NATIONAL AND KAPODISTRIAN UNIVERSITY OF ATHENS
&
UNIVERSITY OF PATRAS

SCHOOL OF SCIENCES
DEPARTMENT OF INFORMATICS AND TELECOMMUNICATIONS AND DEPARTMENT OF PHYSICS
&
SCHOOL OF ENGINEERING
DEPARTMENT OF ELECTRICAL AND COMPUTER ENGINEERING AND DEPARTMENT OF MECHANICAL ENGINEERING AND ASTRONAUTICS

CROSSDEPARTMENTAL MASTER OF SCIENCE (MSc.) PROGRAM
“SPACE TECHNOLOGIES, APPLICATIONS AND SERVICES - STAR”

MSc. THESIS

Design of a CubeSat-Based Multi-Regional Positioning Navigation and Timing System in Low Earth Orbit

G. Tzanoulinos

Supervisors: **Vaios Lappas,** Professor, NKUA
Nori Ait-Mohammed, System Engineer, ESA

ATHENS

OCTOBER 2024

ΕΘΝΙΚΟ ΚΑΙ ΚΑΠΟΔΙΣΤΡΙΑΚΟ ΠΑΝΕΠΙΣΤΗΜΙΟ ΑΘΗΝΩΝ
&
ΠΑΝΕΠΙΣΤΗΜΙΟ ΠΑΤΡΩΝ

ΣΧΟΛΗ ΘΕΤΙΚΩΝ ΕΠΙΣΤΗΜΩΝ
ΤΜΗΜΑ ΠΛΗΡΟΦΟΡΙΚΗΣ ΚΑΙ ΤΗΛΕΠΙΚΟΙΝΩΝΙΩΝ ΚΑΙ ΤΜΗΜΑ ΦΥΣΙΚΗΣ
&
ΠΟΛΥΤΕΧΝΙΚΗ ΣΧΟΛΗ
ΤΜΗΜΑ ΗΛΕΚΤΡΟΛΟΓΩΝ ΜΗΧΑΝΙΚΩΝ ΚΑΙ ΤΕΧΝΟΛΟΓΙΑΣ ΥΠΟΛΟΓΙΣΤΩΝ ΚΑΙ ΜΗΧΑΝΟΛΟΓΩΝ ΚΑΙ ΑΕΡΟΝΑΥΠΗΓΩΝ ΜΗΧΑΝΙΚΩΝ

ΔΙΑΤΜΗΜΑΤΙΚΟ ΠΡΟΓΡΑΜΜΑ ΜΕΤΑΠΤΥΧΙΑΚΩΝ ΣΠΟΥΔΩΝ
“ΔΙΑΣΤΗΜΙΚΕΣ ΤΕΧΝΟΛΟΓΙΕΣ, ΕΦΑΡΜΟΓΕΣ και ΥΠΗΡΕΣΙΕΣ”

ΔΙΠΛΩΜΑΤΙΚΗ ΕΡΓΑΣΙΑ

Σχεδιασμός ενός πολύ-περιφεριακού συστήματος εντοπισμού θέσης, πλοήγησης και μέτρησης χρόνου σε χαμηλή γήινη τροχιά, βασισμένο σε CubeSat

Γ. Τζανουλίνος

Επιβλέπων: **Βάιος Λάππας,** Καθηγητής**,** ΕΚΠΑ
Nori Ait-Mohammed, System Engineer, ESA

ΑΘΗΝΑ

ΟΚΤΩΒΡΙΟΣ 2024

MSc. THESIS

Design of a CubeSat-Based Multi-Regional Positioning Navigation and Timing System in Low Earth Orbit

Georgios Tzanoulinos
ID: 7115172200022

Supervisors: **Vaios Lappas,** Professor, National and Kapodistrian University of Athens
Nori Ait-Mohammed, System Engineer, ESA

Examination Committee: **Vaios Lappas,** Professor, National and Kapodistrian University of Athens
Antonis Paschalis, Professor, National and Kapodistrian University of Athens
Stelios Georgantzinos, Associate Professor, National and Kapodistrian University of Athens

October 2024

ΔΙΠΛΩΜΑΤΙΚΗ ΕΡΓΑΣΙΑ

Σχεδιασμός ενός πολύ-περιφεριακού συστήματος εντοπισμού θέσης, πλοήγησης και μέτρησης χρόνου σε χαμηλή γήινη τροχιά, βασισμένο σε CubeSat

Γεώργιος Τζανουλίνος
Α.Μ.: 7115172200022

Επιβλέπων: **Βάιος Λάππας,** Καθηγητής, Εθνικό και Καποδιστριακό Πανεπιστήμιο Αθηνών
Nori Ait-Mohammed, System Engineer, ESA

Εξεταστική Επιτροπή: **Βάιος Λάππας,** Καθηγητής, Εθνικό και Καποδιστριακό Πανεπιστήμιο Αθηνών
Αντώνης Πασχάλης, Καθηγητής, Εθνικό και Καποδιστριακό Πανεπιστήμιο Αθηνών
Στυλιανός Γεωργαντζίνος, Αναπληρωτής Καθηγητής, Εθνικό και Καποδιστριακό Πανεπιστήμιο Αθηνών

Οκτώβριος 2024

Abstract

Global Navigation Satellite Systems (GNSS) provide critical positioning, navigation, and timing (PNT) services worldwide, enabling a wide range of applications from everyday use to advanced scientific and military operations. The importance of Low Earth Orbit (LEO) PNT systems lies in their ability to enhance GNSS by offering increased signal strength, reduced latency, and improved accuracy and coverage, particularly in challenging environments such as urban canyons or polar regions, thereby addressing limitations of traditional Medium Earth Orbit (MEO) GNSS systems. This thesis presents a comprehensive literature survey on current LEO-based PNT systems, exploring the technological advancements and methodologies employed by leading organizations and institutions related with LEO PNT applications.

Building upon this foundation, the thesis details the design of a novel CubeSat-based multi-regional PNT system tailored for deployment in LEO. The proposed system leverages on a miniaturized CubeSat-compatible PNT payload that includes a chip-scale atomic clock and relies to MEO GNSS technologies, to deliver positioning and timing information across multiple regions. Based on the findings of the literature survey, a Mission Statement is formulated, which in turn informs the development of the Mission and System Requirements that govern the design of the proposed system.

Through simulations and analysis, the thesis evaluates the system's effectiveness in meeting specified mission requirements and success criteria. The findings indicate that the proposed CubeSat-based PNT system offers a viable solution for enhancing global navigation and timing services, with potential commercial, scientific, and dual-use applications. This work contributes to the growing body of knowledge on LEO-based PNT systems and lays the groundwork for future research and development in this rapidly evolving field.

SUBJECT AREA: System engineering of LEO PNT Satellite Systems

KEYWORDS: LEO, PNT, CubeSat, Atomic clocks, Constellation, STK, MATLAB, SPENVIS, DRAMA

ΠΕΡΙΛΗΨΗ

Τα παγκόσμια δορυφορικά συστήματα πλοήγησης παρέχουν κρίσιμες υπηρεσίες εντοπισμού θέσης, πλοήγησης και χρονομέτρησης παγκοσμίως, επιτρέποντας ένα ευρύ φάσμα εφαρμογών από την καθημερινή χρήση έως τις προηγμένες επιστημονικές και στρατιωτικές επιχειρήσεις. Η σημασία των συστημάτων PNT σε χαμηλή γήινη τροχιά έγκειται στην ικανότητά τους να βελτιώνουν τα GNSS προσφέροντας αυξημένη ισχύ σήματος, μειωμένη καθυστέρηση και βελτιωμένη ακρίβεια και κάλυψη, ιδίως σε δύσκολα περιβάλλοντα όπως αστικά φαράγγια ή πολικές περιοχές, αντιμετωπίζοντας έτσι τους περιορισμούς των παραδοσιακών συστημάτων GNSS σε MEO. Η παρούσα διατριβή παρουσιάζει μια ολοκληρωμένη βιβλιογραφική έρευνα σχετικά με τα τρέχοντα συστήματα PNT σε χαμηλή γήινη τροχιά, διερευνώντας τις τεχνολογικές εξελίξεις και τις μεθοδολογίες που χρησιμοποιούνται από κορυφαίους οργανισμούς και ιδρύματα.

Βασιζόμενη σε αυτά τα θεμέλια, η διατριβή περιγράφει λεπτομερώς το σχεδιασμό ενός νέου συστήματος PNT με βάση τον CubeSat, προσαρμοσμένου για ανάπτυξη σε LEO. Το προτεινόμενο σύστημα αξιοποιεί ένα μικροσκοπικό ωφέλιμο φορτίο PNT συμβατό με CubeSat που περιλαμβάνει ατομικό ρολόι σε κλίμακα τσιπ και βασίζεται σε τεχνολογίες MEO GNSS, για να παρέχει πληροφορίες εντοπισμού θέσης και συγχρονισμού σε πολλαπλές περιοχές. Με βάση τα ευρήματα της βιβλιογραφικής έρευνας, διαμορφώνεται μια αποστολή, η οποία με τη σειρά της καθορίζει την ανάπτυξη των απαιτήσεων της αποστολής και του συστήματος που διέπουν το σχεδιασμό του προτεινόμενου συστήματος.

Μέσω προσομοιώσεων και αναλύσεων, η διατριβή αξιολογεί την αποτελεσματικότητα του συστήματος όσον αφορά την εκπλήρωση των καθορισμένων απαιτήσεων της αποστολής και των κριτηρίων επιτυχίας. Τα ευρήματα δείχνουν ότι το προτεινόμενο σύστημα PNT που βασίζεται σε CubeSat προσφέρει μια βιώσιμη λύση για την ενίσχυση των παγκόσμιων υπηρεσιών πλοήγησης και χρονομέτρησης, με πιθανές εμπορικές, επιστημονικές και διπλής χρήσης εφαρμογές. Η εργασία αυτή συμβάλλει στον ανάπτυξη γνώσεων σχετικά με τα συστήματα PNT σε LEO και θέτει τις βάσεις για μελλοντική έρευνα και ανάπτυξη σε αυτόν τον ταχέως εξελισσόμενο τομέα.

ΘΕΜΑΤΙΚΗ ΠΕΡΙΟΧΗ: Μηχανική δορυφορικών συστημάτων LEO PNT

ΛΕΞΕΙΣ ΚΛΕΙΔΙΑ: LEO, PNT, CubeSat, Ατομικό ρολόι, Δορυφορικός αστερισμός, STK, MATLAB, SPENVIS, DRAMA

ACKNOWLEDGEMENTS

This thesis became possible due to a series of key events, thanks to the support of several individuals, for whom I am truly grateful. All started when Prof. Lappas provided me with a letter of recommendation for ESA Academy’s Navigation Training Course 2023. Shortly after, I was informed by Lef Karagiannis from the ESA Academy team that I was placed on the reserve list. When one of the selected participants couldn't attend, I was offered the opportunity to join. During the course, I had the chance to meet Jörg Hahn, and after following up with him, he introduced me to Nori from ESA's LEO-PNT team, setting the next steps in motion.

I was able to carry out this thesis because Prof. Lappas gave me the opportunity to work as a system engineer on the ERMIS CubeSat mission, where I gained the relevant experience. In addition to gaining valuable knowledge on systems engineering, had the opportunity to work with a great team. I would like to express my gratitude to all the members of the ERMIS systems team for their willingness to answer any questions I had. Chronologically, I want to thank Sofia for her guidance on requirements, Varvara for advising me on operations, Paraskevi for providing insights regarding the Link Budget, Konstantinos for his inputs about thermal analysis, Dimitris for his assistance with CAD, Spiros for his support about the theory about maneuvers, and Alexandros for his help with the DRAMA software. And, of course, a special thanks to the other Spyros for his invaluable moral support throughout both the duration of the MSc and the ERMIS project. Also, a big thank you to the "Tartufos Team" from Space Upstream who made the journey of the STAR MSc so enjoyable.

Finally, I would like to express my gratitude to my supervisors, Nori and Prof. Lappas, who generously dedicated their time to guide me throughout this journey. Their support and expertise were crucial in helping me produce what I believe to be a great thesis—something I definitely could not have achieved without their assistance.

ΕΥΧΑΡΙΣΤΙΕΣ

Η παρούσα διατριβή ήταν δυνατή λόγω μιας σειράς γεγονότων, χάρη στην υποστήριξη πολλών ατόμων, για τα οποία είμαι πραγματικά ευγνώμων. Όλα ξεκίνησαν όταν ο κ. Λάππας μου έδωσε συστατική επιστολή για το Navigation Training Course 2023 του ESA Academy. Στη συνέχεια, όπως μου είπε ο Λευτέρης Καραγιάννης από την ομάδα της ESA Academy μπήκα στο reserve list . Όταν ένας από τους επιλαχόντες δεν μπόρεσε να παραστεί, μου δόθηκε η ευκαιρία να συμμετάσχω. Κατά τη διάρκεια του μαθήματος, είχα την ευκαιρία να γνωρίσω τον Jörg Hahn, και μετά από επικοινωνία μαζί του, με σύστησε στον Nori από την ομάδα LEO-PNT της ESA, θέτοντας σε κίνηση τα επόμενα βήματα.

Ο λόγος που μπόρεσα να εκπονήσω αυτή τη διατριβή είναι επειδή ο καθηγητής Λάππας μου έδωσε την ευκαιρία να εργαστώ ως μηχανικός συστήματος στην αποστολή ERMIS, όπου απέκτησα τη σχετική εμπειρία. Εκτός από την απόκτηση πολύτιμων γνώσεων σχετικά με τη μηχανική συστημάτων, είχα την ευκαιρία να συνεργαστώ με μια σπουδαία ομάδα. Θα ήθελα να εκφράσω την ευγνωμοσύνη μου σε όλα τα μέλη της ομάδας για την προθυμία τους να απαντήσουν σε οποιαδήποτε απορία είχα. Χρονολογικά, θέλω να ευχαριστήσω τη Σοφία για την καθοδήγησή της σχετικά με τα requirements, τη Βαρβάρα για τη συμβουλή της σχετικά με τις operations, την Παρασκευή για την παροχή πληροφοριών σχετικά με το Link budget, τον Κωνσταντίνο για τις εισηγήσεις του σχετικά με τη θερμική ανάλυση, τον Δημήτρη για τη βοήθειά του με το CAD, τον Σπύρο για την υποστήριξή του σχετικά με τη θεωρία για τους ελιγμούς και τον Αλέξανδρο για τη βοήθειά του με το λογισμικό DRAMA. Και, φυσικά, ένα ιδιαίτερο ευχαριστώ στον άλλο Σπύρο για την ανεκτίμητη ηθική υποστήριξή του καθ' όλη τη διάρκεια τόσο του ΠΜΣ όσο και του έργου ERMIS. Επίσης, ένα μεγάλο ευχαριστώ στην ομάδα του Ταρτούφου από το Space Upstream που έκανε το ταξίδι του STAR τόσο όμορφο.

Τέλος, θα ήθελα να εκφράσω ένα ευχαριστώ στους επιβλέποντές μου, τον Nori και τον καθηγητή Βάιο Λάππα, οι οποίοι αφιέρωσαν το χρόνο τους για να με καθοδηγήσουν σε όλο αυτό το ταξίδι. Η υποστήριξη και η τεχνογνωσία τους ήταν πάρα πολύ σημαντικές για να με βοηθήσουν να εκπονήσω μια διπλωματική εργασία για την οποία είμαι περήφανος - κάτι που δεν θα είχα πετύχει χωρίς τη βοήθειά τους.

Table of contents

1. Introduction **17**

2. PNT from LEO **19**

3. The State of the Art **20**

3.1. Iridium *20*

3.2. TrustPoint *22*

3.3. Xona Space Systems Inc. *22*

3.4. GeeSpace *24*

3.5. Beijing Future Navigation Technology Co., Ltd. *25*

3.6. ESA's FutureNAV Program *26*

3.6.1. LEO-PNT In Orbit Demonstration 27

3.7. PNT CubeSats *28*

3.7.1. SPATIUM-I 28

3.7.2. MAXWELL 31

3.7.3. CHOMPTT 32

3.7.4. AIOTY-CUBE 35

4. PNT Payloads **39**

4.1. Atomic Clocks *39*

4.2. Clock Performance *42*

4.3. Atomic Clocks in GNSS *42*

4.3.1. Master Clocks 43

4.4. Chip Scale Atomic Clocks *43*

4.5. CubeSat-based PNT Payloads *45*

5. Mission Statement **47**

6. Requirements **49**

7. Mission Architecture **62**

8. Launch Baseline **63**

9. Mission Profile **64**

9.1. Space Segment Overview *65*

10. Mission Design **68**

10.1. Operational Modes *68*

10.1.1. Pointing Profiles 69

10.1.2. Power Profiles 69

10.2. Concept of Operations *71*

10.2.1. Mission Timeline - Mission Phases 71

11. Ground Segment **77**

11.1. Psachna GCS *77*
11.1.1. Psachna GCS Architecture 78

11.2. Nemea GCS *80*

12. Mission Analysis **81**

12.1. Constellation Design *81*
12.1.1. Problem Statement 81
12.1.2. Constellation Tradeoff Analysis 85

12.2. Contacts with Service Area *89*

12.3. Solar Eclipse Analysis *90*

12.4. GCS Visibility Analysis *91*

13. Space Debris Mitigation Analysis **93**

13.1. Space System Fragmentation and Explosion Risk *93*

13.2. Health Monitoring *94*

13.3. Collision Risk Analysis *94*
13.3.1. Collision Risk Assessment – MIDAS 95

13.4. Orbital Decay Analysis – OSCAR *99*

13.5. Spacecraft Re-entry Analysis - SARA *101*

13.6. Passivation Strategy *102*

14. Environmental Design **103**

14.1. Falcon 9 Launch Environment *103*

14.2. Electron Launch Environment *105*

14.3. Vega-C Launch Environment *106*

14.4. Space Environment *108*

14.5. Environmental Qualifications of Components *111*

15. Space Segment **112**

15.1. Spacecraft design *112*
15.1.1. Subsystem Technical Specifications 113
15.1.2. Payload Technical Specifications 124

15.2. Mechanical Design *130*

15.3. System Budgets *131*
15.3.1. Mass Budget 131
15.3.2. Power Budget 133
15.3.3. Link Budget 138
15.3.4. Payload Link Budget 142
15.3.5. ΔV Budget 143
15.3.6. Telemetry Data Budget 145

15.4. Thermal Analysis *146*

15.4.1. Solar Radiation 147
15.4.2. Albedo 148
15.4.3. Planetary Infrared Radiation 149
15.4.4. Internal Heat Dissipation from the Spacecraft 149
15.4.5. Spacecraft's Thermodynamical Equilibrium Equation 150
15.4.6. Emissivity and Absorptivity Coefficients 150
15.4.7. Thermal Simulation Results 151

15.5. System Reliability 152

16. Conclusion 154

17. List of Abbreviations 155

18. Appendix 158

18.1. MATLAB script for Battery SoC - Day in the Life Simulation 158

18.2. MATLAB script for Thermal - Day in the Life Simulation 160

19. Bibliography 162

List of Figures

Figure 1. MEO and LEO footprint and distance comparison 17
Figure 2. Iridium constellation showcasing ISL 20
Figure 3. Iridium NEXT overview 21
Figure 4. Pulsar system overview 22
Figure 5. Pulsar's GNSS independent operation architecture 23
Figure 6. Sherpa-AC 1 system hosting Huginn (a), Huginn payload (b) 23
Figure 7. Pulsar constellation evolution plan 24
Figure 8. The nine GeeSAT-1 satellites 25
Figure 9. Multi-layer PNT system architecture 26
Figure 10. ESA's FutureNAV LEO-PNT IoD system-of-systems overview 27
Figure 11. SPATIUM-I CubeSat 29
Figure 12. Accumulated CSAC counter data (a), calculated count per second (b) 29
Figure 13. Functional block diagram of the SPATIUM-I's payload 30
Figure 14. Figure X. Mission board (a), Supercapacitor board (b) 30
Figure 15. Maxwell mission CONOPs 31
Figure 16. System Block Diagram of MAXWELL CubeSat 32
Figure 17. CHOMPTT 3U CubeSat 33
Figure 18. Top side of the OPTI channel board highlighting the CSAC, TDC-GPX event timer, and the InGaAs APD (a), Bottom side of the OPTI channel board, highlighting the MSP-430 microcontroller (b) 33
Figure 19. OPTI layout 34
Figure 20. AIOTY-CUBE 12U CubeSat (a), ATOMIC payload flight model (b) 36
Figure 21. The subsystems of ATOMIC payload; orbit determination (red), time synchronization (blue), ephemeris generation (yellow) and signal generation (green) 36
Figure 22. ATOMIC payload block diagram and data flow 37
Figure 23. Allan Deviation for free-running (red) vs steered (blue) SA.45s CSAC 37
Figure 24. The basic components of an AFR and how it works 40
Figure 25. An overview showcasing how accuracy and stability are demonstrated in different types of atomic clocks 41
Figure 26. Basic illustration of the workings of a Cs based CSAC 45
Figure 27. Architecture of a CubeSat-Based PNT Payload in line with New Space approach 45
Figure 28. N-CUBE GNSS SDR payload 46
Figure 29. Mission Architecture 62
Figure 30. Spacecraft product tree 65
Figure 31. Basic system overview at high level. Red lines indicate power connections, while black ones indicate data transactions 66
Figure 32. PNT Payload block diagram 67
Figure 33. LEOP - modes state diagram 73
Figure 34. Nominal operations – modes state diagram 75
sFigure 35. GCSs locations 77
Figure 36. UOA's GCS at Psachna, Evia, Greece 78
Figure 37. Psachna GCS architecture 79
Figure 38. The Area Target of Germany with 1° of lat/lon grid granularity 82
Figure 39. GOMspace ANT2150 DUP gain pattern (a) and Gain vs Theta at Phi 45° cut (b) 83
Figure 40. N Asset Coverage Figure of Merit definition 83
Figure 41. Single satellite tracking the area of Germany 84
Figure 42. Walker constellation tracking Germany when in LOS 84
Figure 43. Single satellite in nadir pointing, equipped with a conic sensor with a cone half angle of 85° 85
Figure 44. Constellation tradeoff approach 86

Figure 45. DOP Figure of Merit definition 89
Figure 46. CROC 3D model....95
Figure 47. Number of impacts (a) and catastrophic impacts (b) vs time for objects between 1 mm and 1 cm 96
Figure 48. Number of impacts (a) and catastrophic impacts (b) vs mass for objects between 1 mm and 1 cm 96
Figure 49. Probability of collision vs time (a) and vs mass (b) for objects between 1 mm and 1 cm....97
Figure 50. Number of impacts (a) and catastrophic impacts (b) vs time for objects above 1 cm 97
Figure 51. Number of impacts (a) and catastrophic impacts (b) vs mass for objects above 1 cm 98
Figure 52. Probability of collision vs time (a) and vs mass (b) for objects above 1 cm....98
Figure 53. Orbital decay analysis - Passive disposal after deorbit maneuver....100
Figure 54. SARA re-entry simulation – Altitude vs Downrange....101
Figure 55. SARA re-entry simulation – Altitude vs Time 101
Figure 56. Falcon 9 full octave acoustic MPE (a) and MPE acoustic environment graphs (b) 103
Figure 57. Falcon 9 Payload mechanical interface shock for fairing deployment and Co-Payload separation(s) and for a single separation system values (a) and graph (b) 104
Figure 58. Falcon 9 random vibration MPE values (a) and graph (b) derived at a P95/50 level 104
Figure 59. Falcon 9 maximum fairing spot temperature experienced in the launcher 104
Figure 60. Electron fairing carrying 27 CubeSats....105
Figure 61. Electron acceleration MPE (a) and shock MPE (b)....105
Figure 62. Electron acoustic MPE (a) and random vibration (b) 106
Figure 63. SSMS configurations Hex-1 and Hex-2 (orange blocks) (a) and VAMPIRE 937 MPL Towers (green blocks) (b)....106
Figure 64. Definition of the mission’s duration (a) and orbital parameters (b) in SPENVIS....108
Figure 65. Radiation sources (a) and Trappes proton and electron models 108
Figure 66. Models used for solar particle mission fluences (a) and GCR (b)....109
Figure 67. TID model used 109
Figure 68. TID for 3 years as a function of shielding thickness....110
Figure 69. System diagram at signal level....113
Figure 70. GOMspace NanoDock DMC-3 (a), GOMspace NanoMind A3200 (b)....114
Figure 71. GOMspace NanoDock DMC-3 system diagram 115
Figure 72. A3200 Block diagram 115
Figure 73. NovAtel OEM719 GNSS receiver (a), Tallysman GNSS antenna (b)....116
Figure 74. NanoPower P80 (a), NanoPower BP8 (b), NanoPower DSP-90deg mounted on the 6U structure (c)....117
Figure 75. Block diagram of the NanoPower P80 system....117
Figure 76. Block diagram of power paths in the NanoPower P80....117
Figure 77. NanoPower BP8 functional block diagram....118
Figure 78. NanoPower DSP-90 architecture 118
Figure 79. CubeSpace sensors and actuators 119
Figure 80. CubeSpace ADCS architecture (STR are not applicable in this case) 119
Figure 81. GOMspace NanoCom AX100 (a), GOMspace NanoCom ANT-6F UHF (b) 120
Figure 82. NanoCom Link family product high-level system overview (Slot B is left empty in Link S)121
Figure 83. GOMspace NanoCom Link S (a), GOMspace NanoCom ANT2150-DUP (b) 121
Figure 84. Enpulsion NANO 123
Figure 85. GOMspace 8U structure....124
Figure 86. Microchip SA.45s Chip-Scale Atomic Clock....125
Figure 87. Microchip SA.45s CSAC Block Diagram Overview....125
Figure 88. Microchip SA.45s CSAC Physics Package....126
Figure 89. Frequency Response of the CSAC while exposed to –10°C to +50°C....126
Figure 90. NANOlink-boost Gen2 (a), a corner retroreflector (b) 128
Figure 91. Spacecraft internal view 130

Figure 92. Spacecraft external view 130
Figure 93. System power consumption 134
Figure 94. Battery SoC - Day in the life simulation - Nominal scenario 136
Figure 95. Battery SoC - 5 Days in the life simulation - Nominal scenario...136
Figure 96. GOMspace ANT-6F antenna - Total far field realized gain measured in dBi for 400MHz, 435MHz and 470MHz variants in RHCP. 138
Figure 97. GOMspace ANT-6F antenna - Total far field realized gain measured in dBi for 400MHz, 435MHz and 470MHz variants in LHCP 138
Figure 98. GOMspace ANT-6F antenna radiation pattern 139
Figure 99. GOMspace ANT2150-DUP Mean Half Power Beamwidth 139
Figure 100. Target Sequence – Maneuver..144
Figure 101. Differential Corrector – setting target orbital period 144
Figure 102. Drag and solar pressure vector properties...145
Figure 103. A CubeSat in nadir pointing mode remains oriented towards the center of Earth throughout the orbit 147
Figure 104. Spacecraft temperature - Day in the life simulation – 80% electrical power-to-heat conversion ratio 151
Figure 105. Spacecraft temperature – 5 Days in the life simulation – 80% electrical power-to-heat conversion ratio 151
Figure 106. Spacecraft temperature – 5 Days in the life simulation – 50% electrical power-to-heat conversion ratio 152
Figure 107. Spacecraft temperature – 5 Days in the life simulation – 100% electrical power-to-heat conversion ratio 152

List of Tables

Table 1. Comparison of MEO and LEO based GNSS 21
Table 2. CentiSpace Constellation architecture 26
Table 3. CSAC Mission Board Specifications 31
Table 4. System design standards 48
Table 5. Mission Requirements 49
Table 6. System Requirements 51
Table 7. Mission objectives – Success Criteria 62
Table 8. Launch characteristics 63
Table 9. Bus operational modes 68
Table 10. Payload operational modes 69
Table 11. Pointing profiles 69
Table 12. ADCS components average and maximum power consumption 70
Table 13. ADCS modes power breakdown 70
Table 14. ADCS modes consumption 70
Table 15. System power profiles description 71
Table 16. Mission phases 71
Table 17. LEOP – deployment and initial GCS link 72
Table 18. LEOP – detumbling phase 73
Table 19. LEOP - conditions for state changes 74
Table 20. Nominal operations - conditions for state changes 75
Table 21. UHF Yagi Antenna characteristics 79
Table 22. S-Band Satellite Dish characteristics 79
Table 23. Physical characteristics of the antennae system 80
Table 24. Tradeoffs between altitude, number of satellites and Payload link budget for the inclination of 56° 87
Table 25. Constellation configurations based on inclination at 650 km of altitude 88
Table 26. Service satisfaction for different inclination values at 600 km 88
Table 27. Tradeoffs between altitude, number of satellites and Payload link budget for the inclination of 61° 89
Table 28. Contact times with service area 90
Table 29. Calculation of the revisit time of a single satellite to the area of service 90
Table 30. Solar eclipse calculation 91
Table 31. Solar eclipse - worst case 91
Table 32. Contact times with Psachna GCS 91
Table 33. Contact times with Psachna GCS - worst case 92
Table 34. Contact times with Nemea GCS 92
Table 35. Contact times with Nemea GCS - worst case 92
Table 36. Inputs for CROC 94
Table 37. Calculated cross-sections for each orientation 95
Table 38. MIDAS simulation Input Parameters 95
Table 39. Probability of catastrophic impact before the end of the mission 98
Table 40. OSCAR simulation Input Parameters 100
Table 41. SARA simulation Input Parameters 101
Table 42. Passivation steps 102
Table 43. Falcon 9 Quasi-Static load factors of the CubeSat Dispenser 103
Table 44. Falcon 9 maximum predicted sinusoidal vibration environment 103
Table 45. Vega-C Quasi-Static load factors 107
Table 46. Vega-C Sinusoidal vibration environment test levels 107
Table 47. Vega-C random vibration MPE at SSMS Hexa positions (a) and Shock levels at SSMS Hexagonal module positions and VAMPIRE 937 positions 107

Table 48. TID for different altitudes and shielding thickness for circular orbit with 61° of inclination .110
Table 49. Environmental qualification status of components 111
Table 50. Baseline Configuration....112
Table 51. CDHS highlighted features 114
Table 52. EPS Highlighted features....116
Table 53. UHF link highlighted features....120
Table 54. S-band link highlighted features 121
Table 55. Comparison of Chemical and Electrical Propulsion Systems 122
Table 56. Enpulsion NANO technical specifications....123
Table 57. Characteristics of GOMspace 8U structure 124
Table 58. PNT payload components 124
Table 59. Microchip SA.45s CSAC technical characteristics 125
Table 60. PNT Solution Generator components....127
Table 61. Payload components technical specifications 127
Table 62. PNT Payload technical specifications....127
Table 63. NANOlink-boost Gen2 technical specifications 128
Table 64. Margin philosophy....131
Table 65. Mass Budget – Subsystem level 131
Table 66. Mass Budget – Component level....131
Table 67. Positive Mass Margin of Deployer Pod....133
Table 68. Power generation for different scenarios....133
Table 69. Spacecraft power storage characteristics....133
Table 70. Power Budget for modes with extended operation times 135
Table 71. P80 input channels 137
Table 72. P80 output channels 137
Table 73. UHF uplink budget 140
Table 74. UHF downlink budget 141
Table 75. S band uplink budget 141
Table 76. S band downlink budget 142
Table 77. PNT signal power at ground level....142
Table 78. Phasing duration and ΔV tradeoff....143
Table 79. Stationkeeping ΔV budget 145
Table 80. ΔV Budget for a 10-day phasing maneuver and stationkeeping 145
Table 81. S-Band Telemetry data budget....146
Table 82. UHF Telemetry data budget 146
Table 83. OBC memory budget 146
Table 84. Earth's Albedo depending on the inclination 148
Table 85. Earth's thermal emission depending on the inclination 149

1. **Introduction**

GNSS, standing for Global Navigation Satellite System is a network of satellites that provides global positioning, navigation, and timing information to users on Earth. Current GNSS are located at MEO or GEO and are the United States' GPS, Russia's GLONASS, Europe's Galileo, and China's BeiDou Navigation Satellite System, while other RNSS (Regional Navigation Satellite System) as Japan’s QZSS and India’s NavIC also exist. Nowadays, GNSS have become an essential element in everyday life and are the sole technology that offers free, precise and omnipresent PNT services to users around the world. As highlighted in the EUSPA EO and GNSS Market Report, global revenues from GNSS reached around €260 billion in 2023. By 2033, these revenues are projected to climb to €580 billion, with over 80% of this total coming from services enabled by GNSS devices. Additionally, global shipments of GNSS units are expected to reach 2 billion per year by 2027, with nearly 9 billion GNSS devices anticipated to be in use by 2033. Predominantly, revenues from GNSS components, receivers, system integrators, and software/added-value services are generated by US and European companies. The US accounts for the largest market share at more than 30%, with Europe trailing at close to 25%[1]. Traditionally, navigation satellites have been placed in MEO. In these orbits, the satellites traverse the sky at a slow pace and provide global coverage via low power navigation signals. However, implementing navigation satellites in LEO offers several advantages. A significant benefit of LEO compared to MEO is the reduced spreading loss, which results in stronger signals on the ground. Additionally, LEO provides faster movement across the sky (mean motion), enhancing geometric diversity and leading to multipath whitening. More specifically, the path loss of signals from LEO satellites is so lower than those in MEO, that they could have approximately 1000 times (30 dB) greater signal strength. Thus, they are resistant to interference and are advantageous for navigation in urban and indoor settings. Also, the increased signal strength (however limited by the ITU) makes them more resilient against jamming or spoofing [2].

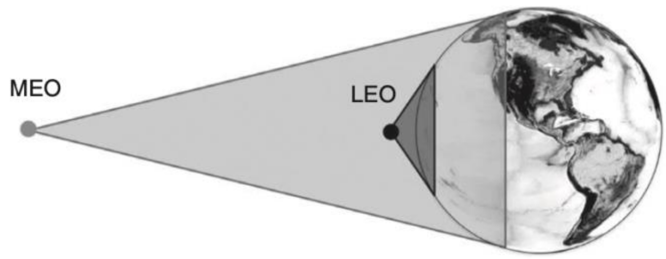

Figure 1. MEO and LEO footprint and distance comparison [2]

Nevertheless, it has to be mentioned that a key drawback of LEO is its smaller satellite footprint, necessitating a significantly larger number of satellites to achieve the same coverage as MEO. As a rule of thumb it takes nine LEO satellites to match the footprint of one MEO satellite, hence requiring many more satellites to cover

Earth. This was one of the fundamental considerations in the design of the current MEO GNSS constellations. In this era, the "New Space" movement is revolutionizing the space industry with innovative approaches that significantly reduce costs and enhance accessibility. Unlike traditional, government-led space activities, New Space focuses on commercial viability, innovation, and cost reduction, making space more accessible and affordable. This sector is marked by the entry of numerous private companies like SpaceX and Blue Origin, fostering competition and technological advancements through faster development cycles and cost-effective manufacturing processes. Public-private partnerships are common, leveraging government support while harnessing private sector efficiency. In this environment, small satellites and nanosatellites are gaining popularity. There is high interest in CubeSats; small, standardized satellites that are much cheaper and quicker to develop than traditional satellites. CubeSats have democratized space exploration by allowing universities, small businesses, and even amateur groups to conduct space missions. They are usually built using COTS components, which further drive down costs and development times. This approach contrasts sharply with the bespoke components typically used in traditional space missions, leading to a more agile and flexible space industry. The combination of New Space initiatives, CubeSats, and COTS components is enabling a broader range of entities to participate in space exploration, fostering innovation, and opening new commercial opportunities in the space sector.

2. PNT from LEO

As the potential of LEO navigation has begun to be explored, the concept of LEO-PNT has emerged. There are three methods for utilizing LEO constellations for positioning: Leveraging LEO Signals of Opportunity (SoO), hosting payloads on satellites designed for PNT applications, Fused payloads embedded within telecommunication payloads [3], [4].

The main motivation of LEO SoO is the recent rise of commercial broadband LEO mega-constellations. The idea behind it is to leverage signals from LEO satellites not specifically designed for PNT. These satellites do not transmit dedicated PNT signals, so the responsibility for PNT processing lies with the receiver. By using measurements such as angle of arrival (AOA), received signal strength, and Doppler shifts, these systems can effectively determine position. This approach offers an alternative means of PNT, especially useful in environments where traditional GNSS signals are insufficient or unavailable. According to the Hosted PNT payload approach, the augmentation of existing GNSS could be possible by introducing LEO PNT systems in the form of constellations of satellites equipped with PNT payloads [4]. Finally, the fused payload approach relies upon LEO telecommunications constellations. By collaborating with the constellation operator and "fusing" PNT with the communications services promising results could be achieved. There is no need for PNT-specific components on orbit. Just by implementing into the transmitted signals PNT related information (e.g. TLEs, ephemeris data) it is possible to reduce the complexity of tracking a dense, low-altitude constellation from the ground and allows the receiver to generate single-epoch stand-alone PNT solutions [5].

3. **The State of the Art**

This chapter outlines the latest advancements that have been done at providing PNT services from LEO.

3.1. Iridium

The Iridium satellite constellation, initially developed by Motorola, to provide global voice and data communication through a network of 66 active satellites. The constellation has the Walker Star pattern with the satellites placed at the altitude of 781 km with an inclination of 86.4°. The satellites are placed into 6 orbital planes that house 11 satellites each. The first-generation satellites with a mass of about 700 kg, launched between 1997 and 2002, were designed to ensure continuous coverage worldwide via L-Band [6]. In order to do so, they introduced cross intersatellite links (ISL), via Ka Band, meaning that each satellite communicates with its nearest two satellites in the same orbital plane (its preceding satellite and the following one) and with a satellite of each of its adjacent orbital planes. Being at the altitude mentioned above, Iridium satellites have an orbital period near 100 minutes and, thus, a single satellite can be visible to a ground user for approximately 7 minutes.

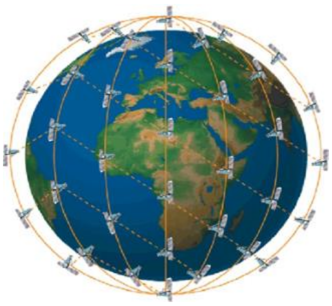

Figure 2. Iridium constellation showcasing ISL [7]

Since the announcement in 2007, about $3 billion has been poured into the Iridium NEXT satellite replacement program. The first Iridium NEXT launched happened in 2017. The satellites were built by Thales Alenia Space and the constellation has the same geometry as the original and comprises 66 operational satellites, supplemented by 9 on-orbit spares and 6 spares on the ground [8].

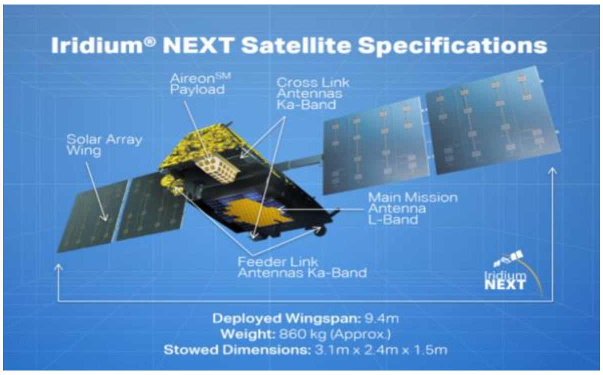

Figure 3. Iridium NEXT overview [9]

Among other services, the company provides Satellite Time and Location (STL) solutions built by Satelles in partnership with Iridium Communications Inc. based on Iridium that started being operational in May 2016. Moreover, in March 2024, Iridium announced the Acquisition of Satelles [10]. Broadcasts are transmitted with the purpose of enabling an STL receiver to achieve accurate time and frequency measurements for determining its PNT. The system is capable of positioning accuracy of 20 m and timekeeping of 1 μs, while it can operate in an indoor environment due to its strong LEO signals. That way, STL can enhance or act as a backup for existing MEO GNSS core constellations by delivering secure measurements even in conditions of high attenuation, jamming, or spoofing. Security is ensured by Iridium’s distinctive architecture, which uses 48 spot beams to concentrate transmissions on localized geographic areas. The intricate overlap of Iridium's spot beams, combined with randomized broadcasts, creates a unique method for location-based authentication resilient to spoofing [2].

Table 1. Comparison of MEO and LEO based GNSS [2]

	MEO	LEO	LEO to MEO ratio
System	GPS	Iridium	-
Altitude (km)	$20{,}200$	780	$1/25$
Spreading loss at zenith (dB)	-97	-69	28
Footprint (km^2)	1.73×10^8	1.93×10^7	$1/9$
Footprint radius (km)	7900	2500	$1/3$
Mean motion $\left(\frac{deg}{sec}\right)$	0.008	0.06	7
Orbital period (hr)	12	1.67	$1/7$
Multipath decorrelation time (min)	10	1	$1/10$

3.2. TrustPoint

TrustPoint was founded in 2020 and is headquartered in Virginia, US [11]. By deploying a constellation of microsatellites, TrustPoint plans on developing a dual use GNSS. The company's goals among others are to complement GPS by providing services resilient to spoofing and jamming, with better accuracy and faster Time to First Fix. In 2021 the company raised $2 million [12]. The system aims to transmit PNT signals in C Band (~5 GHz), while not being dependent on other MEO GNSS. In April 2023, it launched its first CubeSat, named "It's About Time", as a technology demonstrator to test, calibrate and optimize its PNT small satellite payload [13], [14]. TrustPoint launched its second satellite named "Time We'll Tell" in November 2023 [15]. TrustPoint has partnered with SpiderOak, a cybersecurity company, to create the first-ever zero-trust, end-to-end commercial PNT system across both space and ground segments [16].

TrustPoint is creating a ground network that will monitor the constellation's signals and uplink PNT information to the satellites, making the system not dependent of MEO GNSS. This can be expanded for use outside of TrustPoint and provided as an alternative or supplementary PNT service to other LEO satellites. By delivering ground-based RF PNT broadcasts and incorporating CubeSats equipped with specialized receivers, on-board clocks, and a precision orbit determination system, TrustPoint aim to provide PNT services while being independent of existing MEO GNSS, capable of serving an unlimited number of users simultaneously [17].

3.3. Xona Space Systems Inc.

Xona Space Systems is a California-based company established in 2019 aiming to provide commercial PNT services through developing its own LEO constellation named Pulsar that will consist of about 300 CubeSats [18]. Pulsar satellites are to house radiation tolerant and low SWaP clocks for time keeping. By leveraging on both MEO GNSS and ground stations they will be able to deliver cm-level accuracy while being resistant to interference [19].

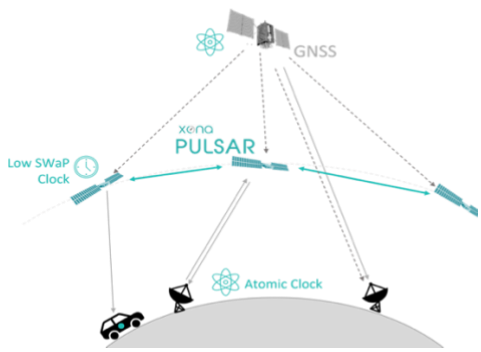

Figure 4. Pulsar system overview [19]

However, the system can be GNSS independent by achieving clock synchronization through inter-satellite links. This design enables atomic clocks to be located at specific nodes within the network, whether on the ground or in space, instead of being placed on every satellite [20].

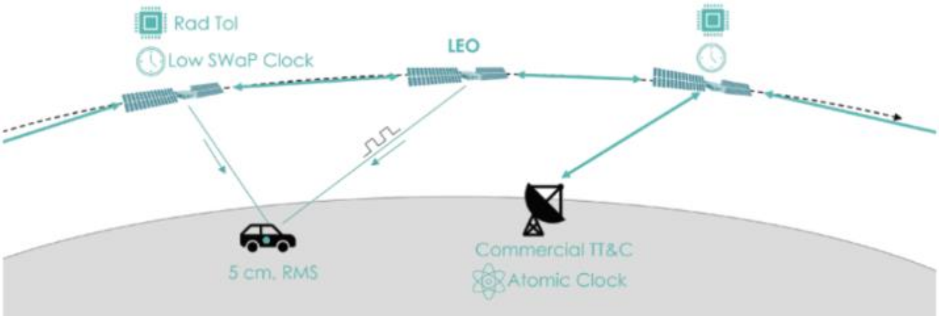

Figure 5. Pulsar's GNSS independent operation architecture [20]

In May 2022, Xona Space Systems successfully launched their first on orbit demonstration payload, named Huginn in an SSO with an altitude of 525 km and an inclination of ~97º [20], [21]. Huginn has the form of a hosted payload onboard a free flying satellite deployer named Sherpa-AC 1. The Sherpa-AC system features a flight computer, ADCS, an electrical power system (including solar panels and batteries), and two-way RF communications. Beyond deploying multiple satellites, Sherpa-AC is also ideal for hosting payloads in LEO [22].

	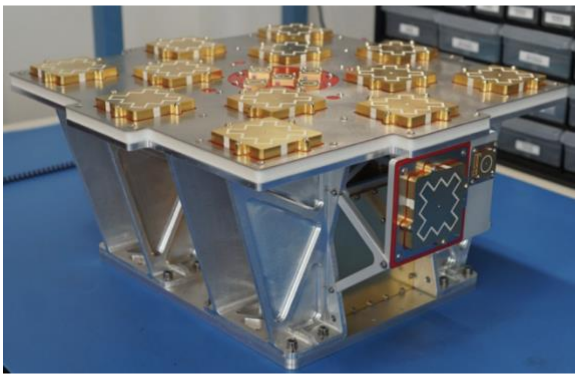
(a)	(b)

Figure 6. Sherpa-AC 1 system hosting Huginn [22] (a), Huginn payload [23] (b)

Huginn successfully broadcasted demo PNT signals to the ground in L-band and C-band and validated Xona's patented distributed clock architecture, which is crucial for providing precision PNT without the need for large atomic clocks onboard[20], [24]. Xona has built a second satellite named Muninn that was set to launch in 2023

[25]. The plan is to build the Pulsar constellation in four phases. By increasing the number of satellites after each phase the PNT services shall also be enhanced.

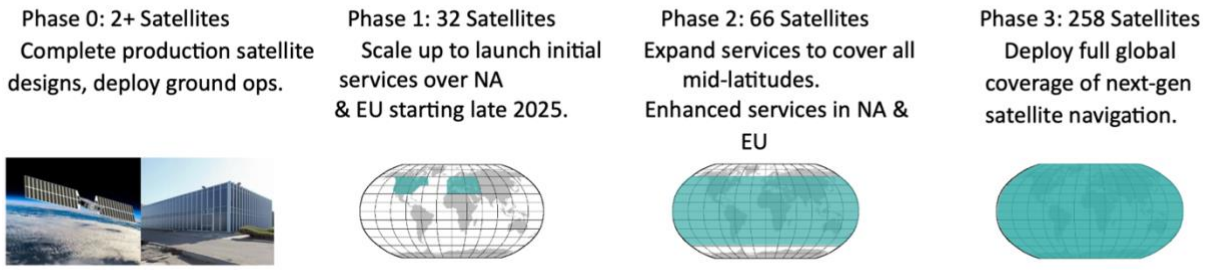

Figure 7. Pulsar constellation evolution plan [19]

3.4. GeeSpace

Geespace is a satellite technology and commercial services company founded in 2018 by Zhejiang Geely Holding Group. It focuses on developing, launching, and operating LEO satellites to provide high-precision positioning, connectivity, and remote sensing services. Geespace's major project is the "Geely Future Mobility Constellation," which aims to integrate communication, navigation, and remote sensing within a single satellite network.

The company's satellites are part of a broader effort to support autonomous driving and smart connectivity for Geely's automotive brands, such as Zeekr. The constellation's goal is to offer commercially global cm-level Precise Point Positioning, Real-Time Kinematic (PPP-RTK) services and connectivity support for use by automotive brands in the Geely Holding portfolio, with the first phase targeting the deployment of 72 satellites by 2025 and an eventual expansion to 240 satellites [26]. Moreover, the constellation supports the operation of OmniCloud, a satellite-based AI cloud platform developed by Geespace that aims to enhance urban traffic management, PNT data for autonomous vehicles, and improving public transportation fleet management, ride-hailing, and ride-sharing services. The platform also extends its capabilities to the industrial sector, where it helps monitor, control, and maintain manufacturing equipment remotely using connected sensors.

GeeSAT 1-01 and GeeSAT 1-02, were Geespace's first satellites and were launched in December 2021. They focused on navigation and communication and each had a mass of 130 kg [27]. In June 2022, successfully launched 9 GeeSAT-1 satellites in LEO to form the constellation's first orbital plane [26]. In February 2024,11 GeeSAT-2 satellites were launched completing the second orbital plane of the Geely Future Mobility Constellation [28].


Figure 8. The nine GeeSAT-1 satellites [29]

3.5. Beijing Future Navigation Technology Co., Ltd.

Beijing Future Navigation Technology Co., Ltd., established in 2017, specializes in developing advanced satellite navigation and augmentation systems. The company is notable for its CentiSpace satellite constellation, which enhances the performance of China's BeiDou navigation system and enables PPP applications by providing additional L1 and L5 signals from LEO to improve PNT accuracy [30].

In September 2018, CentiSpace-1 S1 was launched into an orbit with an altitude between 695 and 708 km and an inclination of 98.2 degrees. CentiSpace-1 S1 has a mass of 97 kg and its goal was to test GNSS augmentation techniques including laser ISL communications. In July 2020, CentiSpace-1 S2 was launched but it failed to get into orbit. Following that in September 2022, CentiSpace-1 S3 and S4 were successfully launched [31]. In October 2022, CentiSpace-1 S5 and S6 satellites were launched to enhance BeiDou navigation signals [32].

The Centispace constellation is planned to consist of three sub-constellations, meaning that the satellites will be in multiple orbital planes with different altitudes and inclinations. Sub-constellation I shall consist of satellites in Walker 120/12/1 pattern with an altitude of 975 km and inclination of 55 degrees. The satellites shall have a mass of about 100 kg and a lifetime of 10 years [33]. Sub-constellation II shall consist of 30 satellites in Walker 30/3/1 pattern at 1100 km altitude with 87.4 degrees of inclination. Sub-constellation III shall consist of 40 satellites in Walker 40/4/1 pattern at 1100 km altitude with 30 degrees of inclination [30].

Table 2. CentiSpace Constellation architecture [30]

	Pattern	Altitude (km)	Inclination (deg)
Sub-constellation I	Walker 120/12/1	795	55
Sub-constellation II	Walker 30/3/1	1100	87.4
Sub-constellation III	Walker 40/4/1	1100	30

3.6. ESA's FutureNAV Program

Approved at the 2022 ESA Ministerial Council meeting in Paris, ESA's FutureNAV program is designed to respond to emerging trends and demands in satellite navigation, pushing towards the development of a multi-layer PNT system and ensuring Europe remains at the cutting edge of this vital technology. Three contracts with a combined value of €233.4 million have been awarded by ESA for the first two missions of FutureNAV programme; Genesis and LEO-PNT. GENESIS aims to create an exceptionally accurate International Terrestrial Reference Frame (ITRF), improving navigation and Earth observation accuracy down to the millimeter level, while having a long-term stability of 0.1 mm per year. This mission integrates multiple geodetic techniques—satellite navigation ranging, Very Long Baseline Interferometry (VLBI), Satellite Laser Ranging (SLR), and the Doppler-based 'DORIS' radio positioning system—into a single, well-calibrated satellite platform. The GENESIS mission will provide essential data for various applications, including climate change monitoring, natural hazard prediction, and land management [34]. A contract valued at €76.6 million was awarded for the Genesis mission to a consortium led by OHB Italia, which consists of 14 different entities. This consortium is tasked with the development, manufacturing, qualification, calibration, launch, and operation of the satellite and its payloads. The Genesis satellite is scheduled for launch in 2028. On the other hand, LEO-PNT mission aims to enhance PNT services through LEO constellations.

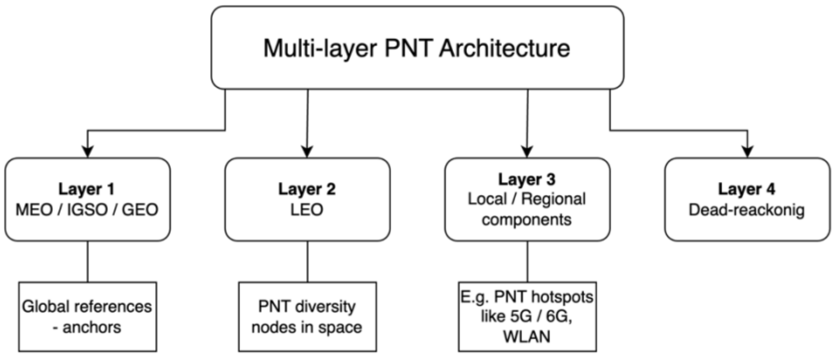

Figure 9. Multi-layer PNT system architecture [35]

3.6.1. LEO-PNT In Orbit Demonstration

Regarding ESA's LEO-PNT mission, two contracts valuing € 78.4 million each have been awarded for the development, launch and operation of two LEO constellations, primarily composed of satellites with a mass of about 70 kg, capable of demonstrating end-to-end PNT services in a variety of frequencies (targeting UHF, L, S, Ku/Ka bands) leading to faster position fixes, enabling two-way authentication checks and enhancing signal availability in high-latitude and polar regions [35].

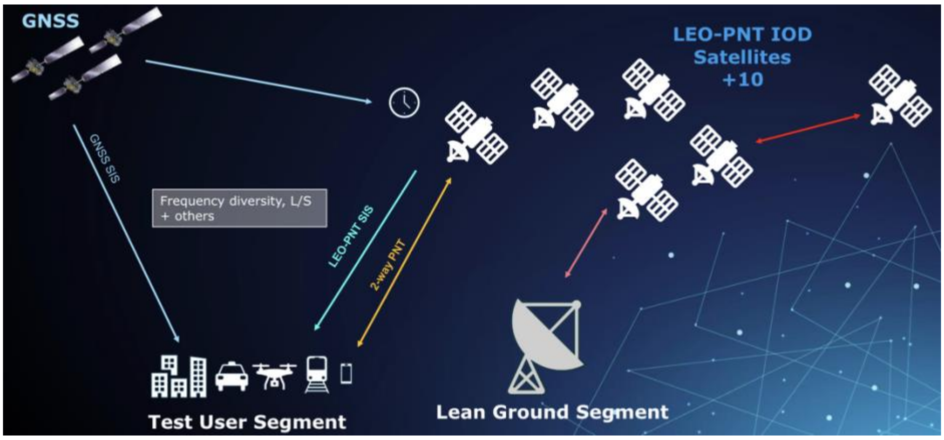

Figure 10. ESA's FutureNAV LEO-PNT IoD system-of-systems overview [35]

The one consortium is led by GMV Aerospace and Defence S.A.U. (ES), with OHB Systems AG (DE) being a core partner and the space segment prime. Other core partners in this project are Alén Space, Beyond Gravity and Indra. This consortium will develop and launch a constellation of 5 satellites. Aside from designing and developing the satellites along with their payloads, they will also be responsible for launching the constellation, providing a ground segment as a service (GSaaS), developing the test user receiver, operating the system and demonstrating its PNT services with end users. The first IOD CubeSat platform shall be provided by Alén Space, while the other 4 LEO satellites shall be manufactured by OHB in Bremen. Beyond Gravity will be focusing on the development of the PNT payloads and Indra will coordinate the experimentation and validation campaign. The system will also showcase an innovative feature known as the "LEO shield," which can evaluate the integrity of GNSS signals received by the LEO satellites in real-time and notify users if there is a malfunction [34], [36], [37], [38].

Thales Alenia Space France S.A.S (FR) was awarded the other contract, in which Thales Alenia Space SPA (IT) has the role of space segment prime. Another partner is Telespazio, which will be supporting the operation and the performance analysis of the system. The ground receivers for this project shall be manufactured by Syntony. The contract covers the development of space, ground and users' segment, the launch, operation and deorbit of the satellites and the overall demonstration of the

PNT services. Overall, those two consortia are formed by 50 entities from 14 countries [39], [40], [41].

According to GMV, he LEO-PNT constellation will transmit PNT signals in different frequency bands from LEO and implement a multi-layer system-of-systems approach by working alongside Galileo and other GNSS. The transmitted signals shall be in UHF, S, L and C band [37]. By doing so, the robustness of current MEO GNSS will be enhanced against natural phenomena (e.g. weather, ionospheric disturbances) and interferences. Moreover, by introducing stronger signal power and a diverse geometry LEO-PNT signals can penetrate urban areas and indoors where MEO GNSS are not efficient. Additionally, the mission will demonstrate the ability of a LEO navigation constellation to monitor the signals of Galileo and EGNOS from space. Finally, the interoperability of space based PNT services with open communication standards, such as 5G/6G, will be demonstrated. That initiative could potentially enable new capabilities in the domain of automotive, autonomous vehicles, IoT and emergency services [39].

3.7. PNT CubeSats

3.7.1. SPATIUM-I

SPATIUM-I, which stands for Space Precision Atomic-clock TIming Utility Mission I, was a 2U Cubesat developed by NTU in Singapore and Kyutech in Japan. It was launched on 23 Sep 2018 from ISS Japanese Kibo module and deorbited on 23 Sep 2021 and was the first CubeSat to successfully demonstrate a CSAC operating in LEO. The SPATIUM-I was launched in a LEO orbit at an altitude of 400 km with 51.6 deg inclination and had a mass of 2.66 kg [42].

The primary scientific objective of the mission was to develop a platform to 3D map the ionosphere TEC based on the phase-shift in satellite clock signal from multiple ground stations and potentially from a constellation of CubeSats hosting a CSAC. The mechanism that this is based on is that since the satellite signals pass through the ionosphere and interact with the ionospheric plasma there is a delay in signal transmission known as propagation delay, which is inversely related to the square of the signal's frequency. On top of this, atmospheric effects are anticipated to introduce an additional phase delay to the radio signal that must be accounted for, too. It was an In-orbit demonstration mission that aimed to demonstrate a COTS CSAC as reliable reference clock for a CubeSat mission, the transmission of Spread Spectrum signals modulated at 467 MHz that used the CSAC as clock source, dual-UHF transmission (at 400 MHz and 467 MHz), reception and demodulation of Spread Spectrum signal at ground station, time-synchronization of several ground stations [43].

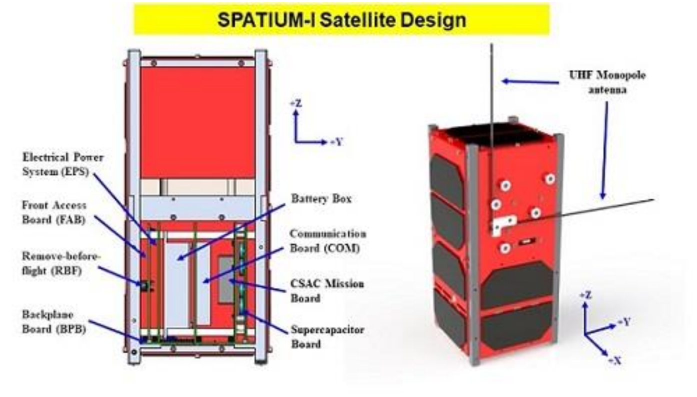

Figure 11. SPATIUM-I CubeSat [43]

The main functions of the payload board were to generate the precise CSAC 10 MHz clock signal, the PPS and telemetry data and relay them to the communication subsystem. The clock's counter value was analyzed through the whole duration of the mission and ended up being extremely stable and no discernible drift was noted in the count per second.

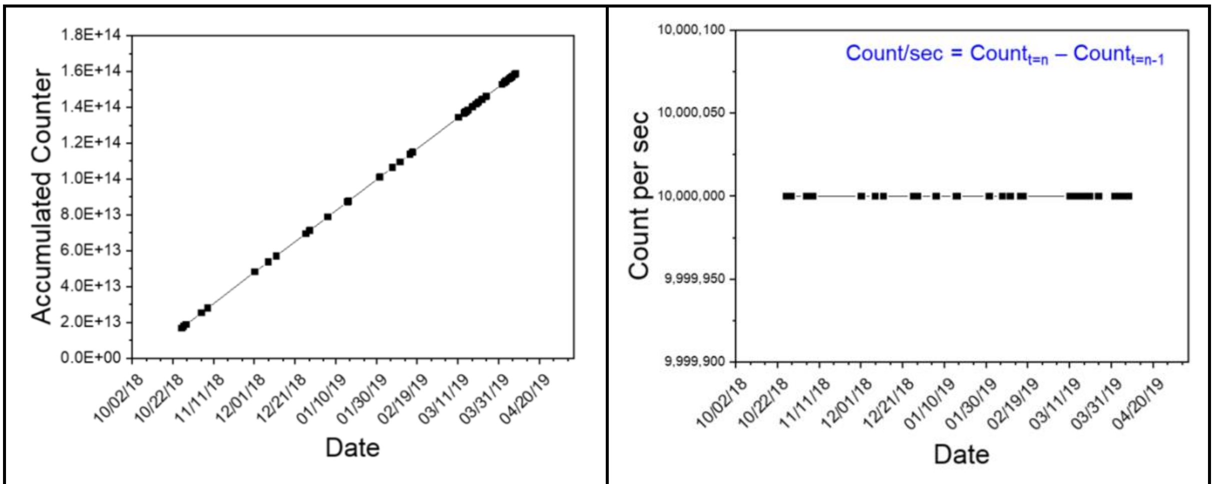

(a)	(b)

Figure 12. Accumulated CSAC counter data (a), calculated count per second (b) [43]

The basic components of the CSAC mission were a CSAC chip (Microsemi SA.45s CSAC), a temperature sensor, ripple counter, and a MCU (Micro-Controller Unit). To ensure stable operation, a low noise, low-dropout voltage (LDO) regulator supplied a constant 3.3 V voltage input to both the CSAC and other onboard components. A frequency counter was specifically designed to count the CSAC's 10 MHz oscillation signal.

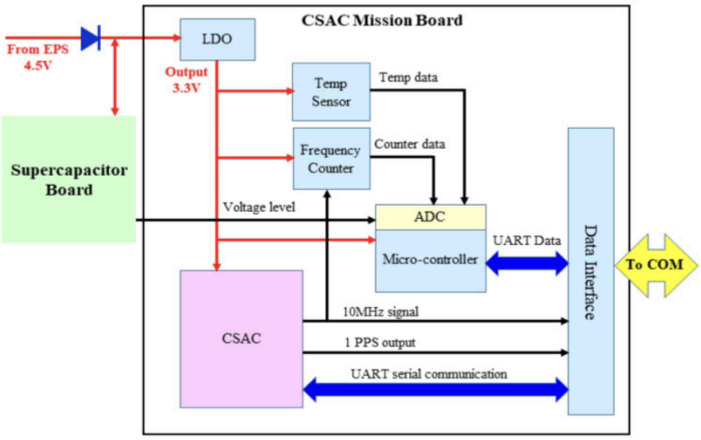

Figure 13. Functional block diagram of the SPATIUM-I's payload [43]

This counter served to confirm the CSAC's clocking precision and to calculate the phase variance in signal transmission for TEC modeling purposes. Every second, triggered by the 1PPS signal from the CSAC, the MCU captured the counter value data along with other pertinent information such as temperature sensor readings and supercapacitor voltage data. Subsequently, this data was processed within the MCU and transmitted to the communication subsystem via UART. To prevent any potential power disruptions to the CSAC during eclipse, a supercapacitor module served as a backup power source for the CSAC board.

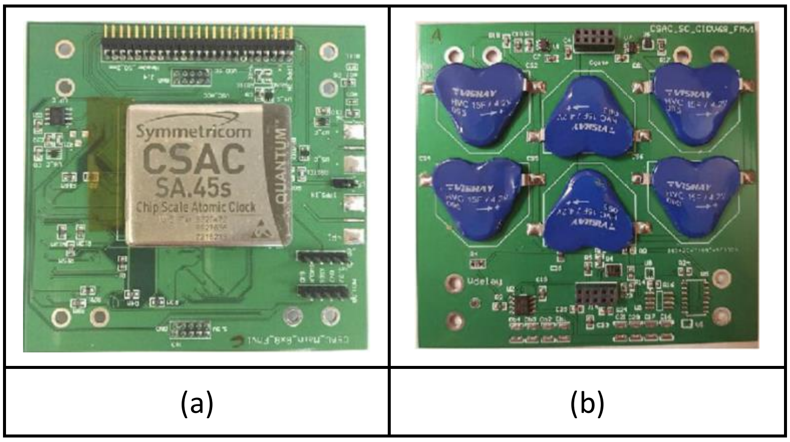

Figure 14. Figure X. Mission board (a), Supercapacitor board (b) [43]

Table 3. CSAC Mission Board Specifications

CSAC Mission Board Specifications [43]	
Dimensions	86.3 mm x 90 mm x 21 mm
Mass	113 gr
Voltage	4.5 V
Power Consumption	0.35 W
Warm-up Time	< 180 s
Data Interfaces	CSAC data: UART (Baud rate: 57,600 bps) Operation data: UART (Baud rate: 128,000 bps)

3.7.2. MAXWELL

MAXWELL (Multiple Access X-band Wave Experiment Located in LEO) is a 6U CubeSat mission that is to be designed, built, and tested at the University of Colorado Boulder. The mission objectives include showcasing cutting-edge RF communications technologies, and the characterization of the Allan Variance of a CSAC on orbit [44].

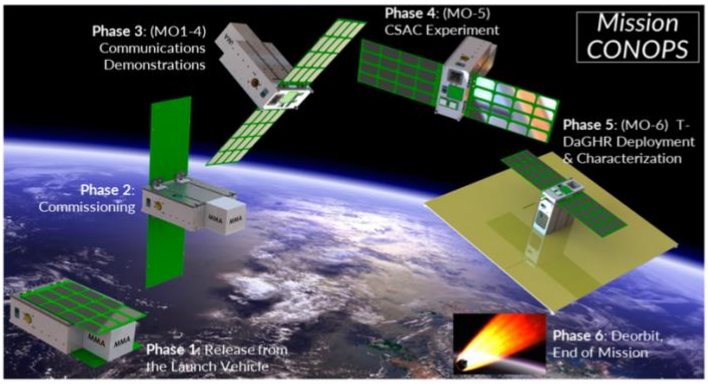

Figure 15. Maxwell mission CONOPs [44]

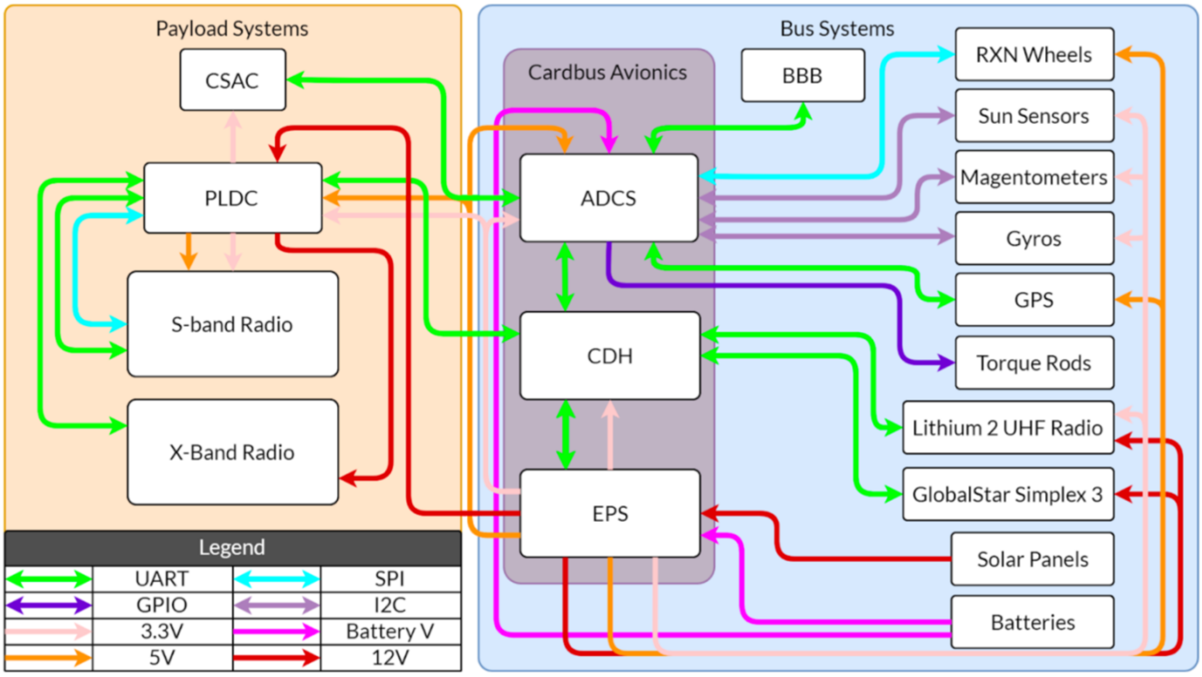

Figure 16. System Block Diagram of MAXWELL CubeSat [44]

The Phase 4 of the mission is the CSAC Experiment. The experiment is to be initiated by a command transmitted from the UHF ground station in Boulder. Upon confirmation, the CSAC is activated, warmed up, and subsequently linked with the Novatel OEM729 GPS unit for clock pulse comparison. The CSAC experiment typically entails a five-day period of data collection, during which the spacecraft maintains this mode. Since the CSAC experiment happens passively without the need for active control, the satellite goes in sun pointing mode to maximize power generation while TT&C is done via the UHF antenna for its health and status to be monitored. The CSAC experiment aims to assess the Allan deviation of the CSAC component while in orbit [44] .

3.7.3. CHOMPTT

CHOMPTT (CubeSat Handling of Multisystem Precision Time Transfer) was an in-orbit demonstration CubeSat mission that showcased ground-to-space time-transfer via a laser link. Led by the University of Florida, the project was a joint effort with NASA Ames Research Center. The CHOMPTT mission integrated the innovative 1U payload named OPTI (Optical Precision Time-transfer Instrument), created by the Precision Space Systems Laboratory (PSSL) at the University of Florida (UF), along with a 3U CubeSat bus designed by the NASA Ames Research Center (ARC). The CHOMPTT CubeSat was successfully launched into LEO on December 16, 2018, aboard NASA's ELaNa XIX mission, to a circular orbit of 500 km altitude with an inclination of 85º [45].

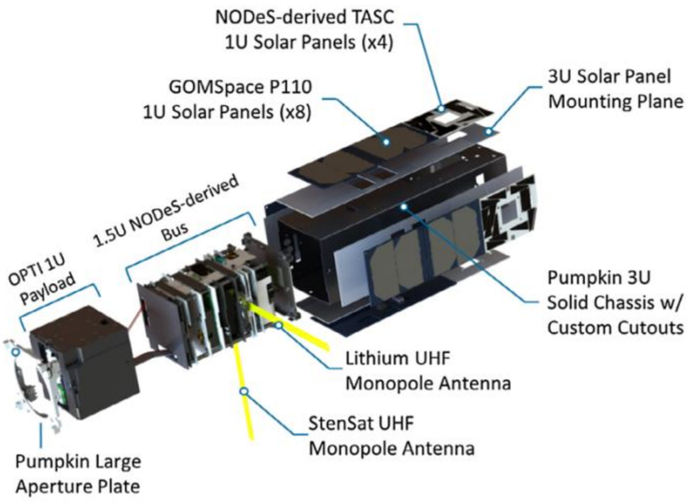

Figure 17. CHOMPTT 3U CubeSat [46]

3.7.3.1. OPTI payload

The Optical Precision Time-transfer Instrument (OPTI) is a compact device weighing 1 kilogram and occupying 1U of space. It encompasses all the essential components required for conducting optical time-transfer from ground to space. Its electronic components consist of two primary instrument channels labeled as A and B, along with a Supervisor and an optical beacon. Both instrument channels are identical, ensuring redundancy. Each channel includes one CSAC, an event timer, an avalanche photodetector (APD), a microcontroller, and the supporting electronics for each of these components.

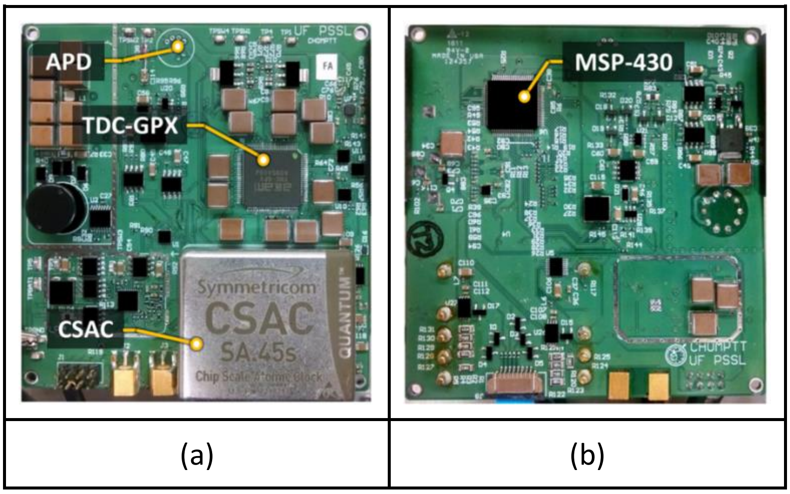

Figure 18. Top side of the OPTI channel board highlighting the CSAC, TDC-GPX event timer, and the InGaAs APD (a), Bottom side of the OPTI channel board, highlighting the MSP-430 microcontroller (b) [46]

The Supervisor functions as the payload controller and serves as the single electrical connection to the spacecraft bus. It employs a Texas Instruments MSP-430 microcontroller to manage commands and collect data from both channels. This data is stored in flash memory on the Supervisor electronics board until it's needed by the spacecraft bus. During periods when the instrument does not implement time-transfer operations, the microcontroller transitions it into a low-power 'clock counting mode'. In this mode, only one channel is operational, with that channel solely counting clock cycles for the local CSAC.

The Supervisor MSP-430 is the one controlling the electronics responsible for operating an optical beacon that assists in tracking the CubeSat by the SLR facility. The beacon electronics drive four VCSELs diode arrays, each with a power output of 0.5W. These arrays emit uncollimated light at a wavelength of 808nm with a collective divergence angle of 14 degrees (half-angle). While the current source for each laser array is integrated onto the Supervisor electronics board, the VCSEL arrays are fixed onto the nadir face of OPTI and linked to the Supervisor with a ribbon cable. Additionally, a single retroreflector array consisting of six hollow retroreflectors each with an effective diameter of 1cm is affixed to the nadir face of OPT [47]. The Supervisor, Channels A and B, the retroreflector array, and the optical beacon, are integrated into a custom Al 6061 structure.

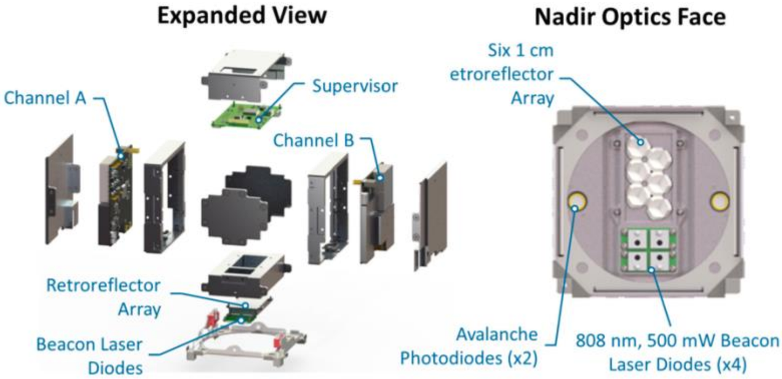

Figure 19. OPTI layout [46]

As mentioned above, the OPTI payload integrates two SA.45s CSACs produced by Microsemi Frequency & Time Corporation, with one clock allocated to each instrument channel. On the other hand, the SLR facility accommodates a rubidium-based SA.31m miniature atomic clock (MAC), also manufactured by Microsemi Frequency & Time Corp. The main output from the CSAC is a 10 MHz square wave, which is routed to the event timer, channel board microprocessor, and Supervisor via clock distribution electronics. Additionally, the CSAC furnishes temperature and other pertinent health and safety data to the Supervisor.

3.7.3.2. The time-transfer experiment

During operational flight, an experimental SLR facility situated at the Kennedy Space Center in Florida will emit 2.5 ns-long infrared laser light pulses at 1064 nm towards the CubeSat. These pulses bounce off a retroreflector array affixed to the nadir face of the satellite and return to the ground. The laser ranging facility then records the round-trip light-travel time of these pulses. Simultaneously, one of the APDs on the nanosatellite captures their arrival time. By merging these datasets, the disparity between the ground and space clocks can be determined, along with the satellite's range. Laboratory assessments of the payload reveal a short-term time-transfer precision of less than 200 picoseconds, translating to a range accuracy of 6 centimeters. During a single contact between the SLR facility and the satellite, approximately 5,000 such measurements will be conducted over a period of around 100 seconds to assess the time transfer precision across time intervals of this scale, and to determine the average frequency offset between the atomic clocks on the ground and the space segment. In this context, the recorded time by each clock is defined based on the count of clock oscillations since a specific epoch, which is established when the respective clock counters were turned on.

The utilization of an optical time-transfer scheme offers superior timing precision compared to radio frequencies due to the increased available bandwidth that allows for higher precision and accuracy, and the lowered level of uncertainty in the propagation delay when traversing through the ionosphere (an electromagnetic wave with frequency f experiences a delay proportional to $\frac{1}{f^2}$ relative to propagation in a vacuum) [47].

3.7.4. AIOTY-CUBE

AIOTY-CUBE is a 12U CubeSat made by Rapid Cubes and Technical University of Berlin that among other goals aims to host and validate the ATOMIC (Autonomous Time and Orbit Determination for Microsatellite Constellations) payload to enhance current GNSS with PNT signals from LEO [48]. At the same time, it depends on the existing GNSS for orbit determination and time synchronization (ODTS). The mission's objective is to demonstrate ODTS performance with less than 20 cm orbit error and with timing precision of 2 ns.

The platform is developed by Rapid Cubes GmbH and it is based on the RapidCube-20 CubeSat bus. The pointing requirement of the satellite is to have the GNSS antenna to continuously point at zenith, which translates to a pointing accuracy of <±5°. AIOTY-CUBE is scheduled for launch in 2024 aboard the second flight of ISAR Aerospace's Spectrum rocket [3].

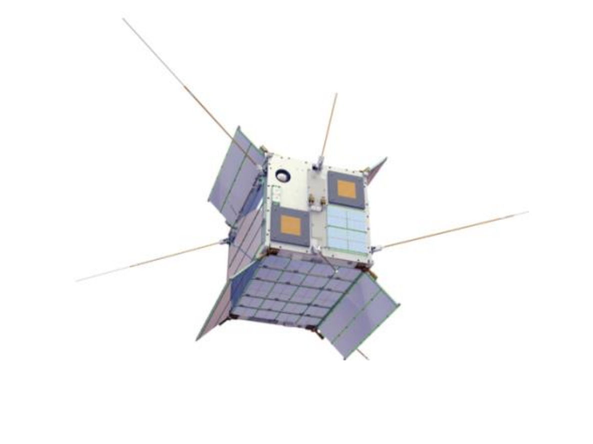

(a)

(b)

Figure 20. AIOTY-CUBE 12U CubeSat (a), ATOMIC payload flight model (b) [3]

Apart from its coupling with GNSS, the payload stays independent from external data sources to reduce dependency on both the satellite bus and ground segment. Its time and frequency synchronization with existing GNSS constellations guarantees compatibility and interoperability and, thus, there is no need for a dedicated ground segment. The hosted payload is built by COTS components and it encompasses a multi-frequency GNSS receiver, a CSAC, a navigation computer and a signal generator.

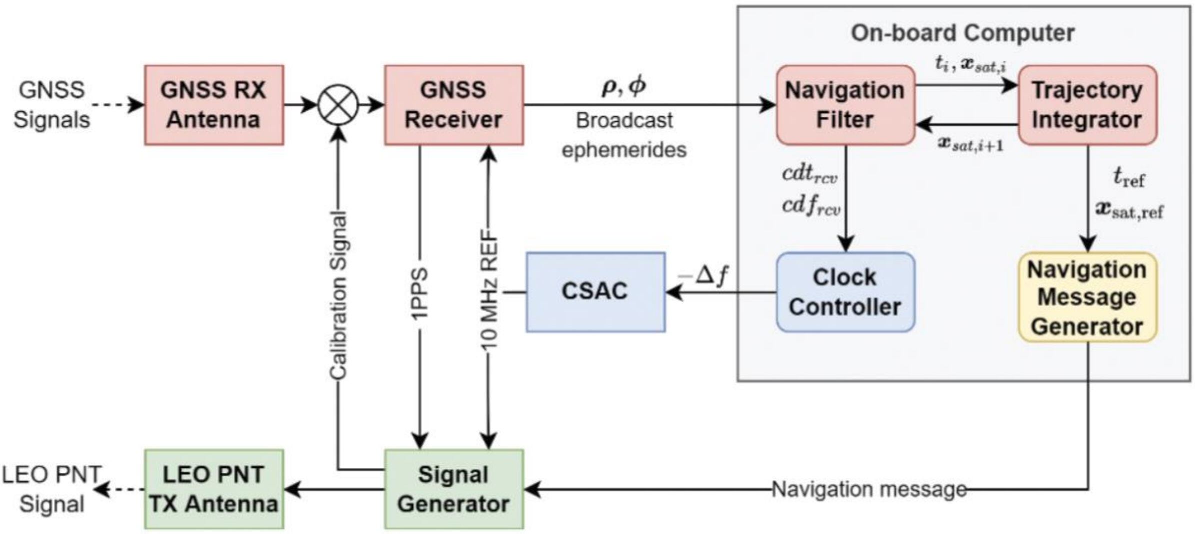

Figure 21. The subsystems of ATOMIC payload; orbit determination (red), time synchronization (blue), ephemeris generation (yellow) and signal generation (green) [3]

As illustrated in the figure above, by acquiring the GNSS signals and applying a real-time navigation filter, precise ODTS can be achieved. Then, the satellite's projected trajectory is utilized to generate its ephemeris. The CSAC that functions as an on-board time and frequency reference for both the GNSS receiver and signal generator has its phase and frequency continuously adjusted to match the GNSS time by using the on-board navigation solution. An internal calibration signal ensures absolute synchronization of the signal generator's phase with respect to GNSS. This enables the generation of GNSS-synchronized ranging and navigation signals, which can be utilized for navigation in conjunction with GNSS signals.

A primary focus in the payload design is low Surface, Weight, and Power (SWaP) characteristics, ensuring compatibility with small spacecraft and potential scalability for larger LEO constellations. The payload weighs less than 1 kg and has a maximum power consumption of 2.5 W. In line with the New Space approach, the payload hardware was chosen from COTS components that were integrated into a single PCB housed in an aluminum casing.

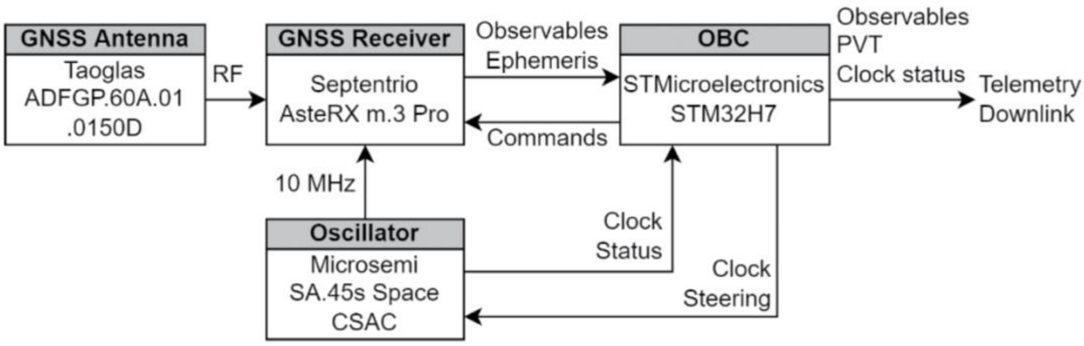

Figure 22. ATOMIC payload block diagram and data flow [3]

3.7.4.1. Time synchronization

The time synchronization is maintained by utilizing the on-board CSAC as a time and frequency reference. Unlike the extremely stable atomic clocks found on GNSS satellites, the Microsemi SA.45s employed in AIOTY-CUBE exhibits significantly lower stability, with an Allan deviation (ADEV) ranging from 10^{-10} to 10^{-11} for sample times between 1 to 1,000 seconds.

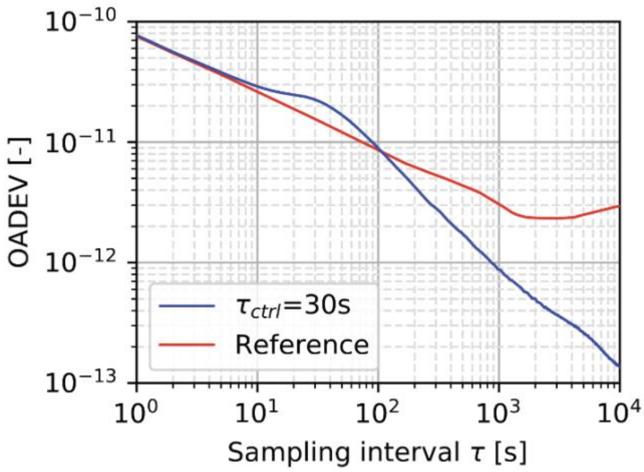

Figure 23. Allan Deviation for free-running (red) vs steered (blue) SA.45s CSAC [3]

In GNSS clock offsets can typically be predicted using second-order polynomials across validity intervals that extend to several hours. However, given that LEO satellite passes last less than 20 minutes for observers on Earth, the statistical uncertainty of the CSAC's timing error would surpass 10 nanoseconds (or 3 meters). As a result, polynomial clock predictions for the payload become impractical. To mitigate this statistical error, the clock state derived from the navigation filter is utilized to synchronize the CSAC's output frequency with the GNSS time scale through continuous clock steering. By employing the CSAC as the frequency reference for the GNSS receiver, the clock offset and drift calculated by the navigation filter match with the CSAC's phase deviation and fractional frequency offset concerning GNSS broadcast time. This approach compensates for the mid- to long-term instabilities of the CSAC caused by random walk frequency modulation (RWFM), while preserving the short-term stability of the CSAC.

With the synchronization of the CSAC's output frequency, the payload can produce signals aligned with GNSS at nanosecond level, enabling their use alongside existing GNSS signals. Precisely synchronizing the navigation payload with GNSS broadcast time effectively eliminates the need for a proprietary time scale within the LEO PNT system.

For the generated signals to be aligned with the GNSS time scale the pulse-per-second (PPS) signal generated by the on-board GNSS receiver is used. However, the precision of PPS is inadequate for synchronizing the payload at nanosecond level. Hence, another calibration signal is implemented that follows the coarse PPS alignment. This signal, generated by the signal generator and employing established GNSS modulations, is coupled with the GNSS receiver. By measuring the calibration signal and comparing it with data from actual GNSS satellites, the navigation filter can detect any systematic phase offsets in the on-board generated navigation signals, ensuring complete synchronicity with GNSS time at the required accuracy [3].

4. **PNT Payloads**

Space-based navigation systems utilize stable atomic clocks aboard satellites in well-defined orbits, emitting RF signals to Earth. These satellites establish a space-time reference frame, offering time and positioning information. A minimum of four satellite signals is necessary to accurately determine both position and time. Additional satellite signals enhance precision and aid in detecting discrepancies and potential issues within the data. For such systems, a Time epoch, defined with a specified reference frame that includes a location (e.g. center of Earth) and starting time (e.g. UTC), is necessary.

The philosophy behind this kind of systems is based upon integrating atomic frequency references (AFR) aboard satellites that maintain a consistent frequency output, which is utilized by other electronic components to generate signals for transmission to Earth. Code data and timestamps are implemented into the signals before their final transmission to the ground. However, noise, timing variability, and environmental influences that are beyond the AFRs, impact the overall performance of the system.

The clocks onboard must consistently deliver a precise and stable frequency along with a clearly defined Time epoch. Any inaccuracies or instability in the clock time, or unpredictable frequency drifts, will result in accumulating errors in the pseudorange solution. To illustrate, one could consider that GNSS systems demand such stable clocks that for instance, to achieve a 1-meter precision in measurements, a timing uncertainty of approximately 3 nanoseconds is required for signals traveling at the speed of light. Maintaining such timing uncertainty for a day necessitates a fractional frequency instability of approximately $3.5 \times 10^{-14} \left(= \ 3\frac{ns}{86000}\ s\right)$. This level of stability is attainable with high-quality atomic clocks, but not with other existing clock technologies or oscillators [2].

4.1. Atomic Clocks

An AFR comprises four fundamental subsystems: a local oscillator (LO) alongside a frequency synthesizer, a group of atoms exhibiting a high-Q transition between quantized energy levels, a totalizing counter that tracks time from a designated starting epoch and a feedback control system to regulate and stabilize the clock's frequency output.
The AFR operates by stabilizing the frequency of a frequency-tunable oscillator to match the quantum transition of the atoms. These atomic quantum states exist at discrete energy levels, with the difference between levels denoted as $\Delta E = h v_a$, where h represents Planck’s constant, and v_a provides a consistent frequency that acts as the clock's oscillation frequency. This is the mechanism that ensures the stability and accuracy of the atomic clock's timekeeping.

As seen in the figure below, an AFR is actualized by having a collection of atoms with high-Q transition, a system with the ability to excite them and measure their quantum state and a control system capable of tuning the frequency of the LO to the frequency that corresponds to the one of the atomic transitions. The Q factor delineates whether an oscillator is underdamped, overdamped, or critically damped. A higher Q value signifies that the oscillations decay relatively slow, indicating a lower rate of energy dissipation compared to the stored energy within the resonator. That way, the AFR produces a consistent and reliable frequency output referenced to the atomic transition. By utilizing an accumulating counter to track the number of oscillations since a predefined epoch, the clock can measure time intervals accurately and provide time information as an atomic clock [2].

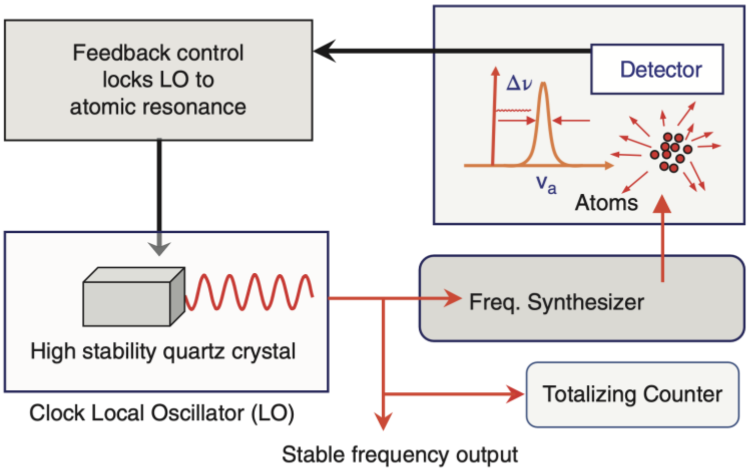

Figure 24. The basic components of an AFR and how it works [2]

The term "atomic clock" is commonly used to describe an AFR that offers a stable and potentially accurate output oscillation frequency. However, such devices typically do not provide time or have a time epoch reference, so they don't function as conventional clocks for timekeeping purposes. To qualify as an actual "atomic clock," the oscillator of the AFR must be connected to a totalizing counter that's synchronized with a universally agreed-upon starting epoch.

In the realm of AFRs, "stability" and "accuracy" carry specific meanings, serving as metrics to evaluate their performance. Accuracy in the context of atomic clocks refers to how precisely the frequency is known compared to the Cs hyperfine transition frequency, which defines the internationally accepted unit of time, the "second," at $9{,}192{,}631{,}770\ Hz$. Stability, on the other hand, measures the variation of the frequency of the atomic reference over time. It's typically expressed as a fractional frequency instability for a specified measurement time interval, an example of this could be that $\frac{\Delta f}{f} = 1 \times 10^{-12}\ at\ \tau = 1\ s$, indicating the degree of consistency in frequency output over a given duration.

The figure below illustrates varying frequency drifts and frequency offsets over time for different types of clocks and oscillators. In this context, f_{atom} portrays the preferred precise frequency of unperturbed atoms that the frequency reference aims to achieve. Cs beam clocks exhibit good frequency accuracy, closely matching f_{atom}, but they display small fluctuations around the mean value, resulting in less stability on shorter time scales compared to other examples. Hydrogen masers demonstrate good short-term stability, yet they may experience unpredictable small offsets in frequency from the intrinsic frequency of the hydrogen atom. Lastly, Quartz crystals exhibit excellent stability on extremely short timescales but suffer from frequency drift over time, making them unable to provide high accuracy over extended periods [2].

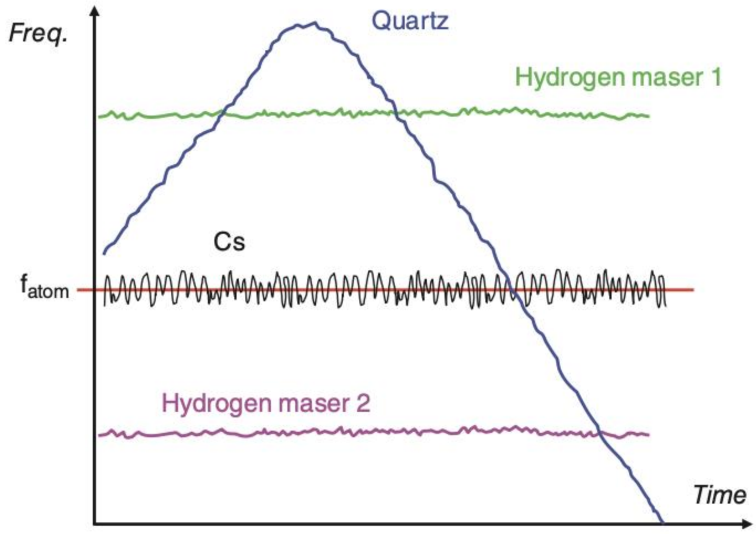

Figure 25. An overview showcasing how accuracy and stability are demonstrated in different types of atomic clocks [2]

The environmental sensitivities of AFRs are crucial specifications to consider, too. Variations in environmental conditions and other system parameters typically play a significant role in clock timing errors over extended periods. These factors encompass external temperature fluctuations, magnetic fields, pressure changes, accelerations, vibrations, and other phenomena. Predictable gradual drifts in AFRs, like aging effects or frequency shifts caused by environmental factors can generally be monitored by comparing with other atomic clocks. While these changes may not severely impact the overall performance of GNSS, they necessitate monitoring, correction and compensation by the control systems.

The environmental sensitivities of atomic clocks tend to have a strong influence on timing errors over time. Predictable gradual frequency drifts and fixed time offsets can be mitigated through independent measurements with other clocks.

4.2. Clock Performance

The most popular technique for assessing the stability of an AFR is the Allan variance $\sigma_y^2(\tau)$ or Allan Deviation $\sigma_y(\tau)$, where y denotes the fractional frequency and τ signifies the averaging time. This method is typically derived from a continuous stream of frequency (or phase) readings of the AFR under examination, in comparison to a known frequency reference assumed to be more stable. Each frequency reading $y_i(\tau)$ or phase reading is taken over a specified averaging period τ, and the Allan variance quantifies the difference between the average frequency across adjacent time intervals τ. A series of measurements, denoted as i, are conducted over a duration τ, followed by averaging the discrepancies between consecutive measurements.

$$\sigma_y^2(\tau) = \frac{1}{2\tau^2}\left\langle \left\{ \int_{t_i + \tau}^{t_i + 2\tau} y(t)dt - \int_{t_i}^{t_i + \tau} y(t)dt \right\} \right\rangle$$

This method effectively mitigates the influence of gradual, predictable shifts and offers valuable insights into the sources of noise, such as the white frequency noise of AFRs and the flicker frequency noise of quartz oscillators. In the case of an AFR, its short-term stability $(\tau < 1 \; to \; 10 \; s)$ is typically governed by the LO, and then it begins to enhance as $\frac{1}{\sqrt{\tau}}$ as the typically white frequency noise from the atoms averages out. Over longer time periods, AFRs have a "flicker floor" and stability does not improve with averaging. In GNSS systems, the short-term frequency instability of the AFR is not typically the primary constraint; instead, it's the multitude of factors affecting timing accuracy over extended durations. Environmental sensitivities of atomic clocks usually dominate timing errors over longer time scales [2].

4.3. Atomic Clocks in GNSS

Three types of AFRs are currently in use by GNSS: rubidium (Rb) vapor cells, cesium (Cs) atomic beams, and hydrogen (H) masers. As it was stated above, these clocks rely on quantum transitions occurring at microwave frequencies between hyperfine levels within the ground state of the atoms.

GNSS satellites are equipped with multiple atomic clocks, typically ranging from 3 to 4 units, to ensure backup redundancy and potentially enhance system capabilities and diagnostics. While at least one clock remains operational, the others are kept in standby mode, ready to step in to replace the active clock or conduct system checks. In the event of a malfunctioning or failed active clock on a satellite, it can be substituted with one of the backup clocks to maintain uninterrupted system operation. Despite some GNSS clocks experiencing failure due to the challenging conditions of space, their overall performance and robustness have been notably commendable, boasting an average lifespan of 15 years. The specific type and quantity of atomic clocks installed onboard the satellites vary depending on the GNSS system and its generation.

4.3.1. Master Clocks

The atomic clocks utilized in GNSS ground control systems demand higher performance compared to those deployed on satellites. These AFRs in ground control systems are responsible for generating precise time and frequency references, maintaining exceptional accuracy and stability. They serve as the primary master reference for the AFRs aboard satellites, ensuring the overall synchronization and coordination of the GNSS system [1].

An example of the types of AFRs used in GNSS ground systems is the ground control system of the GPS. The system's "Master Clock" is operated by the US Naval Observatory (USNO) in Washington D.C. It is composed of an extensive array of high-performance AFRs that includes around a dozen H-masers, fifty cesium atomic beam AFRs, and four cold-atom rubidium (Rb) atomic fountain clocks developed at USNO [1]. These AFRs operate concurrently, with their outputs carefully monitored and averaged to produce an ensemble AFR and "GPS Time Scale" that surpasses the stability and accuracy of any individual clock, ensuring robust and highly reliable timekeeping [5]. Additionally, the USNO and Air Force have set up a slightly smaller set of AFRs serving as the "Alternative Master Clock" at Schriever Air Force Base in Colorado, co-located with the GPS master control center.

The ground control systems utilize master clocks along with supplementary data from international time scales to assess and confirm the frequencies of GNSS space clocks. Accounting for frequency fluctuations and drifts in the space clocks, the ground control system can adjust time offsets or modify frequencies of the space segment as necessary to enhance the overall performance of the system [2].

4.4. Chip Scale Atomic Clocks

Over the past decades, research and development efforts have focused on miniaturizing atomic clocks for commercial use, led by DARPA, which recognized the potential for small, battery-powered versions suitable for military applications. Starting in 2000, DARPA funded a program that resulted in the development of the Miniature Atomic Clock (MAC) in 2008 and the Chip-Scale Atomic Clock (CSAC) in 2011, aimed at enhancing secure GPS signal acquisition. This program's success, driven by collaboration among universities, industry, and government labs, culminated in the commercialization of CSACs by a team at Symmetricom (now Microsemi-Microchip Inc.). Today's CSAC take less volume than $17cm^3$ while weighting about $35\ g$. Moreover, they tend to have extremely low power consumption ($< 120\ mW$) and they can function across a broad temperature spectrum ranging from $-40\ to\ 85$ degrees Celsius.

The conceptual groundwork for CSACs originated from research on laser technology and fiber-optic networks. Two key technological breakthroughs facilitated the downsizing of the atomic clock: (i) the development of low-power semiconductor VCSELs (Vertical Cavity Surface Emitting Lasers) capable of emitting wavelengths suitable for optical pumping of Cs (852 nm or 895 nm) and Rb (780 nm or 795 nm) at power levels below $5\ mW$; and (ii) the advances in semiconductor MEMS (Micro-Electro-Mechanical Systems) techniques that made it possible to manufacture high-quality miniature atomic vapor cells [2].

CSACs can work with either Rb or Cs. It involves a miniature VCSEL that is precisely adjusted to the atomic resonance transition. The injection current of the VCSEL is modulated by a microwave source to generate sidebands, resulting in two optical output frequencies aligning with the atomic resonance lines of Cs (or Rb). The frequency difference between those corresponds to the ground-state "clock" transition frequency (approximately $9.2\ GHz$ for Cs and $6.8\ GHz$ for 87Rb). When this frequency difference aligns with the clock transition, the atoms are "optically pumped" into a non-absorbing "dark state" via the CPT (Coherent Population Trapping) mechanism and, thus, intense laser light passes through the miniature vapor cell [1]. The basis of a CSAC is the CPT, which occurs when a fraction of the alkali atoms become trapped in a coherent superposition between two ground states and cannot get excited out by a photon [49]. Conversely, if the frequency difference (controlled by the modulation frequency applied to the laser) does not match the clock transition frequency, less laser light is transmitted through the vapor cell. Therefore, the atomic clock (serving as a frequency reference) is established by adjusting the microwave modulation frequency to achieve peak DC optical transmission through the vapor cell.

As it is shown in the figure below, by using a microwave source at $4.6\ GHz$ the VCSEL can be modulated to produce sidebands on the laser carrier frequency. That way, the frequency difference is set to match the one of the Cs clock transition frequency ($9.2\ GHz = 2 \times 4.6\ GHz$) in the $6S_{\frac{1}{2}}$ ground state. Afterwards, the laser travels through the Cs vapor cell that includes a buffer gas, and the laser power is measured by a photodiode and amplifier [1]. In this case, apart from the Cs, a buffer gas comprised of various gasses is employed. The composition, temperature, and pressure of these gasses are determined through several balancing processes. The goal is to optimize the characteristics of the atomic transitions crucial to the clock's operation, while also minimizing their dependence on pump light and environmental fluctuations [49].

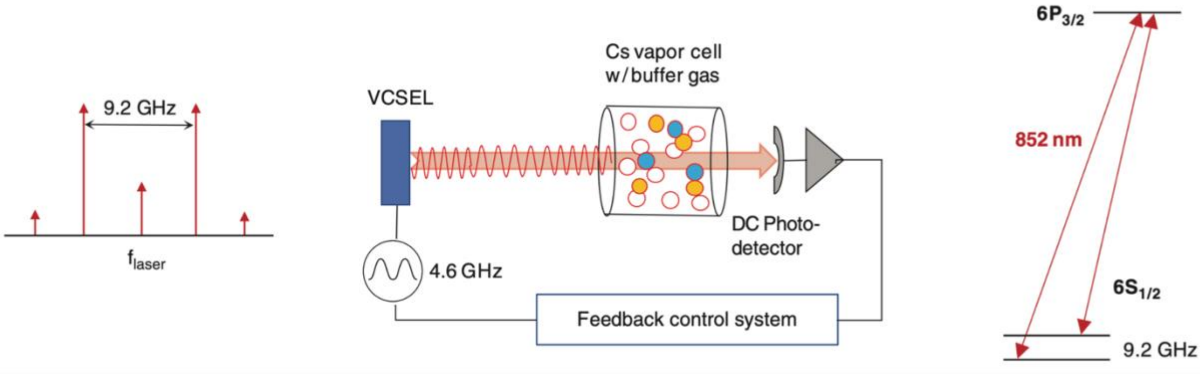

Figure 26. Basic illustration of the workings of a Cs based CSAC [2]

4.5. CubeSat-based PNT Payloads

To comply with the CubeSat specifications, a PNT payload designed for such a platform must adhere to strict constraints regarding mass, power consumption, and volume. Thus, by utilizing COTS components already employed in CubeSats as building blocks, it is possible to develop a PNT payload that meets these constraints. However, given that CSACs are not yet widely adopted in the CubeSat market, a custom PCB could be designed to integrate a CSAC and interface it with other components. Finally, in line with the New Space approach, the objective is for a CubeSat-based PNT system to function independently of the extensive ground segment required by MEO GNSS systems. This can be achieved by utilizing GNSS observables for precise orbit determination (POD) and synchronizing the CubeSat's time reference with GNSS time, thereby eliminating the need for master clocks.

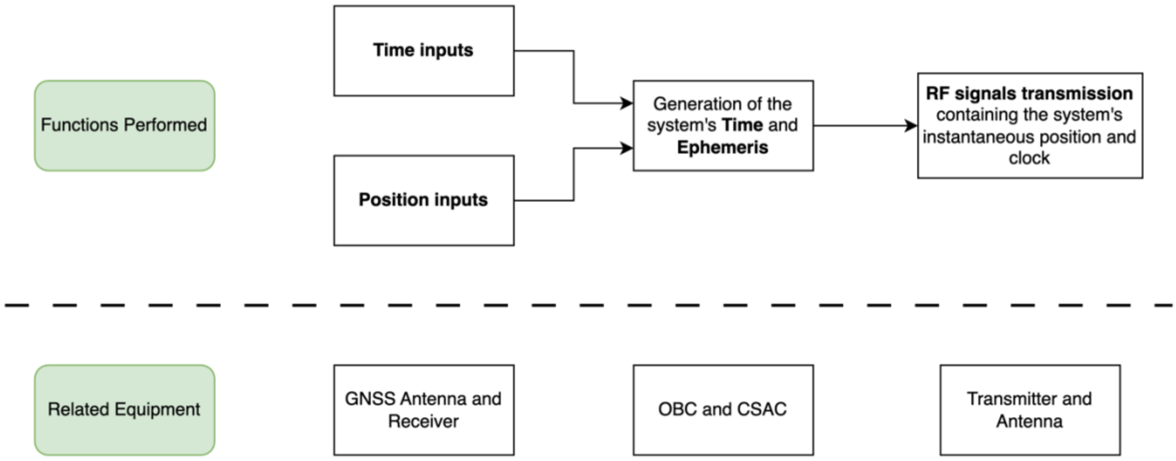

Figure 27. Architecture of a CubeSat-Based PNT Payload in line with New Space approach

A payload of this kind is the ATOMIC that is housed in AIOTY-CUBE, while other space actors have stepped into this domain with Syrlinks having developed a GNSS SDR payload named N-CUBE. The N-CUBE combines a GNSS receiver, a GNSS signal processor, and an RF output stage to enable real-time Precise Onboard Orbit Determination (< 30 cm of accuracy) and time synchronization, supporting multiple GNSS constellations. N-CUBE incorporates two parallel GNSS transmitters, equipped with RF amplifiers, operating in L-Band and S-Band. This design allows for the retransmission of GNSS signals, enabling LEO PNT applications [50].

Figure 28. N-CUBE GNSS SDR payload [50]

5. Mission Statement

The purpose of the mission is to design a LEO CubeSat Constellation that has the capability of providing persistent PNT signals in specific areas of interest, with the size of a country, around the globe. This shall be done by the CubeSats relying on MEO GNSS for orbit determination and time synchronization (ODTS). Time and frequency synchronization to existing GNSS constellations ensures compatibility and interoperability. No dedicated ground segment is needed for timekeeping, while the requirements for space infrastructure are kept at a minimum. The mission shall be based on heritage from the ERMIS mission and, thus, the two missions shall have a similar BUS as long as analysis concludes this as an acceptable and optimal solution.

Following a low cost approach and the New Space philosophy, a PNT payload shall be housed onboard consisting at minimum of a multi-frequency GNSS receiver along with an antenna, a chip-scale atomic clock (CSAC), a navigation computer, a transmitter and an additional antenna to transmit the PNT signals. That way, the GNSS data is processed through a real-time navigation filter to achieve accurate ODTS. The satellite's predicted trajectory is used to create its ephemeris. The CSAC plays a critical role as the onboard time and frequency reference. Its phase and frequency are consistently adjusted to align with the GNSS broadcast time, using the onboard system. A calibration signal ensures that the signal generator's phase is fully synchronized with GNSS. This enables the generation of GNSS-synchronized navigation and ranging signals, which can be used alongside GNSS signals for single point positioning (SPP). This kind of system can provide services to an unlimited number of users. Additionally, Satellite Laser Ranging (SLR) shall be used to confirm the satellite's orbit when it passes over an SLR capable GS.

Furthermore, COTS components with publicly available datasheets that contain the necessary information for the system design shall be preferred. This shall be the primary drive of the system's performance and, thus, the system shall be a realistic one by following market trends in the LEO PNT domain. Regarding the PNT payload, limited information is publicly available without an NDA and due to that, in the current analysis it shall be considered as a "black box" and its mass, dimensions, power consumption, thermal emissions, connection interfaces are to be educated guesses based on relevant research when needed to.

The missions's Ground Segment shall consist of UOA's Ground Station, along with other Ground Stations that are available as a service. KSAT's network should be prioritized due to their involvement with the ERMIS mission. The CubeSat constellation shall be deployed through multiple launches, requiring consideration of a range of different launch providers. The number of CubeSats in the constellation shall be kept in a reasonable number. According to the literature survey done on LEO PNT systems, LEO PNT satellite constellations comprise of a few hundreds satellites. The fact that the mission at hand constrains the area of interest to one with the size of a country the maximum number of satellites shall be 200.

Each spacecraft shall undergo LEOP, a Commissioning phase, and a Payload validation phase before starting its Nominal operations phase. Each satellite shall have an operational lifetime of at least 3 years. After the end of the mission, the spacecrafts shall be deorbited according to the relevant regulations and laws in place.

As stated above, the system is aimed to provide persistent PNT services to specific areas/countries. This design allows for service in multiple areas in similar latitudes, while minimizing the payload duty factor. In this thesis the main focus is the European region and, thus, the area is selected to be Germany since it is a Central European country of substantial area, where many major metropolitan districts are located.

Overall, such a satellite system would enhance current PNT services over Germany by implementing strong signals from LEO and new geometries that are not achievable by MEO GNSS. This would enhance applications like drone mobility, autonomous driving, precision agriculture, and emergency response.

Table 4. System design standards

Satellite type	Number of satellites	Type of components	Service area form factor	Service area location	Payload functions	Mission duration
CubeSat	< 200	COTS	size of a country	Central Europe	PNT signal generation and transmittion, SLR	3 years

6. **Requirements**

In order to proceed with the system design, the mission and system requirements had to be identified. In this section the requirements that seemed fit with the scope and the depth of this thesis are presented. Any requirements that are considered to be beyond that were not taken into consideration.

Table 5. Mission Requirements

ID	Requirement	Justification	Parent	Verification Methods
MR-MIS-010	The CubeSat constellation shall provide PNT signals in specific areas of interest, with the size of a country, around the globe.	Specified in the Mission Statement	Mission Statement	A
MR-MIS-020	Spacecrafts shall implement the hosted payload approach, relying on MEO GNSS for ODTS	Specified in the Mission Statement	Mission Statement	A
MR-MIS-030	No dedicated ground segment shall be needed to support the PNT payload.	Specified in the Mission Statement	Mission Statement	A
MR-MIS-040	The spacecrafts shall support SLR capabilities.	Specified in the Mission Statement	Mission Statement	I, A, T
MR-MIS-050	Provide services to an unlimited number of users.	Specified in the Mission Statement	Mission Statement	A
MR-MIS-060	Spacecrafts shall de-orbit within 5 years of the end of mission following the requirement imposed by the baseline launch provider.	Exolaunch requires all cubesats launched to follow the new FCC 5-year deorbit regulation effective for launches after 29 September. 2024, regardless of the origin of their on-orbit license.	Mitigation of Orbital Debris Regulation	A
MR-MIS-070	In the context of the thesis, industry grade Software Tools like STK, GMAT, Inventor etc shall be used.	Specified in the Mission Statement	Mission Statement	R
MR-MIS-080	The spacecrafts shall be able to remain operational for the full 3 year mission duration.	Specified in the Mission Statement	Mission Statement	R, A
MR-MIS-090	The system shall provide persistent PNT services to Germany.	Specified in the Mission Statement	Mission Statement	A
[redacted]				
MR-CON-010	The constellation shall be in LEO	Specified in the Mission Statement	Mission Statement	R
MR-CON-020	The constellation's geometry shall be a more complex one than the ones of MEO GNSS.	Specified in the Mission Statement	Mission Statement	A
[redacted]				

MR-BUS-010	The BUS design shall be based on heritage from the ERMIS mission.	Specified in the Mission Statement	Mission Statement	R
MR-BUS-020	The system design shall be based on COTS components, prioritizing the ones with available and complete datasheets.	Specified in the Mission Statement	Mission Statement	R, A
MR-BUS-030	The system design shall implement a low cost approach.	Specified in the Mission Statement	Mission Statement	R
MR-BUS-040	The BUS shall be able to support all aspects of the mission.	Necessary for the success of the mission.	MR-MIS-010	A
MR-PLD-010	The PNT payload housed onboard shall consist at minimum of a multi-frequency GNSS receiver along with an antenna, a CSAC, a navigation computer, a transmitter and an additional antenna to transmit the PNT signals.	Specified in the Mission Statement	Mission Statement	R
MR-PLD-020	The transmitted PNT signals shall be of similar or higher strength, at ground level, than those of MEO GNSS.	Specified in the Mission Statement	Mission Statement	A
MR-PLD-030	Spacecrafts shall generate PNT signals autonomously when needed to.	Specified in the Mission Statement	Mission Statement	R
MR-LCH-010	Spacecrafts should be launched via SpaceX's Falcon 9, Rocket Lab's Electron, or Arianegroup's Vega-C.	Specified in the Mission Statement that multiple launchers should be considered.	Mission Statement	R
MR-LCH-020	The launch broker is baselined to be Exolaunch.	Exolaunch provides launch broker services for European actors launching with SpaceX, and is involved with ERMIS mission.	MR-LCH-010	R
MR-GRS-010	The Ground Segment used shall include UOA's GCS at Psachna, Greece.	Specified in the Mission Statement	Mission Statement	R
MR-GRS-011	The Space segment shall be compatible with UOA's GCS at Psachna, Greece.	It is a condition that has to be met to ensure coherent operation of the system.	MR-GRS-010	A
MR-GRS-020	GS as a service options should be considered.	Specified in the Mission Statement	Mission Statement	R
MR-GRS-030	KSAT's GS services should be prioritized.	Specified in the Mission Statement	Mission Statement, MR-GRS-020	R
MR-GRS-031	KSAT's GCS at Nemea, Greece	It is a GCS of KSAT's network at the	MR-GRS-030	R

	should be considered.	Greek region, and thus, it is a preferable option.		

Table 6. System Requirements

ID	Requirement	Justification	Parent	Verification Methods
SR-MIS-010	The system shall be able to provide continuously 4-fold coverage to Germany.	Quadruple spacecraft access coverage is necessary for PNT services of this kind.	MR-MIS-090	A
SR-MIS-020	The system's service availability should be over 97%.	The desired service availability value is set to be 97% due to the maturity of the technology.	MR-MIS-010	A, T
[redacted]				
SR-CON-010	The constellation shall consist of less than 200 spacecrafts.	Specified in the Mission Statement	Mission Statement	R
SR-CON-020	The constellation's configuration should aim for a GDOP less than 6.	GDOP quantifies how the satellite geometry affects positioning accuracy, with lower GDOP values indicating better accuracy and less error. A value of 6 is considered acceptable taking into account that COTS are to be used.	MR-MIS-010	A
SR-CON-030	The constellation's orbit shall conform with the components' radiation exposure ratings. TID shall be less than any component's minimum TID rating.	In order for the spacecrafts to be operational during the whole mission they need to be able to withstand the radiation environment of their orbit.	MR-MIS-080	A
SR-CON-040	The constellation should consist of 10 or less orbital planes.	Assuming that satellites in different orbital planes correspond to different launches and following the New Space low cost approach, the number of launches shall be kept under a minimum.	Mission Statement	R, A
SR-CON-050	The spacecrafts' altitude shall conform with the service's received power requirements at ground level.	Higher altitudes correspond to lower received power levels at ground level.	MR-PLD-021, MR-PLD-0211	A
[redacted]				
SR-BUS-010	PPS signal shall be distributed to all relevant components.	The provision of a 1 PPS clock reference signal from the platform GNSS receiver is crucial for precise synchronization and coordination of satellite operations and payload functions, ensuring optimal mission performance.	MR-MIS-010	A, T
SR-BUS-020	No spacecraft deployable items or other components shall obscure the payload	This restriction ensures unobstructed communication for the payload antennas, preventing interference and ensuring the effectiveness of the	MR-MIS-010	R

	antennas by extending above the antenna surface.	spacecraft's communication systems.		
SR-BUS-030	Spacecrafts shall be equipped with LRAs	LRAs shall be used in order for the SLR laser to be reflected.	MR-MIS-040	R
SR-EPS-010	The system power shall be generated by solar cells.	The requirement for power generation by a solar panel array, coupled with battery charging, is vital to ensure uninterrupted power availability for the CubeSat throughout its mission, especially during orbital eclipses.	CubeSat Design Specification Rev. 14.1 [51]	A, T
SR-EPS-020	The system shall be power positive during nominal operations	This is necessary to ensure the system's robustness.	SR-EPS-010	A
SR-EPS-030	The satellite shall be power positive while detumbling.	During detumbling the DSPs have not been deployed yet. By being power positive during this phase the system's robustness is increased.	SR-EPS-010	A
SR-EPS-040	The battery discharge rate should be under 5% per month when in storage.	The battery charging will be performed before inserting the spacecrafts into the launcher. Each battery discharges with a rate indicated by the manufacturer. The final power of the battery after storing must be adequate to support the satellite in the detumbling mode before the solar panels are fully deployed.	SR-EPS-030	A, T
SR-EPS-050	The EPS should be able to trickle charge	Trickle charging is a method of charging a rechargeable battery at a very low and constant rate, typically at a rate that is significantly lower than the battery's capacity. The purpose of trickle charging is to be able to charge the spacecraft in case of anomalies.	SR-EPS-010	A
SR-EPS-060	The EPS shall be able to provide current in excess of the maximum current of each subsystem it supplies	The requirement for the EPS to provide current in excess of each subsystem's maximum is essential to ensure system reliability and accommodate unpredictable power demands.	SR-EPS-010, MR-MIS-010	A
SR-EPS-070	The solar panels shall be deployed automatically after detumbling.	The solar panels shall be deployed after detumbling to power the CubeSat system and start the battery charging.	SR-EPS-010, MR-MIS-010	A, T
SR-ACS-010	The spacecrafts shall achieve attitude control accuracy to support the mission.	Attitude control is needed of a mission of this complexity.	Mission Statement, MR-MIS-010	A
SR-ACS-020	The spacecrafts' ADCS shall support nominal operations.	The spacecrafts shall achieve attitude control accuracy to support S-Band links with the GS, PNT payload operation and SLR.	SR-ACS-010	A, T
SR-ACS-030	The ADCS shall be able to reference roll, pitch, yaw for 3 axis control.	It is necessary to support spacecraft operations.	SR-ACS-010, SR-ACS-020	R, T
SR-ACS-040	The ADCS shall be able to detumble the spacecraft.	It is necessary to support spacecraft operations.	SR-ACS-010	A
SR-ACS-050	The ADCS shall be able to	It is necessary to support spacecraft operations.	SR-ACS-010,	A

	perform sun pointing.		SR-ACS-020	
SR-ACS-060	The ADCS shall be able to perform nadir pointing.	It is necessary to support spacecraft operations.	SR-ACS-010, SR-ACS-020	A
SR-ACS-070	The ADCS shall be able to perform ground target tracking.	It is necessary to support spacecraft operations.	SR-ACS-010, SR-ACS-020	A
SR-ACS-080	The pointing accuracy shall be of less than 5 degree.	A preliminary analysis concluded that Payload and S-Band TTC antennas are to have HPBW above 30 deg and, thus, this amount of accuracy is considered sufficient. Additionally, this agrees with a similar analysis from the ERMIS mission. Finally, this accuracy deems sufficient for SLR according to a relevant study, while it is also the one mentioned in the case of AIOTY-CUBE [3], [52].	SR-ACS-010	A
SR-ACS-090	The ADCS sensor drift shall be able to be measured and calibrated.	The requirement to measure and calibrate ADCS sensor displacement is driven by the mission's need for accurate attitude control, data accuracy, operational efficiency and long-term reliability.	SR-ACS-010	A, T
SR-ACS-100	The ADCS should detumble the satellite within 4 orbits.	The goal of detumbling the satellite within 4 orbits is to minimize the time it spends in an uncontrolled state, reducing the risk of collisions and ensuring a faster transition to operational status.	SR-ACS-010	A
SR-ACS-110	The ADCS shall include 4 reaction wheels in pyramid configuration.	RWs in pyramid configuration are popular in CubeSats, while this is also considered heritage from the ERMIS mission.	MR-BUS-010	R
SR-CDH-010	The CDHS shall monitor the health status and functionality of all subsystems.	The regular health status checks ensure proactive monitoring and rapid response to any subsystem issues, thus increasing robustness.	MR-MIS-010	A, T
SR-CDH-020	The CDHS shall handle TM&TCs.	It is necessary to support the mission.	MR-MIS-010	A, T
SR-CDH-030	The CDHS shall control the spacecraft's operation modes.	It is necessary to support the mission.	MR-MIS-010	A, T
SR-CDH-040	The CDHS shall initiate and monitor all payload actions through a CAN bus or I2C interface. A second interface should be used for redundancy.	CAN bus and I2C are popular protocols in the COTS market.	SR-CDH-010, SR-CDH-020	A, T
SR-CDH-050	The CDHS shall derive the S-band and UHF telemetry data to be transmitted to the GCS.	It is necessary to support the mission.	SR-CDH-020	A, T
SR-CDH-060	Apart from housekeeping, the CDHS shall execute TC in specific times predetermined by the	It is necessary to support the mission.	SR-CDH-020	A, T

	satellite operators.			
SR-CDH-070	The CDHS shall monitor the spacecraft’s battery levels.	By monitoring the battery levels it is possible to avoid mission critical situations.	SR-CDH-010	A, T
SR-CDH-080	The CDHS shall save the log files in its local storage.	By doing this, the system is robust against multiple GCS pass misses. Also, this supports FDIR processes.	SR-CDH-010	A, T
SR-CDH-081	The CDHS shall log the telemetry of the last 36 hours.	By doing this, the system is robust against multiple GCS pass misses. Also, this supports FDIR processes.	SR-CDH-080	A, T
SR-CDH-082	The CDHS shall log all received TCs in the last 36 hours.	By doing this, the system is robust against multiple GCS pass misses. Also, this supports FDIR processes.	SR-CDH-080	A, T
SR-CDH-090	The software shall be robust to power failure or interruption of any kind.	It is necessary to support the mission.	MR-MIS-010	A, T
SR-CDH-100	The CDHS shall be recovered from the back-up image after corruption or TC.	It increases the system's robustness.	SR-CDH-090	T
SR-CDH-110	Default CDHS image shall be stored in non-volatile read-only protected memory.	It increases the system's robustness.	SR-CDH-090	T
SR-CDH-120	The CDHS shall have the capability to update its firmware in-orbit, using an image uploaded from the Ground Control Station.	It increases the system's robustness.	SR-CDH-090	T
SR-CDH-130	The CDHS shall sync the CDHS clock with the GS	It is necessary to support the mission.	MR-MIS-010	T
SR-CDH-140	The CDHS shall provide memory dump functionality for debugging purposes.	It increases the system's robustness.	SR-CDH-090	T
SR-CDH-150	The CDHS shall ensure operation of the spacecraft and subsystems within thermal limits.	It is necessary to support the mission.	MR-MIS-010	T
[redacted]				
SR-TTC-010	The data rate for UHF TTC uplink and downlink shall be at least 9.6 kbps.	Based on preliminary analysis, this data rate is shown to ensure that the minimum amount of necessary data are transmitted during a pass over a GCS.	MR-BUS-010	R, A, T
SR-TTC-020	The data rate for S-band TTC uplink and downlink shall be at least 512 kbps.	Based on preliminary analysis, this data rate is shown to ensure that the optimal amount of data are transmitted during a pass over a GCS.	MR-BUS-010	R, A, T
SR-TTC-030	The spacecraft’s UHF antenna shall be deployable	Deployable UHF antennas are proven in the CubeSat industry. This is considered heritage from ERMIS mission.	MR-BUS-010	R, T
SR-TTC-040	Spacecrafts shall have a directive patch antenna to enable the communication	S-Band patch antennas are proven in the CubeSat industry. This is considered heritage from the ERMIS mission.	MR-BUS-010	R, T

	link in S-band.			
SR-TTC-050	The UHF channel shall be used as a backup TTC channel and for LEOPs only.	Redundant communications links in case the S-Band comms fail and for Safe Mode.	MR-BUS-010,MR-BUS-040	T
[redacted]				
SR-PRO-010	The propulsion subsystem shall be able to phase the satellites in each orbital plane according to the constellation configuration.	Spacecrafts of the same orbital plane shall be launched in a single launch. Afterwards, they shall acquire their slot via their propulsion subsystem.	MR-CON-010, MR-CON-020	A
SR-PRO-020	Propulsive maneuvers shall be delayed at least seven days after separation from launcher.	Stated in Falcon User's Guide.	Falcon User's Guide [53]	R
[redacted]				
SR-PLD-010	The PNT payload shall include an S-Band patch antenna.	This agrees with CubeSat market trends, while minimizing deployable components along with the relevant risks.	MR-PLD-50	R
SR-PLD-021	The minimum received power at ground level shall be higher than -159 dBW	Based on the fact that the Minimum Received Power of the Galileo signals is -157 dBW, signals with -159 dBW at ground level are acceptable.	MR-PLD-010, Galileo OS SIS ICD [54]	A
SR-PLD-0211	The minimum received power at ground level should be close to or higher than -157 dBW.	Stronger signals than MEO GNSS at ground level add to the service’s value.	MR-PLD-021	A
SR-PLD-030	In the case of no datasheet availability of a PNT payload, the payload shall be assumed to be a Black Box with properties and architecture similar to those of another LEO PNT CubeSat	Specified in the Mission Statement	Mission Statement	R
MR-PLD-031	In case of no available datasheets, the PNT payload should be considered as one with similar properties to the ones of AIOTY-CUBE’s ATOMIC payload.	AIOTY-CUBE is a LEO PNT CubeSat with plenty of publicly available information.	MR-PLD-030	R
MR-PLD-040	The PNT signals shall be transmitted in S-Band	Based on the COTS market analysis and publicly available information, transmission of PNT signals in S-Band is an acceptable solution.	Mission Statement, MR-MIS-010	R
[redacted]				
SR-LCH-010	The spacecrafts shall comply with the fleet Acceptance / Protoflight Random Vibration as defined by the launch provider document.	For CubeSats launching through Falcon 9, Exolaunch requires the Random Vibration test to be completed. The same applies for different launch providers.	EXOpod User Manual [55]	A, T

SR-LCH-020	The isolation circuit shall be able to maintain the spacecrafts powered-off during the launch	The isolation circuit shall be able to maintain the spacecraft powered-off during the dynamic event and show that the boot counter of the EPS/CDHS does not increase during test.	EXOpod User Manual	T
SR-LCH-030	The Spacecrafts shall accommodate ascent venting.	The inclusion of ascent venting in the CubeSat design is essential to ensure proper pressure regulation during launch, preventing potential structural and electronic damage.	CubeSat Design Specification Rev. 14.1	R
SR-LCH-040	The spacecraft thermal design shall keep all units within their operational and non-operational temperature limits during all phases of the mission.	This action ensures the spacecraft’s survivability in the thermal environment that derives from its orbit and operation.	EXOpod User Manual	A, T
SR-LCH-050	The spacecrafts shall be designed to withstand the mechanical environment during launch.	This is done to ensure that the spacecraft shall be healthy when deployed. It is specified in the Launch Provider Manual.	Falcon User's Guide, Electron Payload User’s Guide, SSMS Vega-C User’s Manual	A, T
SR-LCH-060	The spacecrafts shall comply with the sine vibration loads defined in table "Maximum Predicted Sinusoidal Vibration Environment"	Specified in the Launch Provider Manual.	Falcon User's Guide, Electron Payload User’s Guide, SSMS Vega-C User’s Manual	A, T
SR-LCH-070	The spacecrafts shall comply with the acoustic environment during launch defined in table "Full Octave acoustic MPE" and figure "Maximum projected acoustic environment".	Specified in the Launch Provider Manual.	Falcon User's Guide, Electron Payload User’s Guide, SSMS Vega-C User’s Manual	A, T
SR-LCH-080	The spacecrafts shall comply with shock environments experienced during flight defined in table "Payload Mechanical Interface Shock " and figure "Payload Mechanical Interface Shock".	Specified in the Launch Provider Manual.	Falcon User's Guide, Electron Payload User’s Guide, SSMS Vega-C User’s Manual	A, T
SR-LCH-090	Each CubeSat shall have a maximum mass of 16 kg according to launch providers manual.	Specified in the Launch Provider Manual.	EXOpod User Manual	I, A, T
SR-LCH-100	CubeSats shall have, at a minimum, one deployment switch, which is actuated while integrated in the dispenser.	The inclusion of a deployment switch in the CubeSats, actuated within the dispenser, ensures a controlled and timely release, enhancing mission reliability and safety.	CubeSat Design Specification Rev. 14.1	I, T
SR-LCH-110	In the actuated state, the CubeSat deployment switch shall electrically disconnect the power system from the powered functions.	In the actuated state, disconnecting power from CubeSat's systems enhances safety by preventing accidental activations and conserving energy during non-operational periods.	CubeSat Design Specification Rev. 14.1	T

SR-LCH-120	The deployment switch shall be in the actuated state at all times while integrated in the dispenser. In the actuated state, the CubeSats deployment switch should be at or below the level of any external surface that interfaces with the dispenser or neighboring CubeSat.	This ensures that the switch will not damage or interfere with the contacting surface.	CubeSat Design Specification Rev. 14.1	T
SR-LCH-130	If the CubeSat deployment switch toggles from the actuated state and back, the satellite shall reset to a pre-launch state, including reset of transmission and deployable timers	If the CubeSat deployment switch toggles inadvertently, resetting the satellite to its pre-launch state ensures operational integrity by preventing unintended deployments and timing errors.	CubeSat Design Specification Rev. 14.1	T
SR-LCH-140	CubeSats shall include an RBF pin, which cuts all power to the satellite once inserted.	This is done to ensure that the spacecrafts are powered off when it is needed to.	CubeSat Design Specification Rev. 14.1	I
SR-LCH-150	The RBF pin shall be removed from the CubeSat before integration into the dispenser, if the dispenser does not have access ports, or after integration if there are ports.	To ensure that the battery discharge is minimal while in storage and that the spacecraft is operational after deployment.	CubeSat Design Specification Rev. 14.1	I
SR-LCH-160	The RBF pin shall protrude no more than 6.5 mm from the CubeSat rail surface when it is fully inserted into the satellite.	The RBF pin's limited protrusion ensures compatibility with CubeSat deployment systems, preventing interference or damage during satellite integration.	CubeSat Design Specification Rev. 14.1	I
SR-LCH-170	Spacecrafts shall comply with the deployer's maximum 8U CubeSat dimensions as defined in table "Maximum cubesat dimensions"	The CubeSats shall adhere to the deployer's maximum 8U CubeSat dimensions, as specified in the "Maximum CubeSat Dimensions" table, to ensure compatibility and successful deployment.	CubeSat Design Specification Rev. 14.1, EXOpod User Manual	I
SR-LCH-180	The spacecrafts shall comply with the launcher's requirements on pressurized items as defined in the Launch Provider Manual.	This ensures that no damage will be done to the spacecraft itself, the launcher or other rideshare satellite passengers.	Falcon User's Guide, Electron Payload User's Guide, SSMS Vega-C User's Manual	A, T
SR-LCH-190	Spacecrafts shall have no elastic natural frequencies below a specific frequency and a specific quality factor as stated in the Launcher User's Guide.	Stated in the Launcher User's Guide (Falcon 9, Electron, Vega-C)	Falcon User's Guide, Electron Payload User's Guide, SSMS Vega-C User's Manual	A, T
SR-LCH-200	Spacecrafts shall be able to withstand the Quasi-Static load factors of the CubeSat Dispenser, as stated in the Launcher User's Guide	Stated in the Launcher User's Guide (Falcon 9, Electron, Vega-C)	Falcon User's Guide, Electron Payload User's Guide, SSMS Vega-C User's	A, T

			Manual	
SR-LCH-201	Spacecrafts shall be able to withstand the expected Quasi-Static load at its expected X_{PL} direction when adapted into the launcher as this is defined in the Launcher User's Guide.	Stated in the Launcher User's Guide (Falcon 9, Electron, Vega-C)	Falcon User's Guide, Electron Payload User's Guide, SSMS Vega-C User's Manual	A, T
SR-LCH-202	Spacecrafts shall be able to withstand the expected Quasi-Static load at its expected Y_{PL} and Z_{PL} directions when adapted into the launcher as these are defined the Launcher User's Guide.	Stated in the Launcher User's Guide (Falcon 9, Electron, Vega-C)	Falcon User's Guide, Electron Payload User's Guide, SSMS Vega-C User's Manual	A, T
SR-SDM-010	Impacts with space debris and meteoroids larger than 1 mm and smaller than 1 cm shall be calculated.	To ensure that no space debris is generated.	ESSB-ST-U-007 Issue 1	A
SR-SDM-020	Impacts with space debris and meteoroids larger than 1 cm shall be calculated.	To ensure that no space debris is generated.	ESSB-ST-U-007 Issue 1	A
SR-SDM-030	The cumulative collision probability of each spacecraft shall not exceed a maximum value of 10^{-4}.	To ensure that no space debris is generated.	ESSB-ST-U-007 Issue 1	A
SR-SDM-040	An orbital decay analysis shall be performed with DRAMA.	To ensure compliance with the 5-year deorbit requirement.	MR-MIS-060	A
SR-SDM-050	Spacecraft re-entry analysis shall be performed with DRAMA.	To ensure that the spacecraft completely disintegrates in the atmosphere.	ESSB-ST-U-007 Issue 1	A
SR-SDM-060	The spacecrafts shall have recurrent manoeuvre capabilities.	Stated in ESSB-ST-U-007 Issue 1.	ESSB-ST-U-007 Issue 1	A
SR-SDM-070	The spacecrafts shall have recurrent manoeuvre strategy.	Stated in ESSB-ST-U-007 Issue 1.	ESSB-ST-U-007 Issue 1	A
SR-THM-010	A Thermal Mathematical Model shall be generated for the satellite, as described in the ECSS-E-ST-31C	A Thermal Mathematical Model is crucial for accurate temperature control and performance prediction, ensuring the mission success	ECSS-E-ST-31C – Thermal control	A
SR-THM-030	Spacecrafts shall pass a thermal bakeout test and a thermal cycling test.	This ensures that the spacecrafts are able to withstand the thermal environment in space.	MR-MIS-080	T
SR-RAD-010	The TID limits of each	If the ionization limit of each subsystem is below the	MR-MIS-080	A

	subsystem should be higher than the TID induced throughout the nominal mission duration	Total Ionizing Dose (TID) experienced throughout the mission within the chosen orbital altitude, it will result		
SR-RAD-020	The TID rating for components with no publicly available information should be considered 15 krad.	This is an educated guess based on experience.	MR-MIS-080	R
SR-AIV/T-010	The CubeSat shall meet manufacturer specifications for cleanliness, ensuring that the maximum number of particles and molecules mass per unit area is within acceptable limits, adhering to the ECSS-Q-ST-70-01C guidelines. According to visibly clean inspection criteria, the maximum allowable particulate contamination level on all exposed surfaces, including witnesses, shall not exceed 300 mm2/m2 while for molecular contamination, the CubeSat shall maintain a maximum of 1 x 10^-6 g/cm2 organic contamination on any surface.	The "visibly clean" inspection criteria mandate that particulate contamination on exposed surfaces, including witnesses, remains within acceptable limits and the molecular contamination shall be limited to ensure operational integrity. All integration and testing activities related to payload components must be conducted in a cleanroom facility compliant with designated cleanliness class requirements.	ECSS-Q-ST-70-01C – Cleanliness and contamination control	T
SR-AIV/T-020	Leak testing shall be performed post environmental testing.	Stated in the Launcher User's Guide	Falcon User's Guide, Electron Payload User’s Guide, SSMS Vega-C User’s Manual	T
SR-AIV/T-030	Random Vibration testing shall be performed at MPE spectrum for 1 minute in each of 3 axes	Stated in the Launcher User's Guide	Falcon User's Guide, Electron Payload User’s Guide, SSMS Vega-C User’s Manual	T
SR-AIV/T-040	Electromagnetic Compatibility testing shall be performed. Elementary Compatibility can be met by verifying the mechanical battery isolation inhibit system during vibration testing. This can be accomplished by verifying that the isolation circuit successfully maintains the spacecraft powered-off during the dynamic event and showing that the boot counter of the EPS/CDHS does not increase during test.	Stated in the Launcher User's Guide	Falcon User's Guide, Electron Payload User’s Guide, SSMS Vega-C User’s Manual	T

SR-AIV/T-050	Combined Thermal Vacuum and Thermal Cycle testing shall be performed at ±5 °C beyond acceptance for 20 cycles total.	Stated in the Falcon User's Guide	Falcon User's Guide	T
SR-AIV/T-060	The spacecraft shall undergo a radiation testing campaign	To ensure that he spacecrafts shall be able to remain operational for the full 3 year mission duration.	MR-MIS-080	T
SR-AIV/T-070	The Qualification Model approach shall be implemented.	To enable the production of a large number of spacecrafts within an efficient timeline.	SR-CON-010	T
SR-OPS-010	The CubeSats' subsystems activation, monitoring, and control actions shall be performed during the LEOP phase.	LEOP starts with the Initial Checkouts and detumbling of the CubeSat and continues with the Initial Deployment phase during which the solar arrays and the antennas are deployed.	MR-MIS-080	A, T
SR-OPS-020	The satellites will have a critical mode in case of major subsystem failure or loss of solar panels	The critical mode is essential to ensure mission continuity and system resilience in the event of major subsystem failure or solar panel loss	MR-MIS-080	A, T
SR-OPS-030	The satellites shall enter safe mode if required to do so due to low power generation or any other malfunction of its nominal mode of operations.	Calibration of ADCS subsystem and contingency plan (Safe mode) in case of subsystem malfunction	MR-MIS-080	A, T
SR-OPS-040	All deployables such as booms, antennas, and solar panels shall wait to deploy a minimum of 30 minutes after the CubeSat's deployment switch(es) are activated during dispenser ejection.	The 30-minute delay ensures safe separation from the dispenser, allowing time for potential collision avoidance and minimizing the risk of unwanted deployments.	CubeSat Design Specification Rev. 14.1	A, T
SR-OPS-050	CubeSats shall not generate or transmit a signal earlier than 45 minutes after in-orbit deployment	Stated in the CubeSat Design Specification.	CubeSat Design Specification Rev. 14.1	A, T
SR-OPS-060	The spacecraft shall be in ground tracking while in PNT operations.	It is necessary for the provision of the services.	MR-MIS-090	A
SR-GRS-010	The UHF/S-band Ground Control Stations should have UHF/S-band link capabilities.	These are the bands in which the spacecrafts are able to perform communication links.	MR-BUS-010	I, T
SR-GRS-020	The GCS S-Band antenna shall have switchable LHCP and RHCP polarization	Switchable LHCP (Left-Hand Circular Polarization) and RHCP (Right-Hand Circular Polarization) in the GCS S-Band antenna enhances signal resilience. It enables adaptability to varying satellite polarizations, ensuring robust communication, especially in challenging propagation environments, ultimately bolstering mission reliability.	MR-BUS-010	R, T

SR-GRS-030	At least one GCS shall be equipped with laser capable of SLR	Necessary for the SLR operation.	MR-MIS-040	I, T

7. Mission Architecture

To address the objective of the mission a 8U CubeSat Platform shall be utilized that shall transmit S-band PNT signals. In order to provide the coverage needed as stated in the Requirements section, a Walker Delta 61°: 100/10/1 at 550 km shall be utilized.

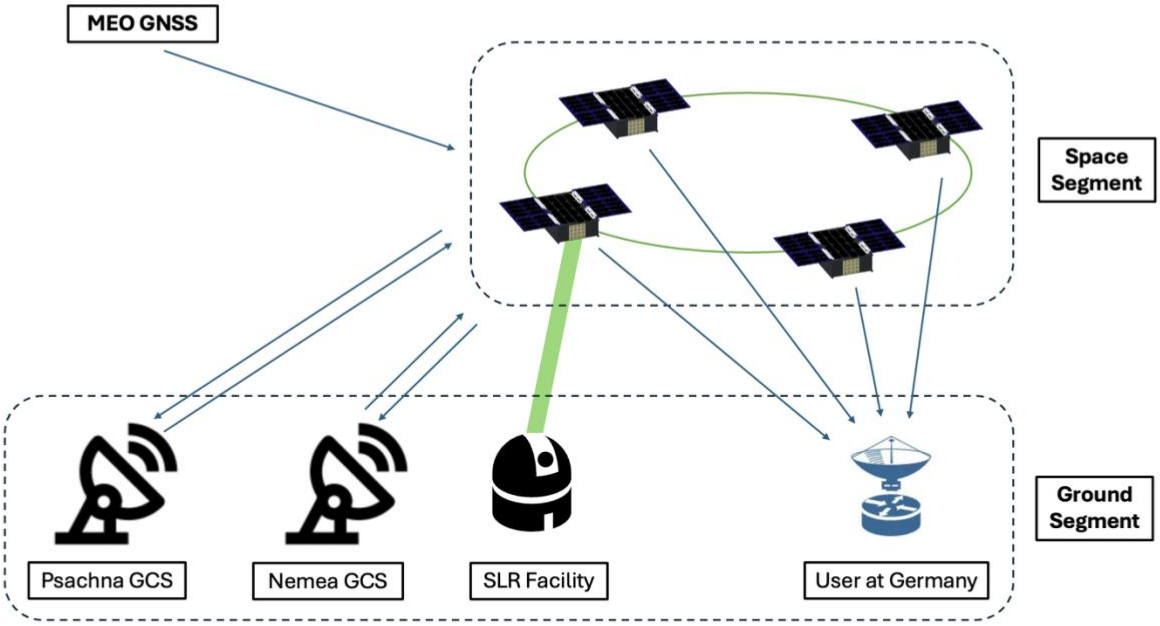

Figure 29. Mission Architecture

Table 7. Mission objectives – Success Criteria

Objective Number	Mission Objective	Success Criteria
Objective 1	Spacecrafts shall perform ODTS by relying on MEO GNSS.	At least one spacecraft shall perform ODTS once by relying on MEO GNSS throughout the mission duration.
Objective 2	The mission shall demonstrate SLR.	The altitude of a single spacecraft in orbit shall be measured via SLR technique at least once.
Objective 3	The system shall provide PNT services to Germany.	A user at ground level in Germany shall be able to determine its 3D position via the system at least once throughout the mission duration.
Objective 4	Spacecrafts shall remain operational for the full 3 year mission duration.	At least one spacecraft shall be operational for 3 years in orbit.

8. Launch Baseline

As stated in the requirements section, due to the large number of spacecrafts in the constellation a variety of launchers is considered. The target orbit has an altitude of 550 km and an inclination of 61°, while the constellation shall consist of 10 orbital planes. The number of orbital planes dictate the minimum number of launches to take place, since spacecrafts shall not have thrust capabilities to change orbital planes. However, the spacecrafts' thrust capabilities shall support phasing within the orbital planes, collision avoidance maneuvers and deorbiting. These orbital parameters make the constellation deployment to consist of multiple dedicated launches to the target orbital planes that are mentioned in the Mission Analysis section. In the context of this mission, there is particular interest in Microlaunchers. Within the scope of the thesis three different launch vehicles are considered; SpaceX's Falcon9, Rocket Lab's Electron and Arianegroup's Vega-C.

Table 8. Launch characteristics

Target Altitude	Target Inclination	Launch Type
550 km	61°	Multiple Dedicated launches

9. **Mission Profile**

The mission consists of 100 spacecrafts that share the same bus design and are placed in a Walker Delta 61°: 100/10/1 at 550 km. Thus, the same LEOP and commissioning procedures are applicable to all satellites.

After LEOP and commissioning have concluded successfully, a phase to validate and calibrate the payloads shall take place. Afterwards, the spacecrafts shall be able to enter nominal operation phase, using their payloads in a regular manner to provide PNT services.

Based on the expected lifetime of the subsystems used and the decay analysis, all satellites have a projected lifetime of 3 years minimum. After the end of their operational life, the satellites shall be decommissioned in a way that ensures safe disposal.

9.1. Space Segment Overview

In this section the space segment is described at a high level.

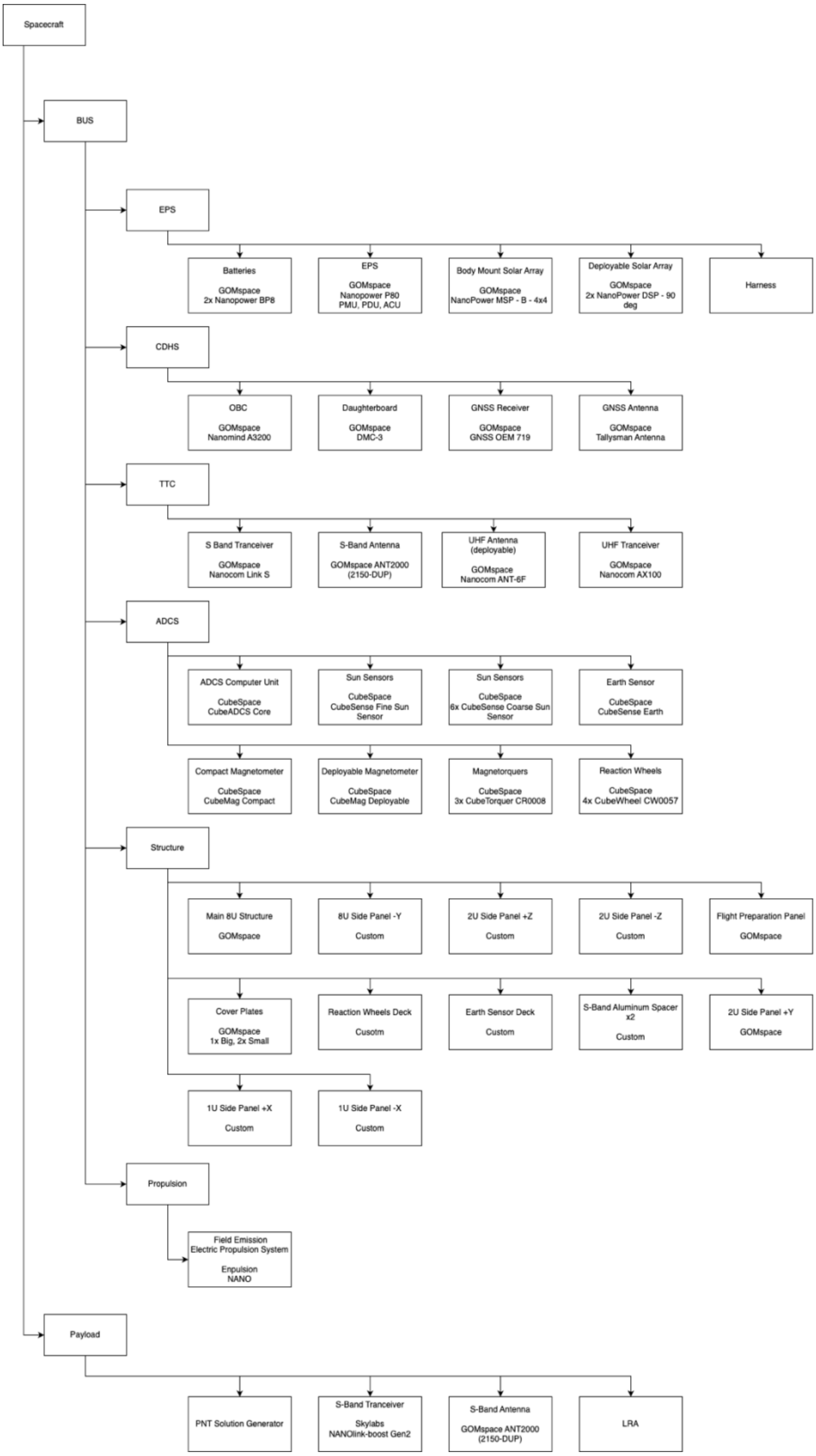

Figure 30. Spacecraft product tree

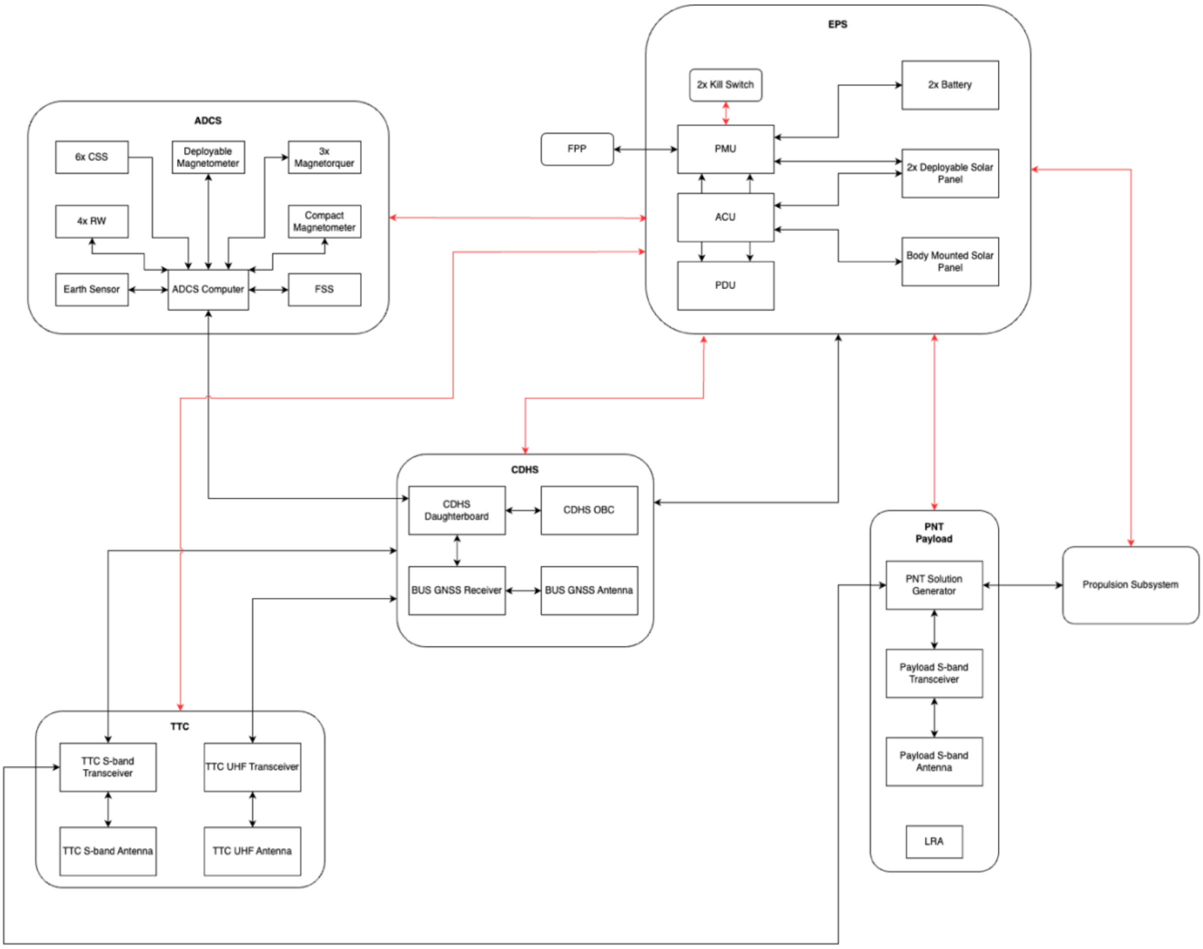

Figure 31. Basic system overview at high level. Red lines indicate power connections, while black ones indicate data transactions

9.1.1.1. Payload Architecture

In this section the payload is described in detail. The main goal of this thesis is to create a system based on COTS for which information is available online, which is not the case for such a payload. Thus, instead of a COTS component the payload is designed at a high level.

The philosophy implemented is similar to the one of AIOTY-CUBE CubeSat's ATOMIC payload.

MEO GNSS signals shall be received by a GNSS antenna and a receiver. A navigation filter shall be implemented in real time to achieve precise ODTS and the projected satellite trajectory shall be used to generate the satellite's ephemeris. For this an OBC shall be used, while a CSAC shall be included for precise timekeeping. Finally, a transmitter and an antenna shall broadcast the PNT signals. Additionally, an LRA shall be included in the exterior of the satellite in order for LSR to be performed.

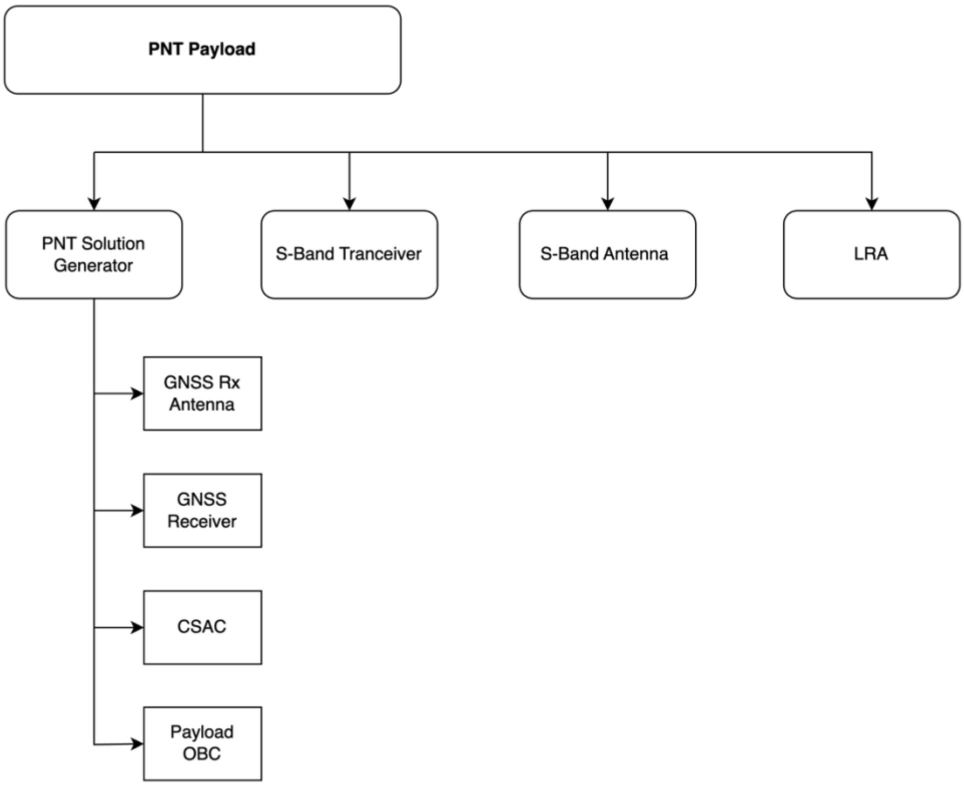

Figure 32. PNT Payload block diagram

10. Mission Design

10.1. Operational Modes

In the following table, the Operational Modes of the satellites are defined. By using them as building blocks, the CONOPS shall be defined in a latter chapter. Each Operational Mode is associated with a Pointing Profile that defines the operational status of the ADCS and a Power Profile that defines the power consumption of the various subsystems during that time. Pointing Profile and Power Profile shall be defined in the next paragraphs.

Table 9. Bus operational modes

Operational Modes – Bus				
Operational Mode	**Mission Phase**	**Pointing Profile**	**Power Profile**	**Description**
Critical Mode	Any	Passive (ADCS off)	Critical Mode	Critical power mode, all subsystems except EPS, CDHS and UHF(Rx) are off and non operational
Deployment	LEOP	Magnetic Detumbling	Deployment Mode	Only vital systems active, solar array, antenna, magnetometer deployment, magnetorquers active
Detumbling	LEOP	Magnetic Detumbling	Detumbling Mode	Only vital systems active, magnetorquers active
Safe Mode	Any	Magnetic Detumbling Safe-mode sun-pointing spin (if detumbling is complete)	Safe Mode	Only vital systems active, magnetorquers active.
Sun-Tracking	Commissioning, Phasing and Payload Validation, Nominal Operation	3-Axis Control	Sun Tracking	Use sun tracking modes to optimise power generation
UHF Link	Any	3-Axis Control	UHF link	Transmit telemetry data to the ground station via UHF
S-Band Link	Phasing and Payload Validation, Nominal Operation	3-Axis Control	S-Band link	Transmit telemetry data to the ground station via S-band
Phasing Maneuver	Phasing and Payload Validation	3-Axis Control	Phasing Maneuver	A pair of burns is performed to change the spacecraft's phase.

Table 10. Payload operational modes

Operational Modes - Payload				
Operational Mode	**Mission Phase**	**Pointing Mode**	**Power Mode**	**Description**
PNT Service Mode	Phasing and Payload Validation, Nominal Operation	3-Axis Control (Ground target tracking)	PNT Service Mode	Transmits PNT signals via the Payload Antenna
SLR	Phasing and Payload Validation, Nominal Operation	3-Axis Control (Ground target tracking)	SLR link	The satellite points the LRA towards the SLR facility, so that laser bounces back from the LRA.

10.1.1. Pointing Profiles

In the following table the Pointing Profiles are defined as it contains the information about which sensors and actuators are operational in each Pointing Profile.

Table 11. Pointing profiles

Pointing Profile	Mission Phases/Modes	Sensor Dependency	Actuator Dependency	Description
Passive	Critical Mode	N/A	N/A	ADCS is powered off
Magnetic Detumbling	LEOP	Magnetometer	Magnetorquers	Use 3 magnetorquers to place the satellite under a stable, low speed spin.
Sun Facing Spin	LEOP, Commissioning	Magnetometer Coarse Sun Sensors	Magnetorquers	Use the magnetorquers to face the solar array face towards the sun, while in Y-Thomson Spin
3-Axis Control	Phasing and Payload Validation, Nominal Operations	Magnetometer Coarse Sun Sensor Fine Sun Sensor Earth Sensor	Magnetorquers 3-axis wheels	In this mode the satellite has 3-axis control. Among other things it can be used for Sun Tracking, Nadir Pointing and Ground Target Tracking.

10.1.2. Power Profiles

To establish the system's power profiles, the ADCS power modes must first be defined. The electrical consumption of the ADCS component is shown in the table below [56], [57].

Table 12. ADCS components average and maximum power consumption

Component	Average Power (W)	Maximum Power (W)
CubeComputer	0.23	0.33
CubeMag Compact	0.05	0.23
CubeMag Deployable	0.05	0.23
CubeSense Sun	0.1	0.17
CubeSense Earth	0.2	0.28
CubeWheel CW0057 x4	3.08	10.8
CubeTorquer CR0008 x3	N/A	1.35

In total there are three ADCS power profiles: Magnetic Detumbling, Sun Facing Spin and 3-Axis Control. The projected power consumption for each component is detailed in the table below, the assumed percentages are based on calculations from the ERMIS mission.

Table 13. ADCS modes power breakdown

Component	ADCS Modes		
	Magnetic Detumbling (W)	Sun Facing Spin (W)	3-Axis Control (W)
CubeComputer	100% of Avg Power	100% of Avg Power	100% of Avg Power
CubeMag Compact	100% of Avg Power	100% of Avg Power	100% of Avg Power
CubeMag Deployable	100% of Avg Power	100% of Avg Power	100% of Avg Power
CubeSense Sun	0% of Avg Power	100% of Max Power	100% of Max Power
CubeSense Earth	0% of Avg Power	0% of Avg Power	100% of Max Power
CubeWheel CW0057 x4	0% of Avg Power	0% of Avg Power	15% of Max Power
CubeTorquer CR0008 x3	33% of Max Power	33% of Max Power	5% of Max Power

Table 14. ADCS modes consumption

Component	ADCS Modes		
	Magnetic Detumbling (W)	Sun Facing Spin (W)	3-Axis Control (W)
CubeComputer	0.23	0.23	0.23
CubeMag Compact	0.05	0.05	0.05
CubeMag Deployable	0.05	0.05	0.05
CubeSense Sun	0	0.17	0.17
CubeSense Earth	0	0	0.28
CubeWheel CW0057 x4	0	0	1.5
CubeTorquer CR0008 x3	0.45	0.45	0.07
Total	**0.78**	**0.95**	**2.52**

With the ADCS modes being defined, it is possible to proceed and outline the system's power profile.

Table 15. System power profiles description

Subsystem	Power Consumption	Power Margin	Power w/ Margin(W)	Critical Mode	Deployment Mode	Safe Mode / Detumbling	Sun-Tracking	UHF link	S-Band link	Phasing Maneuver	SLR	PNT Service Mode
Deployment Mechanism	2	20%	2.4	0.00%	100.00%	0.00%	0.00%	0.00%	0.00%	0.00%	0.00%	0.00%
Battery Heaters	1	10%	1.1	0.00%	100.00%	100.00%	100.00%	100.00%	100.00%	100.00%	100.00%	100.00%
EPS	0.6	5%	0.6	100.00%	100.00%	100.00%	100.00%	100.00%	100.00%	100.00%	100.00%	100.00%
GNSS kit	1.4	5%	1.5	0.00%	0.00%	0.00%	100.00%	100.00%	100.00%	100.00%	100.00%	100.00%
CDHS	0.3	5%	0.3	0.00%	100.00%	100.00%	100.00%	100.00%	100.00%	100.00%	100.00%	100.00%
ADCS - Magnetic Detumbling	0.8	10%	0.9	0.00%	0.00%	100.00%	0.00%	0.00%	0.00%	0.00%	0.00%	0.00%
ADCS - Sun Facing Spin	1.0	10%	1.0	0.00%	0.00%	0.00%	0.00%	0.00%	0.00%	0.00%	0.00%	0.00%
ADCS - 3-axis control	2.5	10%	2.8	0.00%	0.00%	0.00%	100.00%	100.00%	100.00%	100.00%	100.00%	100.00%
UHF Rx	0.5	5%	0.5	0.00%	90.00%	90.00%	90.00%	100.00%	0.00%	0.00%	0.00%	0.00%
UHF Tx	3	5%	3.2	0.00%	10.00%	10.00%	10.00%	100.00%	0.00%	0.00%	0.00%	0.00%
S-Band TxRx	17	5%	17.9	0.00%	0.00%	0.00%	0.00%	0.00%	100.00%	0.00%	0.00%	0.00%
Propulsion	40	5%	42.0	0.00%	0.00%	0.00%	0.00%	0.00%	0.00%	100.00%	0.00%	0.00%
PNT Solution Generator	2.5	20%	3.0	0.00%	0.00%	0.00%	100.00%	0.00%	100.00%	0.00%	100.00%	100.00%
PNT Signal Transmission	31.25	20%	37.5	0.00%	0.00%	0.00%	0.00%	0.00%	0.00%	0.00%	0.00%	100.00%
Mode Consumption (W)				**0.6**	**4.7**	**3.4**	**9.1**	**9.3**	**25.3**	**45.8**	**8.3**	**39.6**
Mode Consumption w/Magin (W)				**0.6**	**5.2**	**3.7**	**10.1**	**10.0**	**27.1**	**48.3**	**9.3**	**46.8**
Mode Consumption w/ system margin (W)		**20%**		**0.8**	**6.3**	**4.4**	**12.1**	**12.0**	**32.6**	**57.9**	**11.1**	**56.1**

10.2. Concept of Operations

10.2.1. Mission Timeline - Mission Phases

Table 16. Mission phases

Time	Mission Phase	Phase Description
T+0	LEOP	Launch, deployment of the deployables, achievement of the first link with a GCS & detumbling.
T+1 weeks	Commissioning	Health check for all subsystems & payloads. Calibration and verification of the operational fitness of the ADCS.
T+ 6 weeks	Phasing and Payload Validation	Phase the spacecrafts into the orbital plane. Calibrate and verify the operational fitness of the payload. Conduct experiments that evaluate payload operations and performance.
T+ 3 years	Nominal Operations	Conduct nominal operations as described in the mission objectives.
-	Decommissioning	The spacecraft shall be passivated and decay into the atmosphere in compliance with applicable legal regulations.

LEOP is divided into two sub-phases, deployment & detumbling. The first is automated and is concluded when communication with the GCS is confirmed. In the second one, each command is issued by the GCS, after reviewing the satellite's telemetry. This allows for more control during these critical steps, but with a time/scheduling disadvantage, since the commands are linked to a GCS overpass.

LEOP - Deployment

Upon Deployment, the CubeSat is released from the launch vehicle, initiating the LEOP. Through the release of the killswitch the satellite is activated and a 45-minute inactivity timer is set. After this period, the UHF antenna and solar panels are deployed, along with the magnetometer. Subsequently, the beacon signal transmission is activated. This phase ends when the GCS link is established, ensuring successful communication with the satellite.

Table 17. LEOP – deployment and initial GCS link

Time	Phase duration	Mission Phase	Phase Description
T=0	45 min	Launcher separation	Separation from CubeSat Deployer, killswitch release, satellite activation and hold timer initiation.
T+ 45 min	5 min	Deployment	UHF antenna deployment, magnetometer deployment, solar panels deployment, beacon signal transmission activation.
T+ 50 min	24-48 hrs	GS Link Establishment	Initiate processes for establishing a link with the Ground Station.

A maximum of 2 days is assumed between deployment and first successful GCS link establishment.

LEOP - Detumbling

During Detumbling, the initial calibration of gyros and magnetometers is performed. Following this, the magnetorquers are commissioned to control the satellite's attitude. The goal is to achieve a rotation rate of less than 0.5 degrees per second, which is a requirement for the successful completion of the LEOP phase.

For the Detumbling subphase, the first successful TTC exchange is considered as time 0. Regarding the Detumbling sequence, a decision to keep the mission automation to a minimum at the early stages of satellite deployment has been made, taking a safer approach. Thus, decisions and command shall be made from the ground station during overpasses. In the following table, time margins/extra overpasses are considered for high rotational rates, erroneous sensor or actuator configurations resulting in rate increases, etc.

Table 18. LEOP – detumbling phase

Time	Phase duration	Mission Phase	Phase Description
T+ 0	24 hrs	Detumbling with timeout	First successful TTC exchange. Detumbling activation. Gyro & Magnetometer Initial Commissioning.
T+ 1 day	5 days	Safe Detumbling	3-axis Magnetorquers Commissioning
T+ 6 days	1 day	Post Comm. Detumbling	Continued Detumbling.
T+ 7 days	-	Detumbling success	Detumbling procedure completed

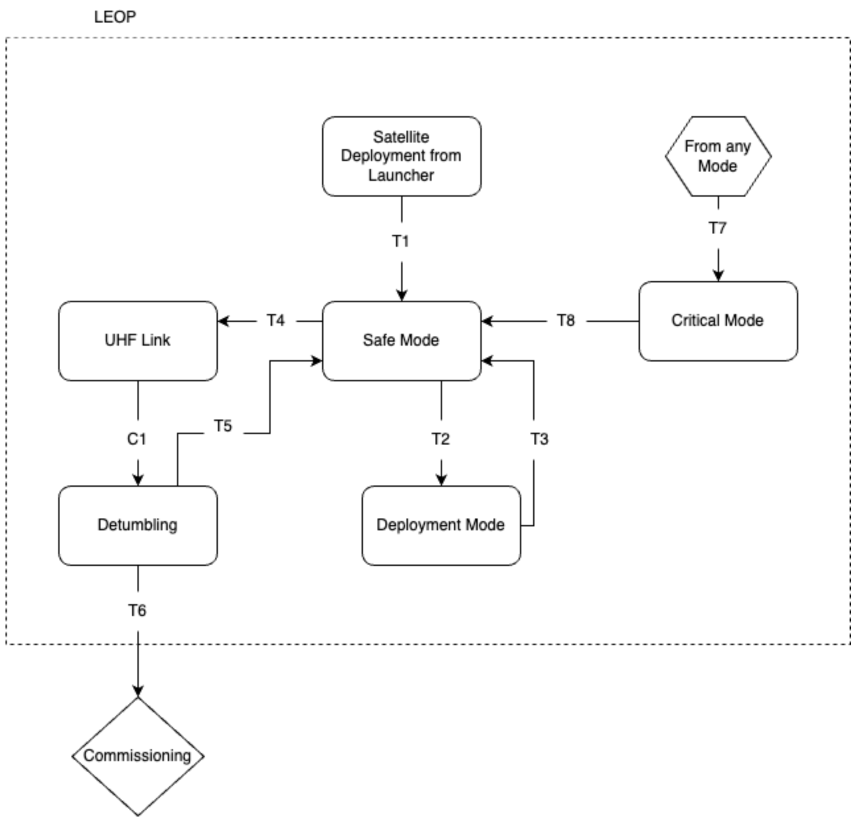

Figure 33. LEOP - modes state diagram

Table 19. LEOP - conditions for state changes

T1	Killswitch Release
T2	Deployment Timer and Deployment Incomplete
T3	Deployment Timeout or Deployment Complete
T4	Deployment Complete or Deployment/Detumbling failure and battery charge over 98%
T5	Detumbling failure
T6	Detumbling successful
T7	Battery < Critical Voltage
T8	Battery > Safe Voltage
C1	GCS Command to initiate Detumbling

During the Commissioning Phase, health checks and self-tests will be conducted for all components, while calibration and functional verification activities will be carried out for all BUS subsystems.

Following the completion of the Commissioning Phase, the Phasing and Payload Validation phase will commence. The initial task is to position the satellites into their designated slots within their respective orbital planes. Afterward, the Payload Validation phase begins, which involves calibrating and verifying the operational readiness of the payload, as well as conducting experiments to assess its performance and functionality.

The PNT payload will be calibrated and tested for its ability to determine the satellite’s position by comparing its measurements with those from the BUS’s GNSS kit. The timekeeping accuracy of the CSAC will also be assessed, and finally, the quality of the transmitted PNT signals will be evaluated.

Under nominal mission conditions, the spacecraft will transmit PNT signals to Germany during each overhead pass, which lasts approximately 10 minutes and occurs about seven times per day. Additionally, around two S-Band links with a ground control station (GCS) are expected daily. These passes will be pre-programmed into the flight plan and uploaded to the spacecraft when a GCS link is established. Moreover, SLR operations may be conducted to assess with accuracy the spacecraft's altitude.

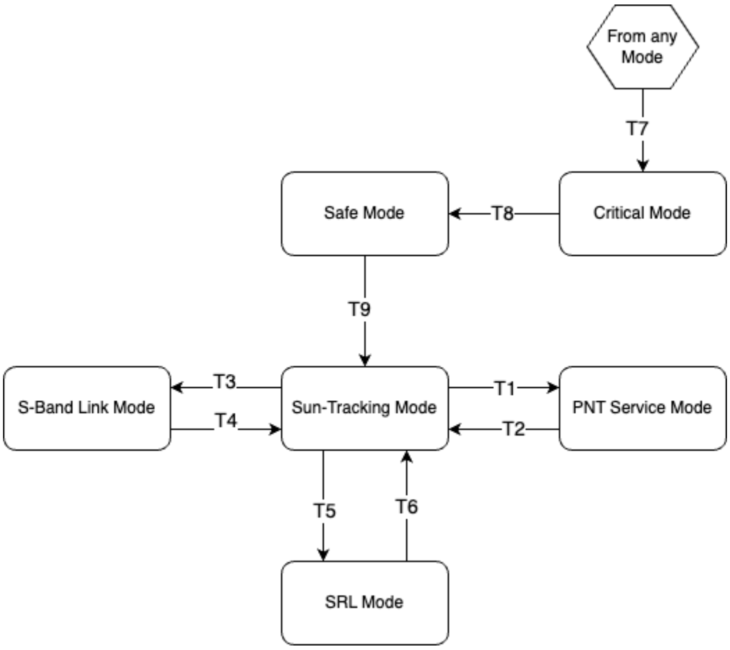

Figure 34. Nominal operations – modes state diagram

Table 20. Nominal operations - conditions for state changes

T1	Timer to initiate PNT Service Mode
T2	End of PNT Service Mode duration
T3	Timer to initiate S-band Link Mode
T4	End of S-band Link Mode duration
T5	Timer to initiate SLR Mode
T6	End of SLR Mode duration
T7	Battery < Critical Voltage
T8	Battery > Safe Voltage
T9	FDIR completed

Error Recovery

If a subsystem encounters an error or failure, the system transitions into the Error Recovery Phase. Upon detecting the issue, the satellite shifts to safe mode, disabling all non-essential functions and subsystems. It will then restart in safe mode to counter any transient radiation effects. In this low-power state, Mission Control will establish communication with the spacecraft to perform diagnostics and retrieve telemetry logs to identify the cause of the failure. Once the issue is diagnosed, the extent of the damage is evaluated, and a recovery procedure is executed based on the specific fault. After completing the recovery process, the spacecraft resumes normal operations. However, in the case of severe system failures, significant modifications to the operational strategy may be required.

Decommissioning Phase

After completing nominal operations, the decommissioning phase begins. During this phase, a spacecraft undergoes passivation before decaying into the atmosphere. The passivation process includes a two-step procedure to prevent accidental activation. Prior to initiating passivation, it must be confirmed that the spacecraft has successfully completed its primary mission and transmitted all critical data to the ground station. Relevant space agencies and authorities will be notified of the passivation and deorbit plan. All FDIR software modules will be disabled, and non-essential subsystems and payloads will be powered down, with the spacecraft entering safe mode. The solar panels will be deactivated to stop power generation, and the batteries will be safely discharged to eliminate any remaining energy. Additionally, all communication, including uplink and downlink, will be terminated. However, the spacecraft will continue to be monitored to ensure it remains in a passive state without risk of unintentional reactivation.

11. Ground Segment

The Ground Segment is composed by two bands; UHF and S-Band, with S-Band being the main TTC link and UHF being the backup and the main one during LEOP. The main GCS shall be the one that UOA has been developing at Psachna, Greece. However, a second GCS is considered to ensure successful handling of the constellation. Since UOA does not own another GCS, GCS as a service is the go to option. For this, KSAT's GCS at Nemea, Greece is baselined.

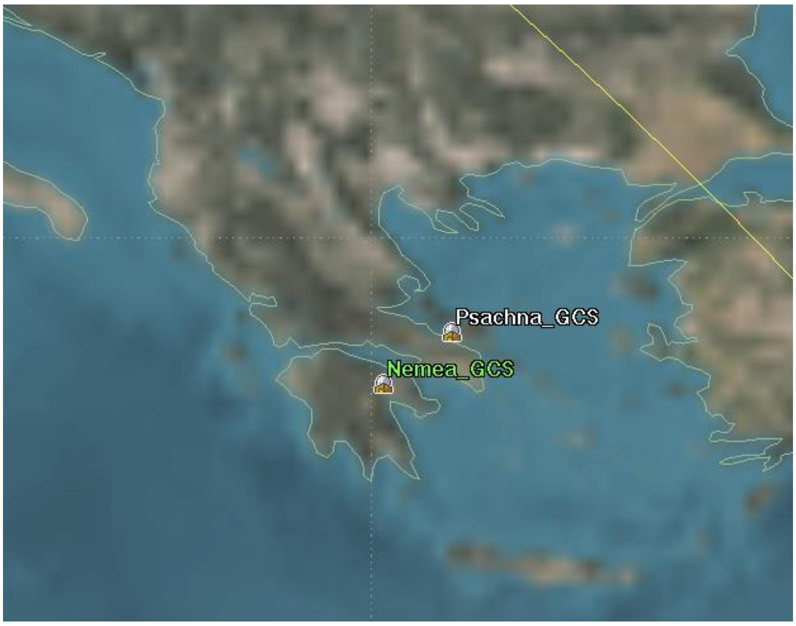

Figure 35. GCSs locations

11.1. Psachna GCS

At Psachna a UHF/VHF and S-Band GCS is under development at UOA's Department of Aerospace Science and Technology building. It is located at 38°34'10.39"N, 23°38'54.55"E (WGS'84) with an elevation of 42 m (above sea level). All the outdoor equipment will be established at the rooftop of the building, which adds an extra height of 5 m. All the GCS antennas have a pointing view over the horizon.

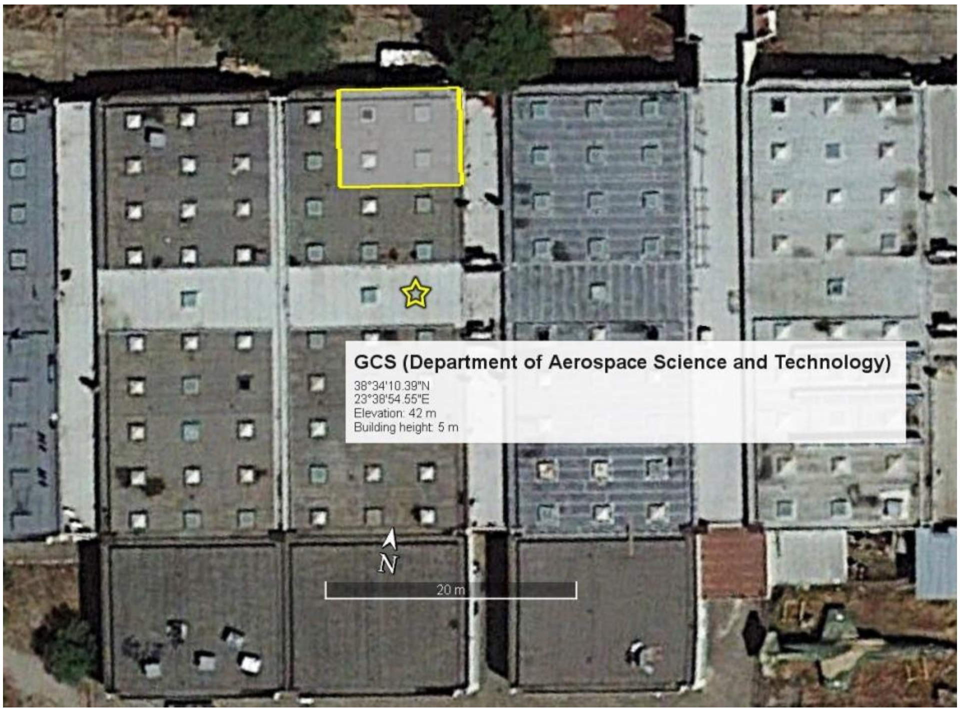

Figure 36. UOA's GCS at Psachna, Evia, Greece

Additionally, the outdoor equipment is being installed far from any metallic surfaces to avoid random reflections, and away from any electric device that could induce interference in the spurious domain.

11.1.1. Psachna GCS Architecture

The indoor equipment of the RF GCS system is organized from top to bottom as follows: The rotator controller, which manages both the azimuth (Az) and elevation (El) pointing directions, is positioned at the top. Below it is the SDR rack, which includes several key components: a rack-mounted radio unit for the VHF/UHF antenna that connects directly to the outdoor low-noise amplifiers (LNAs), a rack-mounted radio unit for the S-band antenna (reception) connected to the outdoor low-noise converter (LNC), and a rack-mounted radio unit for the S-band antenna (transmission). It also consists of the Power rack, which supplies the necessary power to the SDR rack. Additionally, there is a rack-mounted server containing software critical for satellite control and communication (Mission Control). This server is interconnected with both the rotator controller rack and the SDR rack and is equipped with an ethernet Gigabit (Gbit) interface for remote access.

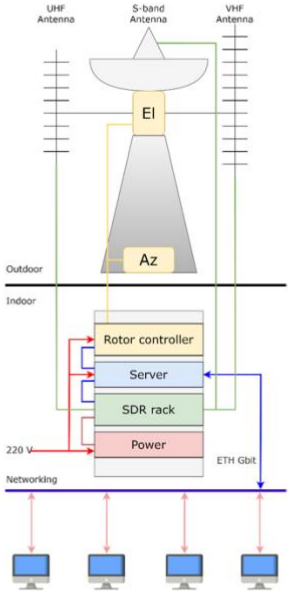

Figure 37. Psachna GCS architecture

Table 21. UHF Yagi Antenna characteristics

Frequency Range	At least 380 – 512 MHz
Beamwidth	$\leq 36°$
Gain	$\geq 14\ dBic$
Front-to-Back Ratio	$\geq 18\ dB$
LNA Gain	$>\ 10\ dB$
LNA noise figure	$<\ 2.0\ dB$
Polarization	LHCP or RHCP

Table 22. S-Band Satellite Dish characteristics

Frequency Range	Uplink	2025 – 2110 MHz
	Downlink	2200 – 2290 MHz
Beamwidth	$\leq 5.1°$	
Gain	$\geq 30\ dBic$	
Front-to-Back Ratio	$>\ 25\ dB$	
LNA Gain	$>\ 25\ dB$	
LNA noise figure	$<\ 2.0\ dB$	
Polarization	LHCP or RHCP	

Table 23. Physical characteristics of the antennae system

Maximum tower mass with S-band and two Yagi antennas	300 kg
Maximum base foundation area	4.5 m x 4.5 m
Maximum heigh from ground to cross boom	2.3 m
S-Band antenna diameter	1.9 m
S-Band antenna length	0.8 m
VHF Yagi dimension	1.2 m
UHF Yagi dimension	1.1 m
Azimuth Turning angle	0-360°
Azimuth Turning speed	3.5 °/sec
Elevation Turning angle	0-180°
Elevation Turning speed	2 °/sec
Rotor accuracy	0.3°

11.2. Nemea GCS

KSAT has developed a GCS at Nemea, Greece that is compatible with KSATlite services. KSATlite is a GCS as a service option that is tuned to be compatible with most small satellites. Among others, they provide downlink/uplink capabilities in S-band, which is the reason it was picked for the current mission. Although the GCS's precise location is not available online, Nemea's coordinates, which are 37.82° N and 22.66° E ,are used for analysis purposes.

12. **Mission Analysis**

12.1. Constellation Design

12.1.1. Problem Statement

As mentioned in the Mission Statement, the system shall provide persistent PNT services over the area of Germany. That means that a satellite constellation shall be designed in a way that at least 4 spacecrafts are covering the area of service at all times.

It is essential that the spacecrafts are placed into circular orbits with the same altitude in order to ensure that the distance between spacecrafts and ground users and GCSs is the same for all spacecrafts throughout the mission. Additionally, the constellation's configuration should be one that remains constant at all times. Thus, Walker constellations are evaluated. Since the area of service is not located in a polar area, Walker Delta geometries are the ones under inspection, with single shell constellations being considered sufficient for the purposes of this thesis. For this STK was used, in which tradeoffs between constellation parameters can be made with the Analyzer tool. However, UOA's educational version does not include it and tradeoffs between different scenarios were performed manually.

Moreover, the design of the constellation has to conform with other parameters, like the Payload link budget, the TTC link budget, the expected radiation dose, the power budget, deorbit plan etc.

Some of those criteria, which are considered critical with the essence that there is no assurance that they are met are analyzed in depth in this chapter, while other criteria, for which preliminary analysis has shown that their margin surplus is high enough so that the possibility of them being met is high, are not under consideration at this point. How the latter criteria are met and the tradeoffs that took place are described in the relevant sections.

Regarding the contact analysis between space and ground assets, regardless if it is about the contact between the spacecrafts and the end users on the ground or between the spacecrafts and the GSs, a constraint on the elevation angle is established. A minimum elevation angle of 5° is assumed, meaning that for lower elevation angles no contacts are considered.

STK simulations of the constellation configuration were performed between the altitudes of 550 km and 800 km. The minimum value of 550 km is selected as it is a standard launch altitude for LEO missions and no altitude-lowering maneuvers shall be done.

In the STK simulation, Germany was defined as an “Area Target” object, and based on it a “Coverage Definition” object was created that creates a grid over the specific area. The grid is defined so that its resolution is set to 1° of Lat/Lon. It has to be noted that different grid resolutions can conclude in different results. The value of 1° is the minimum possible and corresponds to the highest quality analysis results.

Figure 38. The Area Target of Germany with 1° of lat/lon grid granularity

The philosophy behind the coverage is that the spacecrafts shall have their Payload antennas mounted on the nadir side and track the area of service as they pass near it.

That way, the area covered by each spacecraft is constrained by the FOV of the Payload antenna. The Payload antenna is chosen to be GOMspace ANT2150 DUP, which has the gain pattern seen below. In the simulation, the FOV of the Payload antenna is chosen to be a cone with a half angle of 30° that corresponds to a 5.5 dB antenna gain. The antenna coverage can be simulated in STK by defining a sensor on-board the satellites at their nadir side with the stated FOV properties.

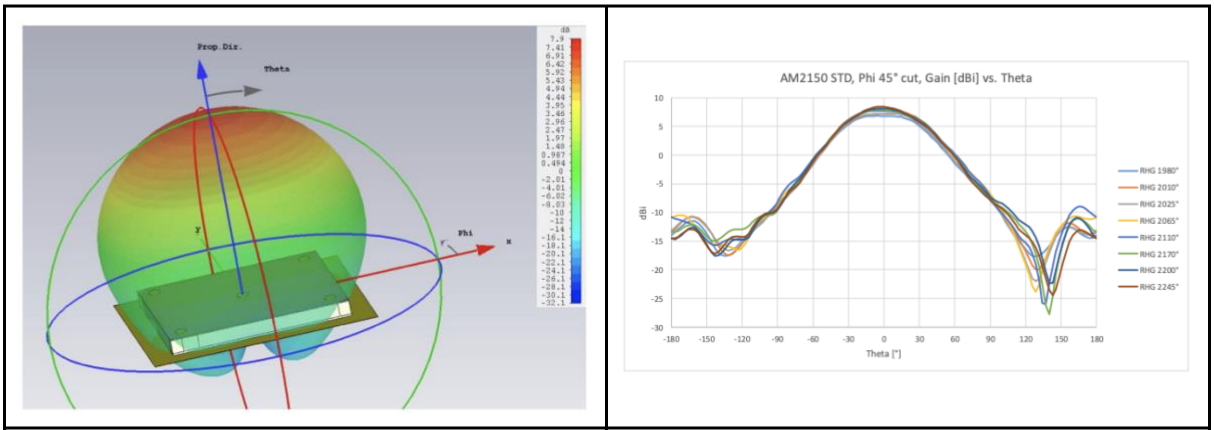

(a) (b)

Figure 39. GOMspace ANT2150 DUP gain pattern (a) and Gain vs Theta at Phi 45° cut (b)

After defining the satellite constellation via the Walker tool, which is set to track the service area, the Sensors of the constellation must be grouped into a single object. This is done by inserting a new "Constellation" object that contains all the sensors of the constellation. Now, this "Constellation" object can be set as an "Asset" to the "Coverage Definition" object and the coverage quality can be assessed via a "Figure of Merit" object of the type "N asset coverage".

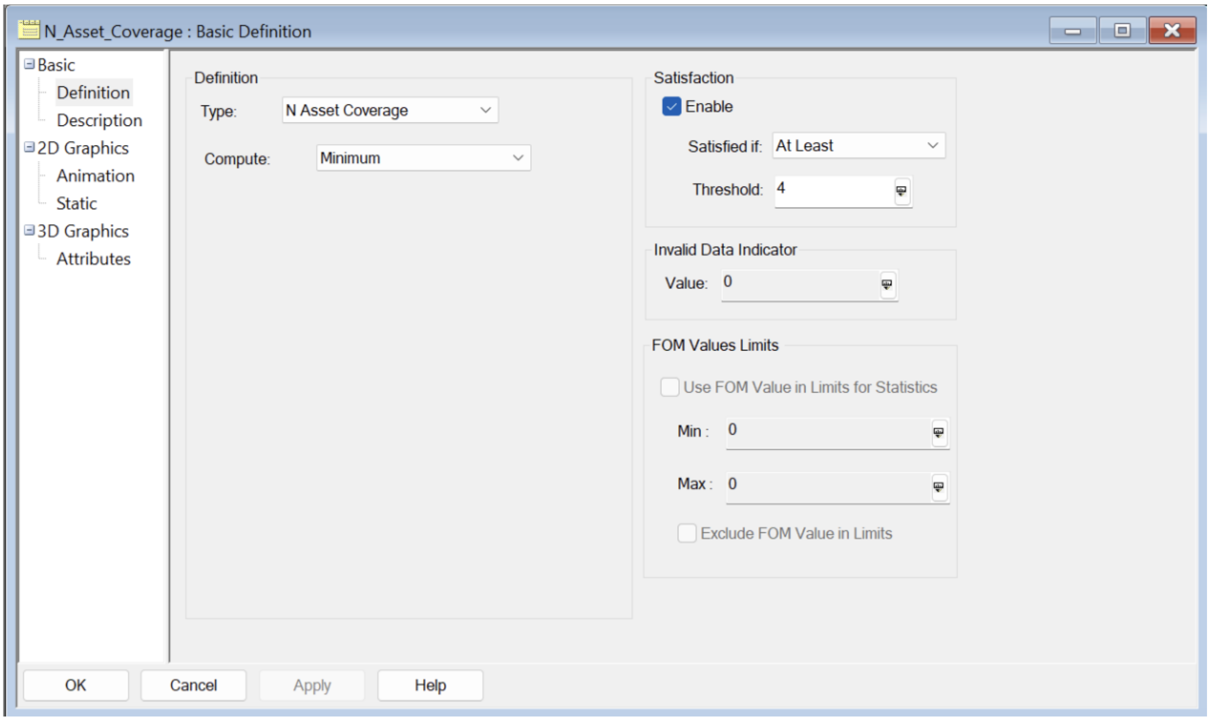

Figure 40. N Asset Coverage Figure of Merit definition

By generating the "Percent Satisfied" report it is possible to calculate the percentage of grid points over Germany that are always covered by a minimum of 4 satellites for the duration of one year. However this kind of analysis does not take into account any minimum elevation constraints.

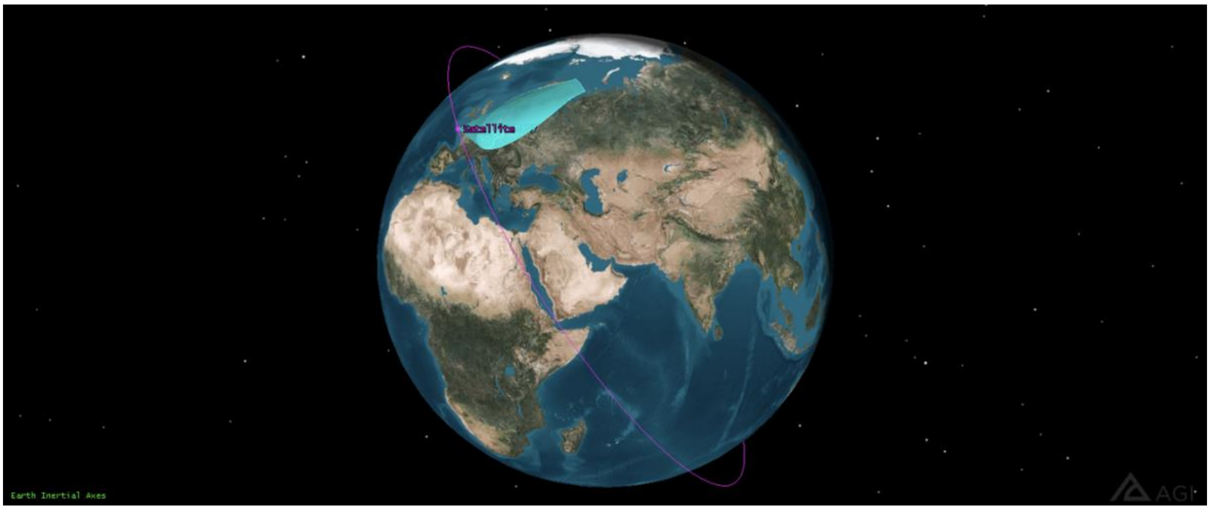

Figure 41. Single satellite tracking the area of Germany

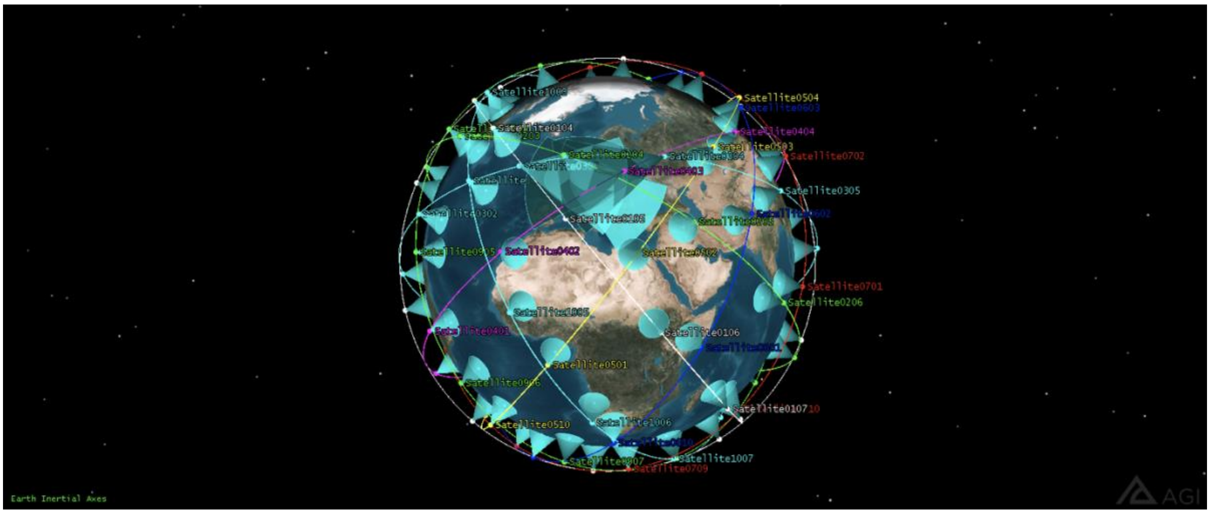

Figure 42. Walker constellation tracking Germany when in LOS

In order to also include the elevation constraint into this analysis with the UOA’s educational STK license, a creative solution was found. By creating a different scenario in which the sensors’ conic half angle is set to 85° and the satellites are always maintaining nadir pointing attitude, by performing the exact same procedure it is feasible to essentially solve the same coverage problem while discarding any contact times with less than 5° of elevation.

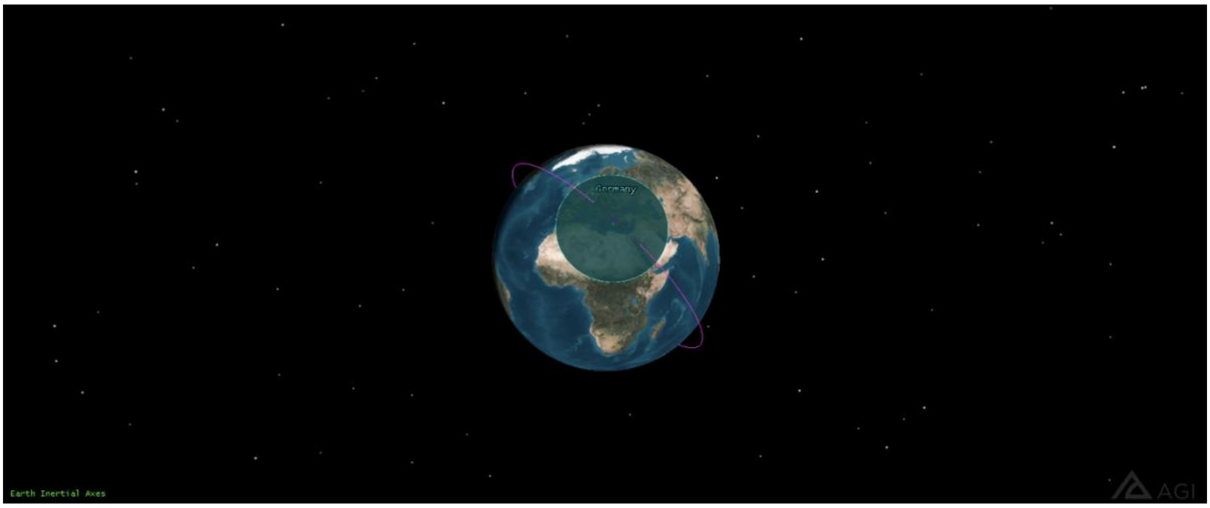

Figure 43. Single satellite in nadir pointing, equipped with a conic sensor with a cone half angle of 85°

12.1.2. Constellation Tradeoff Analysis

In order to design a Walker Delta constellation the parameters that need to be defined are:

- Altitude
- Inclination
- Number of equally spaced orbital planes
- Number of satellites in every orbital plane
- The relative spacing between satellites in adjacent planes

The critical parameters are assessed to be the altitude and the number of satellites and the main aim is to minimize them. Additionally, it is recommended to find the minimum number of orbital planes for each specific number of satellites. This would be beneficial for the launch campaign since one launch would be nominally associated with satellites in a single orbital plane.

What needs to be done at this point is a multivariable optimization of the constellation between altitude, inclination, number of orbital planes and total number of satellites. Such a tradeoff analysis could be done via the Analyzer tool in STK, but UOA's educational license does not support it. Thus, what essentially needs to be done is to break down the problem into smaller manageable pieces. An iterative approach is taken and it is described in the following diagram.

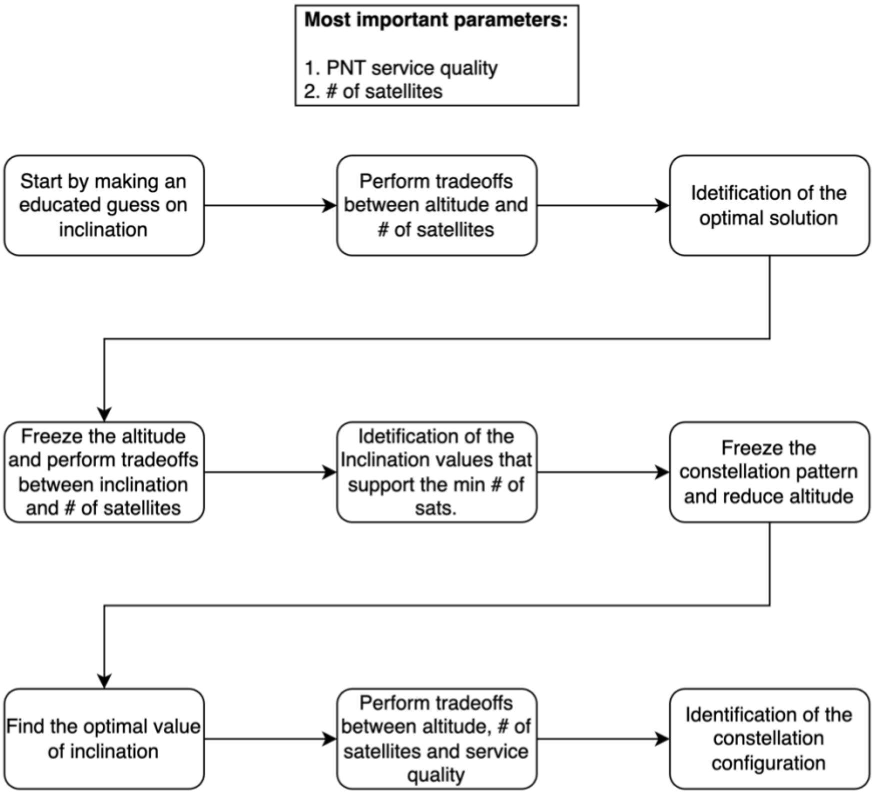

Figure 44. Constellation tradeoff approach

The first step for such an analysis shall be to do a preliminary tradeoff analysis between altitude, which directly translates to Payload Link Budget and TID, and constellation configuration. As stated above only Walker Delta geometries are to be considered. For the purposes of this analysis, scenarios with a specific inclination, but different altitudes are simulated. The inclination is selected to be 56° to match the one of Galileo, because Galileo is a system optimized for coverage over Europe and even though this is a comparison between a LEO and a MEO system, at this point, it is considered an acceptable educated guess.

The relative spacing between satellites in adjacent planes is not considered a parameter whose value needs to be a specific one, since the same thrust requirements apply in any case due to the fact that satellites in the same plane are launched together and satellites in every orbital plane are evenly spaced in it. So, different relative spacing between satellites in adjacent planes are considered for the purpose of finding out if a specific value results in better coverage. The values of relative spacing between satellites in adjacent planes that are considered are 1,2,3 and 4. However, preliminary analysis showed that as a rule of thumb when set to 1, the 4-asset coverage is better and as a result this is mainly the case under inspection.

Table 24. Tradeoffs between altitude, number of satellites and Payload link budget for the inclination of 56°

Altitude (km)	Min # of satellites	Min # of orbital planes	Min received power at ground level (dB)	TID in 3 years at Solar Maximum. Shielding: 1.5 mm of Al (krad)
800	90	10	-159.2	20.6
750	90	10	-158.9	17.4
700	100	10	-158.5	14.8
650	100	10	-158.1	12.1
600	110	10	-157.7	10.7
	110	11		
550	110	11	-157.2	9

All in all, the only constellation that conforms with all the relevant requirements is a constellation at 650 km that comprises 100 satellites in 10 orbital planes. This is the baseline constellation for the next steps, a Walker Delta 56°: 100/10/1 at 650 km.

By keeping the altitude at 650 km and performing simulations as described above, it was found that such a constellation can provide the required coverage to Germany for multiple inclinations varying from 56° to 69°. So, for each different value of inclination the coverage analysis is rerun in order to find whether or not there is a constellation configuration that fulfills the coverage requirements with a lower number of total satellites.

Table 25. Constellation configurations based on inclination at 650 km of altitude

Altitude of 650 km		
Inclination (deg)	Min # of satellites	Min # of orbital planes
56	100	10
57	100	10
58	100	10
59	100	10
60	90	10
61	90	10
62	90	10
63	90	10
64	90	10
65	100	10
66	100	10
67	100	10
68	100	10
69	100	10

At this point, new simulations are run for the highlighted inclination values to determine whether or not these constellation configurations could align with the coverage requirements at the lower altitude of 600 km.

Table 26. Service satisfaction for different inclination values at 600 km

Configuration	Satisfaction of 4-asset coverage
Walker Delta 60°: 90/10/1 at 600 km	68 %
Walker Delta 61°: 90/10/1 at 600 km	100 %
Walker Delta 62°: 90/10/1 at 600 km	93 %
Walker Delta 63°: 90/10/1 at 600 km	81 %
Walker Delta 64°: 90/10/1 at 600 km	68 %

The optimal value of inclination has been identified and is considered to be directly related to the selection of the service area. Now, the initial tradeoff table is recreated. At this point GDOP is also included in order to conclude the constellation's configuration.

GDOP can be calculated via a "Figure of Merit" object of the type "Dilution of Precision". For this analysis the time step is set to 1 hr and the grid resolution is set to 2° in order to limit computational resources. By generating the "Stats by Region" report it is possible to calculate the GDOP over Germany over the duration of one year.

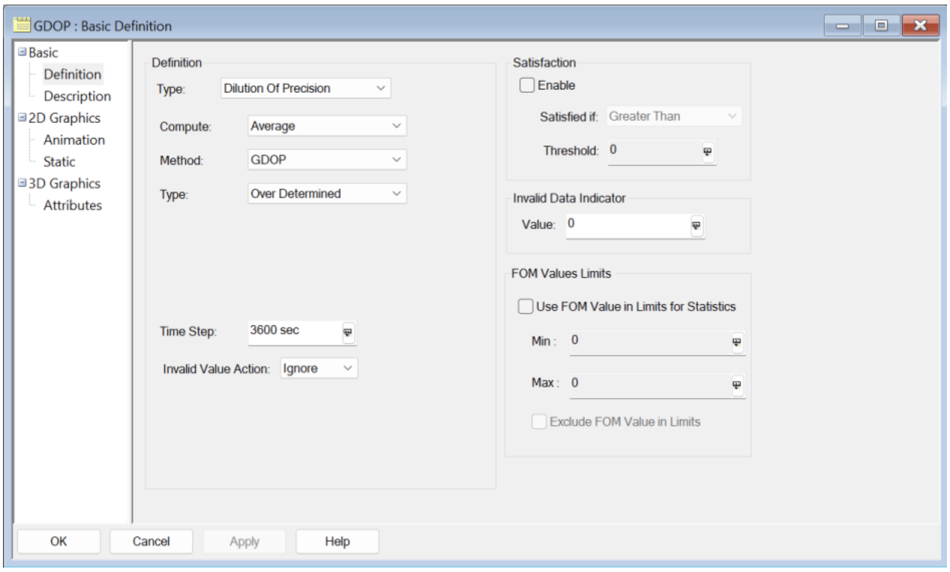

Figure 45. DOP Figure of Merit definition

Table 27. Tradeoffs between altitude, number of satellites and Payload link budget for the inclination of 61°

Altitude (km)	Min # of satellites	Min # of orbital planes	Min received power at ground level (dB)	TID in 3 years (Solar Max) for 1.5 mm	ΔV for phasing* (m/s)	Avg GDOP
750	80	10	-158.9	22.6	57.0	7
	81	9				4.5
700	90	10	-158.5	19.5	57.2	4.1
650	90	10	-158.1	17	57.4	5.5
600	90	10	-157.7	14.5	57.6	7.7
550	100	10	-157.2	12.2	57.8	5.3

*Phasing is assumed to have a duration of 3 days. It is calculated w/o margin.

As it is shown in the table, the sole solution that conforms with all requirements is a Walker Delta 61°: 100/10/1 at 550 km, which is the baseline for this thesis. This corresponds to an Orbital Period of 1.59 hr or 95.4 min.

12.2. Contacts with Service Area

The constellation has constant coverage over the service area - Germany. In this STK analysis a minimum elevation of 5 is set as a constraint. Additionally, satellites in the same orbital plane are assumed to demonstrate similar performance. In the following tables are shown the calculated contact and revisit times.

Table 28. Contact times with service area

Orbital Plane ID	Avg Contact Duration (min)	Min Contact Duration (min)	Max Contact Duration (min)	Contacts per day
1	10.7	0.2	12.3	7.2
2	10.7	1	12.3	7
3	10.7	0.1	12.3	7.2
4	10.7	0.3	12.3	7.2
5	10.7	0.2	12.3	7.2
6	10.7	0.3	12.3	7.2
7	10.7	0.6	12.3	7.2
8	10.7	0.1	12.3	7.2
9	10.7	0.6	12.3	7.2
10	10.7	0.5	12.3	7.2

Table 29. Calculation of the revisit time of a single satellite to the area of service

Orbital Plane ID	ART (hr)	MRT (hr)
1	3	13.8
2	3	13.8
3	3	13.8
4	3	13.8
5	3	13.8
6	3	13.8
7	3	13.8
8	3	13.8
9	3	13.8
10	3	13.8

12.3. Solar Eclipse Analysis

In this section the number and duration of solar eclipses are calculated for every orbital plane via STK.

Table 30. Solar eclipse calculation

Orbital Plane ID	Avg Eclipse Duration (min)	Min Eclipse Duration (min)	Max Eclipse Duration (min)	Eclipses per day
1	31.5	0.3	35.6	13.5
2	31.5	1	35.6	13.5
3	31.4	0.4	35.6	13.5
4	31.3	0.3	35.6	13.6
5	31.2	2.3	35.6	13.9
6	31.4	1.2	35.6	13.9
7	31.1	0.4	35.6	14
8	31.1	1.3	35.6	13.7
9	30.9	0.5	35.6	13.6
10	31.2	1.8	35.6	13.5

Table 31. Solar eclipse - worst case

Worst case - max eclipse values			
Avg Eclipse Duration (min)	Min Eclipse Duration (min)	Max Eclipse Duration (min)	Worst case Eclipses per day
31.5	2.3	35.6	14

12.4. GCS Visibility Analysis

In this section the contact times with GCSs are calculated. In the STK analysis performed, a minimum elevation of 20° was assumed and any contact with a duration less than a minute was considered insufficient for establishing a link and was discarded.

Table 32. Contact times with Psachna GCS

Orbital Plane ID	Avg Contact Duration (sec)	Min Contact Duration (sec)	Max Contact Duration (sec)	Contacts per day
1	268	61	337	2.7
2	267	60	337	2.7
3	268	63	337	2.7
4	268	62	337	2.7
5	268	61	337	2.7
6	268	60	337	2.7
7	267	61	337	2.7
8	268	61	337	2.7
9	267	60	337	2.7
10	267	61	337	2.7

Table 33. Contact times with Psachna GCS - worst case

Worst case - min contact times			
Avg Contact Duration (sec)	Min Contact Duration (sec)	Max Contact Duration (sec)	Contacts per day
267	60	337	2.7

Table 34. Contact times with Nemea GCS

Orbital Plane ID	Avg Contact Duration (sec)	Min Contact Duration (sec)	Max Contact Duration (sec)	Contacts per day
1	268	61	337	2.6
2	268	60	337	2.6
3	267	62	337	2.6
4	268	62	337	2.6
5	268	60	337	2.6
6	268	61	337	2.6
7	267	62	337	2.7
8	268	62	337	2.6
9	267	61	337	2.7
10	268	64	337	2.7

Table 35. Contact times with Nemea GCS - worst case

Worst case - min contact times			
Avg Contact Duration (sec)	Min Contact Duration (sec)	Max Contact Duration (sec)	Contacts per day
267	60	337	2.6

13. **Space Debris Mitigation Analysis**

13.1. Space System Fragmentation and Explosion Risk

The mission plan does not involve any intentional break-up in orbit. The components susceptible to accidental breaking-up and releasing debris are the two GOMspace NanoPower BP8 battery packs, the CubeSpace RWs and the Enpulsion NANO propulsion system.

The BP8 battery packs themselves are composed of lithium-ion battery cells in an aluminum case, with an integrated protection system, cell balancing, cell fault detection and heating system. Each lithium cell (GOMspace NanoPower Battery 3000mAh - Lithium Ion 18650 cells), is “equipped with a current-interrupt device (CID) and a vent. The CID is triggered by an increase of an internal pressure because of overcharging or overheating of the cell. The estimated threshold is 1.017 MPa. Triggering the CID causes disconnecting conductive paths inside of a cell to prevent further (dis)charge and it causes a permanent open circuit across the cell. The vent is triggered by an internal pressure exceeding an estimated value of 1.906 MPa, which results into releasing accumulated gases inside of the cell to prevent or reduce a risk of a rupture or an explosion.” All the above, in conjunction with flight acceptance testing by the manufacturer, ensure the compliance and reserve risk minimizing mitigation measures for a battery cell/pack failure contingency.

To address the potential fragmentation risks posed by the RWs, several proactive measures shall be implemented. The identification and assessment of risks such as mechanical overloads, bearing wear, and electrical failures—factors that can lead to overheating or uncontrolled spins—shall be a priority. Mitigation strategies will be integrated into the system's design, including over-speed protection systems to automatically shut down reaction wheels when they exceed safe limits, and thermal loads monitoring and management to prevent overheating. Additionally key parameters like temperature, vibration, and speed shall be monitored, enabling early detection of any degradation. Predictive analytics could also have a role in optimizing maintenance schedules, reducing the risk of unexpected failures. Finally, safe failure mechanisms, such as fragmentation shields are be incorporated in CubeSpace reaction wheels.

To minimize fragmentation and explosion risks posed by a CubeSat’s electrical propulsion subsystem, the following strategy should be considered. Firstly, identifying and assessing the risks associated with high-voltage electrical arcing, thermal overload, and potential propellant leaks need to be addressed, as these can lead to overheating or overpressure failures. To mitigate these risks, the system design should include robust high-voltage insulation and advanced thermal management solutions. More detailed information from the provider regarding the Enpulsion NANO propulsion system is required, particularly to confirm whether pressure relief mechanisms are incorporated to safely vent excess propellant pressure. Additionally, further data on the propellant tank is needed, including the presence of sensors for monitoring pressure and temperature, as well as the specifications of the enclosure container. Evaluating whether graceful shutdown systems are in place to automatically disengage high-voltage components during a failure is also a priority. Together, these strategies will significantly reduce the likelihood of system fragmentation or explosion.

13.2. Health Monitoring

System health monitoring is facilitated through an array of sensors that capture the functional and environmental state of all subsystems throughout mission lifetime. Solar arrays are equipped with temperature sensors, and all power channels are constantly monitored for voltage and power. Every subsystem offers a diagnostic function that reports the health status of the system, such as operational capability, temperature, voltage supply levels etc.
Using this feedback the operators can deduce the system health status and intervene if required. Additionally, automatic failsafes are incorporated on the electrical power system, protecting channels from short-circuits, disconnecting batteries in the event of a malfunction and placing the satellite in a safe mode should a fault condition be detected.

13.3. Collision Risk Analysis

The main requirement is that the cumulative collision probability of each spacecraft shall not exceed a maximum value of 10^{-4} for spacecrafts in LEO.

The first step that needs to be done is to calculate the spacecraft's cross section for different orientations, via the DRAMA - CROC (CROss Section of Complex Bodies - v.2.1.0) tool. The spacecraft is an 8U CubeSat equipped with two deployable Solar Panels, whose characteristics are shown in the table below.

Table 36. Inputs for CROC

Main Structure	454 mm x 226.3 mm x 100 mm
Single Deployed Solar Panel (x2)	326.55 mm x 167.17 mm x 5.2 mm
Mass	11.3 kg

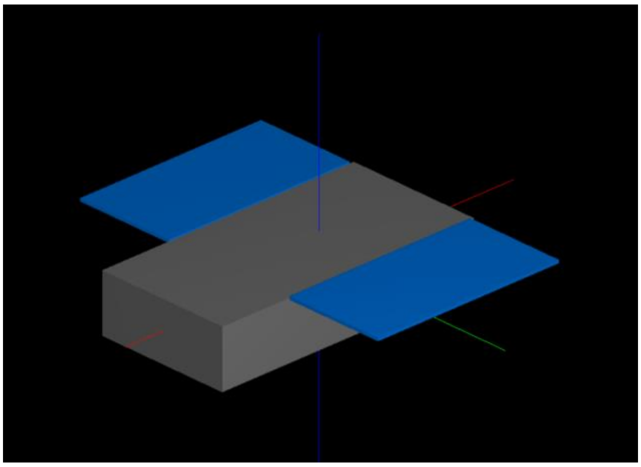

Figure 46. CROC 3D model

Table 37. Calculated cross-sections for each orientation

Minimum Cross Section normal operation - 2U side	Average Cross Section (randomly tumbling case)	Maximum Cross Section
$243\ cm^2$	$1294\ cm^2$	$2133\ cm^2$

13.3.1. Collision Risk Assessment – MIDAS

According to ESSB-ST-U-007 Issue 1, in order to mitigate the risk of accidental break-up caused by a collision, the developer of a spacecraft operating in Earth orbit shall quantify the probability that space debris or meteoroid impact causes the spacecraft to break-up, including the impacts with space debris and meteoroids larger than 1 mm and smaller than 1 cm, and the impacts with space debris and meteoroids larger than 1 cm [58]. The DRAMA - MIDAS (MASTER-based Impact Flux and Damage Assessment Software) tool is used to model the collision flux and damage statistics.

Table 38. MIDAS simulation Input Parameters

Begin date	11/01/2027
End date	11/01/2030
Semi-major axis	6928.1 km
Inclination	61°
Eccentricity	0.001
S/C cross-section	0.21 (worst case)
Drag coefficient - C_D	2.2
Reflectivity coefficient - C_r	1.2
Mass	$11.3\ kg$

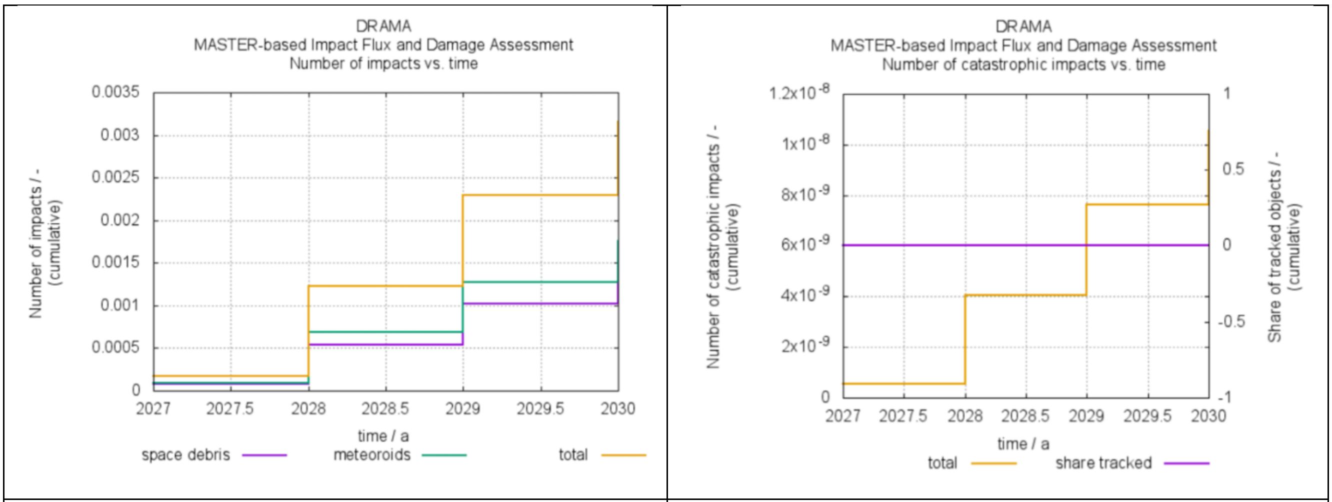

(a) (b)

Figure 47. Number of impacts (a) and catastrophic impacts (b) vs time for objects between 1 mm and 1 cm

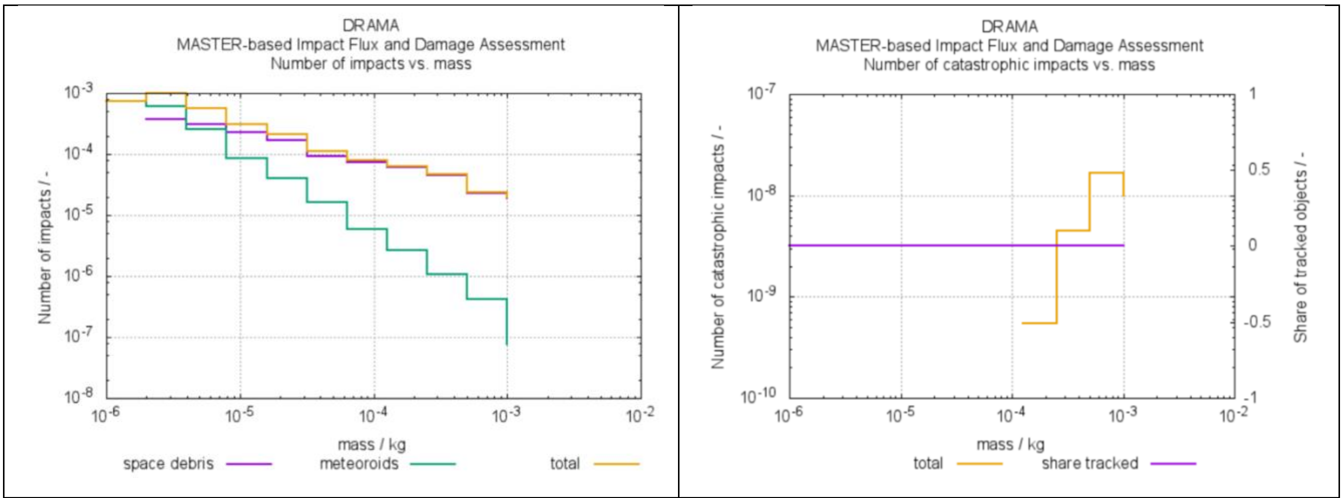

(a) (b)

Figure 48. Number of impacts (a) and catastrophic impacts (b) vs mass for objects between 1 mm and 1 cm

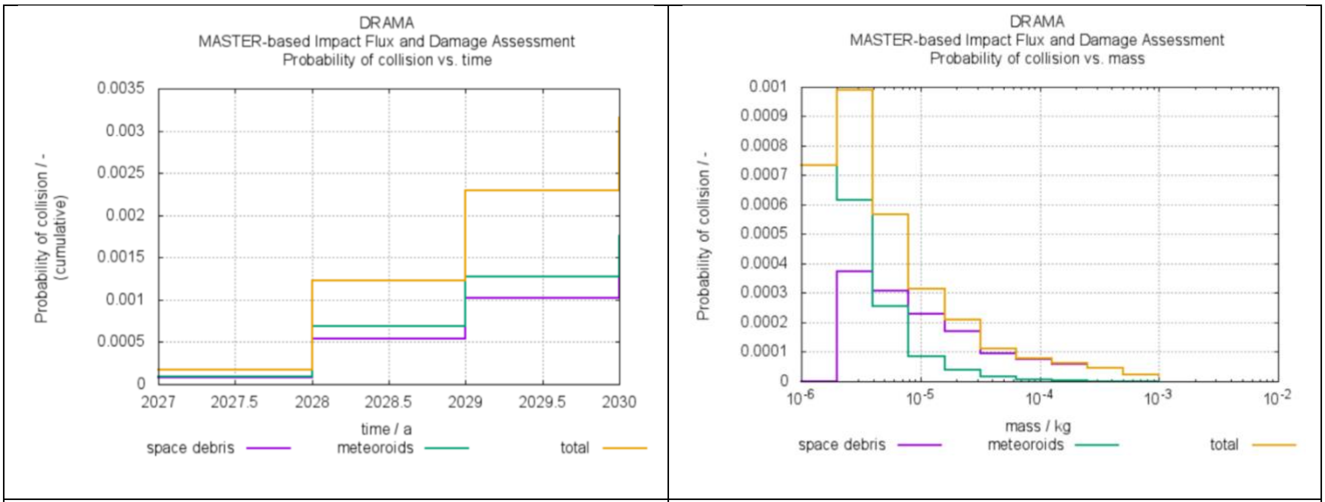

(a) (b)

Figure 49. Probability of collision vs time (a) and vs mass (b) for objects between 1 mm and 1 cm

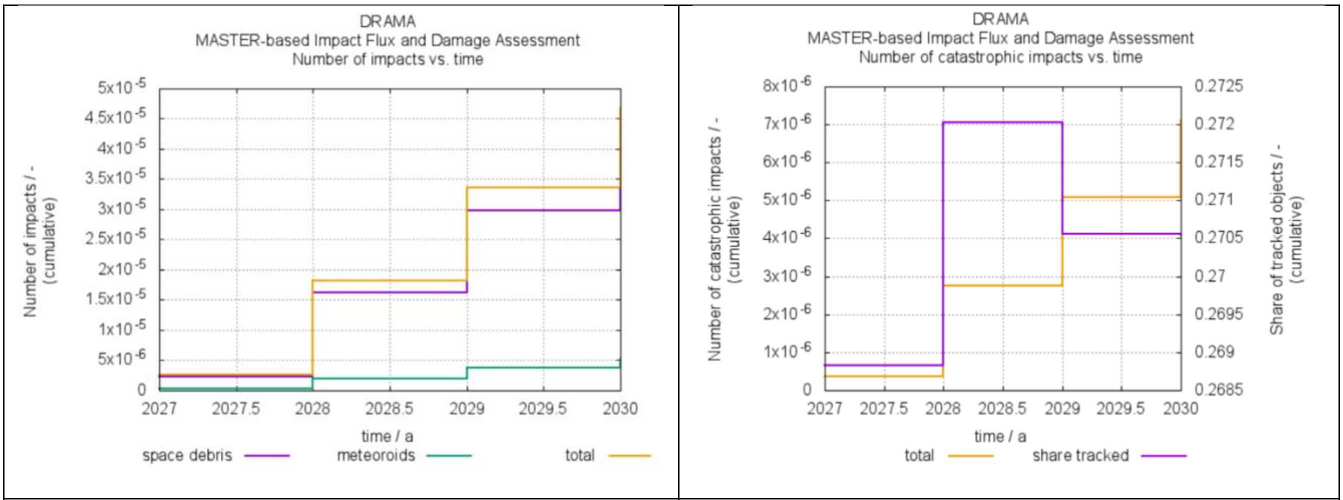

(a) (b)

Figure 50. Number of impacts (a) and catastrophic impacts (b) vs time for objects above 1 cm

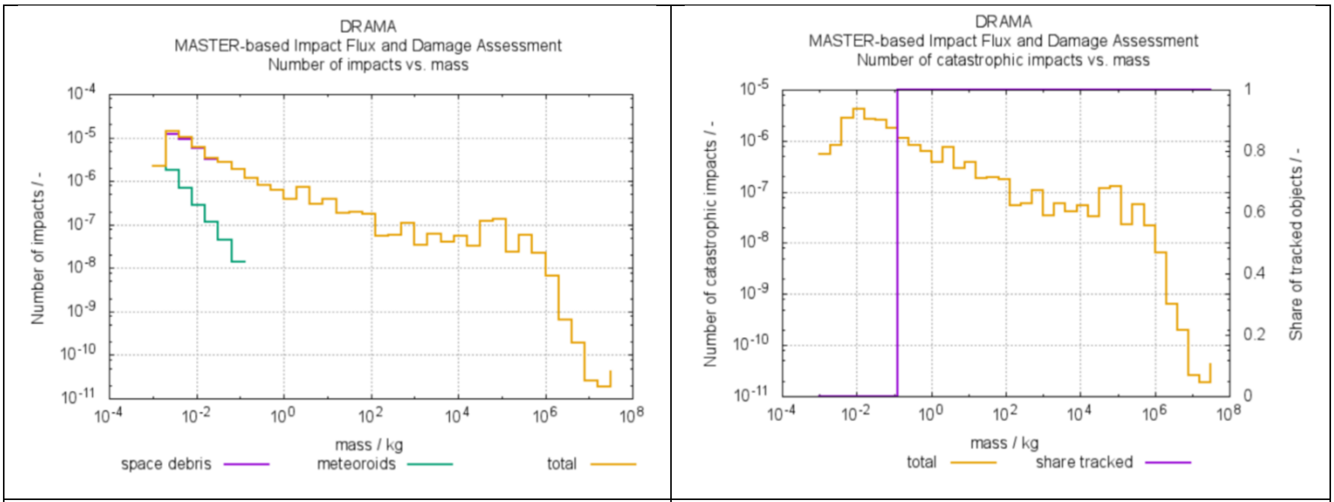

(a) (b)

Figure 51. Number of impacts (a) and catastrophic impacts (b) vs mass for objects above 1 cm

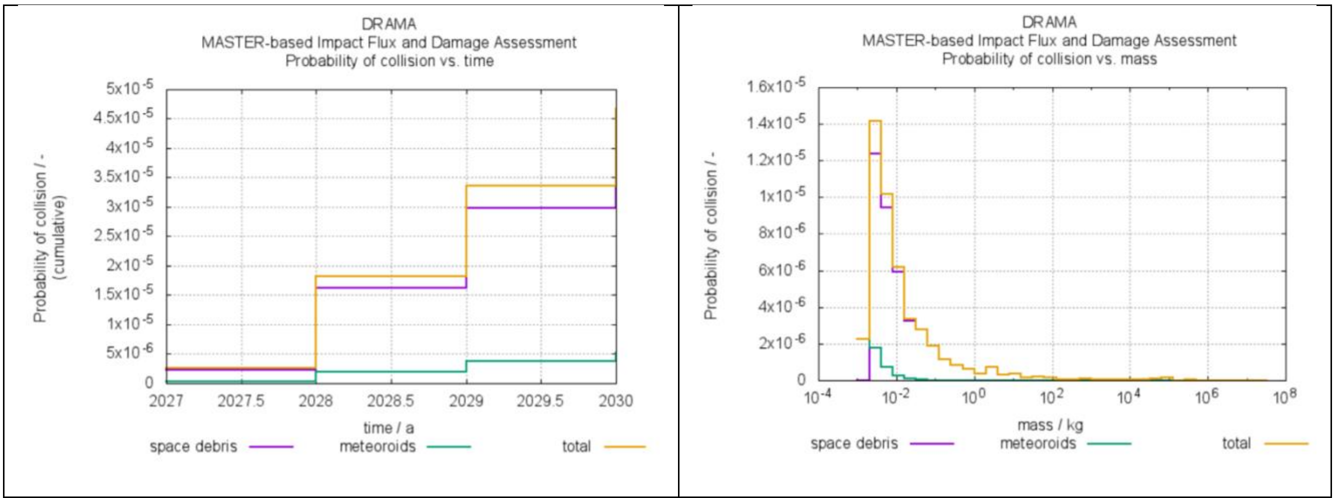

(a) (b)

Figure 52. Probability of collision vs time (a) and vs mass (b) for objects above 1 cm

Since the total number of catastrophic impacts N is known, the probability of catastrophic impacts can be calculated via: $P_{cat} = 1 - e^{-N}$ [59]

Table 39. Probability of catastrophic impact before the end of the mission

Object Diameter	1 mm to 1 cm	Above 1 cm
Probability of catastrophic impact during 2029	$7.63 \cdot 10^{-9}$	$5.09 \cdot 10^{-6}$
Probability of catastrophic impact during 2030	$1.06 \cdot 10^{-8}$	$7.11 \cdot 10^{-6}$

The probability of catastrophic impact is l below the 10^{-4} limit for a LEO mission.

13.4. Orbital Decay Analysis – OSCAR

Three different sets of space debris requirements are applicable to the Spacecrafts: Greek national law (assuming they are owned by UOA), European regulations, FCC regulation to which USA based launchers are subject to. The strictest of the three requirements must be followed to ensure full compatibility with all regulatory authorities involved. Greek law requires the submission of an environmental impact study, which will be evaluated following “european regulation and established good practices” (Greek legislation does not specify any national regulations for the environmental impact report). ESA and FCC regulations both require that “spacecraft disposal as soon as practicable but no later than 5 years after mission ends”. Therefore, the spacecrafts shall fulfill the 5-year decay requirement (MR-MIS-060).

The spacecrafts shall have stationkeeping capabilities and, thus, their original altitude of $550\ km$ shall be maintained for the full 3-year nominal operations phase. Based on the ΔV budget, in the worst case $70\ m/s$ will be allocated to lower the spacecraft's altitude before allowing them to passively decay. It is assumed that a single maneuver of $70\ m/s$ is performed in a random point of the initial orbit. Then, via the Vis-viva equation it is possible to calculate the new orbit after the maneuver.

$$u^2 = GM\left(\frac{2}{r} - \frac{1}{a}\right)$$

where
u is the orbital velocity of the satellite
r is the distance between the satellite and the Earth’s center
a is the length of the semi-major axis
G is the gravitational constant ($6.67 \cdot 10^{-11}\ N \cdot m^2 \cdot kg^{-2}$)
M is the Earth’s mass ($5.972 \cdot 10^{24}\ kg$)

The orbital velocity of spacecraft in a circular orbit with 550 km of altitude (or semi-major axis $a = 6928$) is 7.59 km/s. By performing a retrograde burn of 70 m/s and using the spacecraft’s r and new orbital velocity as inputs to the Vis-viva equation, the new semi major axis is calculated to be $a' = 6811\ km$.
Since a retrograde burn was performed at a point of circular orbit, that point is the point of the apoapsis. So, the point of periapsis can be calculated via: $r_p + r_a = 2a\ \ or\ \ r_p = 2a - r_a = 6694.96$. Finally, the eccentricity of the new orbit is calculated via $e = \frac{r_a - r_p}{r_a + r_p} = 0.017$.
By having these elements to be used as inputs in DRAMA – OSCAR tool, the orbital decay analysis can be performed. It results that the spacecraft shall deorbit in 1.7 years.

Table 40. OSCAR simulation Input Parameters

Begin date	$01/11/2030$ (solar min)
Semi-major axis	6811 km
Inclination	61°
Eccentricity	0.017
S/C cross-section	0.1 (tumbling S/C)
Drag coefficient - C_D	2.2
Reflectivity coefficient - C_r	1.2
Mass	11.3 kg
Solar & Geomagnetic activity model	Latest prediction

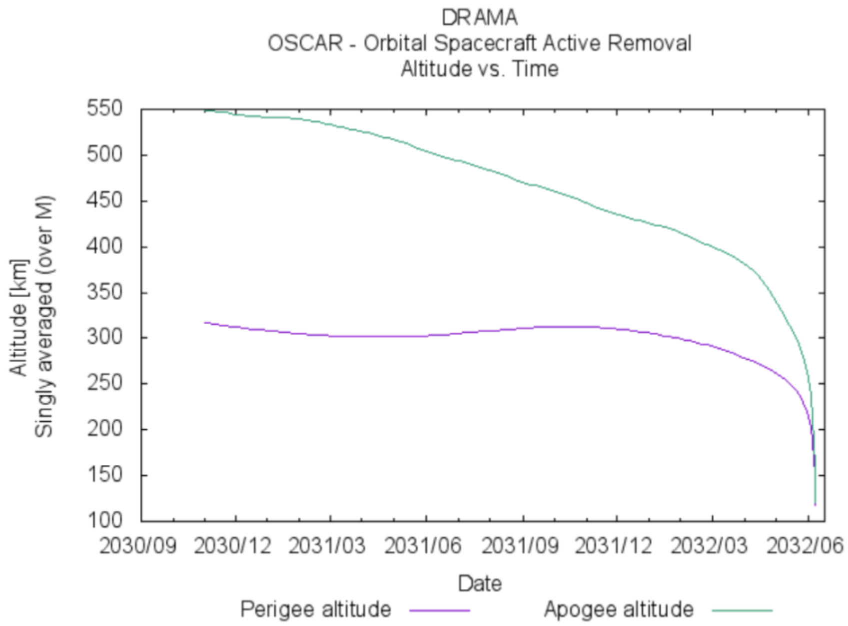

Figure 53. Orbital decay analysis - Passive disposal after deorbit maneuver

In the worst case in which a ΔV of $70\ m/s$ is used to lower the spacecraft's altitude, the mission is compliant with the 5-year deorbit requirement.

13.5. Spacecraft Re-entry Analysis - SARA

The spacecraft's re-entry is modeled through DRAMA's SARA (Spacecraft Entry Survival Analysis) tool.

Table 41. SARA simulation Input Parameters

Begin date	01/11/2032
Semi-major axis	6498 km
Inclination	61°
Eccentricity	0
Shape	Sphere
Radius	0.1 m^2 (because it corresponds to an object with a mass of 11.8 kg)
Model Properties	Solid object
Material	Drama-AA7075

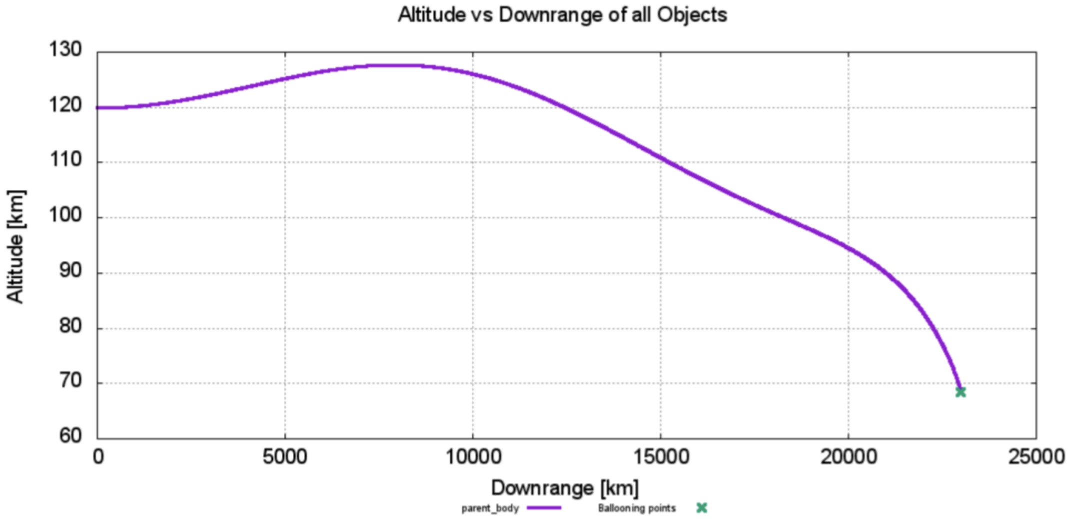

Figure 54. SARA re-entry simulation – Altitude vs Downrange

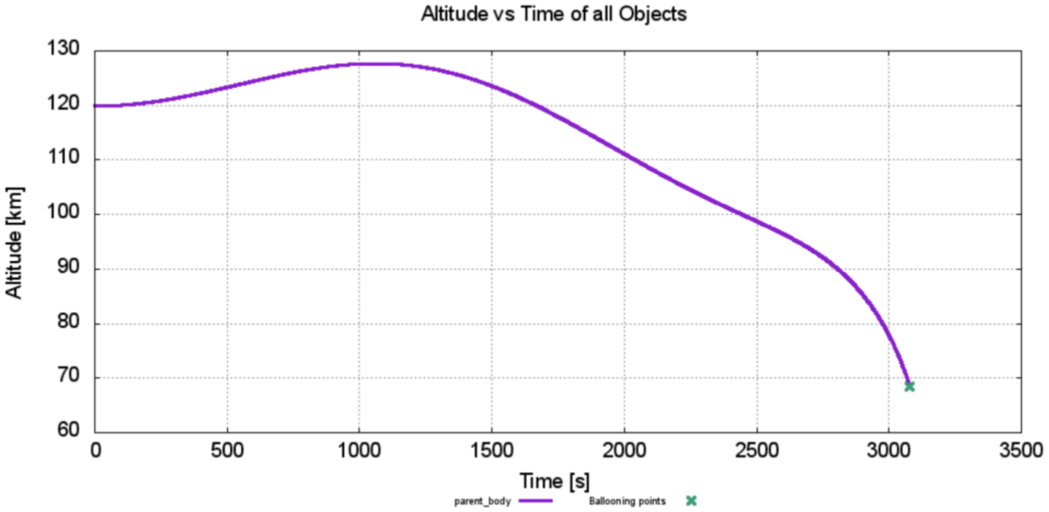

Figure 55. SARA re-entry simulation – Altitude vs Time

The analysis concluded that the spacecraft is completely disintegrated at 68.4 km.

13.6. Passivation Strategy

After nominal operations have been concluded the cubesats are passivated before being left to decay into the atmosphere. The passivation process is initiated via a two-step activation process, to protect against accidental passivation.

Table 42. Passivation steps

1	Before starting the passivation process, ensure that the CubeSat has completed its primary mission objectives and that all important data and mission information have been transmitted to the ground station.
2	Inform relevant space agencies and authorities of the passivation plan and the CubeSat's deorbit process.
3	The propulsion subsystem shall exhaust all propellant through depletion burn(s).
4	All nonessential subsystems and payload are switched OFF.
5	The CubeSat safe mode is activated.
6	Deactivation of the Solar Panels to stop the power generation.
7	Discharge the batteries to a safe level to ensure that no excess energy remains in the batteries.
8	Terminate all communication with the CubeSat from ground stations, as well as any uplink or downlink operations.
9	Ensure the CubeSat remains in a passive state by monitoring for unintentional system reactivation.

14. Environmental Design

In this section is described the expected launch environment for three different launch vehicles; SpaceX's Falcon9, Rocket Lab's Electron and Arianegroup's Vega-C.

14.1. Falcon 9 Launch Environment

The spacecrafts shall be able to withstand the Quasi-Static load factors of the CubeSat Dispenser, as stated in Falcon Payload User's Guide. So, spacecrafts shall be able to withstand a Quasi-Static load of 17g at their expected Y_{PL} and Z_{PL} directions and 10g at their expected X_{PL} direction when adapted into the launcher as this is defined in Falcon Payload User's Guide.

Table 43. Falcon 9 Quasi-Static load factors of the CubeSat Dispenser

Axial (X_{PL}) Load Factor (g)	Lateral (RSS Y_{PL}, Z_{PL}) Load Factor (g)
10	17

The load factors stated above are defined as "combined loads," which include all contributions from static loads, low frequency loads (<100 Hz), and high frequency loads (> 100 Hz). Additionally, spacecrafts shall be able to survive under the sinusoidal MPE, acoustic MPE, shock response spectrum MPE, random vibration MPE and the thermal environment inside the launcher fairing.

Table 44. Falcon 9 maximum predicted sinusoidal vibration environment

Frequency (Hz)	Sinusoidal Vibration MPE (g)	
	Axial X_{PL}	Lateral Y_{PL}, Z_{PL}
5	1.4	1.5
100	1.4	1.5

Frequency (Hz)	Acoustic MPE
31.5	126.1
63	128.6
125	132.6
250	134.5
500	132.3
1000	127.4
2000	123.8
4000	120.8
8000	117.8
OASPL (dB)	139.3

(a)

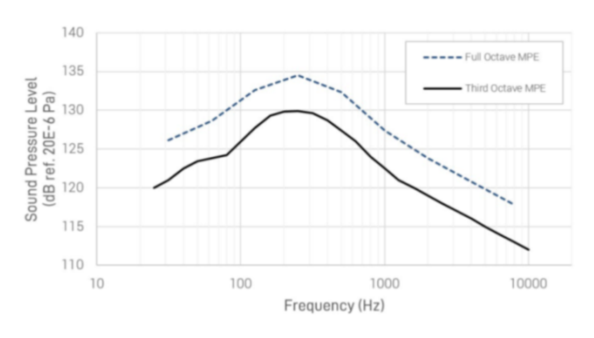

(b)

Figure 56. Falcon 9 full octave acoustic MPE (a) and MPE acoustic environment graphs (b)

Frequency (Hz)	MPE Induced by Launch Vehicle and Co-Payload(s) SRS (g)	Maximum Allowable Induced by Payload Separation System SRS (g)
100	30	30
1000	1000	--
1950	--	2850
10000	1000	2850

(a)

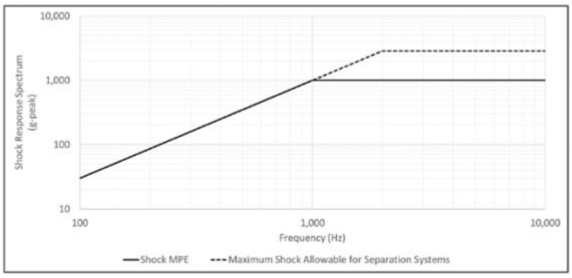

(b)

Figure 57. Falcon 9 Payload mechanical interface shock for fairing deployment and Co-Payload separation(s) and for a single separation system values (a) and graph (b)

Frequency (Hz)	Random Vibration MPE (P95/50), All Axes
20	0.01
50	0.015
700	0.015
800	0.03
925	0.03
2000	0.00644
GRMS	**5.57**

(a)

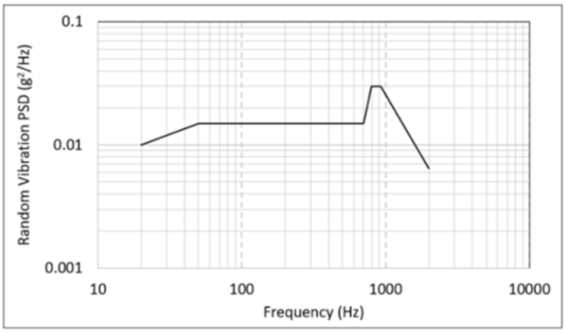

(b)

Figure 58. Falcon 9 random vibration MPE values (a) and graph (b) derived at a P95/50 level

The Launch Vehicle fairing is designed such that the temperature seen by the Falcon Payload never exceeds the temperature shown below.

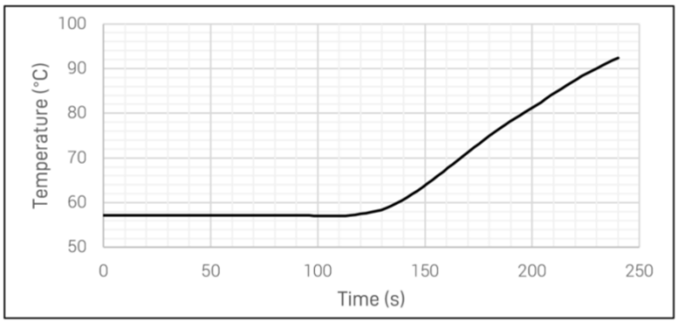

Figure 59. Falcon 9 maximum fairing spot temperature experienced in the launcher

14.2. Electron Launch Environment

Electron can accommodate a diverse array of payload configurations, ranging from a single primary microsatellite to multi-satellite missions that include multiple microsats and CubeSats [60].

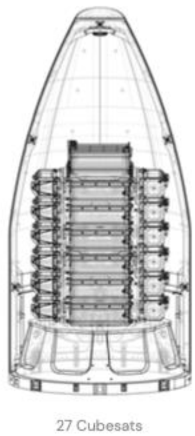

Figure 60. Electron fairing carrying 27 CubeSats

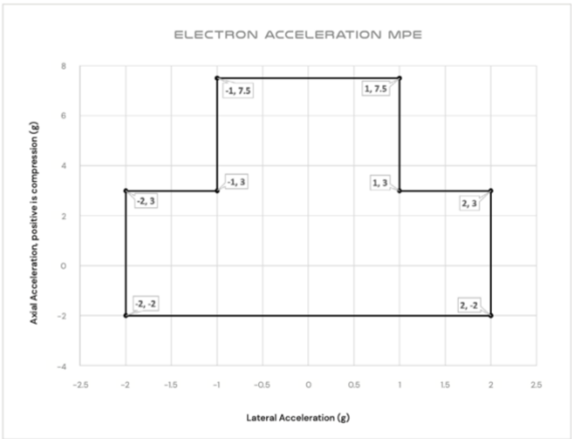

(a)

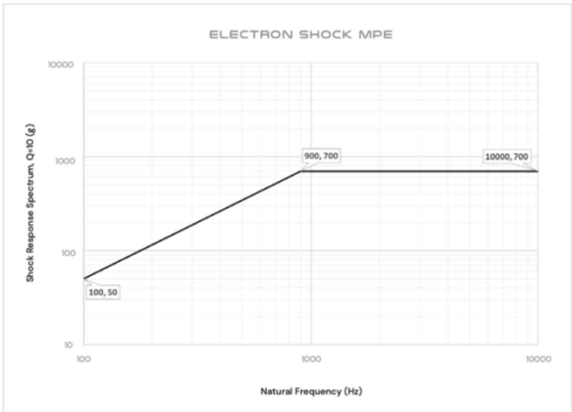

(b)

Figure 61. Electron acceleration MPE (a) and shock MPE (b)

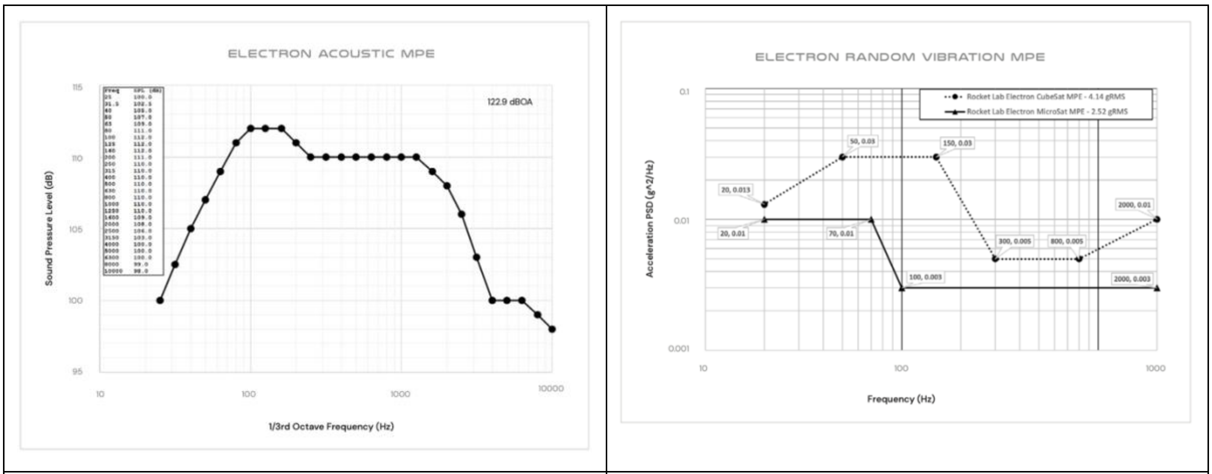

(a) (b)

Figure 62. Electron acoustic MPE (a) and random vibration (b)

14.3. Vega-C Launch Environment

According to SSMS Vega-C User's Manual, it uses several carrying systems to carry and deploy Small S/C. The ones used to mount CubeSat deployer PODs are the SSMS modular carrying system (primarily used for a cluster of small spacecrafts of varying sizes and masses) at Hexa positions and the VAMPIRE 937 MPL (used for a primary large payload accompanied by up to six nanosatellites) in the Towers positions [61].

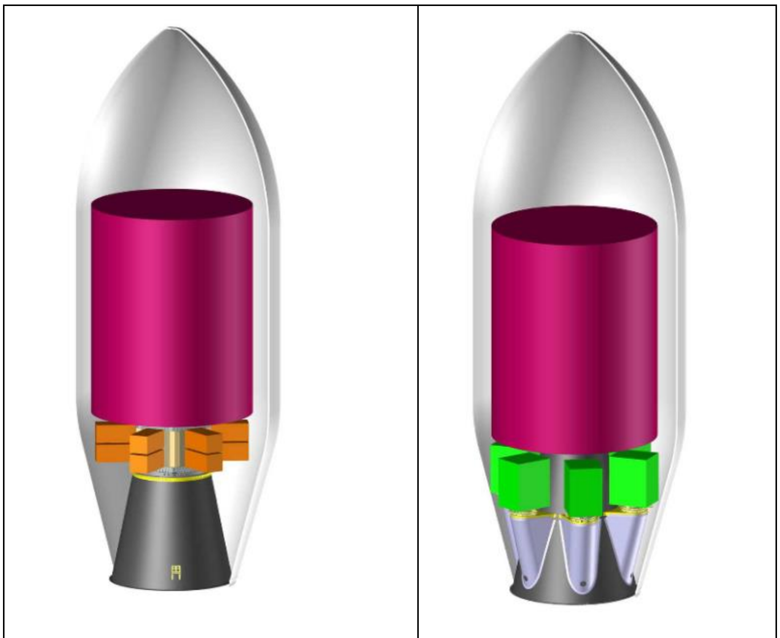

(a) (b)

Figure 63. SSMS configurations Hex-1 and Hex-2 (orange blocks) (a) and VAMPIRE 937 MPL Towers (green blocks) (b)

Table 45. Vega-C Quasi-Static load factors

Quasi-Static load factors	
Lateral direction load factor (g)	Longitudinal direction load factor (g)
10	10

Table 46. Vega-C Sinusoidal vibration environment test levels

Sine environment (0-peak) [g]			
Longitudinal direction			
Frequency band [Hz]	5 - 70	70 - 110	110 - 125
Qualification levels (O-peak) [g]	2.5	1.25	1.25
Acceptance levels (O-peak) [g]	2.0	1.0	1.0
Lateral direction			
Frequency band [Hz]	5 - 70	70 - 110	110 - 125
Qualification levels (O-peak) [g]	2.5	1.25	1.25
Acceptance levels (O-peak) [g]	2.0	1.0	1.0

Table 47. Vega-C random vibration MPE at SSMS Hexa positions (a) and Shock levels at SSMS Hexagonal module positions and VAMPIRE 937 positions

Random levels (SSMS Hexagon Positions)	
Frequency Band [Hz]	PSD, Power Spectral Density (1) (10^{-3} g^2/Hz)
20 - 50	7.1
50 - 100	7.1 – 14.2
100 - 200	14.2 – 35.5
200 - 500	35.5
500 - 1000	35.5 – 14.2
1000 - 2000	14.2 – 7.1
G_{RMS}	5.4 g
Duration	60 s

(a)

Frequency (Hz)	Flight limit level (dB) - Launch Vehicle event (SSMS Hexagon Positions and VESPA+R inner position and VAMPIRE 937 positions)
100	30
2 000	1500
10 000	1500

(b)

14.4. Space Environment

In order to ensure the nominal operation of the spacecrafts during their 3 year lifespan, the radiation environment they are to be exposed to shall be identified. Thus, the expected Total Ionising Dose (TID) needs to be calculated. This is done via SPENVIS in the following steps:

1. Define trajectory

The duration of the mission is set to 3 years and it is set to start in 2024. This is done to account for the worst case scenario of a Solar Maximum, that according to NOAA's Space Weather Prediction Center it should happen between late 2024 and early 2026 [62].

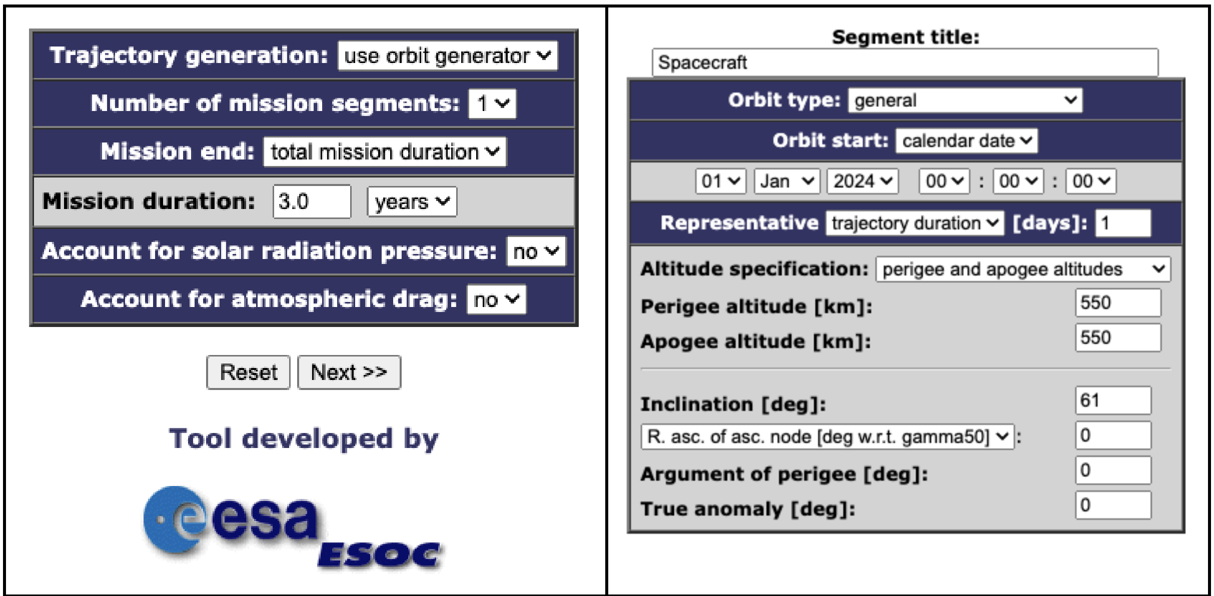

(a) (b)

Figure 64. Definition of the mission's duration (a) and orbital parameters (b) in SPENVIS

2. Include Radiation Sources and Effects into the model

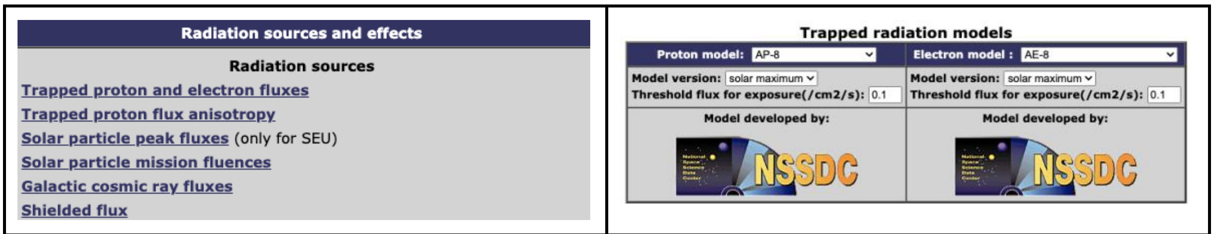

(a) (b)

Figure 65. Radiation sources (a) and Trappes proton and electron models

Add this step the solar maximum models are used, while the threshold flux for exposure is set to a minimal value for increased accuracy.

The trapped proton anisotropy was calculated with the Badhwar & Konradi 1990 MAX model. Solar particle peak fluxes were simulated via the CREME-96 model that accounted for the worst day in terms of radiation environment for ions from hydrogen (H) to uranium (U). Tha same range of ios was used to calculate the solar particle mission fluences and the GCR spectra via NASA's ESP-PSYCHIC model and ISO-15390 standard model respectively. To account for the worst case, the GCR effects are calculated during a solar minimum period because during that time the shielding from the Sun's magnetic field is at its minimum.

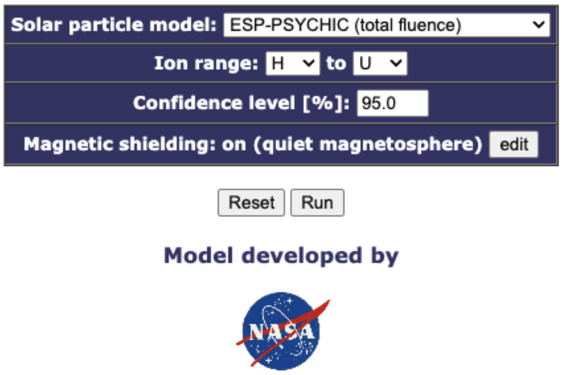

(a)

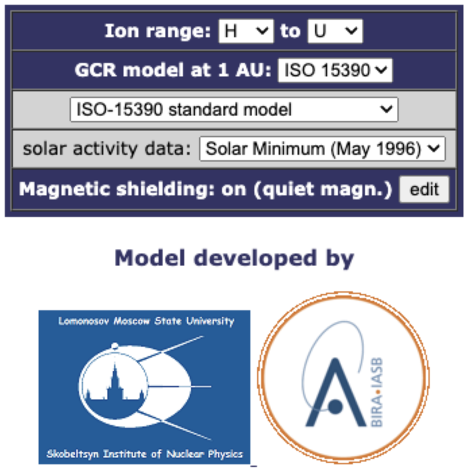

(b)

Figure 66. Models used for solar particle mission fluences (a) and GCR (b)

3. Calculate TID

After considering the radiation sources stated above, the TID was calculated via SHIELDDOSE-2 dose model. The shielding configuration used was the "center of Al spheres" as this deemed to be the most suitable one for a CubeSat mission. Due to Cubesats' small form factor that promotes minimal shielding, all of their components are subjected to radiation flux from all directions and, thus, a spherical model would be the optimal available option.

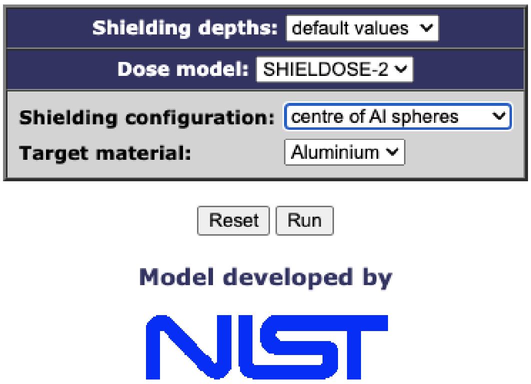

Figure 67. TID model used

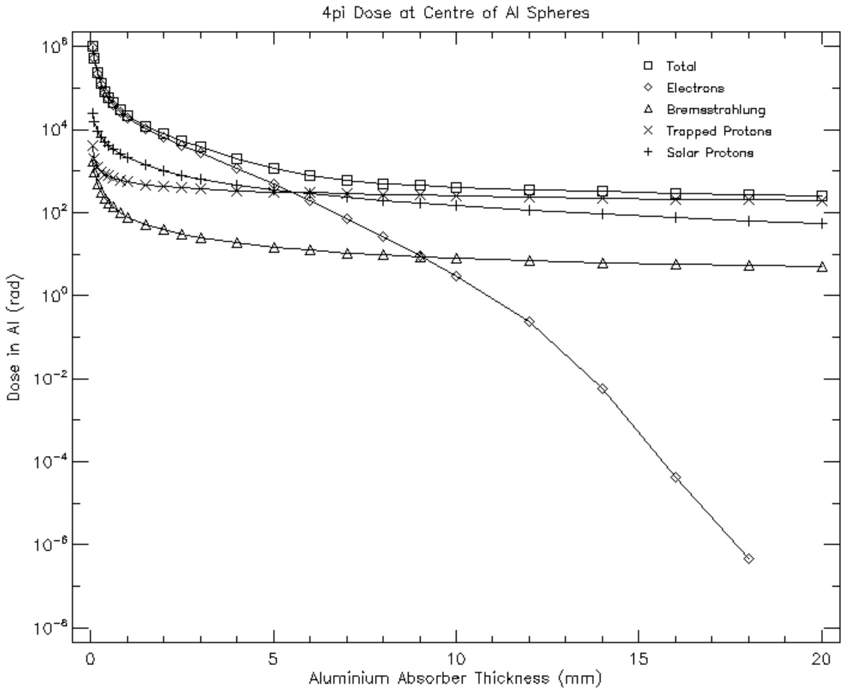

Figure 68. TID for 3 years as a function of shielding thickness

Even though the mission is baselined for an altitude of 550 km, in the following table are presented the TIDs that correspond to the altitudes and shielding thickness that were considered in the orbital design trade off. Two shielding thickness options, 1.5 mm and 2 mm, of Aluminum were considered. The current baseline is 2 mm of Aluminum, however the option of 1.5 mm is used to account for the worst case.

Table 48. TID for different altitudes and shielding thickness for circular orbit with 61° of inclination

Altitude (km)	TID in 3 years (Solar Max) for 1.5 mm of Al (kRad)	TID in 3 years (Solar Max) for 2 mm of Al (kRad)
750	22.6	14.6
700	19.5	12.6
650	17	11
600	14.5	9.4
550	12.2	7.9

Based on the environmental simulation presented, 12.2 kRad is induced to the subsystems for the nominal 3 years mission duration. By comparing the component TID qualification level against the calculated TID it is possible to evaluate the capability of the equipment to withstand the expected space environment conditions. Since all components have higher TID ratings the system is expected to operate nominally for 3 years of mission.

14.5. Environmental Qualifications of Components

In the following table, the environmental ratings of the components are presented. Educated guesses are used when no information was found.

Table 49. Environmental qualification status of components

Components	Temperature Qualification (°C)	Radiation Tolerance (kRad)	Random Vibration (gRMS)
NanoDock DMC-3	-40 to +85	Not applicable (no active components)	14.1
NanoMind A3200	-30 to +85	20	14.1
NovAtel OEM-719 GPS kit	-40 to +85	18	14.1
NanoPower P80 System	-40 to +85	20	14.1
NanoPower BP8	-10 to +50	15	14.1
NanoPower DSP-90deg	-55 to +95	20	14.1
Nanopower MSP-B-4x4	-55 to +175	20	14.1
ADCS Computer	-40 to +85	24	14.16
CubeTorquer CR0008	-20 to +70	24	14.16
CubeSpace Cubewheel CW0057	-20 to +80	24	14.16
CubeSense FSS	-20 to +80	24	14.16
CubeSense CSS	-20 to +80	24	14.16
CubeSense Earth	-20 to +80	24	14.16
CubeMag Compact/Deployable	-20 to +80	24	14.16
NanoCom AX100	-30 to +85	22	14.1
ANT-6F	-40 to +85	20	14.1
NanoCom Link S	-40 to +85	20	14.1
NanoCom ANT2150 DUP	-40 to +85	20	14.1
Enpulsion NANO	-20 to +40	N/A	N/A
PNT Payload	N/A	N/A	N/A

15. Space Segment

15.1. Spacecraft design

Table 50. Baseline Configuration

Subsystem	Components
CDHS	GOMspace NanoMind A3200 GOMspace DMC-3 GomSpace GPS Kit (OEM 719 +Antenna)
EPS	GomSpace NanoPower P80 System 2 x GomSspace NanoPower BP8 Body Mount Solar Array GomSpace NanoPower MSP-B-4x4 Body Mount Solar Array GomSpace NanoPower MSP-B-4x1 Deployable Solar Array GomSpace NanoPower DSP-90deg x2
ADCS	Cubespace CubeADCS Core Cubespace CubeTorquer CR0008 x3 CubeSpace Cubewheel CW0057 x4 Cubespace CubeSense Fine Sun Sensor x1 Cubespace CubeSense Coarse Sun Sensors x 6 Cubespace CubeSense Earth Cubespace CubeMag Compact Cubespace CubeMag Deployable
TTC	GomSpace NanoCom AX100 GomSpace NanoCom ANT-6F (UHF)
	GomSpace NanoCom Link-S GomSpace NanoCom ANT2150-DUP
Propulsion	Enpulsion NANO
Structure	GomSpace 8U Structure
	GomeSpace 6U Side Panels GomSpace NanoUtil MSP-FPP Flight Preparation Panel Custom mounting components (in-house)
PNT Payload	PNT Solution Generator NANOlink-boost Gen2 Transceiver GomSpace NanoCom ANT2150-DUP (S-Band) LRA

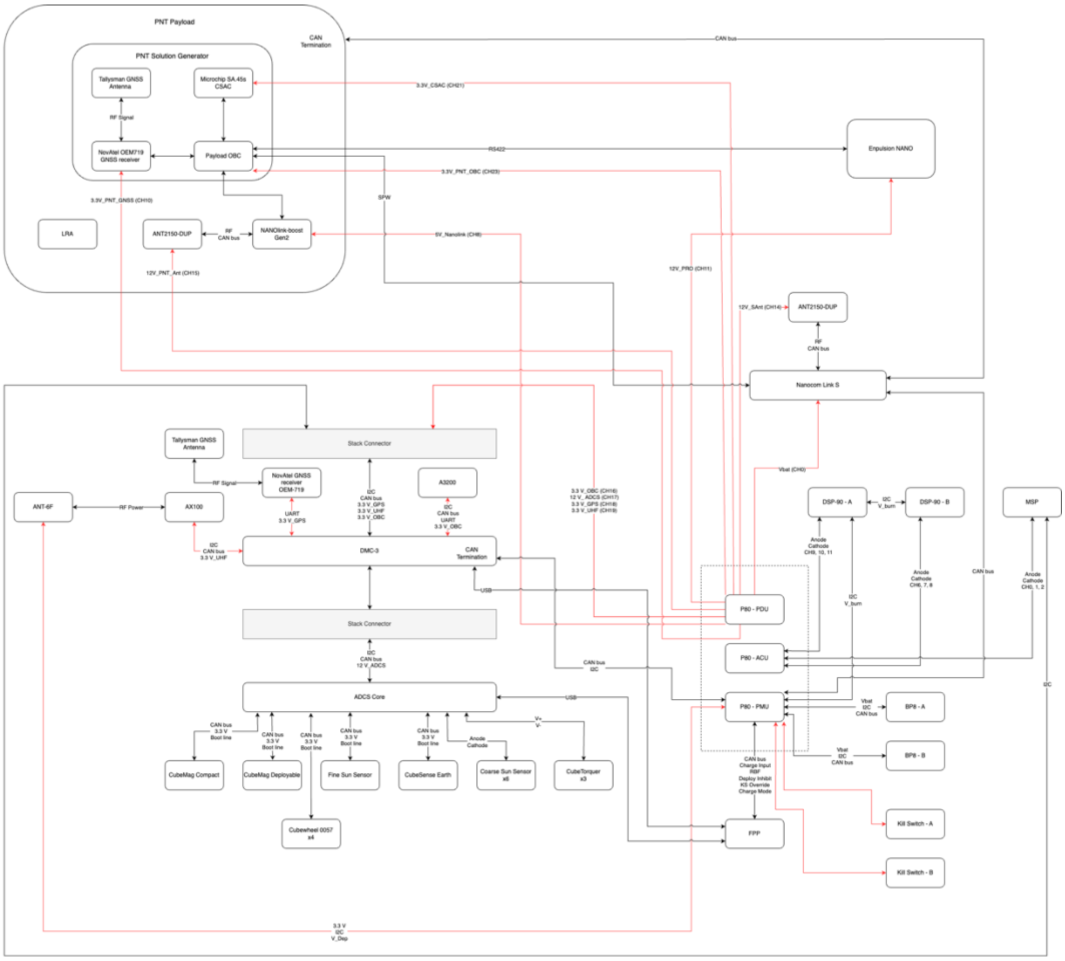

Figure 69. System diagram at signal level*

* The Propulsion subsystem is directly connected with the Payload OBC and not the BUS OBC, because the RS422 protocol that is implemented in Enpulsion NANO is not supported by GOMspace A3200. However, the Payload OBC could incorporate such an option since it is not defined yet. The product GOMspace NanoMind HP MK3 supports RS422 and it could be a viable option.

15.1.1. Subsystem Technical Specifications

15.1.1.1. Command and Data Handling Subsystem

The CDHS consists of the following components that have the features shown in the table below:

- GOMspace NanoDock DMC-3
- GOMspace NanoMind A3200
- NovAtel OEM-719 GPS kit
    - NovAtel OEM719 GNSS receiver
    - Tallysman GNSS antenna

Table 51. CDHS highlighted features

GOMspace NanoDock DMC-3	GOMspace NanoMind A3200	NovAtel OEM-719 GPS kit
• Carrier for up to 4 daughterboards • Mass 51 grams (without 4 daughterboards) • Dimensions 91.9 x 88.7 x 8.6 mm • Operating Temperature -40°C to +85°C • Provision for mounting a GPS receiver (in place of 2 daughterboards) • 4x 20-position FSI one-piece connector for daughterboards • USB to UART console interface for easy use in lab setup	• High-performance AVR32 MCU with advanced power saving features • Mass 24 gr • Dimensions 65 x 40 x 7.1 • Typical Power Consumption 0.17 W • Max Power Consumption 0.9 W • Operating Temperature -30 °C to +85 °C • Clock frequency from 8 MHz to 64 MHz • 512 KB build-in flash • Multiple CSP data interfaces: I2C, UART, CAN-Bus • 128 MB NOR flash (On two dies of 64 MB each) • 32 kB FRAM for persistent configuration storage • 32 MB SDRAM • On-board temperature sensors • Includes 3-Axis magneto resistive sensor and 3-Axis gyroscope	• Consists of: NovAtel OEM719 GNSS receiver and Tallysman GNSS antenna • Precision, position: 1.5 m • Precision, velocity: 0.03 m/s • Power: 3.3 V and <400 mA • Mass: 31 g • Size: 46 x 72 x 11 mm

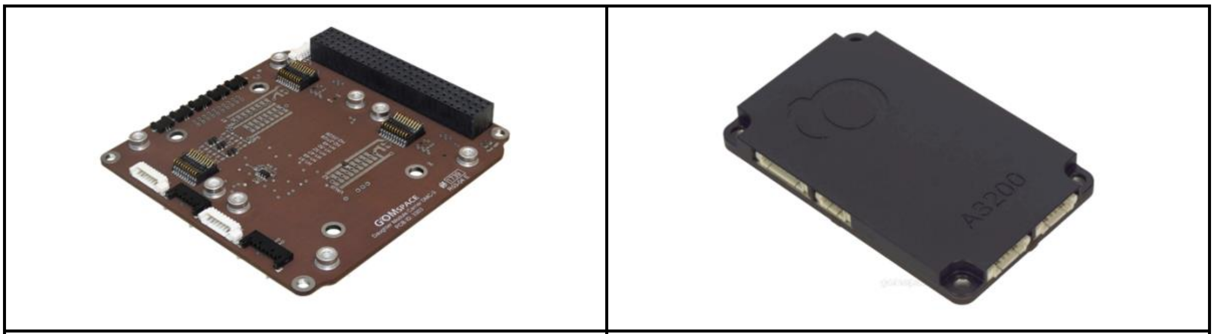

(a) (b)

Figure 70. GOMspace NanoDock DMC-3 (a), GOMspace NanoMind A3200 (b)

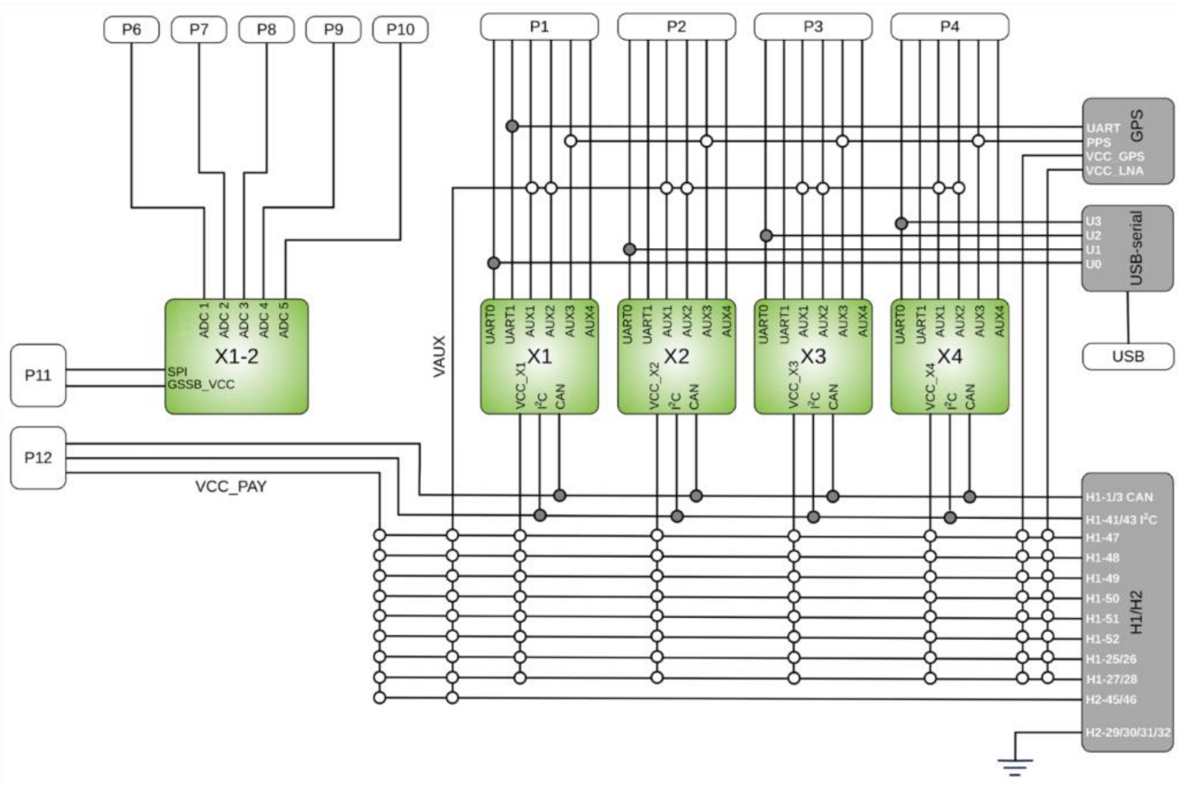

Figure 71. GOMspace NanoDock DMC-3 system diagram

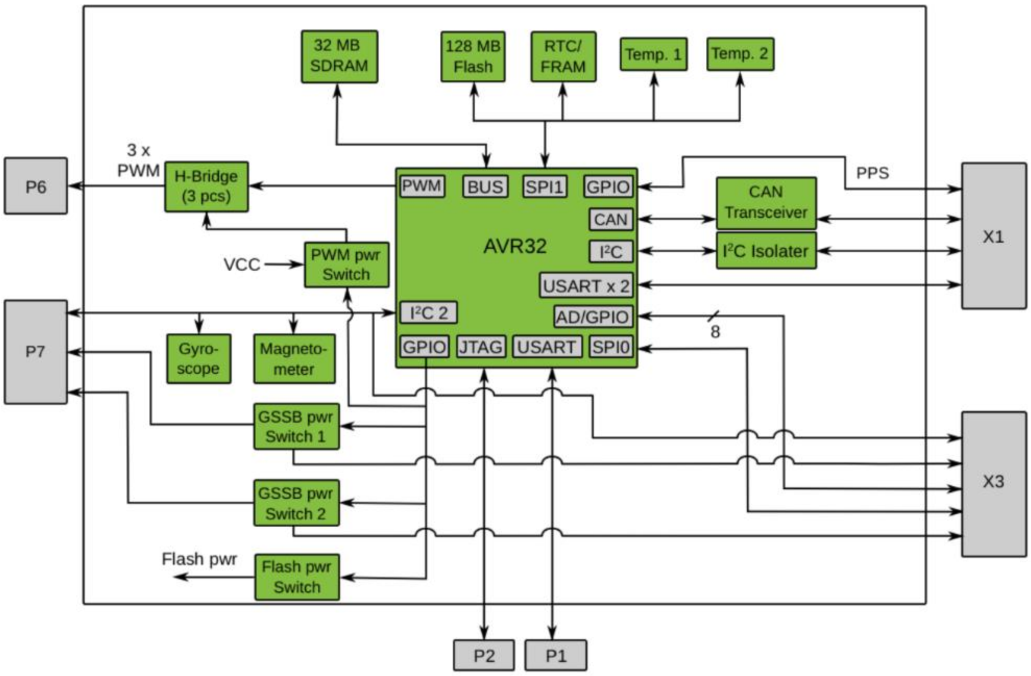

Figure 72. A3200 Block diagram

(a)

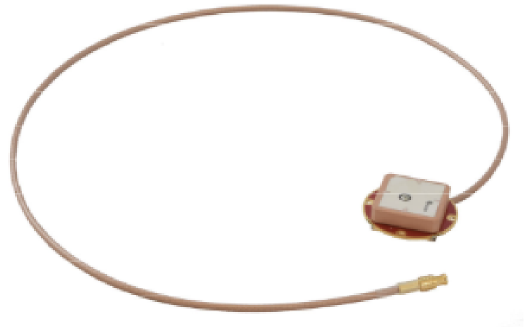

(b)

Figure 73. NovAtel OEM719 GNSS receiver (a), Tallysman GNSS antenna (b)

15.1.1.2. Electrical Power Subsystem

The EPS consists of the following components:

1. GOMspace Nanopower P80 PMU
2. GOMspace Nanopower P80 ACU
3. GOMspace Nanopower P80 PDU
4. GOMspace Nanopower BP8 x2
5. GOMspace NanoPower DSP-90deg x2
6. GOMspace Nanopower MSP-B-4x4
7. GOMspace Nanopower MSP-C-4x1

Table 52. EPS Highlighted features

GOMspace EPS (P80, BP8 and SP)
• Kill switch (KS) logic • Real-time clock (RTC) backup • 2x6 Maximum Power Point Tracking (MPPT) boost converters • KS/Remove Before Flight (RBF) inhibit switch • Software and hardware Latch-up protection (LUP). • 12 low voltage LUP channels, fed by 4 converters. All low voltage channels can be configured to an arbitrary converter in hardware. • 12 high voltage LUP channels - raw battery channels. • Nominal voltage of 28,8 V (charge to 32 V) • Maximum charge and discharge current of 4 A • Operating Temperature -40°C to +85°C • Battery Capacity 86 Wh

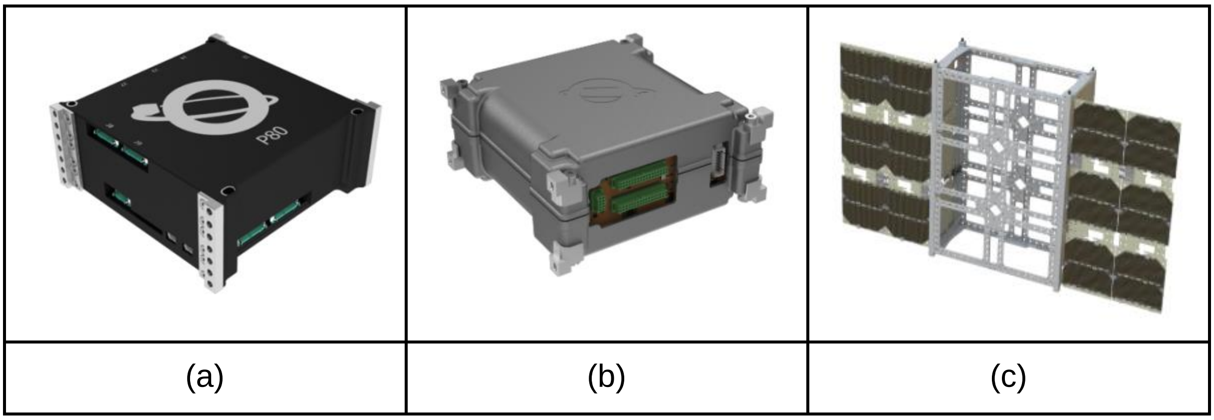

Figure 74. NanoPower P80 (a), NanoPower BP8 (b), NanoPower DSP-90deg mounted on the 6U structure (c)

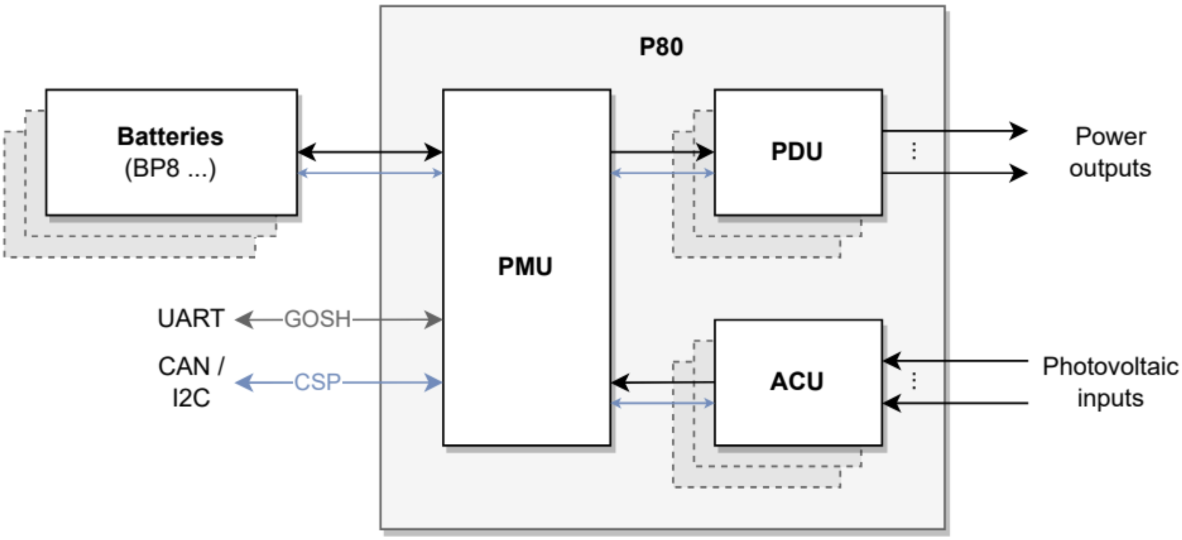

Figure 75. Block diagram of the NanoPower P80 system (The black arrows show the power paths and the blue shows communication)

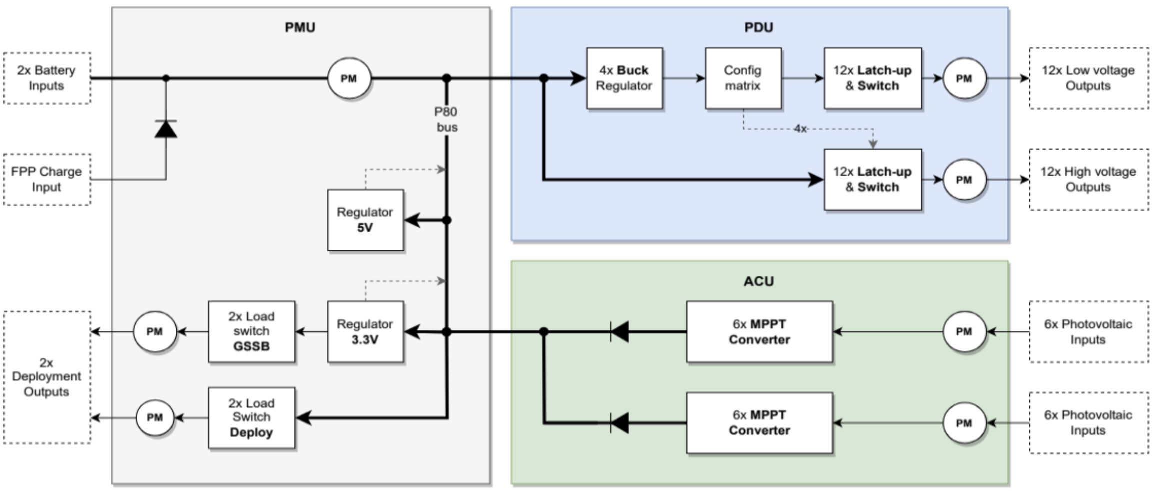

Figure 76. Block diagram of power paths in the NanoPower P80 (PM-modules indicate voltage and current readings)

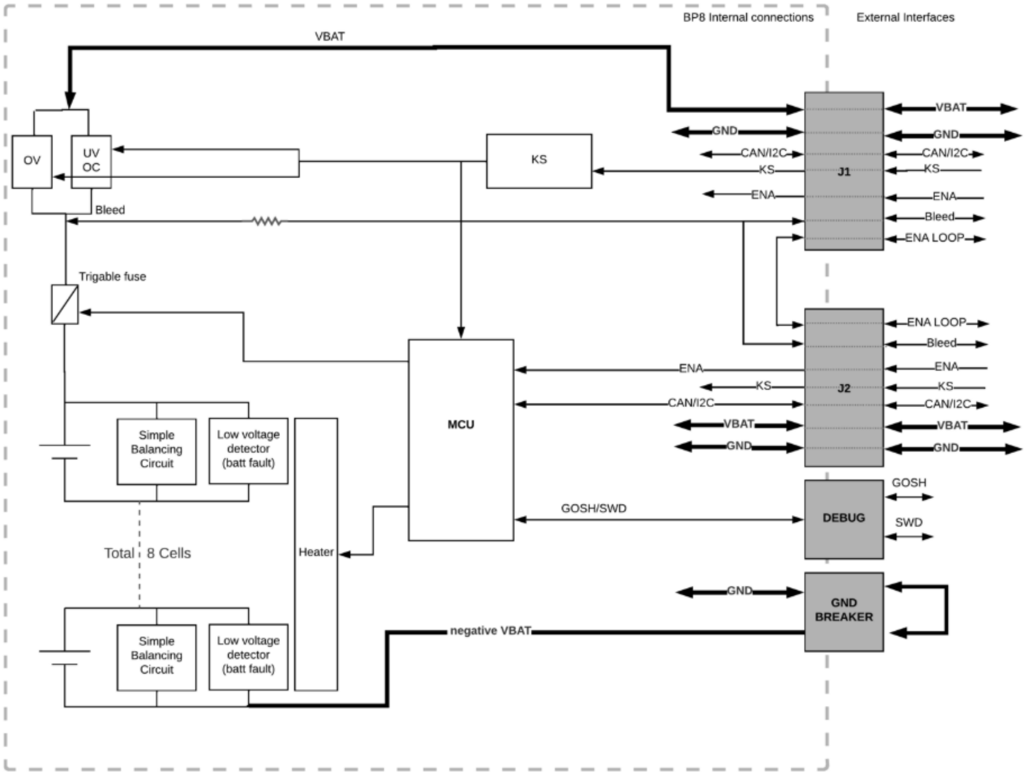

Figure 77. NanoPower BP8 functional block diagram

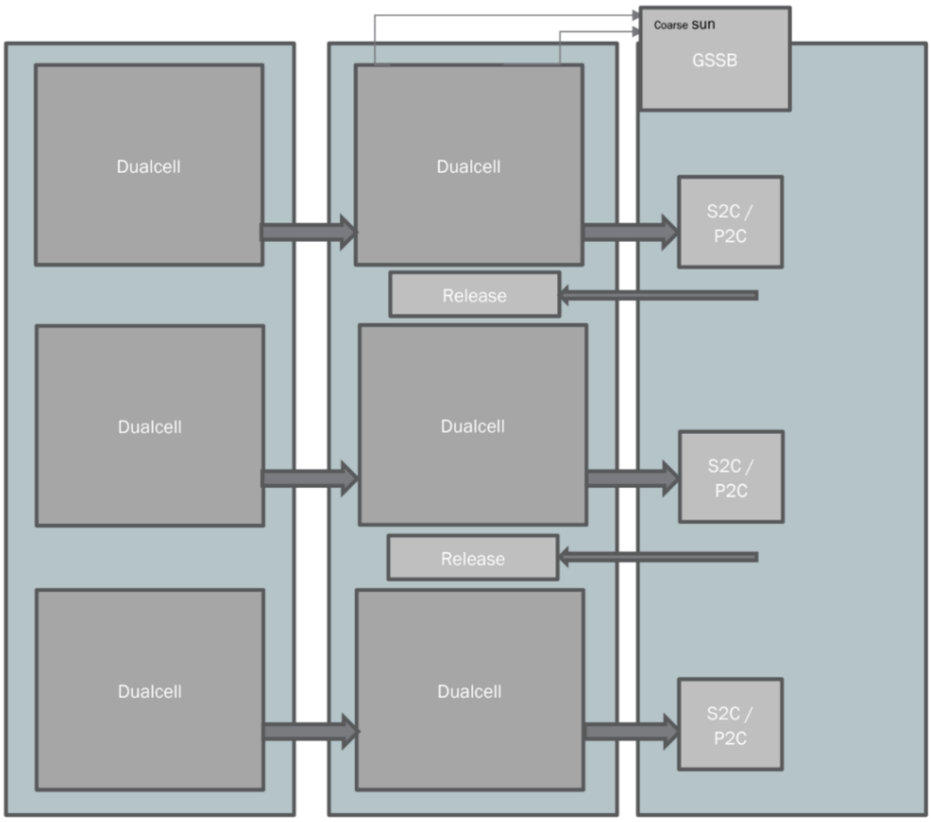

Figure 78. NanoPower DSP-90 architecture

15.1.1.3. Attitude Determination and Control Subsystem

In order for each SC to be able to determine and control its attitude a Cubespace ADCS is baselined.

Moreover, NovAtel OEM-719 GPS kit is used as the SC's main GNSS receiver and antenna. These are directly mounted onto NanoDock DMC-3 and are compatible with GOMspace's OBC.

The AOCS consists of the following components:

1. CubeSpace ADCS Computer
2. CubeSpace CubeTorquer CR0008 x3
3. CubeSpace Cubewheel CW0057 x4
4. CubeSpace CubeSense Coarse Sun Sensor x6
5. CubeSpace CubeSense Sun Sensor x1
6. CubeSpace CubeSense Earth
7. Cubespace CubeMag Compact
8. Cubespace CubeMag Deployable

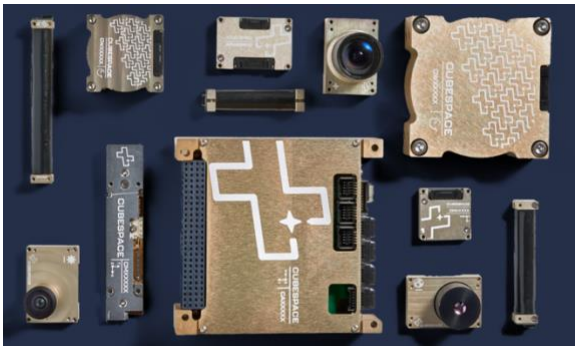

Figure 79. CubeSpace sensors and actuators

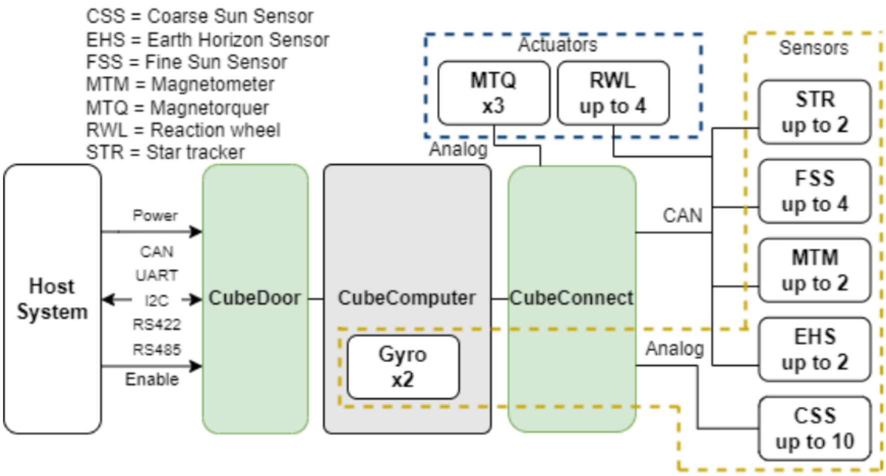

Figure 80. CubeSpace ADCS architecture (STR are not applicable in this case)

15.1.1.4. Telemetry and Telecommand Subsystem

The TTC is designed in order to be capable of achieving two-way links in two bands; UHF and S-band. The UHF link is mandatory for the first contact acquisition with the spacecraft after deployment from the launcher. This is because after being deployed from the CubeSat Deployer, the spacecraft shall be in a tumbling state, which creates the need for an omnidirectional antenna and subsequently a UHF communication link. After LEOP the baselined TTC link shall be the one in S-band, and UHF shall be used as a backup TTC link.

The UHF link consists of the following components:

1. GOMspace NanoCom AX100
2. GOMspace ANT-6F UHF

Table 53. UHF link highlighted features

GOMspace NanoCom AX100	GOMspace ANT-6F UHF
• Advanced high performance narrow-band transceiver for UHF • Dimensions 65 x 40 x 6.5 mm • Mass 24.5 g • Supply Voltage (min - max) 3.3 - 3.4 V • Operating Temperature -30 °C to +85 °C • Transmit Power 24 to 30 dBm • FSK/MSK/GFSK/GMSK • Data rates from 0.1 kbps to 115.2 kbps • Class leading sensitivity down to –137 dBm at 100 bps with FEC • RF carrier frequency and FSK deviation programmable in 1 Hz steps • Transmitter with adjustable 24 to 30 dBm output power at > 45 % PAE • RF parameters are fully configurable on-orbit.	• Multiples of choices of top layer hardware • Dimensions 221.7 x 116.7 x 5.3 mm • Mass 90 g • Supply Voltage (min - max) 3.3 V • Operating Temperature -40 °C to +85 °C • Dual pole design to provide redundancy in case of a transceiver failure • Omnidirectional Canted Turnstile Antenna • Frequency range: 340-680 MHz • Max. gain: 0.8 dB at 161 MHz • Rigid antenna tubes • Safe antenna rod stowage system • Matched to 50 Ω

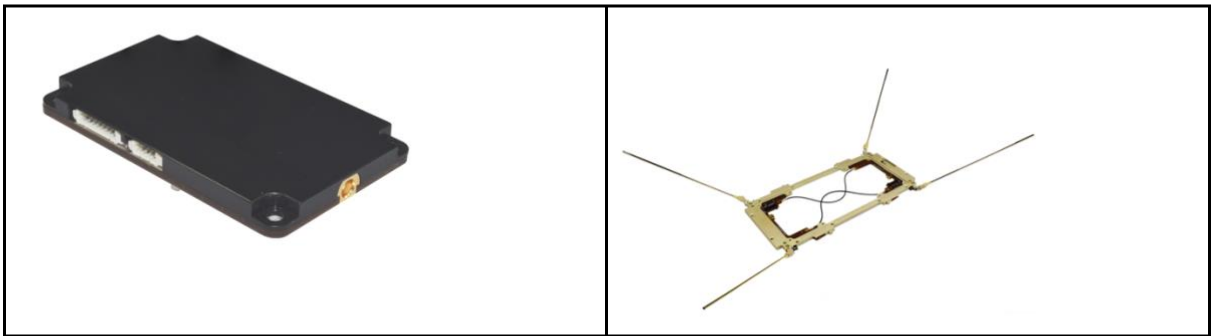

(a) (b)

Figure 81. GOMspace NanoCom AX100 (a), GOMspace NanoCom ANT-6F UHF (b)

The S-band link consists of the following components:

1. GOMspace NanoCom Link S
2. GOMspace NanoCom ANT2150-DUP

Table 54. S-band link highlighted features

GOMspace NanoCom Link S	GOMspace NanoCom ANT2150-DUP

• Qualified for >5 years operation in space according to the GomSpace qualification program.
• CAN bus interface for CubeSat Space Protocol based control and telemetry.
• RS422 full duplex interface for low-speed payload data transfer.
• 3x SpaceWire LVDS interfaces for high-speed payload data transfer.
• Full duplex continuous mode Rx and Tx based on the CCSDS 131.0-B-4 standard with:
    o GomSpace Stream Encapsulation, GSSE.
    o Idle byte insertion.
    o BPSK and QPSK modulation support.
• Symbol rates 0.5MBd to 7.5MBd (symbols/sec).
• Transmit frequency range: 2200 to 2290MHz in steps of 1Hz.
• Receiver frequency range: 2025 to 2110MHz in steps of 1Hz.
• Adjustable output power up to 32dBm.
	• Dimensions 98 x 98 x 20.1 mm
	• Mass 110 g
	• Power Supply 11 W
	• Operating temperature -40 °C to 85 °C
	• Integrated antenna and PA/LNA results in low loss and optimum RF performance.
	• Duplex filter based design results in optimum co-existence with other RF transceivers on-board.
	• Shielded electronics.
	• Flexible power interface (VIN 8-18 V).
	• Default CAN-bus control interface.
	• Medium gain (8 dBi) patch antenna with circular polarization.
	• ANT2150 DUP version supports full duplex with RX in 2025-2110 MHz and TX in 2200-2290 MHz.
	• Temperature sensors and input current sensor

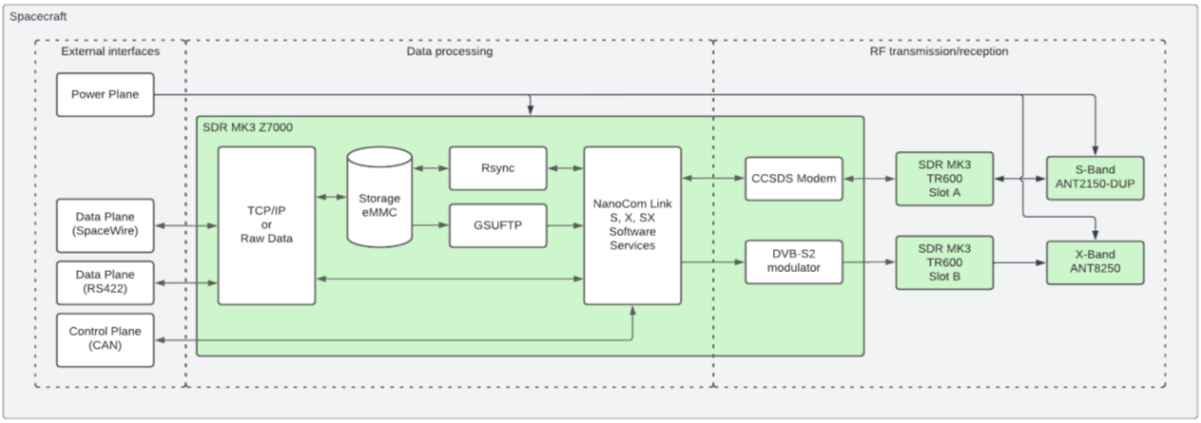

Figure 82. NanoCom Link family product high-level system overview (Slot B is left empty in Link S)

	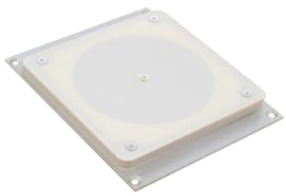
(a)	(b)

Figure 83. GOMspace NanoCom Link S (a), GOMspace NanoCom ANT2150-DUP (b)

15.1.1.5. Propulsion Subsystem

The propulsion subsystem will primarily be used for phasing the spacecrafts within the orbital planes and stationkeeping. Additionally, it may be employed for collision avoidance maneuvers and to lower the spacecraft's altitude prior to passivation. As it was the case with all the BUS components, propulsion subsystems with available datasheets were prioritized.

Before beginning the subsystem selection process, it is essential to determine whether a chemical or electrical propulsion system is more suitable for the mission. In general, chemical propulsion systems provide high thrust for short, impulsive maneuvers, are simpler, and have lower power requirements but are less fuel-efficient. In contrast, electrical propulsion systems offer much higher fuel efficiency and specific impulse, ideal for long-duration missions or fine orbital adjustments, though they require more complex systems, higher power, and longer maneuvering times. The two types of systems are compared in the table below for a comprehensive overview.

Table 55. Comparison of Chemical and Electrical Propulsion Systems

Parameter	Chemical Propulsion	Electrical Propulsion
Thrust	High (rapid acceleration, several Newtons)	Low (gradual thrust, in microNewtons)
Specific Impulse (Isp)	Moderate (150-450 s)	Very High (1000-5000+ s)
Power Requirements	Low to moderate	High
Size and Mass	Larger and heavier due to fuel storage	Compact and lighter, but may impose stricter power and thermal requirements
System Complexity	Moderate	High
Responsiveness	Fast (seconds to minutes)	Slow (minutes to hours)

The primary drawback of electric propulsion is its slow response time and the longer duration required for maneuvers. However, the DRAMA analysis concluded that the probability of collision is minimal, aligning with LEO satellite debris mitigation requirements. As a result, system responsiveness is considered a secondary concern. Additionally, this mission does not require high-thrust maneuvers.

Furthermore, CubeSats are subject to strict mass and volume limitations, making it essential to select a propulsion subsystem that is optimally suited for this mission. Combined with the EPS's ability to manage high power consumption, this makes electric propulsion the more suitable choice.

As mentioned in the requirements section, components with publicly available information are to be selected. Thus, the propulsion subsystem selected is the Enpulsion NANO, which is a light and compact solution that aligns with the system’s

ΔV, power, mass and volume requirements and has already flown to space 170 times.

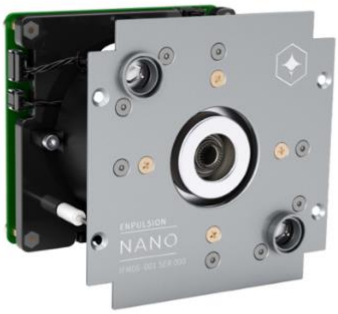

Figure 84. Enpulsion NANO [63]

Table 56. Enpulsion NANO technical specifications

Enpulsion NANO [64], [65], [66]	
Dynamic thrust range	$10\ \mu N\ to\ 350\ \mu N$
Nominal thust	$330\ \mu N$
Propellant	Indium
Specific Impulse	$1500\ to\ 5000\ s$
Propellant mass	$220\ g\ \pm\ 5\%$
Total Impulse	$>\ 5000\ Ns$
Total system Power	$8\ -\ 40\ W$
Power at nominal thrust	$40\ W$
Dimensions	$100^{*}\ \times\ 100^{*}\ \times\ 82.5\ mm$
Mass (dry / wet)	$600/900\ g$
Heat-up power	$4\ -\ 10\ W$
Hot standby power	$3\ -\ 5\ W$
Supply voltage	$12\ V\ or\ 28\ V$
Command interface	$RS422\ or\ RS485$
Operating Temperature	$-20℃\ to\ 40℃$
Survival Temperature	$-40℃\ to\ 105℃$

*Can be customized

By using the Tsiolkovsky rocket equation the total available ΔV is calculated.

$$\Delta V = I_{sp} g_0 ln \frac{m_{initial}}{m_{final}}$$

The satellite’s mass is assumed to be 11.3 kg, out of which 200g is the propellant. Assuming that in the worst case the Isp is 1500 s, the ΔV is calculated to be >260 m/s.

15.1.1.6. Structure Subsystem

The GOMspace 8U Nanosatellite boasts several key features, including countersunk holes for internal mounting rings, holes designed for central covering plates, and dedicated holes for attaching solar panels (NanoPower MSP). Additionally, it is equipped with mounting holes to accommodate various external systems, ensuring versatility in its design and application.

Figure 85. GOMspace 8U structure

Table 57. Characteristics of GOMspace 8U structure

Dimensions	454 x 226.3 x 100.0 mm
Mass	838 g
Material	Alu 7075-T7351
Kill Switches	4

15.1.2. Payload Technical Specifications

As it was already mentioned, since limited information is publicly available on components capable of generating PNT signals (PNT Solution Generator), this part of the payload is to be considered a black box. Its physical properties are based on AIOTY-CUBE's ATOMIC payload.

Table 58. PNT payload components

PNT Payload	PNT Solution Generator NANOlink-boost Gen2 Transceiver GomSpace NanoCom ANT2150-DUP* LRA

For the PNT Solution Generator to function, GNSS inputs are needed, which can be obtained through a GNSS antenna and a GNSS receiver. For this, the same GNSS kit as the one used for BUS functions shall be used; the NovAtel OEM-719 kit that comprises of the NovAtel OEM719 GNSS receiver and the Tallysman GNSS antenna.

Additionally, a CSAC is mandatory for timekeeping and for this purpose SA.45s CSAC from Microchip is selected. It is a passive atomic clock that utilizes the interrogation method of coherent population trapping (CPT) and functions based on the D1 optical resonance of cesium atoms.

Figure 86. Microchip SA.45s Chip-Scale Atomic Clock [67]

Table 59. Microchip SA.45s CSAC technical characteristics

Dimensions	40.6 x 35.3 x 11.4 mm
Supply Voltage	3.3 V
Mass	35g
monitoring and control interface	RS-232, PPS
power consumption	120mW
Storage Temperature	–55°C to +85°C

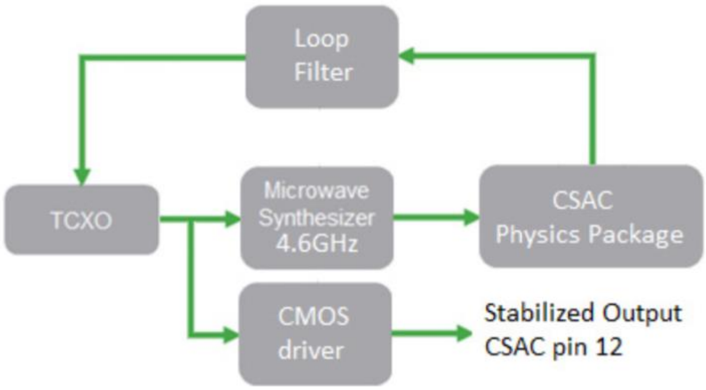

Figure 87. Microchip SA.45s CSAC Block Diagram Overview [67]

The primary RF output from the CSAC is generated by a temperature-compensated crystal oscillator (TCXO), buffered by a CMOS logic gate, and delivered through the CSAC output pin 12. During standard operation, the TCXO's frequency is continuously compared to and adjusted based on the ground state hyperfine frequency of cesium atoms within the physics package. This process enhances the TCXO's stability and reduces its sensitivity to environmental factors by four to five orders of magnitude.

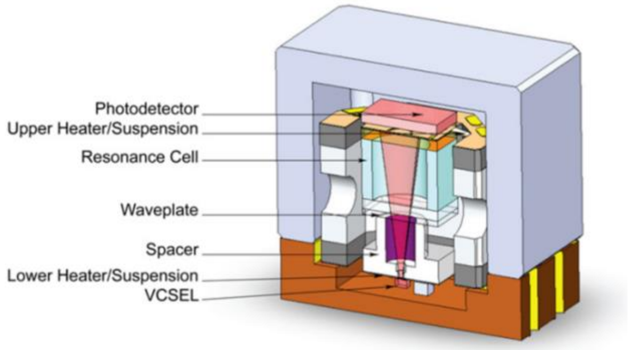

Figure 88. Microchip SA.45s CSAC Physics Package [68]

The architecture of this CSAC enables it to function with minimal frequency errors for a vast temperature range, that enables it to operate in the thermal conditions of space. However, test results have shown that its best performance is around 20℃.

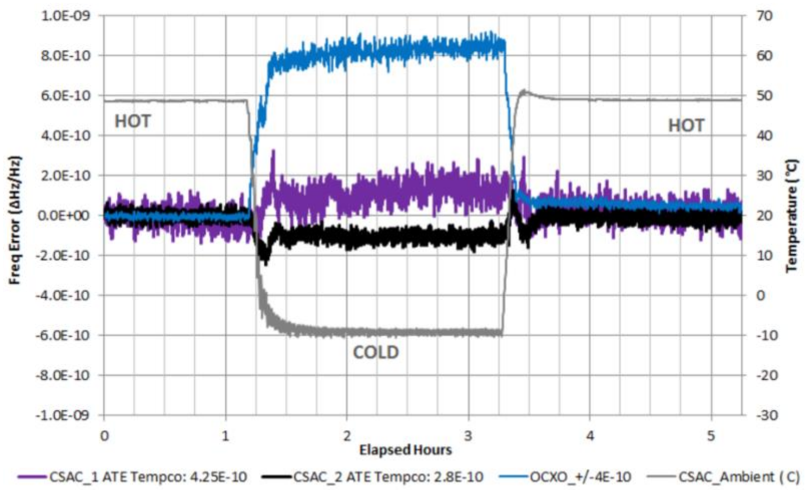

Figure 89. Frequency Response of the CSAC while exposed to –10°C to +50°C [68]

The final component of the PNT Solution Generator is the Payload OBC, which apart from handling the generation of the PNT information that is to be downlinked, it shall also act as a clock monitoring system and it shall perform clock steering required for the system to operate nominally. For these reasons, it is assumed that the PNT Solution Generator shall have a duty cycle of 100% during Nominal Operations.

Table 60. PNT Solution Generator components

PNT Solution Generator	Tallysman GNSS Antenna NovAtel OEM719 GNSS receiver Microchip SA.45s CSAC Payload OBC

Table 61. Payload components technical specifications

Payload component	Mass (gr)	Max power consumption (W)	dimensions (mm x mm x mm)
PNT Solution Generator	1000 [3]	2.5 [3]	N/A (less than 0.5 U)
NANOlink-boost Gen2 Transceiver	248	17	95 x 91 x 22
GomSpace NanoCom ANT2150-DUP *	110	11.75	98 x 98 x 20.1
LRA	200	-	10 x 10 x 10 (each CRR)

* GomSpace NanoCom ANT2150-DUP is considered to be modified to be able to handle 5W of RF power.

Table 62. PNT Payload technical specifications

	Mass (gr)	Max power consumption (W)	dimensions (mm x mm x mm)
PNT Payload	1558	31.25	1U (assumed)

	
(a)	(b)

Figure 90. NANOlink-boost Gen2 (a), a corner retroreflector (b) [69]

Table 63. NANOlink-boost Gen2 technical specifications

Characteristic	Description
Output power	Adj. up to 37 dBm (5W)
Supported modulations	OQPSK (other upon request)
Noise figure	< 5 dB
Data rates	default 4 Mbps @ 2.5 MHz (OQPSK)
Baseband bandwidth	up to 56 MHz
Frequency band Transmitter Receiver	 2.200 - 2.300 GHz 2.025 - 2.110 GHz
On-board Communication interfaces	CAN bus, LVDS (support for additional interfaces upon request e.g. UART, SPI, I2C)
Supply voltage	5 V DC (+/- 10%)
Power consumption	< 17 W (Rx + Tx @ 5W output power)
Dimensions	95 x 91 x 22 mm
Operation temperature	-10°C to +50°C
Storage temperature	-20°C to +65°C
Mass	< 248 g

The design of the LRA shall be based on other CubeSat missions like CHOMPTT, LightSail-A and LightSail-B. All these missions were equipped with RRAs consisting of six to thirteen 1 cm sized corner cubes made of BK7 [45], [70], [71]. For this mission a total of 8 RRAs are considered, which are assumed to have a total mass of less than 200 gr (due to lack of information, mass value is assumed to be higher than expected as a risk mitigation measure).

15.2. Mechanical Design

In this section are displayed CAD renders of the spacecraft.

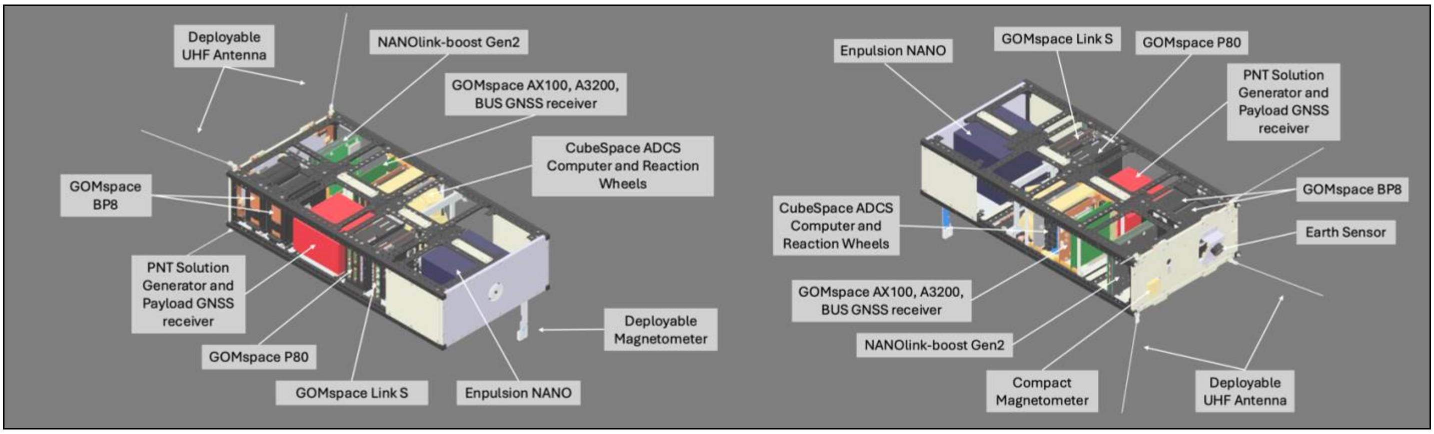

Figure 91. Spacecraft internal view

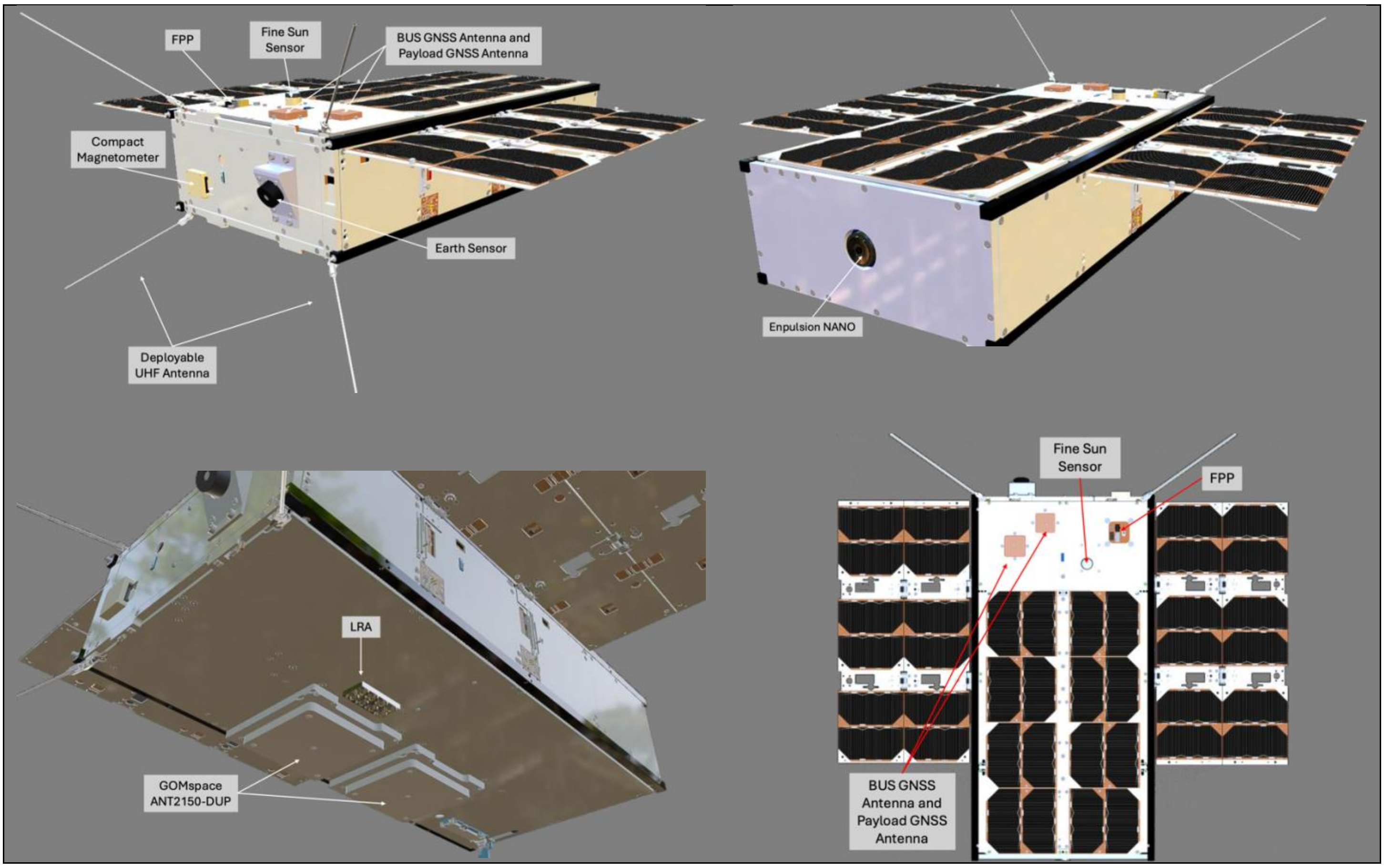

Figure 92. Spacecraft external view

15.3. System Budgets

Table 64. Margin philosophy

Mass & Power	System level	20%
	New developments or existing units requiring major modifications	20%
	Existing units requiring minor modifications	10%
	Existing units	5%
Data	On-board memory	50%
Propulsion	ΔV margin	50%
Communication	Link margin above	5dB

15.3.1. Mass Budget

Table 65. Mass Budget – Subsystem level

Subsystem	Mass (g)	Mass with Margins (g)
ADCS	819.0	860.0
CDHS	132.0	138.6
EPS	2564.0	2692.2
Harness	374.3	393.0
Payload	1558.0	1821.4
PRO	900.0	945.0
Structure	1873.0	2024.0
TTC	540.0	567.0
Total	**8760.3**	**9441.1**
Total with 20% system margin	**11329.3**	

Table 66. Mass Budget – Component level

Name	Provider	Mass (g)	Design Maturity Margin (DMM)	Mass with Margins (g)
ADCS Computer	CubeSpace	214.0	5%	224.7
CubeTorquer CR0008 x3	CubeSpace	70.0	5%	73.5
CubeSpace Cubewheel CW0057 x4	GOMspace	940	5%	987
CubeSense Coarse Sun Sensor x 6	CubeSpace	10.0	5%	10.5
CubeSense Sun Sensor	CubeSpace	15.0	5%	15.8
CubeSense Earth	CubeSpace	18.0	5%	18.9
CubeMag Compact	CubeSpace	6.0	5%	6.3

CubeMag Deployable	CubeSpace	16.0	5%	16.8
Nanopower P80 (1x PMU, 1x ACU, 1x PDU)	GOMSpace	361.0	5%	379.1
Nanopower BP8 x2	GOMSpace	970.0	5%	1018.5
NanoPower DSP-90deg	GOMSpace	390.0	5%	409.5
NanoPower DSP-90deg	GOMSpace	390.0	5%	409.5
Nanopower MSP-B-4x4	GOMSpace	453.0	5%	475.7
NanoDock DMC-3	GOMSpace	51.0	5%	53.6
NanoMind A3200	GOMSpace	24.0	5%	25.2
NovAtel OEM-719 GPS kit	GOMSpace	57.0	5%	59.9
NanoCom AX100	GOMSpace	25.0	5%	26.3
NanoCom ANT-6F UHF	GOMSpace	90.0	5%	94.5
NanoCom Link-S	GOMSpace	315.0	5%	330.8
NanoCom ANT2150-DUP	GOMSpace	110.0	5%	115.5
8U Nanosatellite Structure	GOMSpace	838.0	5%	879.9
8U Side Panel	Custom	438.0	10%	481.8
2U Side Panel	Custom	55.0	10%	60.5
2U Side Panel	Custom	133.0	10%	146.3
NanoUtil MSP-FPP	GOMSpace	10.0	10%	11.0
Cover plate Big x2	GOMSpace	10.0	5%	10.5
Cover plate Small x1	GOMSpace	3.0	5%	3.2
2U Side Panel	Custom	121.0	10%	133.1
Custom Stack Breakout	Custom	62.0	20%	74.4
S band aluminum spacer x2	Custom	64.0	10%	70.4
1U Side Panel x2	Custom	74.0	10%	81.4
Custom Reaction Wheels Deck	Custom	65.0	10%	71.5
PNT Solution Generator	Custom	1000.0	20%	1200.0
NANOlink-boost Gen2	Skylabs	248.0	5%	260.4
NanoCom ANT2150-DUP (modified)	GOMSpace	110.0	10%	121.0
LRA	N/A	200.0	20%	240.0
Enpulsion NANO	Enpulsion	900.0	5%	945.0
Cables/Harness	Custom	374.3	5%	393.0

Below, it is shown the positive mass margin available when comparing the margined system mass with the limit of the Deployer Pod. The maximum mass that is to be fit inside the Exolaunch's Deployer Pod for 6U and 8U CubeSats is 16 kg.

Table 67. Positive Mass Margin of Deployer Pod

Margined System Mass (gr)	Mass Margin of Deployer Pod (gr)
11329.3	4670.7

15.3.2. Power Budget

15.3.2.1. Power Generation

The spacecraft is equipped with 40 solar cells in total; 16 body mounted and 24 deployable solar cells. According to GOMspace, each solar cell can generate up to 1.2 W in LEO. However, for the following analysis it is assumed that a solar cell can generate 1 W when it is exposed vertically to sunlight.

Table 68. Power generation for different scenarios

Scenario	Average Power Generation (in sunlight)
Sun Tracking - fully deployed array	40 W
Sun Tracking - deployment failure	16 W
Tumbling - fully deployed array	20* W
Tumbling - deployment failure (non-deployable cells active only)	8* W

* It is assumed that when tumbling the spacecraft can generate half the power that it would in Sun Tracking mode.

Table 69. Spacecraft power storage characteristics

Cell Chemistry	Li-Ion
Cell Configuration	8S1P
Battery BOL Capacity (Wh)	75
Battery EOL Derating	33%
Battery EOL Capacity (Wh)	50
Number of Batteries	2

Total Battery EOL Capacity (Wh)	100
Max battery operational voltage (V)	32
Min battery operational voltage (V)	21.5
Maximum Combined Discharge Current (A)	8
Maximum Combined Charge Current (A)	8

15.3.2.2. Power Consumption

As outlined in the CONOPS section, 11 operational modes have been identified, each with its corresponding power consumption profile. he defined modes include Critical Mode, Deployment Mode, Safe Mode, Detumbling Mode, Sun-Tracking, UHF Link, S-Band Link, Phasing Maneuver, PNT Service Mode, and SLR Mode. Among those, the Safe Mode and Detumbling Modes share the same power profile. Among these, the modes expected to be sustained for extended periods are analyzed.

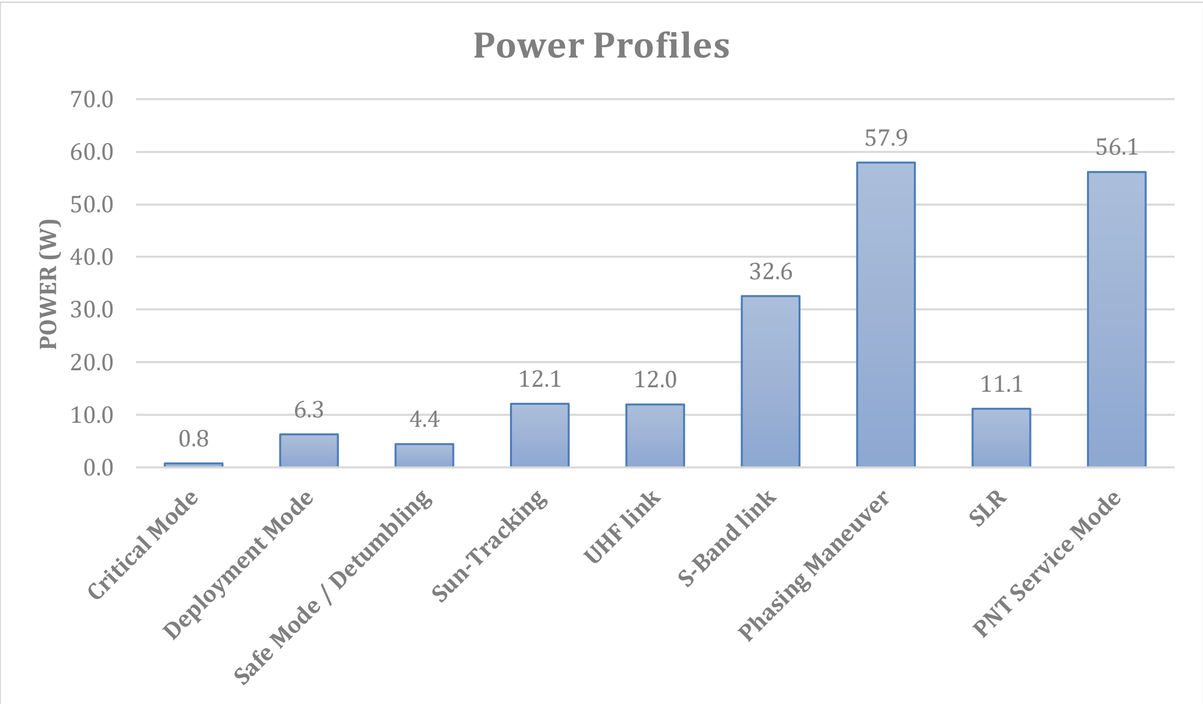

Figure 93. System power consumption

Table 70. Power Budget for modes with extended operation times

	Critical Mode, Deployment Failure	Safe Mode/Detumbling, Deployment Success	Safe Mode/Detumbling, Deployment Failure	Sun Tracking, Deployment Success	UHF Link, Deployment Success
Maximum Eclipse Time (s)	2136.0				
Time in Sunlight (s)	3529.0				
Orbit Period (s)	5665.0				
Power Generation (W)	8.0	20.0	8.0	40.0	20.0
Average eclipse Power consumption (W)	0.8	4.4	4.4	12.1	12.0
Average daytime Power consumption (W)	0.8	4.4	4.4	12.1	12.0
Power balance during daytime (W)	7.2	15.6	3.6	27.9	8.0
Energy Expended during eclipse (Wh)	0.4	2.6	2.6	7.2	7.1
Energy Expended during daytime (Wh)	0.7	4.3	4.3	11.9	11.8
Energy Expended in one orbit (Wh)	1.2	7.0	7.0	19.0	18.9
Energy generated in one orbit (Wh)	7.8	19.6	7.8	39.2	19.6
Energy Balance in one orbit (Wh)	6.7	12.6	0.9	20.2	0.7
EOL Battery Capacity (Wh)	100.0				
DoD	0.45%	2.63%	2.63%	7.17%	7.12%
Battery Charged during one orbit	6.65%	12.64%	0.87%	20.19%	0.72%
Number of Orbits to fully charge	15.0	7.9	114.5	5.0	138.5

15.3.2.3. Day in the life simulation

A MATLAB Day in the life simulation has been done based on the following assumptions. The EOL battery capacity is 50Wh, and since there are two batteries on board, the spacecraft has a total battery capacity of 100Wh. The spacecraft operates in Sun-Tracking Mode that has a constant consumption of 8.5W and is capable of generating 40W of power while exposed to sunlight. Over a 24-hour period, the spacecraft will enter PNT Service Mode an average of 7 times, corresponding to the typical number of daily contacts with the service area. Those are separated by approximately 3 hours, which is the ART to the service area. Each contact, based on STK analysis, lasts an average of 10.7 minutes or 642 seconds. When in PNT Service Mode the power consumption is 52.5W. Additionally, the spacecraft will engage in S-Band Link Mode twice within the same 24-hour period. When in S-Band Link Mode the power consumption is 29W. After completing either an S-Band Link Mode or PNT Service Mode, the spacecraft will return to Sun-Tracking Mode. It is assumed that no power is generated (0W) when the spacecraft is in a different mode than Sun-Tracking Mode. The MATLAB code used can be found in the Appendix.

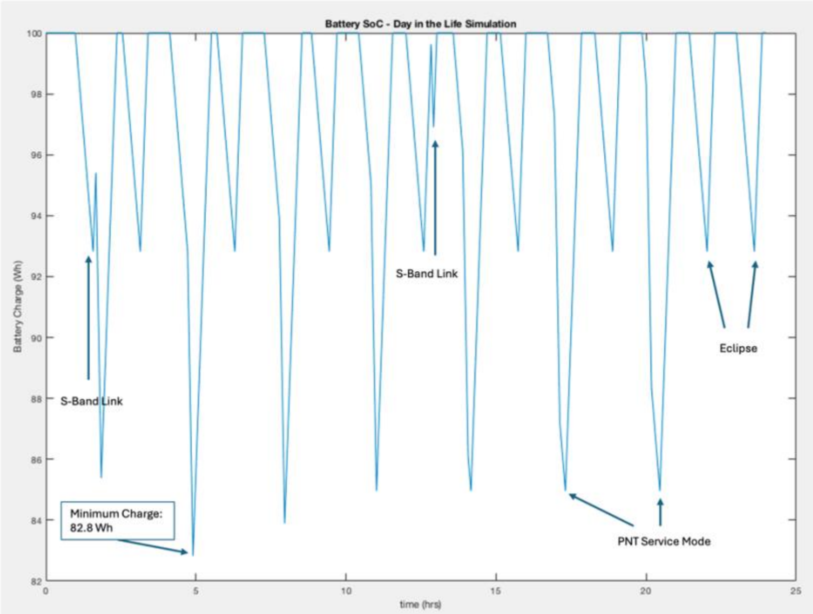

Figure 94. Battery SoC - Day in the life simulation - Nominal scenario

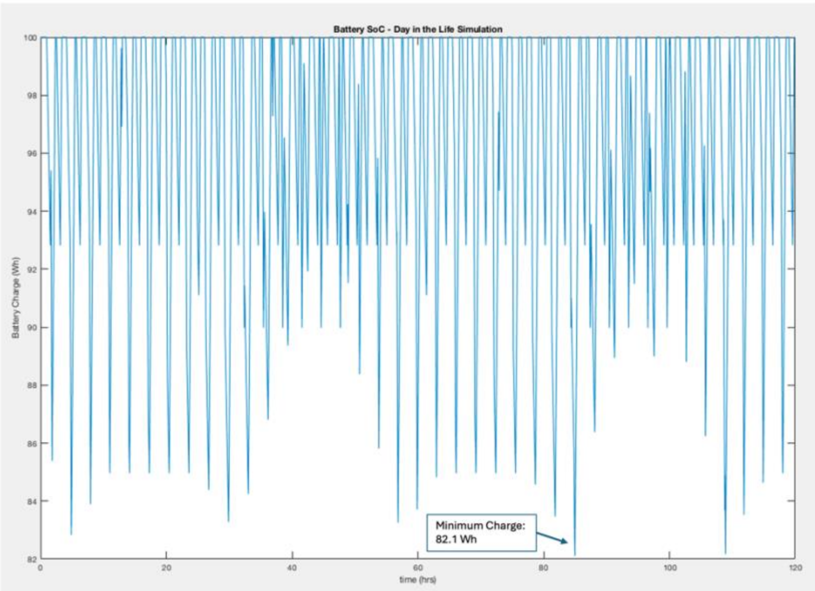

Figure 95. Battery SoC - 5 Days in the life simulation - Nominal scenario

15.3.2.4. Power Channel Allocation

The ACU of GOMSpace P80, features two groups of six channels each, for a total of 12 channels. Each channel supports a maximum current of 1.1 A, and the maximum input voltage is rated at 25 V. It is important to note that the open-circuit voltage (Voc) must remain below the battery voltage (Vbat) for optimal operation. The battery voltage (Vbat) ranges from 19.5 to 33.3 V, with a maximum charge current of 4 A. The open-circuit voltage (Voc) of a single cell is 2.4 V.

Table 71. P80 input channels

Channel	Group	# of Series Cells	# of Parallel Strings	Mounted ON	Voc (V)	Current (A)	Power (W)
0	A	4	1	MSP	9.6	0.5	4
1	A	4	1	MSP	9.6	0.5	4
2	A	4	1	MSP	9.6	0.5	4
3	A	4	1	MSP	9.6	0.5	4
4	A	0	0	-	-	-	-
5	A	0	0	-	-	-	-
6	B	4	1	DSP (B)	9.6	0.5	4
7	B	4	1	DSP (B)	9.6	0.5	4
8	B	4	1	DSP (B)	9.6	0.5	4
9	B	4	1	DSP (A)	9.6	0.5	4
10	B	4	1	DSP (A)	9.6	0.5	4
11	B	4	1	DSP (A)	9.6	0.5	4

Table 72. P80 output channels

Channel	Voltage Options	Max Current (A)	Combined Channel	Channel Allocation
0	Vbat	2	Ch0	Vbat_LinkS
1	Vbat	2	Ch0	
2	Vbat	2	-	
3	Vbat	2	-	
4	Vbat	2	Ch4	
5	Vbat	2	Ch4	
6	Vbat	2	-	
7	Vbat	2	-	
8	Vbat or 3.3, 5, 12 or 18V	2	Ch8	5V_Nanolink
9	Vbat or 3.3, 5, 12 or 18V	2	Ch8	
10	Vbat or 3.3, 5, 12 or 18V	2	-	3.3V_PNT_GNSS
11	Vbat or 3.3, 5, 12 or 18V	2	-	12V_PRO
12	3.3, 5 or 12V	2	Ch12	
13	3.3, 5 or 12V	2	Ch12	
14	3.3, 5 or 12V	2	-	12V_SAnt
15	3.3, 5 or 12V	2	-	12V_PNT_Ant
16	3.3, 5 or 12V	2	Ch16	3.3V_OBC
17	3.3, 5 or 12V	2	Ch16	12V_ADCS
18	3.3, 5 or 12V	2	-	3.3V_GPS
19	3.3, 5 or 12V	2	-	3.3V_UHF
20	3.3, 5 or 12V	2	Ch21	
21	3.3, 5 or 12V	2	Ch21	3.3V_CSAC
22	3.3, 5 or 12V	2	-	
23	3.3, 5 or 12V	2	-	3.3V_PNT_OBC

15.3.3. Link Budget

Here is presented information about the spacecraft antennas that are to be used.

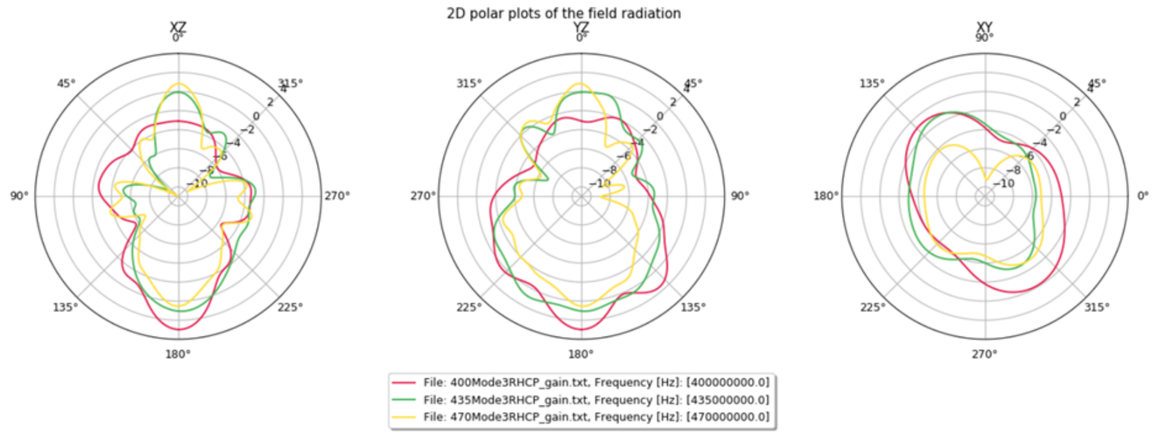

Figure 96. GOMspace ANT-6F antenna - Total far field realized gain measured in dBi for 400MHz, 435MHz and 470MHz variants in RHCP. The illustration is shown in Polar coordinate in three different orientations.

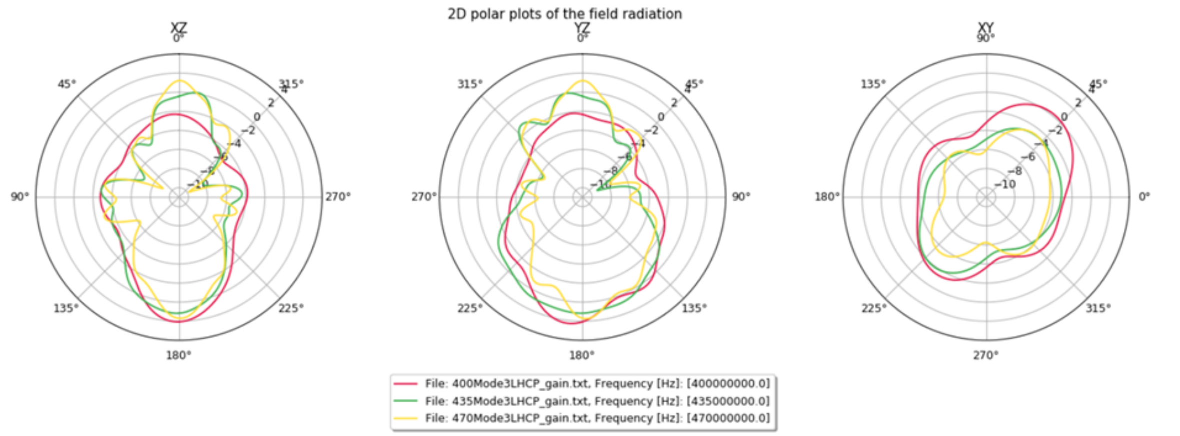

Figure 97. GOMspace ANT-6F antenna - Total far field realized gain measured in dBi for 400MHz, 435MHz and 470MHz variants in LHCP. The illustration is shown in Polar coordinate in three different orientations.

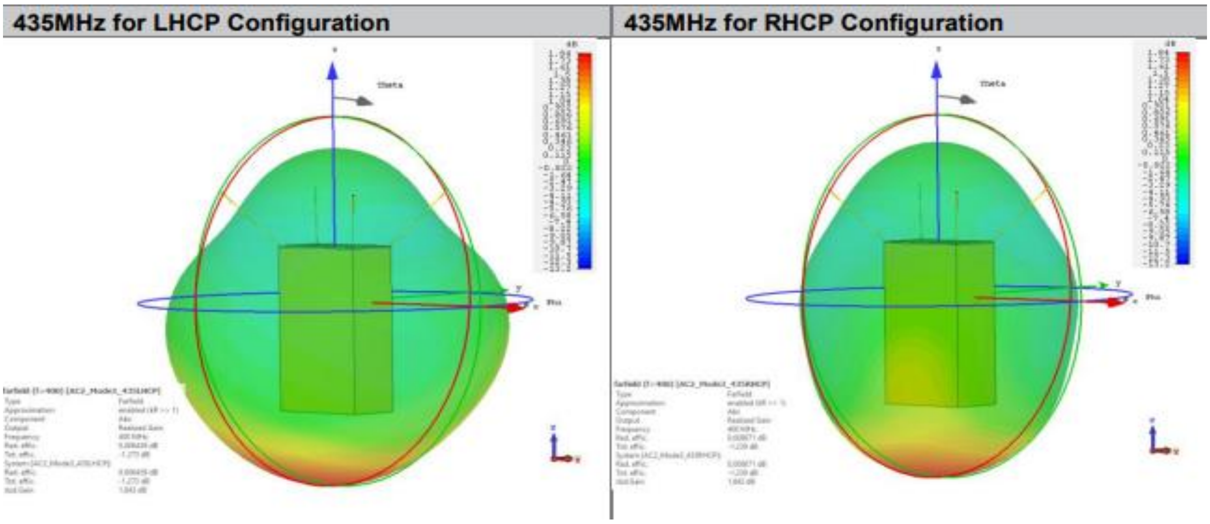

Figure 98. GOMspace ANT-6F antenna radiation pattern

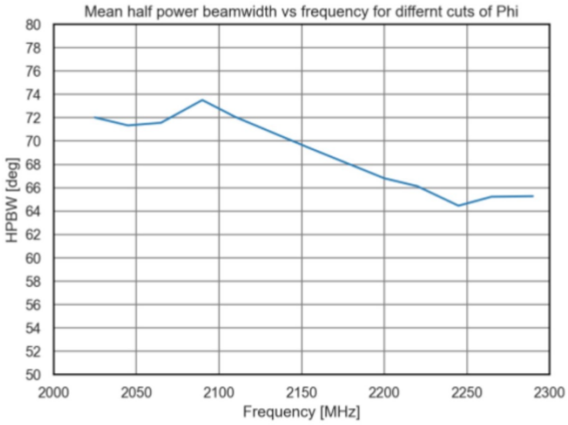

Figure 99. GOMspace ANT2150-DUP Mean Half Power Beamwidth

<u>Link Budget Considered Assumptions</u>

The link budgets are dimensioned for an orbit height of 550 km. UHF link shall operate in the earth exploration frequency band (401-403 MHz). Not sufficient information on KSAT's GCS at Nemea is publicly available and, thus, all calculations are based on the infrastructure at Psachna GCS. All the links budgets were calculated taking into account the worst-case values (conservative assumptions and calculations) of the uplink and downlink segments.

In S-band, all the uplink and downlink excess loss (apart from path loss) were calculated according to ITU Rec. P.618 [72]. The minimum data rate is 512 kbps with a 0.6 MHz channel bandwidth. The threshold Eb/No was selected 9.5 dB, considering a QPSK CCSDS 131.0-B-4 modulation with rate ½ convolutional inner code and R-S (255,223). Also, worst case values are considered regarding the performance characteristics of the GOMspace NanoCom Link S module at spacecraft and ground station equipment, SDR Rack and Antennas. In UHF band, both uplink and downlink segments were considered to operate at a minimum data rate of 9600 bps, accommodated in a 25-kHz bandwidth channel. The threshold Eb/No was selected 7.8 dB, considering a GMSK modulation with Conv. R=1/2, K=7 & R.S. (255,223). Also, worst case values are considered regarding the performance characteristics of the GOMspace NanoCom AX100 module at spacecraft and ground station equipment, SDR Rack and Antennas.

Table 73. UHF uplink budget

Spacecraft Orbit & Link Parameters																			
Mean Orbit Altitude:	550,00																		km
Mean Orbit Radius:	6928,14																		km
Elevation Angle (**ε**):	5,00	10,00	15,00	20,00	25,00	30,00	35,00	40,00	45,00	50,00	55,00	60,00	65,00	70,00	75,00	80,00	85,00	90,00	°
Slant Range (**S**):	2205,90	1815,65	1518,37	1293,77	1123,42	992,87	891,59	812,11	749,14	698,94	658,84	626,89	601,71	582,25	567,79	557,80	551,93	550,00	km
Frequency:	403,00																		MHz
Wavelength (**λ**):	0,7439																		meters
Ground Station																			
Ground Station Transmitter Power Output:	10,00																		Watts
In dBW:	10,00																		dBW
In dBm:	40,00																		dBm
Ground Stn. Total Transmission Line Losses:	6,40																		dB
Antenna Gain:	14,80																		dBi
Ground Station EIRP:	18,40																		dBW
Uplink Path																			
Ground Station Antenna Pointing Loss:	0,50																		dB
Gnd-to-S/C Antenna Polarization Losses:	0,20																		dB
Path Loss:	151,44	149,75	148,20	146,81	145,58	144,51	143,57	142,76	142,06	141,46	140,95	140,51	140,16	139,87	139,65	139,50	139,41	139,38	dB
Gaseous attenuation:	2,10	1,10	1,10	1,10	1,10	0,40	0,40	0,30	0,30	0,30	0,30	0,30	0,30	0,30	0,30	0,30	0,30	0,00	dB
Ionospheric Losses:	0,40																		dBi
Received power at Spacecraft	-136,24	-133,55	-132,00	-130,61	-129,38	-127,61	-126,67	-125,76	-125,06	-124,46	-123,95	-123,51	-123,16	-122,87	-122,65	-122,50	-122,41	-122,08	dBW
Spacecraft (Eb/No Method)																			
Spacecraft Antenna Pointing Loss:	0,30																		dB
Spacecraft Antenna Gain:	2,20																		dBi
Spacecraft Total Transmission Line Losses:	1,20																		dB
Spacecraft System Noise Temperature:	170,00																		K
Spacecraft Figure of Merrit (G/T):	-21,30																		dB/K
Spacecraft Carrier-to-Noise Power Density (C/No)	70,75	73,45	75,00	76,39	77,62	79,39	80,32	81,23	81,93	82,54	83,05	83,48	83,84	84,12	84,34	84,50	84,59	84,92	dBHz
System Desired Data Rate:	9600,00																		bps
In dBHz:	39,82																		dBHz
Command System Eb/No:	30,93	33,62	35,18	36,57	37,79	39,57	40,50	41,41	42,11	42,71	43,23	43,66	44,02	44,30	44,52	44,67	44,77	45,10	dB
Required Eb/No (Threshold):	7,80																		dB
System Link Margin:	23,13	25,82	27,38	28,77	29,99	31,77	32,70	33,61	34,31	34,91	35,43	35,86	36,22	36,50	36,72	36,87	36,97	37,30	dB
Spacecraft (SNR Method)																			
Spacecraft Antenna Pointing Loss:	0,30																		dB
Spacecraft Antenna Gain:	2,20																		dB
Spacecraft Total Transmission Line Losses:	1,20																		dB
Spacecraft System Noise Temperature:	170,00																		K
Spacecraft Figure of Merrit (G/T):	-21,30																		dB/K
Signal Power at Spacecraft LNA Input:	-135,54	-132,85	-131,30	-129,91	-128,68	-126,91	-125,97	-125,06	-124,36	-123,76	-123,25	-122,81	-122,46	-122,17	-121,95	-121,80	-121,71	-121,38	dBW
Spacecraft Receiver Bandwidth:	25000,00																		Hz
Spacecraft Receiver Noise Power (Pn = kTB)	-162,32																		dBW
Signal-to-Noise Power Ratio at G.S. Rcvr:	26,77	29,47	31,02	32,41	33,64	35,41	36,34	37,25	37,96	38,56	39,07	39,50	39,86	40,14	40,36	40,52	40,61	40,94	dB
Analog or Digital System Required S/N:	3,64																		dB
System Link Margin	23,13	25,82	27,38	28,77	29,99	31,77	32,70	33,61	34,31	34,91	35,43	35,86	36,22	36,50	36,72	36,87	36,97	37,30	dB

Table 74. UHF downlink budget

Spacecraft Orbit & Link Parameters																			
Mean Orbit Altitude:	550,00																		km
Mean Orbit Radius:	6928,14																		km
Elevation Angle (ε):	5,00	10,00	15,00	20,00	25,00	30,00	35,00	40,00	45,00	50,00	55,00	60,00	65,00	70,00	75,00	80,00	85,00	90,00	°
Slant Range (S):	2205,90	1815,65	1518,37	1293,77	1123,42	992,87	891,59	812,11	749,14	698,94	658,84	626,89	601,71	582,25	567,79	557,80	551,93	550,00	km
Frequency:	403,00																		MHz
Wavelength (λ):	0,7439																		
Spacecraft																			
Spacecraft Transmitter Power Output:	1,00																		Watts
In dBW:	0,00																		dBW
In dBm:	30,00																		dBm
Spacecraft Total Transmission Line Losses:	2,00																		dB
Spacecraft Antenna Gain:	2,20																		dBi
Spacecraft EIRP:	0,20																		dBW
Downlink Path																			
Spacecraft Antenna Pointing Loss:	0,30																		dB
S/C-to-Ground Antenna Polarization Loss:	0,20																		dB
Path Loss:	151,44	149,75	148,20	146,81	145,58	144,51	143,57	142,76	142,06	141,46	140,95	140,51	140,16	139,87	139,65	139,50	139,41	139,38	dB
Gaseous attenuation:	2,10	1,10	1,10	1,10	1,10	0,40	0,40	0,30	0,30	0,30	0,30	0,30	0,30	0,30	0,30	0,30	0,30	0,00	dB
Ionospheric Losses:	0,40																		dBi
Received power at Ground Station	-154,24	-151,55	-150,00	-148,61	-147,38	-145,61	-144,67	-143,76	-143,06	-142,46	-141,95	-141,51	-141,16	-140,87	-140,65	-140,50	-140,41	-140,08	dBW
Ground Station (Eb/No Method)																			
Ground Station Antenna Pointing Loss:	0,50																		dB
Ground Station Antenna Gain:	14,80																		dB
Ground Station Total Transmission Line Losses:	1,90																		dB
Ground Station System Noise Temperature:	184,00																		K
Ground Station Figure of Merrit (G/T):	-9,75																		dB/K
Ground Station Carrier-to-Noise Power Density (C/No)	64,11	66,80	68,35	69,75	70,97	72,74	73,68	74,59	75,29	75,89	76,41	76,84	77,19	77,48	77,70	77,85	77,94	78,28	dBHz
System Desired Data Rate:	9600,00																		bps
In dBHz:	39,82																		dBHz
Command System Eb/No:	24,29	26,98	28,53	29,92	31,15	32,92	33,86	34,77	35,47	36,07	36,58	37,02	37,37	37,66	37,88	38,03	38,12	38,45	dB
Required Eb/No (Threshold):	7,80																		dB
System Link Margin:	16,49	19,18	20,73	22,12	23,35	25,12	26,06	26,97	27,67	28,27	28,78	29,22	29,57	29,86	30,08	30,23	30,32	30,65	dB
Ground Station (SNR Method)																			
Ground Station Antenna Pointing Loss:	0,50																		dB
Ground Station Antenna Gain:	14,80																		dB
Ground Station Total Transmission Line Losses:	1,90																		dB
Ground Station System Noise Temperature:	184,00																		K
Ground Station Figure of Merrit (G/T):	-9,75																		dB/K
Signal Power at Ground Station LNA Input:	-141,84	-139,15	-137,60	-136,21	-134,98	-133,21	-132,27	-131,36	-130,66	-130,06	-129,55	-129,11	-128,76	-128,47	-128,25	-128,10	-128,01	-127,68	dBW
Ground Station Receiver Bandwidth (B):	25.000,00																		Hz
G.S. Receiver Noise Power (Pn = kTB)	-161,97																		dBW
Signal-to-Noise Power Ratio at G.S. Rcvr:	20,13	22,82	24,38	25,77	26,99	28,77	29,70	30,61	31,31	31,91	32,43	32,86	33,22	33,50	33,72	33,87	33,97	34,30	dB
Analog or Digital System Required S/N:	3,64																		dB
System Link Margin	16,49	19,18	20,73	22,12	23,35	25,12	26,06	26,97	27,67	28,27	28,78	29,22	29,57	29,86	30,08	30,23	30,32	30,65	dB

Table 75. S band uplink budget

Spacecraft Orbit & Link Parameters																			
Mean Orbit Altitude:	550,00																		km
Mean Orbit Radius:	6928,14																		km
Elevation Angle (ε):	5,00	10,00	15,00	20,00	25,00	30,00	35,00	40,00	45,00	50,00	55,00	60,00	65,00	70,00	75,00	80,00	85,00	90,00	°
Slant Range (S):	2205,90	1815,65	1518,37	1293,77	1123,42	992,87	891,59	812,11	749,14	698,94	658,84	626,89	601,71	582,25	567,79	557,80	551,93	550,00	km
Frequency:	2030,00																		MHz
Wavelength (λ):	0,15																		
Ground Station																			
Ground Station Transmitter Power Output:	10,00																		Watts
In dBW:	10,00																		dBW
In dBm:	40,00																		dBm
Ground Stn. Total Transmission Line Losses:	9,30																		dB
Antenna Gain:	26,50																		dBi
Ground Station EIRP:	27,20																		dBW
Uplink Path																			
Ground Station Antenna Pointing Loss:	0,50																		dB
Gnd-to-S/C Antenna Polarization Losses:	0,50																		dB
Path Loss:	165,48	163,79	162,24	160,85	159,62	158,55	157,62	156,81	156,10	155,50	154,99	154,56	154,20	153,92	153,70	153,54	153,45	153,42	dB
Gaseous attenuation:	0,40	0,20	0,14	0,10	0,08	0,07	0,06	0,05	0,05	0,05	0,04	0,04	0,04	0,04	0,04	0,04	0,04	0,04	dB
Cloud and fog attenuation:	0,05	0,02	0,02	0,01	0,01	0,01	0,01	0,01	0,01	0,01	0,00	0,00	0,00	0,00	0,00	0,00	0,00	0,00	dB
Rain attenuation:	0,05	0,03	0,02	0,01	0,01	0,01	0,01	0,01	0,01	0,01	0,01	0,01	0,01	0,01	0,01	0,01	0,01	0,01	dB
Attenuation due to tropospheric scintillation:	0,84	0,37	0,23	0,16	0,13	0,10	0,09	0,08	0,07	0,06	0,06	0,05	0,05	0,05	0,05	0,04	0,04	0,04	dB
Ionospheric Losses:	0,10																		dBi
Received power at Spacecraft	-140,73	-138,31	-136,54	-135,04	-133,75	-132,64	-131,68	-130,85	-130,13	-129,52	-129,00	-128,56	-128,20	-127,91	-127,69	-127,53	-127,44	-127,41	dBW
Spacecraft (Eb/No Method)																			
Spacecraft Antenna Pointing Loss:	0,50																		dB
Spacecraft Antenna Gain:	5,50																		dB
Spacecraft Total Transmission Line Losses:	2,00																		dB
Spacecraft System Noise Temperature:	260,00																		K
Spacecraft Figure of Merrit (G/T):	-20,65																		dB/K
Spacecraft Carrier-to-Noise Power Density (C/No)	66,72	69,14	70,91	72,41	73,70	74,81	75,77	76,60	77,32	77,93	78,45	78,89	79,25	79,54	79,76	79,92	80,01	80,04	dBHz
System Desired Data Rate:	512000,00																		bps
In dBHz:	57,09																		dBHz
Command System Eb/No:	9,63	12,05	13,82	15,32	16,60	17,72	18,68	19,51	20,22	20,84	21,36	21,80	22,16	22,45	22,67	22,82	22,92	22,95	dB
Required Eb/No (Threshold):	11,50																		dB
System Link Margin:	-1,87	0,55	2,32	3,82	5,10	6,22	7,18	8,01	8,72	9,34	9,86	10,30	10,66	10,95	11,17	11,32	11,42	11,45	dB
Spacecraft (SNR Method)																			
Spacecraft Antenna Pointing Loss:	0,50																		dB
Spacecraft Antenna Gain:	5,50																		dB
Spacecraft Total Transmission Line Losses:	2,00																		dB
Spacecraft System Noise Temperature:	260,00																		K
Spacecraft Figure of Merrit (G/T):	-20,65																		dB/K
Signal Power at Spacecraft LNA Input:	-137,73	-135,31	-133,54	-132,04	-130,75	-129,64	-128,68	-127,85	-127,13	-126,52	-126,00	-125,56	-125,20	-124,91	-124,69	-124,53	-124,44	-124,41	dBW
Spacecraft Receiver Bandwidth:	1.200.000,00																		Hz
Spacecraft Receiver Noise Power (Pn = kTB)	-143,66																		dBW
Signal-to-Noise Power Ratio at G.S. Rcvr:	5,93	8,35	10,12	11,62	12,90	14,02	14,98	15,81	16,52	17,14	17,66	18,10	18,46	18,75	18,97	19,13	19,22	19,25	dB
Analog or Digital System Required S/N:	7,80																		dB
System Link Margin	-1,87	0,55	2,32	3,82	5,10	6,22	7,18	8,01	8,72	9,34	9,86	10,30	10,66	10,95	11,17	11,32	11,42	11,45	dB

Table 76. S band downlink budget

Spacecraft Orbit & Link Parameters																			
Mean Orbit Altitude:	550,00																		km
Mean Orbit Radius:	6928,14																		km
Elevation Angle (**ε**):	5,00	10,00	15,00	20,00	25,00	30,00	35,00	40,00	45,00	50,00	55,00	60,00	65,00	70,00	75,00	80,00	85,00	90,00	°
Slant Range (**S**):	2205,90	1815,65	1518,37	1293,77	1123,42	992,87	891,59	812,11	749,14	698,94	658,84	626,89	601,71	582,25	567,79	557,80	551,93	550,00	km
Frequency:	2210,00																		MHz
Wavelength (**λ**):	0,14																		
Spacecraft																			
Spacecraft Transmitter Power Output:	1,00																		Watts
In dBW:	0,00																		dBW
In dBm:	30,00																		dBm
Spacecraft Total Transmission Line Losses:	1,00																		dB
Spacecraft Antenna Gain:	5,50																		dBi
Spacecraft EIRP:	4,50																		dBW
Downlink Path																			
Spacecraft Antenna Pointing Loss:	0,50																		dB
S/C-to-Ground Antenna Polarization Loss:	0,50																		dB
Path Loss:	166,22	164,53	162,98	161,59	160,36	159,29	158,35	157,54	156,84	156,24	155,73	155,30	154,94	154,65	154,43	154,28	154,19	154,16	dB
Gaseous attenuation:	0,40	0,20	0,14	0,10	0,08	0,07	0,06	0,05	0,05	0,05	0,04	0,04	0,04	0,04	0,04	0,04	0,04	0,04	dB
Cloud and fog attenuation:	0,05	0,02	0,02	0,01	0,01	0,01	0,01	0,01	0,01	0,01	0,00	0,00	0,00	0,00	0,00	0,00	0,00	0,00	dB
Rain attenuation:	0,07	0,04	0,02	0,02	0,02	0,01	0,01	0,01	0,01	0,01	0,01	0,01	0,01	0,01	0,01	0,01	0,01	0,01	dB
Attenuation due to tropospheric scintillation:	0,84	0,37	0,23	0,16	0,13	0,10	0,09	0,08	0,07	0,06	0,06	0,05	0,05	0,05	0,05	0,04	0,04	0,04	dB
Ionospheric Losses:	0,10																		dBi
Received power at Ground Station	-164,18	-161,76	-159,98	-158,48	-157,20	-156,08	-155,12	-154,29	-153,57	-152,96	-152,44	-152,00	-151,64	-151,35	-151,13	-150,97	-150,88	-150,85	dBW
Ground Station (Eb/No Method)																			
Ground Station Antenna Pointing Loss:	0,50																		dB
Ground Station Antenna Gain:	26,50																		dB
Ground Station Total Transmission Line Losses:	1,90																		dB
Antenna or "Sky" Temperature	29,53	16,51	12,04	9,80	8,46	7,58	6,95	6,50	6,16	5,89	5,69	5,52	5,40	5,30	5,23	5,19	5,16	5,15	K
Ground Station Effective Noise Temperature:	170,00																		K
Ground Station System Noise Temperature:	199,53	186,51	182,04	179,80	178,46	177,58	176,95	176,50	176,16	175,89	175,69	175,52	175,40	175,30	175,23	175,19	175,16	175,15	K
Ground Station Figure of Merrit (G/T):	1,60	1,89	2,00	2,05	2,08	2,11	2,12	2,13	2,14	2,15	2,15	2,16	2,16	2,16	2,16	2,17	2,17	2,17	dB/K
Ground Station Carrier-to-Noise Power Density (C/No)	65,52	68,23	70,12	71,67	72,99	74,12	75,10	75,94	76,67	77,29	77,81	78,26	78,62	78,91	79,14	79,29	79,39	79,42	dBHz
System Desired Data Rate:	512000,00																		bps
In dBHz:	57,09																		dBHz
Command System Eb/No:	8,43	11,14	13,02	14,58	15,90	17,03	18,01	18,85	19,57	20,19	20,72	21,16	21,53	21,82	22,04	22,20	22,29	22,32	dB
Required Eb/No (Threshold):	11,50																		dB
System Link Margin:	-3,07	-0,36	1,52	3,08	4,40	5,53	6,51	7,35	8,07	8,69	9,22	9,66	10,03	10,32	10,54	10,70	10,79	10,82	dB
Ground Station (SNR Method)																			
Ground Station Antenna Pointing Loss:	0,50																		dB
Ground Station Antenna Gain:	26,50																		dB
Ground Station Total Transmission Line Losses:	1,90																		dB
Ground Station System Noise Temperature:	199,53	186,51	182,04	179,80	178,46	177,58	176,95	176,50	176,16	175,89	175,69	175,52	175,40	175,30	175,23	175,19	175,16	175,15	K
Ground Station Figure of Merrit (G/T):	1,60	1,89	2,00	2,05	2,08	2,11	2,12	2,13	2,14	2,15	2,15	2,16	2,16	2,16	2,16	2,17	2,17	2,17	dB/K
Signal Power at Ground Station LNA Input:	-140,08	-137,66	-135,88	-134,38	-133,10	-131,98	-131,02	-130,19	-129,47	-128,86	-128,34	-127,90	-127,54	-127,25	-127,03	-126,87	-126,78	-126,75	dBW
Ground Station Receiver Bandwidth (B):	1.200.000,0																		Hz
G.S. Receiver Noise Power (Pn = kTB)	-144,81	-145,10	-145,21	-145,26	-145,29	-145,31	-145,33	-145,34	-145,35	-145,36	-145,36	-145,36	-145,37	-145,37	-145,37	-145,37	-145,37	-145,37	dBW
Signal-to-Noise Power Ratio at G.S. Rcvr:	4,73	7,44	9,33	10,88	12,20	13,33	14,31	15,15	15,87	16,49	17,02	17,46	17,83	18,12	18,34	18,50	18,59	18,63	dB
Analog or Digital System Required S/N:	7,80																		dB
System Link Margin	-3,07	-0,36	1,52	3,08	4,40	5,53	6,51	7,35	8,07	8,69	9,22	9,66	10,03	10,32	10,54	10,70	10,79	10,82	dB

15.3.4. Payload Link Budget

Table 77. PNT signal power at ground level

Spacecraft Orbit & Link Parameters																			
Mean Orbit Altitude:	550,00																		km
Mean Orbit Radius:	6928,14																		km
Elevation Angle (**ε**):	5,00	10,00	15,00	20,00	25,00	30,00	35,00	40,00	45,00	50,00	55,00	60,00	65,00	70,00	75,00	80,00	85,00	90,00	°
Slant Range (**S**):	2205,90	1815,65	1518,37	1293,77	1123,42	992,87	891,59	812,11	749,14	698,94	658,84	626,89	601,71	582,25	567,79	557,80	551,93	550,00	km
Frequency:	2210,00																		MHz
Wavelength (**λ**):	0,14																		
Spacecraft																			
Spacecraft Transmitter Power Output:	5,00																		Watts
In dBW:	6,99																		dBW
In dBm:	36,99																		dBm
Spacecraft Total Transmission Line Losses:	1,00																		dB
Spacecraft Antenna Gain:	5,50																		dBi
Spacecraft EIRP:	11,49																		dBW
Downlink Path																			
Spacecraft Antenna Pointing Loss:	0,50																		dB
S/C-to-Ground Antenna Polarization Loss:	0,50																		dB
Path Loss:	166,22	164,53	162,98	161,59	160,36	159,29	158,35	157,54	156,84	156,24	155,73	155,30	154,94	154,65	154,43	154,28	154,19	154,16	dB
Gaseous attenuation:	0,40	0,20	0,14	0,10	0,08	0,07	0,06	0,05	0,05	0,05	0,04	0,04	0,04	0,04	0,04	0,04	0,04	0,04	dB
Cloud and fog attenuation:	0,05	0,02	0,02	0,01	0,01	0,01	0,01	0,01	0,01	0,01	0,00	0,00	0,00	0,00	0,00	0,00	0,00	0,00	dB
Rain attenuation:	0,07	0,04	0,02	0,02	0,02	0,01	0,01	0,01	0,01	0,01	0,01	0,01	0,01	0,01	0,01	0,01	0,01	0,01	dB
Attenuation due to tropospheric scintillation:	0,84	0,37	0,23	0,16	0,13	0,10	0,09	0,08	0,07	0,06	0,06	0,05	0,05	0,05	0,05	0,04	0,04	0,04	dB
Ionospheric Losses:	0,10																		dBi
Received power at Ground Level	-157,19	-154,77	-152,99	-151,49	-150,21	-149,09	-148,13	-147,30	-146,58	-145,97	-145,45	-145,01	-144,65	-144,36	-144,14	-143,98	-143,89	-143,86	dBW

15.3.5. ΔV Budget

15.3.5.1. Phasing Maneuver

In this section the ΔV Budget for the phasing maneuver shall be calculated. The mission requires 10 satellites to be phased within a single orbital plane at an altitude of 550 km, so that they are evenly spaced in it. To account for the worst-case scenario, the ΔV required to phase a single satellite by 180 degrees shall be calculated.

Additionally, it is assumed that after this maneuver is completed N days or approximately $N \cdot 15$ orbital periods of the satellite at its original altitude of 550 km are going to pass before readjusting its orbit to the original one with a second burn.

The philosophy behind these maneuvers is that by performing a burn to change the altitude of the satellite, its period is going to change by $\varDelta T$. More specifically, by lowering the altitude of a satellite that has a period of T, it will change to T' and the periods will be related by the formula $T' = T - \varDelta T$. Over the course of N orbits, this difference in orbital period will accumulate into a 180-degree phase shift, equivalent to half of the original orbit, and then by performing a second burn in the opposite direction the satellite shall return to its original orbit.

This can be expressed mathematically as follows:

$$N \cdot \varDelta T = \frac{T}{2} \quad or \quad \varDelta T = \frac{T}{2 \cdot N}$$

N: the number of orbits

By having knowledge of the spacecraft's initial state and its desired orbital period after the maneuver, it is possible to calculate the ΔV required via STK. This is done using the Astrogator propagator by inserting a "Target Sequence" item with a "maneuver" nested within it.

Table 78. Phasing duration and ΔV tradeoff

Phasing Duration	ΔV required (m/s)	ΔV with 50% margin (m/s)
1 day (15 orbits)	175.2	262,8
3 days (45 orbits)	57.8	86,7
5 days (75 orbits)	35.0	52,5
6 days (90 orbits)	29.2	43,8
7 days (105 orbits)	25.2	37,8
10 days (150 orbits)	18.0	27,0

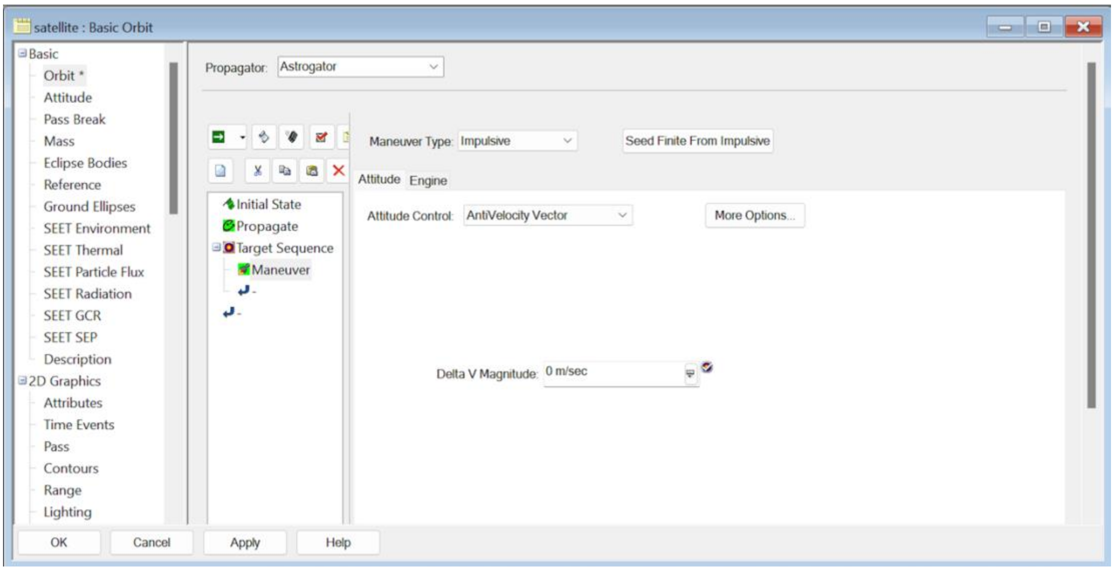

Figure 100. Target Sequence – Maneuver

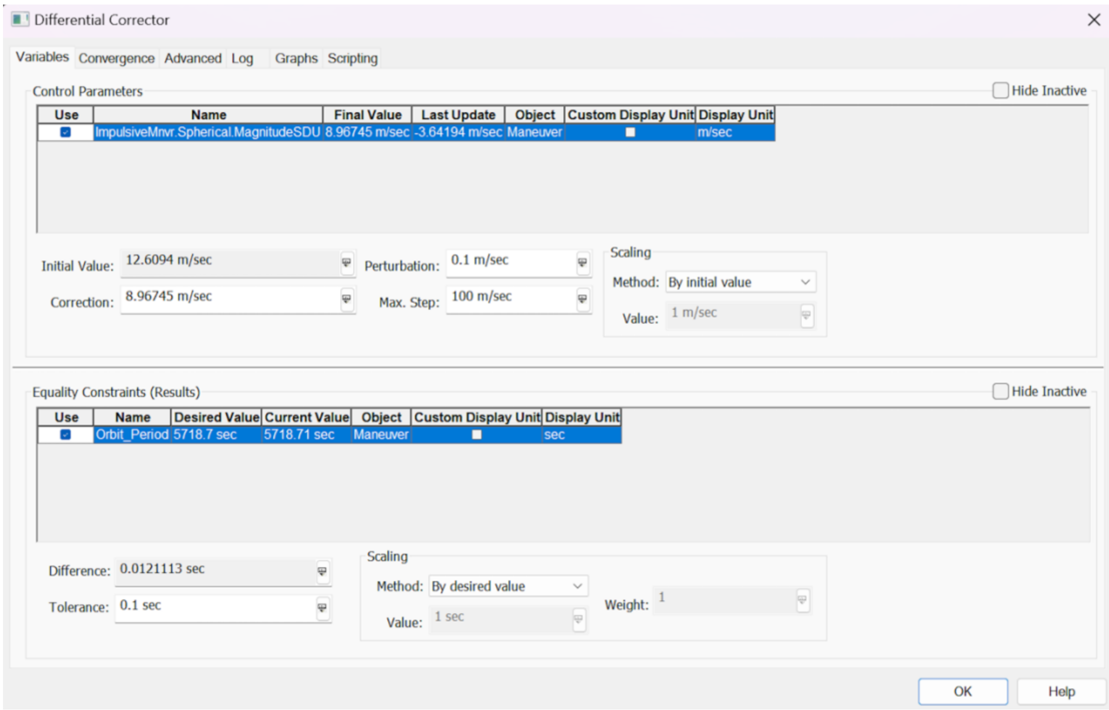

Figure 101. Differential Corrector – setting target orbital period

15.3.5.2. Stationkeeping

The primary causes of a satellite's loss of altitude are atmospheric drag and solar radiation pressure. Their combined vector was modeled in STK, and by analyzing its values over a year, the average deceleration exerted on the satellite can be determined. Therefore, the ΔV required for 3 years of stationkeeping can be calculated.

In the STK simulation, a worst-case scenario was considered, where the satellite's cross-sectional area was assumed to be 2133 cm², and its mass was set at 12.5 kg. This results in an area-to-mass ratio of about 0.02 m²/kg.

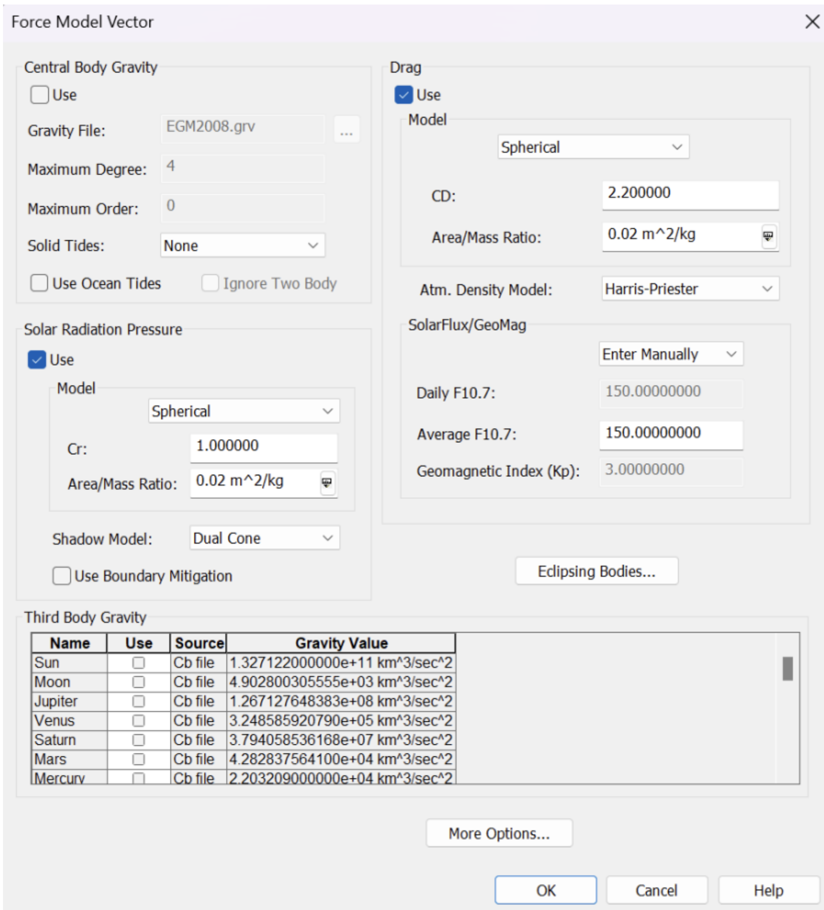

Figure 102. Drag and solar pressure vector properties

Table 79. Stationkeeping ΔV budget

ΔV required (m/s)	ΔV with 50% margin (m/s)
41.7	62.6

Table 80. ΔV Budget for a 10-day phasing maneuver and stationkeeping

ΔV required (m/s)	ΔV with 50% margin (m/s)	Residual ΔV for collision avoidance maneuvers and deorbiting (m/s)
59.8	89.6	170

15.3.6. Telemetry Data Budget

Telemetry is constantly generated and stored on the CDHS OBC on board memory. It is assumed that a full telemetry line representing all telemetry fields requires less than 500 bytes (incl. 50% margin). Telemetry is sampled every 10s as a baseline. This can be decreased to provide more granularity for calibration, failure recovery etc, at the expense of the total duration that can be logged. Full Telemetry logs can be downloaded only through the S-Band link. Under nominal conditions it is expected that such full level of detail is not required regularly. UHF link will be used only for real time issuing of commands and retrieval of responses. The UHF data rate can support a sampling period of 1s, if the increased resolution is required by operations.

Table 81. S-Band Telemetry data budget

Size of a single telemetry line (incl. 50% margin)	500
Sampling Time	10s
Data generated per 24h w/ 50% margin	4.12 MB
Contact Time	260s
Data Rate	1Mbps
Lines Transmitted	65000
Log duration corresponding to transmitted lines	180.5 h
Average Time between contacts	12 h

Table 82. UHF Telemetry data budget

Size of a single telemetry line (incl. 50% margin)	500
Sampling Time	1s
Telemetry generation data rate w/ 50% budget	4 kbps
UHF data rate	9.6 kbps
Data rate margin	140%

Telemetry logs in the OBC are kept for a maximum of 7 days. Telemetry logging follows a FIFO scheme (oldest data overwritten). In the case of CubeADCS, the subsystem onboard memory will be used to store the ADCS logs, in accordance with the manufacturer's suggestions. Essential ADCS data (angular rates of satellite, orientation) will also be stored on the CDHS for redundancy.

Table 83. OBC memory budget

Telemetry log timespan	7 days
Memory required for logs	29 MB
Total memory available on OBC	128 MB

15.4. Thermal Analysis

There are three ways of heat transfer; conduction, convection and via radiation. In the space environment the main method of heat transfer is via radiation. When a satellite is in orbit around a planetary body there are three external heat sources that need to be taken into consideration; the direct solar radiation, the albedo and the thermal emittance from the celestial body. Additionally, the internal heat dissipation of the satellite will be considered.

15.4.1. Solar Radiation

The solar radiation is the main heating source for a spacecraft in space. Its intensity varies regarding the distance between the spacecraft and the Sun. For a satellite orbiting the Earth solar constant has an average value of 1367 W m^{-2}, with a maximum val-ue of 1414 W m^{-2}and a minimum value of 1322 W m^{-2}, which is changing while the Earth orbits the Sun. The above values are recommended by the World Radiation Center in Davos in Switzerland [73]. Another variation of the solar constant is created due to the 11-year solar cycle, but it is in the magnitude of 0.1% and it is considered negligible [73]. The heat gained (W) due to the direct solar flux is:

The heat gained (W) due to the direct solar flux is:

$$Q_{solar} = aS_{solar}A_{sun}$$

Where:
a: the absorptivity coefficient of the spacecraft's surface
S_{solar}: the solar radiation flux (W m^{-2})
A_{sun}: the area of the spacecraft vertical to the solar rays (m^2)

For this analysis, it is considered that the CubeSat maintains nadir pointing attitude, with one of its 8U sides facing to nadir.

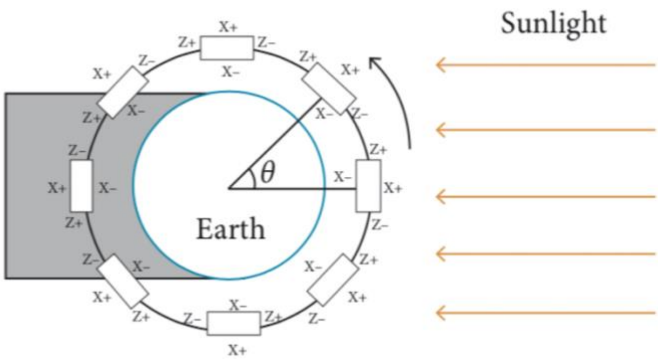

Figure 103. A CubeSat in nadir pointing mode remains oriented towards the center of Earth throughout the orbit [74]

While the CubeSat orbits a celestial body, it rotates in a way that both its 2U sides and its one 8U side (since the other is constantly facing to nadir) are exposed to direct sunlight. If a surface A is inclined at an angle γ to the solar rays, the projected area of the surface vertical to the rays (A_p) is given by:

$$A_p = A \cos\gamma$$

While in orbit, if the given surface performs a complete rotation, the angle γ is constantly changing. Since a surface rotates in and out of the Sunview, the average surface area over a full revolution (i.e., 0 to 2π radians) needs to be determined.

$$A_{p,average} = \frac{1}{2\pi}\int_0^{2\pi} A_p \, d\gamma = \frac{1}{2\pi}\int_0^{2\pi} A \cos\gamma \, d\gamma$$

By considering the zero radians position being with the surface normal facing away from the solar vector. The integral then goes to zero when the surface normal rotates between π/2 and 3π/2 (i.e., the active surface is out of Sunview). Thus, the integral limits can be reduced and the $A_{p,average}$ relation rewritten as [75]:

$$A_{p,average} = \frac{A}{2\pi} \int_{3\pi/2}^{\pi/2} \cos\gamma \, d\gamma = \frac{A}{\pi}$$

The total surface of the CubeSat projected vertically to the solar rays is [75]:

$$A_{p,total} = \frac{1}{\pi}(A_{8U} + A_{2U} + A_{2U}) = \frac{1}{\pi}(A_{8U} + 2 \cdot A_{2U})$$

15.4.2. Albedo

The albedo is the measure of the diffuse reflection of solar radiation out of the total solar radiation and measured on a scale from 0 to 1. The proportion reflected is not only determined by properties of the surface itself, but also by the spectral and angular distribution of solar radiation reaching the Earth's surface. For the Earth the reflectivity is greater over land areas, and generally increases as the local height of the Sun decreases, and when the cloud coverage increases. So, in areas of high geographical latitude where the presence of clouds, snow and ice is strong, and also the Sun is at a relatively small local altitude the albedo tends to increase. In addition, the albedo which is the sunlight reflected from the surface of the Earth, depends on the cosine of the angle between Sun - Earth - Satellite.

Data related to specific satellite orbits from NASA's data library that include the relevant geometric factor and are shown in the table below [76].

Table 84. Earth's Albedo depending on the inclination

Orbit inclination (deg)	Albedo (percent)	
	Min	Max
0-30	18	55
30-60	23	57
60-90	23	57

The heat gained from a surface of the satellite (W) due to the albedo flux is:

$$Q_{albedo} = aS_{solar}a_{albedo}AF_{1-2}$$

Where:

a_{albedo}: a dimensionless albedo constant that describes the reflectivity of the celestial body
F_{1-2}: the view factor from the surface of the celestial body to the spacecraft
A: the CubeSat's surface area exposed to radiation from the planetary body

The view factor is the proportion of the radiation which leaves surface 1 and strikes surface 2 and it has to do with the relative orientation between two surfaces. We consider that the CubeSat is nadir oriented, so it has its sides either vertical or horizontal to the nadir direction (both 2U and both 3U sides are horizontally oriented and one 8U side is vertically oriented, since the other one is constantly facing the zenith direction). The respective view factors can be considered as [77]:

$$F_{ver} = \left(\frac{1}{h^*}\right)^2 \text{and } F_{hor} = -\frac{\sqrt{(h^*)^2-1}}{\pi (h^*)^2} + \frac{1}{\pi} tan^{-1}\left(\frac{1}{\sqrt{(h^*)^2-1}}\right)$$

where

$h^* = \frac{R+h}{R}$, R being the radius of the celestial body radius and h being the altitude.

15.4.3. Planetary Infrared Radiation

All objects, including stars and planets, radiate energy to their surroundings. The heat radiated is described by the Stefan–Boltzmann law and depends on the temperature of the body (T) and its surface emissivity (ε), which is the effectiveness, of the surface material, emitting energy as thermal radiation.
For satellites orbiting the Earth there are data related the orbit's inclination from NASA's data library [76]:

Table 85. Earth's thermal emission depending on the inclination

Orbit inclination (deg)	Emitted Radiation (W/m^2)	
	Min	Max
0-30	228	275
30-60	218	257
60-90	218	244

The heat gained from a surface of the satellite (W) due to planetary radiation is:

$$Q_{planetary-IR} = aS_{planetary-IR}AF_{1-2}$$

with
$S_{planetary-IR}$: the radiation flux of the planetary body (W m^{-2})

15.4.4. Internal Heat Dissipation from the Spacecraft

While the spacecraft is operational, internal heat is generated by its electrical components. In this analysis, the heat dissipation is directly correlated with the spacecraft's CONOPS and its power consumption, with thermal dissipation considered as a portion of the total power used. Three cases are considered; 50%, 80% and 100% of the power consumption is converted to heat emissions.

15.4.5. Spacecraft’s Thermodynamical Equilibrium Equation

By having knowledge about the thermal loads that apply on the satellite and its thermodynamical equilibrium equation, we can have complete knowledge of its thermal state. The CubeSat is considered a compact object that has a uniform thermal capacity and temperature throughout his whole body. The equation is:

$$Q_{in} = Q_{out} + mc \cdot dT/dt$$

where
Q_{in}: the thermal power absorbed by the satellite (W)
Q_{out}: the thermal power radiated from the satellite (W)
$m \cdot c$: the thermal capacity of the satellite (JK^{-1}), with m being the satellite’s mass (kg) and c being the specific heat capacity ($JK^{-1}kg^{-1}$).

The thermal power absorbed by the satellite Q_{in} consists of the thermal power from the Sun Q_{solar}, the thermal power due to albedo Q_{albedo}, the thermal power from the celestial body CubeSat orbits $Q_{planetary-IR}$, and the internal heat dissipation from the CubeSat $Q_{internal}$. While in eclipse, Q_{solar} and Q_{albedo} are considered to be zero.

$$Q_{in} = Q_{solar} + Q_{albedo} + Q_{planetary-IR} + Q_{internal}$$

The thermal power radiated from the satellite Q_{out} is given by the equation:

$$Q_{out} = \varepsilon\sigma A_{total} T^4$$

where
ε: the dimensionless constant of the surface emissivity of the CubeSat
σ: the Stefan-Boltzmann constant (5.67 x $10^{-8} Wm^{-2}K^{-4}$)
A_{total}: the total surface of the satellite (m^2)

The differential is approached by the derivative’s definition. While having defined beforehand the repetition K, the time step Δt and the corresponding temperatures, it is assumed that:

$$dT/dt = \Delta T/\Delta t = (T[K] - T[K-1])/\Delta t$$

This is a proposed method from literature for the transient temperature analysis of objects in orbit [75]. For the calculations we assume that the CubeSat weights 11.3 Kg, that its body is homogenous and has the specific heat capacity of aluminum Al 6061-T6, $C_p = 896 Jkg^{-1}K^{-1}$.

15.4.6. Emissivity and Absorptivity Coefficients

It is assumed that the satellite’s body is made with aluminum alloy Al 6061-T6. It is also assumed that the 60% of the total surface area of the CubeSat is uniformly covered by solar panels. Assuming the panels’ coefficients are $a_{panel} = 0.9$ and $\varepsilon_{panel} = 0.85$ and aluminum’s coefficients are $a_{Al} = 0.16$ and $\varepsilon_{Al} = 0.03$, the CubeSat’s coefficients are: $a = 0.6$ and $\varepsilon = 0.52$ [73], [78].

15.4.7. Thermal Simulation Results

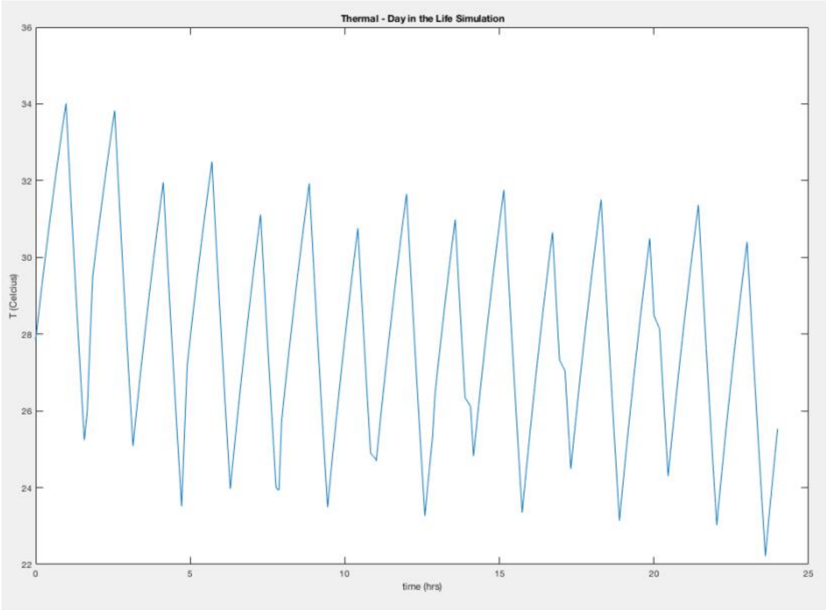

Figure 104. Spacecraft temperature - Day in the life simulation – 80% electrical power-to-heat conversion ratio

Due to the partial ambiguity of the diagram, a longer duration of 5 days was taken into consideration.

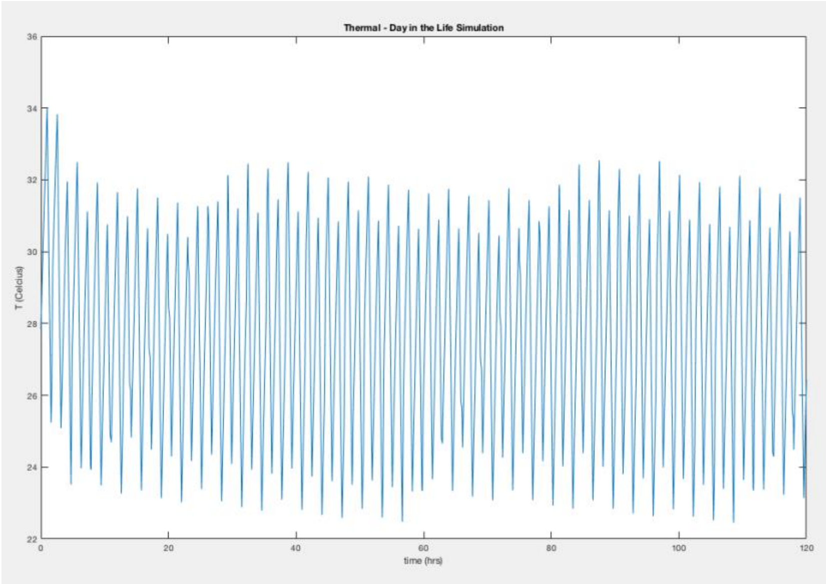

Figure 105. Spacecraft temperature – 5 Days in the life simulation – 80% electrical power-to-heat conversion ratio

However, each component does not convert the same percentage of its power consumption into heat. To ensure the analysis is valid, two worst-case scenarios have been identified: a 50% and a 100% electrical power-to-heat conversion ratio.

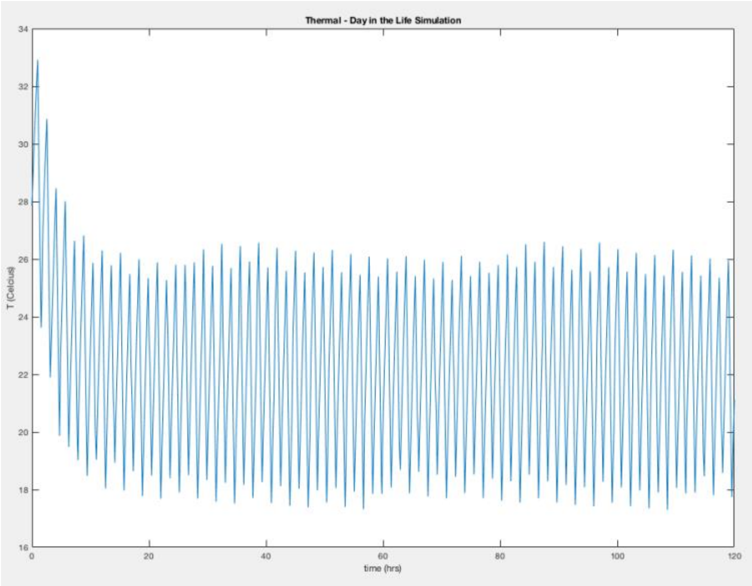

Figure 106. Spacecraft temperature – 5 Days in the life simulation – 50% electrical power-to-heat conversion ratio

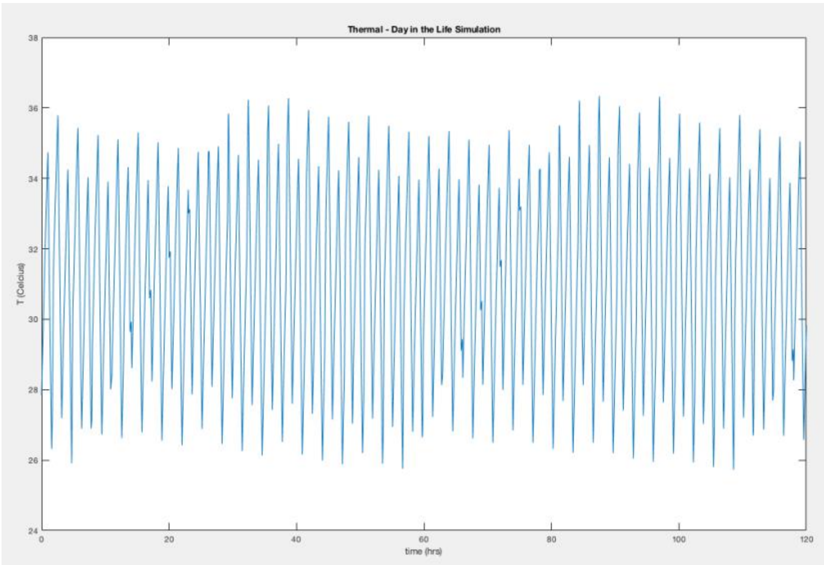

Figure 107. Spacecraft temperature – 5 Days in the life simulation – 100% electrical power-to-heat conversion ratio

The simulations are run for a 5-day period and the combined temperature range is: $17℃ - 36℃$.

15.5. System Reliability

The system's reliability should be evaluated; however, up to this day CubeSat missions do not undergo reliability assessment and since the data are not available yet, it is not applicable on this mission. Instead, the desired goal of service availability is set. As mentioned in the SR-MIS-020 The system should have at least 97% service availability. Thus, it needs to be ensured that spacecrafts are able to operate with minimal interruptions.

To do so, single-event latch-ups (SEL) and single-event functional interrupts (SEFI) mitigation strategies shall be implemented so that the system shall be able to prevent or recover from radiation-induced errors. This includes redundancy in components and connections and the implementation of Error Detection and Correction (EDAC) mechanisms to help detect and automatically correct induced errors. EDAC methodologies such as Hamming codes, which detect and correct single-bit errors or Reed-Solomon codes, which handle multiple errors in data blocks should be considered. Additionally, radiation-hardened components are employed to reduce sensitivity to space radiation, while periodic system resets should be considered to clear transient errors and maintain long-term reliability. Finally, a comprehensive FDIR strategy shall be designed and implemented to allow the spacecraft to autonomously detect, isolate, and recover from faults, minimizing dependence on ground control interventions so that spacecrafts are able to return to nominal operation without the need of a GCS overpass.

16. **Conclusion**

In this thesis, a comprehensive exploration of the state-of-the-art developments in Positioning, Navigation, and Timing (PNT) systems from Low Earth Orbit (LEO) with an emphasis on CubeSats is presented. Moreover, payload technologies for timekeeping in microsatellite and nanosatellite platforms are explored while focusing on atomic clocks.

Based on these advancements, the feasibility of a CubeSat-based LEO PNT system that could offer services to multiple country-sized areas in the same latitude bounds was assessed. A preliminary design of the system that is based solely on COTS components is presented that accounts for every aspect of such a mission. The design is based on the ERMIS mission of the Greek CubeSat In-Orbit Validation (IOV) programme and it concluded that it is possible to provide the PNT services mentioned above with 100 8U CubeSats without the need of a dedicated ground segment dedicated to timekeeping. Instead, the CubeSats shall operate by relying on MEO GNSS and relaying the PNT signals on S-Band.

Since such mission is feasible, a more detailed system analysis is recommended to lead to the CDR of the system. However, in order to proceed additional information is required for the subsystems and the payload, that more probable than not can only be obtained after an NDA with the respective provider.

In EUSPA EO and GNSS Market Report, it was concluded that GNSS downstream market revenues are expected to rise from more than €260 billion in 2023 to around €580 billion in 2033. Moreover, the GNSS cumulative revenues are forecast to reach €4.6 trillion in the next decade with the service revenues accounting for almost 80% in 2033. The current and the predicted economic growth of the PNT market along with the success story of the New Space and the CubeSats suggest that a business offering commercial PNT sevices via a CubeSat-Based Multi-Regional Positioning Navigation and Timing System in Low Earth Orbit is positioned for success in an emerging market.

17. List of Abbreviations

Abbreviation	Meaning
ACS	Attitude Control Subsystem
ADEV	Allan Deviation
ADCS	Attitude Determination and Control Subsystem
AFR	Atomic Frequency References
AIV	Assembly, Integration, and Verification
AOA	Angle of Arrival
APD	Avalanche Photodetector
ARC	Ames Research Center
ART	Average Revisit Time
BPSK	Binary Phase Shift Keying
CCSDS	Consultative Committee for Space Data Systems
CDHS	Control and Data Handling Subsystem
CON	Constellation
COTS	Commercial Off-The-Shelf
CPT	Coherent Population Trapping
Cs	Cesium
CSAC	Chip-Scale Atomic Clock
DARPA	Defense Advanced Research Projects Agency
DC	Direct Current
EMI	Electromagnetic Interference
EMISM	EMI Safety Margin
EPS	Electrical Power Subsystem
EUSPA	European Union Agency for the Space Programme
FOV	Field of View
GEO	Geosynchronous Earth Orbit
GDOP	Geometric Dilution of Precision
GNSS	Global Navigation Satellite System
GPS	Global Positioning System
GCS	Ground Control Station
GRS	Ground Segment
GS	Ground Station
GSaaS	Ground Segment as a Service
H	Hydrogen
I2C	Inter-Integrated Circuit
IOD	In Orbit Demonstration
ISS	International Space Station
ITRF	International Terrestrial Reference Frame
ITU	International Telecommunication Union
Kyutech	Kyushu Institute of Technology
LCH	Launch
LDO	Low-Dropout Voltage
LEOP	Launch and Early Orbit Phase
LEO	Low Earth Orbit
LHCP	Left-Hand Circularly Polarized
LO	Local Oscillator

LRA	Laser Retroreflector Array
LVDS	Low-Voltage Differential Signaling
MAC	Miniature Atomic Clock
MCU	Micro-Controller Unit
MEMS	Micro-Electro-Mechanical Systems
MEO	Medium Earth Orbit
MEOP	Maximum Expected Operating Pressure
MIS	Mission
MPE	Maximum Predicted Environment
MRT	Maximum Revisit Time
NavIC	Navigation with Indian Constellation
NDA	Non-Disclosure Agreement
NTU	Nanyang Technological University
ODTS	Orbit Determination and Time Synchronization
OBC	On-Board Computer
OQPSK	Offset Quadrature Phase Shift Keying
OPS	Operations
PLD	Payload
POD	Precise Orbit Determination
PNT	Positioning, Navigation, and Timing
PPP	Precise Point Positioning
PPP-RTK	Precise Point Positioning Real-Time Kinematic
PRO	Propulsion
PSD	Power Spectral Density
PSSL	Precision Space Systems Laboratory
QPSK	Quadrature Phase Shift Keying
QZSS	Quasi-Zenith Satellite System
RAD	Radiation
RF	Radio Frequency
RHCP	Right-Hand Circularly Polarized
RNSS	Regional Navigation Satellite System
RSS	Radiated Susceptibility
RWFM	Random Walk Frequency Modulation
Rb	Rubidium
Rx	Receive
SC	Spacecraft
SEFI	Single-Event Functional Interrupts
SEL	Single-Event Latch-ups
SLR	Satellite Ranging Laser
SoO	Signals of Opportunity
SPP	Single Point Positioning
STK	Systems Tool Kit
STL	Satellite Time and Location
SWaP	Surface, Weight, and Power
TC	Telecommand
TEC	Total Electron Content
TID	Total Ionizing Dose
TLE	Two-Line Element

THM	Thermal
TM	Telemetry
TT&C	Telemetry, Tracking, and Command
Tx	Transmit
UHF	Ultra High Frequency
UF	University of Florida
UART	Universal Asynchronous Receiver-Transmitter
UOA	University of Athens
US	United States
USNO	United States Naval Observatory
VCSEL	Vertical Cavity Surface Emitting Laser
VLBI	Very Long Baseline Interferometry

18. Appendix

18.1. MATLAB script for Battery SoC - Day in the Life Simulation

```
clc;
close all;
clear all;

scenario_time=86400; % # of days
initial_battery_charge=100.0; %Wh
orbit_period=5665.0; %sec
time_in_eclipse=2136.0; %sec, max eclipse time calculated in STK
time_in_sunlight=orbit_period-time_in_eclipse;

%Create a matrix of scenario_time cells that will simulate eclipse and sunlight by 0s and 1s.
%to do this, first a cycle of 1s followed by 0s is created

cycle= [ones(1, time_in_sunlight), zeros(1, time_in_eclipse)];

%calculate the number of repetitions of this cycle are needed to reach the length of scenario_time
num_repeats=ceil(scenario_time / orbit_period);
sun_status_matrix= repmat(cycle, 1, num_repeats); %repeat the cycle to cover the entire scenario_time cells
sun_status_matrix=sun_status_matrix(1:scenario_time); %trim the matrix to scenario_time elemets

%define Sun Tracking mode's Power Generation and Power Consumption
avg_power_generation=40;
avg_power_consumption=12.1;

power_generation_matrix = sun_status_matrix * avg_power_generation;

%Here, extra power modes are added. When a mode is initiated, power
%generation is assumed to be 0

% add an S-Band link that consumes 32.6 W for 300 secs, at a random point:
% Epoch 3000.

sband_start_time(1)= 3000;
sband_interval = 43200;
number_sband_links=floor(scenario_time/sband_interval);

for i=2:number_sband_links
sband_start_time(i)= sband_start_time(i-1)+sband_interval;
end

sband_duration = 300;
sband_consumption = 32.6;
sband_consumption_matrix = zeros(1,scenario_time)

for i=2:number_sband_links
sband_consumption_matrix(sband_start_time(i):(sband_start_time(i) + sband_duration)) = sband_consumption;
end

% add a PNT service Mode that consumes 56.1 W for 642 secs, at a random point:
% Epoch 6000.
pnt_service_duration = 642;
pnt_service_consumption = 56.1;

pnt_service_start_time(1)= 6000;
pnt_service_interval=11000;
number_of_pnt_service=floor(scenario_time/pnt_service_interval);

for i=2:number_of_pnt_service
pnt_service_start_time(i)= pnt_service_start_time(i-1)+pnt_service_interval;
end

pnt_service_consumption_matrix = zeros(1,scenario_time)

% pnt service is assumed to be ON number_of_pnt_service times in the
```

```
% scenario_time duration§
for i=1:number_of_pnt_service
   pnt_service_consumption_matrix(pnt_service_start_time(i):(pnt_service_start_time(i)+ pnt_service_duration)) =
pnt_service_consumption;
end

power_balance_matrix = power_generation_matrix - avg_power_consumption
battery_soc_matrix = ones(1,scenario_time) * initial_battery_charge; % battery State of Charge

for i=1:scenario_time-1
   if sband_consumption_matrix(i)==0 && pnt_service_consumption_matrix(i)==0
      battery_soc_matrix(i+1) = battery_soc_matrix(i) + power_balance_matrix(i)*(1/3600);
       if battery_soc_matrix(i+1) > 100
          battery_soc_matrix(i+1)= 100;
       end
   elseif sband_consumption_matrix(i) ~= 0
    battery_soc_matrix(i+1) = battery_soc_matrix(i) - sband_consumption_matrix(i)*(1/3600);
    if battery_soc_matrix(i+1) > 100
          battery_soc_matrix(i+1)= 100;
    end
   elseif pnt_service_consumption_matrix(i) ~= 0
    battery_soc_matrix(i+1) = battery_soc_matrix(i) - pnt_service_consumption_matrix(i)*(1/3600);
    if battery_soc_matrix(i+1) > 100
          battery_soc_matrix(i+1)= 100;
    end
   end
end

Time(1)=0; %starting time
for K=2:scenario_time
   Time(K)=Time(K-1)+1;
end

plot(Time(1,:) / 3600,battery_soc_matrix(1,:))
ylabel('Battery Charge (Wh)');
xlabel('time (hrs)')
title('Battery SoC - Day in the Life Simulation')
min_battery_soc=min(battery_soc_matrix);
```

18.2. MATLAB script for Thermal - Day in the Life Simulation

```
clc;
close all;
clear all;

sigma=5.68e-8; % Boltzmann constant
Ssolar=1368; %average solar constant
Splanetary=(244+218)/2; %central body's IR emission
albedo=(0.57+0.23)/2; %albedo
R=6371000;  %central body's radius
scenario_time=5*86400; % # of days

%info regarding the orbital period and eclispe time
orbit_period=5665.0; %sec
time_in_eclipse=2136.0; %sec, max eclipse time
time_in_sunlight=orbit_period-time_in_eclipse;

%Create a matrix of scenario_time cells that will simulate eclipse and sunlight by 0s and 1s.
%to do this, first a cycle of 1s followed by 0s is created
cycle= [ones(1, time_in_sunlight), zeros(1, time_in_eclipse)];
%calculate the number of repetitions of this cycle are needed to reach the length of scenario_time
num_repeats=ceil(scenario_time / orbit_period);
sun_status_matrix= repmat(cycle, 1, num_repeats); %repeat the cycle to cover the entire scenario_time cells
sun_status_matrix=sun_status_matrix(1:scenario_time); %trim the matrix to scenario_time elemets

h=550000;   %altitude
alpha=0.6;
epsilon=0.52;
Cp=896;    %Cp
mass=11.3;   %CubeSat's mass
power_to_heat_ratio=1;

%Surface areas of the CubeSat
A_8u=0.08;
A_3u=0.03;
A_2u=0.02;
A_total=2*(A_8u+A_3u+A_2u);
A_ptotal=(1/pi)*(A_8u+2*A_2u); %average surface area viewing the Sun

%view factors
h_star=(R+h)/R;
F_ver=(1/h_star)^2;
F_hor=-sqrt(h_star^2-1)/pi*h_star^2+(1/pi)*atan(1/sqrt(h_star^2-1));

% thermal power sources
Qsolar=alpha*Ssolar*A_ptotal; %solar thermal power
Qalbedo=alpha*Ssolar*albedo*(A_8u*F_ver+2*A_3u*F_hor+2*A_2u*F_hor);  %albedo thermal power
Qplanetary=alpha*Splanetary*(A_8u*F_ver+2*A_3u*F_hor+2*A_2u*F_hor); %ir thermal power


%Nominally the satellite is in Sun-Tracking mode consuming 12.1 W
%It is assumed that power_to_heat_ratio % of electrical power is converted to thermal
%emissions
for i=1:scenario_time
Qinternal(i)= power_to_heat_ratio*12.1;
end

%add S-Band Mode thermal emissions
% add an S-Band link that consumes 32.6 W for 300 secs, at a random point:
% Epoch 3000.
sband_duration = 300;
sband_consumption = 32.6;
sband_start_time(1)= 3000;
sband_interval = 43200;

number_sband_links=floor(scenario_time/sband_interval);

for i=2:number_sband_links
sband_start_time(i)= sband_start_time(i-1)+sband_interval;
```

```
end

for i=2:number_sband_links
Qinternal(sband_start_time(i):(sband_start_time(i) + sband_duration)) = power_to_heat_ratio * sband_consumption;
end

% add a PNT service Mode that consumes 56.1 W for 642 secs, at a random point:
% Epoch 6000.

pnt_service_interval=11000;
number_of_pnt_service=floor(scenario_time/pnt_service_interval);
pnt_service_start_time(1)= 6000;
for i=2:number_of_pnt_service
pnt_service_start_time(i)= pnt_service_start_time(i-1)+pnt_service_interval;
end

pnt_service_duration = 642;
pnt_service_consumption = 56.1;

% pnt service is assumed to be ON number_of_pnt_service times in the
% scenario_time duration
for i=1:number_of_pnt_service
   Qinternal(pnt_service_start_time(i):(pnt_service_start_time(i)+ pnt_service_duration)) = power_to_heat_ratio *
pnt_service_consumption;
end

Temp_Kelvin(1)=300; %starting temperature
Q_in(1)=Qplanetary+Qinternal(1)+Qsolar+Qalbedo; %starting Qin, starts in sunlight

for K=2:scenario_time
   % determine whether the satellite is in eclipse or not and account for
   % the correspondingthermal load
   if sun_status_matrix(K)==0  %in eclipse
      Q_in(K)=Qplanetary+Qinternal(K);
   else     %while in sunlight
      Q_in(K)=Qplanetary+Qinternal(K)+Qsolar+Qalbedo;
   end
   %The temperature equation is derived from the energy balance
%  mass*Cp*dT/dt = Qin-åóAT^4
% using the derivative definition:
% dT/dt=(T[K]-T[K-1])/Ät, with Ät being 1 sec
   Temp_Kelvin(K)=Temp_Kelvin(K-1)+(1/(mass*Cp))*(Q_in(K-1)-epsilon*sigma*A_total*Temp_Kelvin(K-1)^4);
end

% Convertion to Celcius
for K=1:scenario_time
   Temp_Celcius(K) = Temp_Kelvin(K)-272.15;
end

Time(1)=0; %starting time
for K=2:scenario_time
   Time(K)=Time(K-1)+1;
end

%Diagram: Temperature/time
figure (1)
plot(Time(1,:) / 3600,Temp_Celcius(1,:))
xlabel('time (hrs)')
ylabel('T (Celcius)')
title('Thermal - Day in the Life Simulation')
```

19. Bibliography

[1] EUSPA, “EUSPA EO and GNSS Market Report,” 2024. Accessed: Jul. 16, 2024. [Online]. Available: https://www.euspa.europa.eu/sites/default/files/2024-03/euspa_market_report_2024.pdf

[2] Y. T. J. Morton, F. Diggelen, J. J. Spilker, B. W. Parkinson, S. Lo, and G. Gao, Eds., *Position, Navigation, and Timing Technologies in the 21st Century*. Wiley, 2020. doi: 10.1002/9781119458449.

[3] Inside GNSS, “First Steps Toward a Fully Operational LEO PNT Payload,” Inside GNSS. Accessed: Jul. 16, 2024. [Online]. Available: https://insidegnss.com/first-steps-toward-a-fully-operational-leo-pnt-payload/

[4] F. S. Prol *et al.*, “Position, Navigation, and Timing (PNT) Through Low Earth Orbit (LEO) Satellites: A Survey on Current Status, Challenges, and Opportunities,” *IEEE Access*, vol. 10, pp. 83971–84002, 2022, doi: 10.1109/ACCESS.2022.3194050.

[5] P. A. Iannucci and T. E. Humphreys, “Fused Low-Earth-Orbit GNSS,” Sep. 2020.

[6] M. Wade, “Iridium,” Encyclopedia Astronautica. Accessed: Jul. 16, 2024. [Online]. Available: https://web.archive.org/web/20170722060655/http://www.astronautix.com/i/iridium.html

[7] K. de Jong, M. Goode, X. Liu, and M. Stone, “Precise GNSS Positioning in Arctic Regions,” in *All Days*, OTC, Feb. 2014. doi: 10.4043/24651-MS.

[8] Iridium Communications Inc, “Iridium NEXT: In Review,” Iridium 360 Blog. Accessed: Jul. 16, 2024. [Online]. Available: https://www.iridium.com/blog/iridium-next-review/

[9] Iridium Communications Inc, “What is a Hosted Payload?,” Iridium 360 Blog. Accessed: Jul. 16, 2024. [Online]. Available: https://www.iridium.com/blog/what-is-a-hosted-payload-iridium-aireon/

[10] Satelles Inc, “Iridium Announces Acquisition of Satelles,” Satelles. Accessed: Jul. 16, 2024. [Online]. Available: https://satelles.com/iridium-announces-acquisition-of-satelles/

[11] TrustPoint Inc, “TrustPoint.” Accessed: Jul. 16, 2024. [Online]. Available: https://www.trustpointgps.com/

[12] D. Werner, “TrustPoint Launches PNT Cubesat,” SpaceNews. Accessed: Jul. 16, 2024. [Online]. Available: https://spacenews.com/trustpoint-launches-pnt-cubesat/

[13] TrustPoint Inc, “TrustPoint Advances Commercial PNT System with Upcoming Launch of Second Satellite,” EIN Presswire. Accessed: Jul. 16, 2024. [Online]. Available: https://www.einpresswire.com/article/664842193/trustpoint-advances-commercial-pnt-system-with-upcoming-launch-of-second-satellite

[14] M. Saines, “TrustPoint Launches Commercially Funded PNT Microsatellite,” GPS World. Accessed: Jul. 16, 2024. [Online]. Available:

https://www.gpsworld.com/trustpoint-launches-commercially-funded-pnt-microsatellite/
[15] G. D. Krebs, “It’s About Time,” Gunter’s Space Page.
[16] SatNow, “TrustPoint Partners with SpiderOak to Elevate Security for its GNSS Infrastructure,” SatNow. Accessed: Jul. 16, 2024. [Online]. Available: https://www.satnow.com/news/details/1438-trustpoint-partners-with-spideroak-to-elevate-security-for-its-gnss-infrastructure
[17] P. Anderson, G. Schmitt, and P. Shannon, “Low Earth Orbit Navigation System (LEONS): Scalable GNSS-Independent Time Transfer and Positioning for Space Users,” Feb. 2023, pp. 65–76. doi: 10.33012/2023.18591.
[18] ESA, “Xona Space Systems: Development Status,” eoPortal Directory.
[19] Xona Space Systems Inc, “Xona Space Systems,” Jun. 2023. Accessed: Jul. 16, 2024. [Online]. Available: https://www.unoosa.org/documents/pdf/icg/2023/ICG_WG-S_LEO-PNT_Workshop_June_2023/ICG_LEO-PNT_Workshop_2023_04.pdf
[20] T. Reid, “Launching Xona’s Ravens: Commercial Satnav from LEO,” Inside GNSS. Accessed: Jul. 16, 2024. [Online]. Available: https://insidegnss.com/launching-xonas-ravens-commercial-satnav-from-leo/
[21] ESA, “Xona Space Systems: New Capabilities,” eoPortal Directory. Accessed: Jul. 16, 2024. [Online]. Available: https://www.eoportal.org/satellite-missions/xona#new-capabilities
[22] G. D. Krebs, “Sherpa-AC,” Gunter’s Space Page. Accessed: Jul. 16, 2024. [Online]. Available: https://space.skyrocket.de/doc_sdat/sherpa-ac.htm
[23] B. Chan, “Xona Space Systems,” Nov. 2022. Accessed: Jul. 16, 2024. [Online]. Available: https://www.gps.gov/governance/advisory/meetings/2022-11/chan.pdf
[24] Xona Space Systems Inc, “Xona Broadcasts Demo PNT Signals,” Xona Space Systems Inc. Accessed: Jul. 16, 2024. [Online]. Available: https://www.xonaspace.com/xonademospntsignals
[25] Xona Space Systems Inc, “Xona Secures Investment from First Spark Ventures and Lockheed Martin to Accelerate LEO GPS Alternative,” Xona Space Systems Inc. Accessed: Jul. 16, 2024. [Online]. Available: https://www.xonaspace.com/xonasecuresinvestmentfirstsparklockheedmartin
[26] Geely, “Geespace Successfully Launches First Nine Satellites,” Geely Auto. Accessed: Jul. 16, 2024. [Online]. Available: https://global.geely.com/en/news/2022/geespace-launches-nine-satellites
[27] G. D. Krebs, “GeeSAT 1-01, ..., 74,” Gunter’s Space Page. Accessed: Jul. 16, 2024. [Online]. Available: https://space.skyrocket.de/doc_sdat/geesat-1.htm
[28] Zhejiang Geely Holding Group, “Geespace Launches Eleven Low-orbit Satellites Expanding Geely Future Mobility Constellation,” Zhejiang Geely Holding Group. Accessed: Jul. 16, 2024. [Online]. Available: https://zgh.com/media-center/news/2024-09-03/?lang=en

[29] L. Bruce, “Chang Zheng 2C launches GeeSAT autonomous driving navigation satellites,” NASA SpaceFlight. Accessed: Jul. 16, 2024. [Online]. Available: https://www.nasaspaceflight.com/2022/06/chang-zheng-2c-geesat/

[30] Ltd. Beijing Future Navigation Technology Co., “CENTISPACETM System Experimental Satellites PPP Application Test,” UNOOSA. Accessed: Jul. 16, 2024. [Online]. Available: https://www.unoosa.org/documents/pdf/psa/activities/2023/GNSS2023/GNSS2023_05_04.pdf

[31] G. D. Krebs, “CentiSpace-1 S1, ..., S5,” Gunter’s Space Page. Accessed: Jul. 16, 2024. [Online]. Available: https://space.skyrocket.de/doc_sdat/centispace-1.htm

[32] T. Cozzens, “China launches CentiSpace-1 navigation enhancement satellites,” GPS World. Accessed: Jul. 16, 2024. [Online]. Available: https://www.gpsworld.com/china-launches-centispace-1-navigation-enhancement-satellites/

[33] Yang Long, “The Centispace-1: A LEO Satellite-Based Augmentation System,” in *14th Meeting of the International Committee on Global Navigation Satellite Systems*, 2019. Accessed: Jul. 16, 2024. [Online]. Available: https://www.unoosa.org/documents/pdf/icg/2019/icg14/WGB/icg14_wgb_S5_4.pdf

[34] A. Parsonson, “ESA Awards €233M for Three Navigation Satellites,” European Spaceflight. Accessed: Jul. 16, 2024. [Online]. Available: https://europeanspaceflight.com/esa-awards-e233m-for-three-navigation-satellites/

[35] M. C. Limón, “FutureNAV In Orbit Demonstrator - a first step towards a European LEO-PNT component,” in *UN / Finland Workshop on Applications of Global Navigation Satellite Systems* , 2023. Accessed: Jul. 16, 2024. [Online]. Available: https://www.unoosa.org/documents/pdf/psa/activities/2023/GNSS2023/GNSS2023_05_01.pdf

[36] ESA, “LEO-PNT,” ESA. Accessed: Jul. 16, 2024. [Online]. Available: https://www.esa.int/Applications/Satellite_navigation/LEO-PNT

[37] GMV, “GMV to Lead ESA’s LEO PNT End-to-End In-Orbit Demonstrator Mission,” GMV. Accessed: Jul. 16, 2024. [Online]. Available: https://www.gmv.com/en/communication/press-room/press-releases/positioning-navigation-and-timing/gmv-lead-esas-leo-pnt-end

[38] Alén Space, “Alén Space will participate in the LEO-PNT mission of the European Space Agency ,” Alén Space. Accessed: Jul. 16, 2024. [Online]. Available: https://alen.space/alen-space-leo-pnt-european-space-agency/

[39] ESA, “ESA Kicks off Two New Navigation Missions,” ESA. Accessed: Jul. 16, 2024. [Online]. Available: https://www.esa.int/Newsroom/Press_Releases/ESA_kicks_off_two_new_navigation_missions

[40] Thales Alenia Space, “Thales Alenia Space Won European Space Agency’s One of Two LEO-PNT Orbit Demonstrators,” Thales Alenia Space. Accessed: Jul. 16, 2024. [Online]. Available: https://www.thalesaleniaspace.com/en/press-releases/thales-alenia-space-won-european-space-agencys-one-two-leo-pnt-orbit-demonstrators
[41] Syntony GNSS, “Syntony’s Receivers Selected by ESA for New LEO-PNT Constellation Demonstration,” Syntony GNSS. Accessed: Jul. 16, 2024. [Online]. Available: https://syntony-gnss.com/news/business/syntonys-receivers-selected-by-esa-for-new-leo-pnt-constellation-demonstration
[42] Nanyang Technological University, “SPATIUM (Space Precision Atomic-Clock Timing Utility Mission),” Nanyang Technological University. Accessed: Jul. 16, 2024. [Online]. Available: https://www.ntu.edu.sg/sarc/research-capabilities/satellites/spatium
[43] ESA, “SPATIUM-I: Payload CSAC,” eoPortal Directory. Accessed: Jul. 16, 2024. [Online]. Available: https://www.eoportal.org/satellite-missions/spatium#payload-csac-chip-scale-atomic-clock
[44] A. P. Aboaf, “MAXWELL Mission Handbook,” University of Colorado Boulder. Accessed: Jul. 16, 2024. [Online]. Available: https://www.studocu.com/row/document/multimedia-university-of-kenya/history-of-engineering/507214918-maxwell-mission-handbook-released-5940716043101429/49270606
[45] ESA, “CHOMPTT: Payload Complement of 13 CubeSats,” eoPortal Directory. Accessed: Jul. 16, 2024. [Online]. Available: https://www.eoportal.org/satellite-missions/chomptt#payload-complement-of-13-cubesats
[46] J. Anderson *et al.*, “Sub-nanosecond ground-to-space clock synchronization for nanosatellites using pulsed optical links,” *Advances in Space Research*, vol. 62, no. 12, pp. 3475–3490, 2018, doi: https://doi.org/10.1016/j.asr.2017.06.032.
[47] J. W. Conklin *et al.*, “Preliminary results from the CHOMPTT laser time-transfer mission,” in *33rd Annual AIAA/USU Conference on Small Satellites*, 2019. Accessed: Jul. 16, 2024. [Online]. Available: https://digitalcommons.usu.edu/cgi/viewcontent.cgi?article=4407&context=smallsat
[48] Erik Kulu, “AIOTY-CUBE Satellite.” Accessed: Sep. 02, 2024. [Online]. Available: https://www.nanosats.eu/sat/aioty-cube
[49] E. Commission, J. R. Centre, and M. Travagnin, *Chip-scale atomic clocks – Physics, technologies, and applications*. Publications Office, 2021. doi: doi/10.2760/278540.
[50] Syrlinks, “N-CUBE.” Accessed: Sep. 02, 2024. [Online]. Available: https://www.syrlinks.com/en/spatial/charge-utile-gnss-de-haute-performance
[51] Cal Poly, “CubeSat Design Specification Rev 14.1,” 2020. Accessed: Sep. 02, 2024. [Online]. Available: https://static1.squarespace.com/static/5418c831e4b0fa4ecac1bacd/t/62193b7fc9e72e0053f00910/1645820809779/CDS+REV14_1+2022-02-09.pdf

[52] N. Bartels, P. Allenspacher, S. Bauer, B. Rödiger, F. Sproll, and W. Riede, “Design and qualification of a recessed satellite cornercube retroreflector for ground-based attitude verification via satellite laser ranging,” *CEAS Space Journal*, vol. 11, no. 4, pp. 391–403, Dec. 2019, doi: 10.1007/s12567-019-00255-x.
[53] Space X, “Rideshare Payload User’s Guide,” Dec. 2023. Accessed: Sep. 02, 2024. [Online]. Available: https://storage.googleapis.com/rideshare-static/Rideshare_Payload_Users_Guide.pdf
[54] European Union, “GALILEO OPEN SERVICE SIGNAL-IN-SPACE INTERFACE CONTROL DOCUMENT,” Sep. 2023. Accessed: Sep. 02, 2024. [Online]. Available: https://www.gsc-europa.eu/sites/default/files/sites/all/files/Galileo_OS_SIS_ICD_v2.1.pdf
[55] Exolaunch, “EXOpod User Manual,” Sep. 2022. Accessed: Sep. 02, 2024. [Online]. Available: https://exolaunch.com/documents/EXOpod_User_Manual_September_2022.pdf
[56] Cubespace, “Cubespace Product Catalogue”, Accessed: Sep. 19, 2024. [Online]. Available: https://www.cubespace.co.za/uploads/6249be11-455a-4ee8-b659-563d5e90fabb.pdf
[57] Cubespace, “CubeADCS Gen2 Interface Control Document,” May 2024, Accessed: Sep. 19, 2024. [Online]. Available: https://www.cubespace.co.za/uploads/a9331ba4-34e9-4d93-b486-45bf092d06ca.pdf
[58] ESA Space Debris Mitigation Working Group, “ESA Space Debris Mitigation Requirements, ESSB-ST-U-007 Issue 1,” Oct. 2023. Accessed: Oct. 15, 2024. [Online]. Available: https://technology.esa.int/upload/media/DGHKMZ_6542582e18e33.pdf
[59] X. Oikonomidou, V. Braun, and S. Lemmens, “GUIDELINES FOR SPACE DEBRIS AND METEOROID IMPACT RISK ASSESSMENT WITH DRAMA/MIDAS,” in *8th European Conference on Space Debris*, Darmstadt, Germany: ESA Space Debris Office, 2021. Accessed: Oct. 15, 2024. [Online]. Available: https://conference.sdo.esoc.esa.int/proceedings/sdc8/paper/163/SDC8-paper163.pdf
[60] Inc. Rocket Lab USA, “Electron Payload User’s Guide,” Nov. 2022. Accessed: Oct. 09, 2024. [Online]. Available: https://www.rocketlabusa.com/assets/Uploads/Electron-Payload-User-Guide-7.0.pdf
[61] Arianespace, “SSMS Vega-C User’s Manual,” Sep. 2020. Accessed: Oct. 09, 2024. [Online]. Available: https://www.arianespace.com/wp-content/uploads/2020/10/SSMS-Vega-C-UsersManual-Issue-1-Rev0-Sept2020.pdf

[62] D. Dobrijevic, “Solar maximum: What is it and when will it occur?,” 2024. Accessed: Sep. 03, 2024. [Online]. Available: https://www.space.com/what-is-solar-maximum-and-when-will-it-happen
[63] Enpulsion, “Enpulsion NANO.” Accessed: Oct. 05, 2024. [Online]. Available: https://www.enpulsion.com/order/enpulsion-nano/
[64] Enpulsion, “Enpulsion NANO datasheet,” 2024. Accessed: Oct. 05, 2024. [Online]. Available: https://www.enpulsion.com/wp-content/uploads/ENP2018-001.I-Enpulsion-NANO-Product-Datasheet.pdf
[65] Orbital Transports, “SmallSat Catalog - Enpulsion NANO.” Accessed: Oct. 05, 2024. [Online]. Available: https://catalog.orbitaltransports.com/enpulsion-nano/
[66] Enpulsion, “Enpulsion Brochure,” 2024. Accessed: Oct. 05, 2024. [Online]. Available: https://www.enpulsion.com/downloads/
[67] Microchip Technology Inc., “Chip-Scale Atomic Clock (CSAC) SA.45s User’s Guide,” 2020. Accessed: Oct. 05, 2024. [Online]. Available: https://ww1.microchip.com/downloads/en/DeviceDoc/Chip-Scale-Atomic-Clock-CSAC-SA.45s-Users-Guide-DS50003041.pdf
[68] Microchip Technology Inc., “Chip-Scale Atomic Clock Performance During Rapid Temperature Change White Paper,” 2021. Accessed: Oct. 05, 2024. [Online]. Available: https://ww1.microchip.com/downloads/en/DeviceDoc/Chip-Scale-Atomic-Clock-CSAC-Performance-During-Rapid-Temperature-Changes-White-Paper-DS00003996A.pdf
[69] F. Bard, “Galileo Space Segment,” *Navigation Training Course 2023, ESA Academy*, 2023.
[70] Frank Lemoine, “LightSail.” Accessed: Sep. 02, 2024. [Online]. Available: https://ilrs.gsfc.nasa.gov/missions/satellite_missions/past_missions/litb_reflector.html
[71] ESA, “LightSail Missions of The Planetary Society.” Accessed: Sep. 02, 2024. [Online]. Available: https://www.eoportal.org/satellite-missions/lightsail#spacecraft
[72] ITU, “Recommendation ITU-R P.618-14,” Aug. 2023. Accessed: Sep. 03, 2024. [Online]. Available: https://www.itu.int/dms_pubrec/itu-r/rec/p/R-REC-P.618-14-202308-I!!PDF-E.pdf
[73] D. Gilmore, *Spacecraft Thermal Control Handbook, Volume I: Fundamental Technologies*. Washington, DC: American Institute of Aeronautics and Astronautics, Inc., 2002. doi: 10.2514/4.989117.
[74] S. Sanchez-Sanjuan, J. Gonzalez-Llorente, and R. Hurtado-Velasco, “Comparison of the Incident Solar Energy and Battery Storage in a 3U CubeSat Satellite for Different Orientation Scenarios,” *Journal of Aerospace Technology and Management*, vol. 8, no. 1, pp. 91–102, Mar. 2016, doi: 10.5028/jatm.v8i1.531.
[75] E. A. Silk, *Introduction to Spacecraft Thermal Design*. Cambridge University Press, 2020. doi: 10.1017/9781108149914.
[76] J. R. Wertz and W. J. Larson, *Space Mission Analysis and Design*, 3rd ed. 1999.

[77] G. Broccia, “Solar Radiation profiles for a 3U CubeSat in LEO,” May 2021.
[78] Lai J., “Thermal Analysis for a High Precision Pointing Helios CubeSat,” San José State University, San José,CA, 2015. Accessed: Oct. 08, 2024. [Online]. Available: https://www.sjsu.edu/ae/docs/project-thesis/Justin.Lai-F15.pdf